UNIVERSITY OF LIVERPOOL

Evaluating models of Influenza A virus Infection

Thesis submitted in accordance with the requirements of the University of Liverpool for the degree of Doctor in Philosophy

By

Elsa Gayle Zekeng BSc

March 2019

AUTHOR'S DECLARATION

Apart from the help and advice acknowledged, this thesis represents the unaided work of the author

.....

Elsa Gayle Zekeng, March 2019

This research was carried out in the Department of Infection Biology, Institute of Infection and Global Health, University of Liverpool

ACKNOWLEDGEMENTS

Over the course of my PhD, there are many people who provided me with mental and emotional support without whom I will not be able to get to this point today. It has been a great pleasure to complete my PhD at the University of Liverpool and more importantly, one of the greatest opportunities to do this in the Hiscox laboratory.

First and foremost, I will like to thank God for giving me this opportunity and seeing me through my PhD. To my parents, Dr. & Dr. Mrs. Zekeng; the best gift a parent can give their child is education, you gave me that and so much more. For that, I will like to thank you from the bottom of my heart. For the sacrifices, you have made to give me this opportunity, they didn't go unnoticed, I hope I've made you proud and I am able to pay you back some day. To my sister, Dr. Cherryl Zekeng, thank you for listening to me, for supporting me and pushing me to my full potential. To my other siblings, Miss Rita Tatah and Mr. Leopold Zekeng; thank you for the moral and emotional support. To Miss Zoey Leonore Awah and Mr. Liam Zuriel Awah, thank you for putting a smile on my face from the day you were born.

To my supervisor, Prof. Julian Hiscox, thank you for giving me the opportunity to work with you, it has been my pleasure working with your group. Thank you to the whole of the Hiscox respiratory viruses' group. Thank you to our collaborators in Public Health England; Prof. Miles Carroll, Dr. Anthony Marriott and Dr. Catherine Whittaker. Thank you to Professor Paul Digard at the Roslin Institute, University of Edinburgh for all the scientific support. Thank

you to Prof. James Stewart for your scientific support.

Particular thanks to Dr. Isabel Garcia, Dr. Stuart Armstrong, Dr. Dong Xia, Dr. Nathifa Moyo, Dr. Diane Munday, Dr. Olivier Touzelet, Dr. Simon Clegg and Ms. Jill Hudson for all their scientific support during my PhD. A heartfelt thank you to all my friends in the IC2 in the infection Biology department for their friendship and scientific support over this time.

To my friend, Miss Kabila Gana, thank you very much for your love, mental and emotional support and your continuous encouragement and prayers, I will forever be grateful. To Dr. Irene Afreh-Mensah and Miss Sharon Ngang, thank you for your emotional, mental and physical support. To Mr. Jamaal Brathwaite, thank you very much for your continuous support and love over the last year, it was indeed a very trying year, but your love and support carried and encouraged me through.

Last but certainly not the least, a very special thanks to Dr. Sarah Tade. For the constant love, encouragement, prayers and support during the last five years, I could not have done this without her.

ABSTRACT

High throughput proteomics and transcriptomics has provided a platform to further understand viral – host interaction. This provides a window into the host proteome and transcriptome with and without infection. This leads to identification of potential biomarkers, understanding IAV pathogenesis and also drawing a comparison of how hosts respond to viral infection.

This thesis used two independent high throughput approaches to explore the proteome and transcriptome of samples from hosts (*in vitro* and *in vivo*) infected with influenza A virus (IAV) compared to samples from hosts (*in vitro* and *in vivo*) non-infected with IAV. The independent high throughput approaches used were; proteomics on a Q-Exactive platform and transcriptomics on a MinION sequencer. These approaches were used to further understand IAV infection in these different hosts and secondly to explore and search further for a potential biomarker for the diagnosis of IAV and potential drug targets. To our knowledge, this is the first study that has used high throughput approaches to analyses samples from different hosts. This allowed for comparison across hosts but also provides vast amounts of data that are reliable and consistent.

A549 cells that were mock-infected and IAV- infected were subjected to the Q-Exactive platform and MinION sequencing. This provided insight into the *in vitro* host-viral interaction on a cellular level. For the first time, showed the potential of MinION sequencing as a method for understanding the viral-host interaction of IAV infected cells and identifying potential biomarkers. This highlighted transcripts such as NUP54, RBM42, HPGD, GCLC, ANPEP, AKAP13, RACGAP1, CREB1, MAN2B1 and PRKCI. These transcripts were

identified by bioinformatic analysis as host factors that play a crucial role in replication of IAV in the host. The corresponding proteins to these transcripts were also identified by proteomics. To better understand IAV in hosts, *in vivo,* Non-human primates (NHP) were infected with IAV and the broncho-alveolar fluid (BALF) was collected and compared to BALF from naïve NHP. After analysis on the Q-Exactive platform, the results obtained drew parallels on a cellular level to that observed *in vitro* models. Proteins such as; DDX58, EIF3A, HSP90AA1, MAPK1, MX1 and STAT1 involved in the "replication of IAV" were highlighted. In addition to the cellular changes, the NHP studies provided insight into an immune response similar to that observed in humans following IAV infection. This provided an added dimension in understanding IAV infection. Finally, nasopharyngeal aspirates (NAs) from humans IAV-infected and IAV non-infected from three different cohorts (Alder Hey Children's hospital (AHCH), Liverpool, Great Ormond Street Hospital (GOSH), London and Institute Pasteur Dakar (IPD)) were analysed on the Q-Exactive platform. This provided a full circle loop to compare if the changes observed *in vitro* model – A549 cells and *in vivo* model-NHP were relatable back to humans. Proteins identified *in vitro* and *in vivo* studies were concordant with proteins identified in the human NAs. These proteins include; COPA, STAT1, TUBB and HSPB1. Additionally, three proteins were identified in human NAs across all three cohorts; BPIFA1/SPLUNC1, Lactotransferrin and Fibrinogen A, B and G. These proteins play crucial roles in elucidating IAV infection in the host. This study presents the first time these proteins have been highlighted using label-free Mass spectrometry in human NAs across three cohorts from different geographical locations.

This thesis illustrates how proteomic analysis of IAV-infected samples compared to non-infected samples can be used to identify markers that may serve as potential diagnostic indicators for IAV infection.

TABLE OF CONTENTS

ABBREVIATIONS

Alder Hey Children's Hospital	AHCH
Alveolar macrophages	AM
Bicinchoninic acid	BCA
Bourbon virus	BOUV
Broncho-alveolar fluid	BALF
Centre for Disease Control	CDC
Centre for genomic research	CGR
Chromosomal maintenance 1	CRM1
Chronic obstructive pulmonary disease	COPD
Clara cell secretory protein	CCSP
C-terminal repeat domain	CTD
Cycle threshold	Ct
Cytopathic effect	CPE
Deoxyribonucleic acid	DNA
Differentially expressed	DE
Differential gene expression	DEG
Dulbecco's Modified Eagle Medium	DMEM
Dhori virus (thogotovirus dhori)	DHOV
Endoplasmic reticulum	ER
Foetal bovine serum	FBS
Glyceraldehyde 3-phosphate dehydrogenase	GAPDH
Great Ormond Street Hospital	GOSH
Glycoprotein	Gp
Health Protection Agency Culture Collections	HPACC

Hemagglutinin	HA
Hepatitis B-Virus	HBV
Human Immunodeficiency virus	HIV
human respiratory syncytial virus	HRSV
immunofluorescence	IF
Influenza A virus	IAV
Influenza B virus	IBV
Influenza C virus	ICV
Influenza D virus	IDV
Ingenuity pathway analysis	IPA
Inhaled aerosol	i.a
Institute Pasteur	IPD
Interferon	IFN
Interferon-induced proteins with tetratricopeptide repeats 3	IFIT3
Interferon-stimulated genes	ISGs
International Committee on Taxonomy of Viruses	ICTV
Internal positive control	IPC
Johnston Atoll Virus	JAV
Liquid chromatography Mass Spectrometry	LC-MS
Madin-Darby Canine Kidney	MDCK
Matrix protein	M
Mitochondrial antiviral-signalling	MAVS
Multiplicity of infection	MOI
messenger RNAs	mRNA
Nasopharyngeal aspirates	NAs

Neuraminidase	NA
Next Gneration Sequencing	NGS
Non-human primate	NHP
Nuclear export protein	NEP
Nucleocapsid protein	NP
Oxford Nanopore Technologies	ONT
Polyacrylamide gel electrophoresis	PAGE
Plaque-forming units	PFU
Phosphate Buffered Saline	PBS
Phocine Distemper virus	PDV
Polymerase A protein	PA
Polymerase B1 protein	PB1
Polymerase B2 protein	PB2
polymerase chain reaction	PCR
Poly-vinylidine fluoride	PVDF
Porcine Reproductive and Respiratory Syndrome Virus P	RRSV
Post infection	p.i.
Protein interaction network viewer	PINV
Public Health England	PHE
Quaranfil virus	QRFV
Rabies virus	RBV
Red blood cells	RBCs
Respiratory syncytial virus	RSV
Retinoic acid gene-I	RIG-I
Ribonucleic Acid	RNA

Ribonucleoprotein complex	RNP
RNA dependent RNA polymerase	RdRp
Serum-free media	SFM
Sialic acid	SA
Sodium-Dodecyl sulphate	SDS
Stable isotope labeling by amino acids in cell culture	SILAC
Swine influenza virus	SIV
Toll-like receptor	TLR
Thogotovirus (thogotovirus thogoto)	THOV
Two-dimensional gel electrophoresis	2D-DIGE
University of Liverpool	UOL
Viral ribonucleotides	vRNPs
World Health Organization	WHO

CHAPTER 1: INTRODUCTION

1.1 General introduction

The influenza virus has been associated with human disease and epidemics since 412 BC, as described by Hippocrates. An epidemic in 412 BC, which affected medical personnel, showed the clinical symptoms of debility, coughs, and headaches. These were principal factors associated with the influenza virus (1, 2). This information demonstrates just how long the influenza virus has been associated with humans. Influenza viruses have been, and still are, a major source of morbidity and mortality around the world, affecting large groups of people yearly (3). In the United States alone, influenza virus infections cause an annual mortality of 36,000 (4). In addition to humans being infected by influenza viruses, many animal species can be infected. Four types of influenza virus have been classified; A, B, C, and the recently classified D virus (5, 6). Influenza viruses' A and B cause seasonal disease epidemics. The influenza A virus (IAV) can cause pandemics due to its great genetic diversity. IAV infects a wide range of host species and causes severe disease in humans (7). Some viral proteins have an essential part to play in affecting IAV's virulence, NS1 is an example of such a protein (8). NS1 plays a role in inhibiting an innate host response by targeting interferon (IFN) production and IFN-induced antiviral effectors. NS1 protein has been extensively studied in IAV, but not extensively in influenza B (9). Influenza type C infections do not cause epidemics but rather cause mild respiratory illness. Influenza D viruses mainly affect cattle and its ability to be a potential public health threat in humans is low (4) (10). IAV has given rise to pandemic strains in humans, as in the case of the 2009 H1N1 pandemic. IAV pandemics date back to 1918 (11). In 1918, the human influenza A (H1N1) virus (IAV) spread globally and

killed between 40 and 50 million people. There were similarities in the clinical presentation and pathologic features of IAV in humans and swine. These similarities triggered the hypothesis that the pandemic human influenza, in 1918, infected pigs (12).

IAV was the first swine influenza virus isolated in a laboratory in 1931, where it was recorded and confirmed by laboratory diagnosis (13). Robert Shope successfully transmitted the infectious agent from sick pigs via transmission of secretions to healthy animals. Smith, Andrews, and Laidlaw were able to establish and document IAV infection in the ferret model and subsequently the transmissibility of both human and swine viruses (13). This was the first isolated human influenza virus and so was termed IAV. In 1940, an antigenically different virus was isolated, and after isolation, was termed the influenza type B virus (B/Lee/40) (14). The first influenza C virus was isolated in 1947 (15). The diagnosis of influenza viruses has frequently been via clinical symptoms (which can be similar with other respiratory infections) and the time of the year. Influenza virus infections can present as a sudden onset of three-day fever as well as muscle pain. Influenza viruses can rapidly become epidemic and infect a large percentage of people. For these reasons, influenza viruses have been one of the most studied viruses up until the emergence of the human immunodeficiency virus (HIV), over three decades ago (16).

1.2 Introduction to the classification of families

1.2.1 The Orthomyxoviridae family

The International Committee on Taxonomy of Viruses (ICTV) has recognised a hierarchy of viral taxa as follows: order, family, (subfamily), genus, and species. The viruses within the *Orthomyxoviridae* family are negative sense RNA viruses with seven genera and nine species (17).

Table 1.1 Classification of Family Orthomyxoviridae, according to the International Committee on Taxonomy of Viruses (ICTV) released in 2017 (17)

Genus	Species
Alphainfluenzavirus	*Influenza A virus*
Betainfluenzavirus	*Influenza B virus*
Deltainfluenzavirus	*Influenza D virus*
Gammainfluenzavirus	*Influenza C virus*
Isavirus	*Salmon isavirus*
Quaranjavirus	*Johnston Atoll quaranjavirus*
	Quaranfil quaranjavirus
Thogotovirus	*Dhori thogotovirus*
	Thogoto thogotovirus

Virions of viruses within the *Orthomyxoviridae* family are both spherical and pleomorphic and are 80–120nm in diameter (18). Many members of the *Orthomyxoviridae* family are known animal or human pathogens. For example,

IAV accounts for seasonal epidemics and pandemics, resulting in many deaths over the past century (19).

Unlike influenza viruses, *thogotoviruses* which are in the *Thogotovirus* genus are mainly transmitted through tick vectors and are subsequently called 'tick-borne viruses' (19-21). These viruses are frequently found in domestic animals; sheep, cattle and camels. These viruses can cause neural diseases and abortion (19, 22). Thogotovirus (thogotovirus thogoto [THOV]) and the Dhori virus (thogotovirus dhori [DHOV]) infect humans and are known to cause human deaths (23, 24). Tick vectors are popularly known to transmit THOV and DHOV, but DHOV has been reported to cause human infections in a vector-free manner, perhaps through aerosols (24). This makes the transmission route unclear and not fully characterised. A farmer in the United States was infected, and subsequently killed, by a virus called the 'Bourbon virus' (BOUV). In 2014, this virus was identified and classified as an unknown type of thogotovirus (19, 25). These viruses are capable of harming the human population and their characterisation is important for public health (19).

The envelope of thogotovirus consists of only one glycoprotein (Gp). This glycoprotein is responsible for virus entry, attachment, entry, and fusion (19, 26). Within the *Orthomyxovirdae* family, quaranjavirus is the closest to thogotovirus. The Gp found in quaranjavirus shares a sequence identity of 26% with the thogotovirus Gp.

The quaranjavirus genus contains the two species: Quaranfil virus (QRFV) and Johnston Atoll virus (JAV) (ICTV Report Taxonomy, 2009). In 1964, JAV was first isolated from ticks (*Ornithodoros capensis*) from Sand Island in the central pacific (27, 28). In 1953, the Quaranfil virus was first isolated from children in Quaranfil, Egypt, and subsequently in numerous other geographic areas from ticks and birds (27, 29). Through high throughput sequencing, the QRFV was completely sequenced and classified as a novel *orthomyxovirus*. QRFV had a genome made up of several RNA segments containing proteins that had similarities to other proteins within the orthomyxoviridae family such as polymerase (PA, PB1 and PB2) and hemagglutinin (HA) (27). Considering JAV and Lake Chad virus (LKCV) were both unclassified viruses, they were sequenced and analysed in comparison to QRFV. QRFV and JAV had a high amino acid similarity to each other of 80% and 70% in PB1 and HA respectively. As a result of this and further phylogenetic analyses, QRFV, JAV, and LKCV were proposed to belong to the *Orthomyxoviridae* family (27).

Influenza viruses are categorised in separate genera to thogotovirus and isavirus. Influenza viruses have two major internal proteins; nucleoprotein and matrix protein that influence their classification (30) (31) (32, 33). IAVs affect mammals and birds. These viruses are further classified into subtypes based on the HA and neuraminidase (NA) proteins. These consist of 18 HA and 11 NA proteins (33) (34-36). Newly isolated influenza viruses and laboratory strains frequently differ in shape: filamentous and spherical, respectively (37). All influenza viruses have distinguishing features, which allow the differentiation and categorisation of each virus.

Table 1.2: Differentiation and categorisation of each influenza virus (adapted from talk.ictvonline.org)

Influenza viruses	Influenza virus A (IAV)	Influenza virus B (IBV)	Influenza virus C (ICV)	Influenza virus D (IDV)
Distinguishing features – Genome segments	Eight genome segments.	Eight genome segments.	Seven genome segments and are lacking neuraminidase.	Seven gene segments and is, therefore, identical to ICV.
Glycoproteins	Glycoprotein spikes: HA and NA, matrix protein (M2), and a matrix overlay protein of M1 receptor-destroying enzyme are different.	Similar to IAV, four envelope proteins: hemagglutinin, neuraminidase and instead of M2, NB, and BM2.	Contains HE (HEF) as one major surface protein, which contains receptor-binding and fusion activities.	Contains HEF proteins with a 55% amino acid identity and has an almost identical structural fold to ICV.

			It has correlating functions to HA and NA found in IAV and IBV.	
Conserved sequences	The conserved end sequences of viral RNAs are 5'-AGUAGAAACAAGG and 3'-UCG(U/C)UUUCGUCC	The conserved end sequences of viral RNAs are 5'-AGUAG(A/U)AACAA and 3'-UCGUCUUCGC	The conserved end sequences of viral RNAs are 5'-AGCAG(U/G)AGCAAG and 3'-UCGUCUUCGUC	Due to its similarity to ICV, the 3' and 5' sequences are identical to ICV. The only difference is on the 3' end, where the nucleotide at position 5 is an adenine in IDV but a cytosine in ICV.

Shape and size	Spherical or filamentous and 100nm in diameter	Spherical or filamentous and 100nm in diameter	On infected surfaces, form long cordlike structures – on order of 500μm	

1.3 Antigenic drift, antigenic shift, and recombination

IAV has properties that are a result of the size of the genome and its segmented nature. These properties include the ability to exchange gene segments (called reassortment) within a co-infected cell and mutations, as replication of the IAV genome is prone to errors (38). These mutations and gene segment exchanges can lead to viruses that are genetically different to the parental viruses. These exchanges can occur across species and have the potential to result in epidemics and pandemics in humans, lower animals, and birds (39, 40) (Table 1.3). There are three mechanisms by which IAV change is evolutionary. These are: antigenic drift (mutation – Figure 1.1), antigenic shift (re-assortment – Figure 1.2), and less rarely, a recombination. Reassortment was detected in some IAV strains that circulate seasonally and have epidemiological importance (38, 41-45). Pandemics are known to occur when these gene exchanges allow an IAV strain to be both antigenically novel and also have the ability to spread through a human population (38) (Figure 1.3).

1.3.1 Antigenic drift – mutation

IAV replication is prone to errors due to the absence of proofreading mechanisms in the viral RNA-dependent RNA polymerase. These errors lead to about two mutations for each genome that is replicated (38, 46). These mutations are necessary for IAV adaptation in a new host (47). When IAV is in the host, anti-HA antibodies are directed to HA viral proteins. Mutations that allow IAV to escape host immunity, evade vaccines, and become resistant to

drugs, are a positively selected (40) evolution of IAV (Figure 1.1) and reassortment (Figure 1.2). These anti-HA antibodies encourage antigenic drift, therefore, encouraging antibody escape. The effect of these changes is that the immune system can no longer identify this virus and as a result, immune protection from the host has lost its effectivity (40). Over time, and due to the continuous pressure on the virus to evade host immune response, these mutations contribute to the evolution of the virus and potentially result in a new subtype (40, 48).

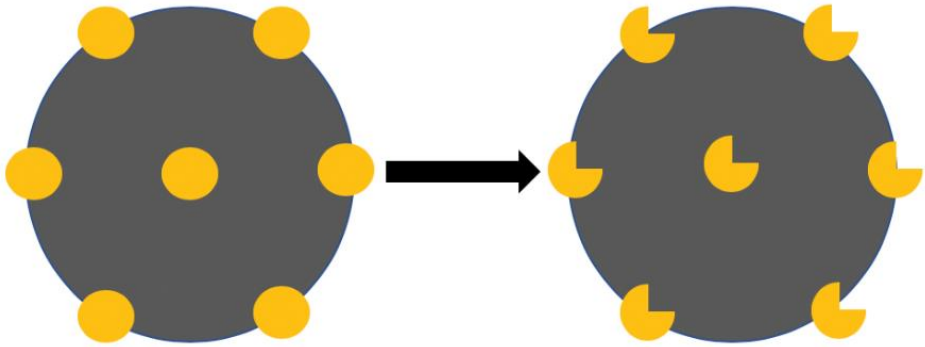

Figure 1.1. Illustration of antigenic drift also known as mutation. The yellow circles represent the gene segments that undergo mutation that causes a change in shape. This can affect antibody binding and thus host immune response.

1.3.2 Antigenic shift – reassortment

Antigenic shift is the process by which RNA segments, from genotypically different IAVs, can be exchanged and is also referred to as reassortment (49). This changes the antigenicity of IAV (38). Reassortment could be a result of transmission between hosts for example the virus from birds to humans. IAV also infects an intermediate host – frequently a pig – or virus transmission from

bird to pig (intermediate host) to humans (50). Pigs can be infected by human IAV strains, as well as avian IAV strains (Figure 1.3). As a result, pigs are called the ‘mixing vessel’. Avian and human IAV have been isolated from naturally and experimentally infected pigs (47). This reassortment can be seen in the 2009 H1N1 pandemic (pH1N1); viruses from avian, human, classical swine, and Eurasian swine circulated in pigs. This was then transmitted into the human population causing a pandemic (47, 51, 52). This can also be seen in the 1957 and 1968 pandemics (38, 53). The 1957 pandemic is thought to have occurred because viral proteins; PB1, HA, and NA from an avian H2N2 virus entered the human population with the already circulating H1N1 and formed the H2N2 pandemic (38). Additionally, the 1968 pandemic occurred as a result of the viral proteins; PB1 and HA from the avian H3 virus entering the human population with the already circulating H2N2, forming the 1968 H3N2 pandemic (38, 54). The result of this reassortment generates a ‘novel’ virus that is capable of creating a pandemic IAV strain (40, 55, 56) (see Figures 1.2 and 1.3).

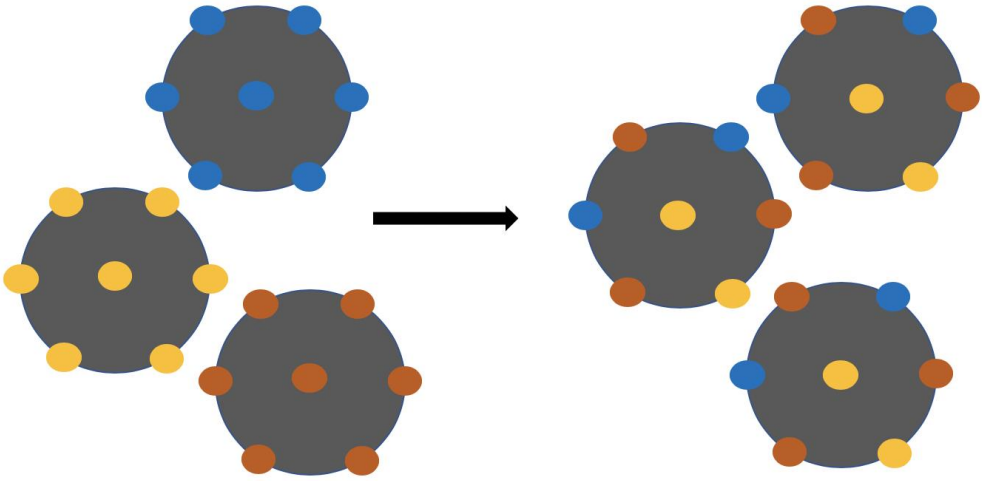

Figure 1.2: Illustration of antigenic shift, also known as reassortment. The coloured circles (yellow, blue, and orange) represent gene segments from different IAV strains that exchange, reassort, and form new subtypes and strains, containing a mix of parental segments. This mix frequently happens in pigs.

1.3.3 Recombination

Recombination is another means by which influenza viruses achieve evolution (40). Genetic recombination produces genetic diversity through two main mechanisms: non-homologous recombination which occurs between two RNA fragments (57, 58) and homologous recombination, that involves the switching of templates and is frequently thought to be absent or rare (59). This mechanism is thought to occur while the polymerase complex is copying the RNA. The process of recombination contributes to genetic diversity and only occurs when viruses replicate within the same cells (40).

i)

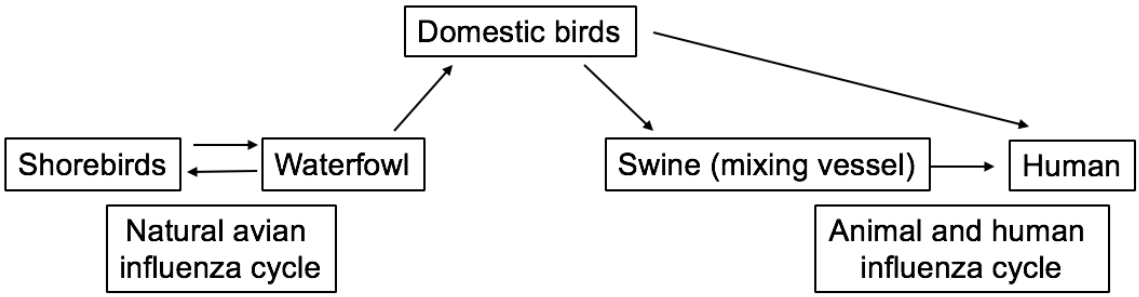

ii)

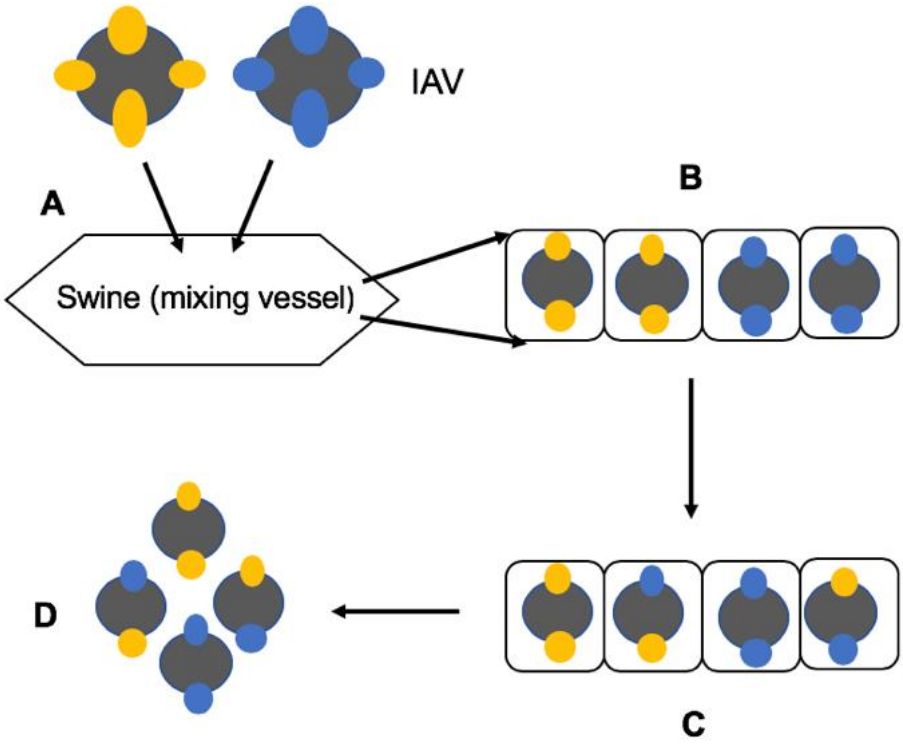

Figure 1.3: (i) Host transfer of the influenza virus in the natural avian cycle, the transfer into the natural reservoir (waterfowl), infection of domestic birds, its transfer to swine (where re-assortment of strains occurs), and infection to human host. This shows the movement of the influenza virus from animal to human hosts; (ii) Adaptation of IAV in swine (mixing vessel) and reassortment. A) Two strains of IAV enter the swine, one human IAV (denoted by yellow circles) and another avian IAV (denoted by blue circles). B) Replication occurs

in the cells of the swine and produce both strain subtypes. C) Gene segments of both IAV strains are exchanged in the same swine cell. D) IAV containing gene segments from both human IAV and avian IAV are produced.

1.4 Influenza epidemics and pandemics

Influenza causes both morbidity and mortality, and the proportion of each depends on the severity of the virus and its fluctuation during each season. For example, the 2015–2016 influenza season was relatively mild. All efforts to reduce the impact of future epidemics or pandemics are essential, through the implementation of the universal influenza vaccination and initiation of antiviral therapy. It is therefore crucial to maintain continual research amidst the variety of emerging viral epidemics such as Ebola and Zika (60). Understanding the state of epidemics and pandemics in the United Kingdom and globally, in recent times, and over the years, is essential to put the severity of IAV infection in context.

1.4.1 Epidemics

Over the years, influenza epidemics have been almost an annual occurrence with unpredictable severity (61). These epidemics tend to occur when it is cold, when there is crowding of people and lower humidity, during the Northern or Southern hemisphere winter periods. Influenza outbreaks are known to be well correlated to seasonal changes in temperature and absolute humidity; the annual climate cycles in tropical countries are much weaker and outbreaks show less seasonality, therefore reducing environmental correlations. Moving beyond the correlation, outbreak patterns between temperate and tropical

countries, are also driven by absolute humidity, and, to a lesser extent, global temperature (62). While environmental factors play a great role in influencing the seasonality of influenza outbreaks, other non-environmental factors, such as seasonal changes in behaviour, family, and social structure, pre-existing immunity, and the nature of the virus to transcend these factors, can affect seasonal epidemics (63). The presence of a variant virus showing antigenic changes from previous strains plays a part in the propagation of epidemics.

1.4.2 Pandemics

For an outbreak to be classified as a pandemic, it arises in a definite geographical area and eventually spreads to new towns, cities and countries. Following this, the percentage of individuals infected increases and there is an increase in mortality rates. This can be as a result of new IAV subtypes introduced in the population prior to the outbreak (16). Pandemics affect 20–40% of the world's population. Pandemics are thought to have occurred over many centuries, although consistent records only date back to the 1918/1919 pandemic (64). See Table 1.3 for the list of IAV outbreaks.

Table 1.3: Influenza A virus outbreaks in the past 40 years (adapted from (6, 65-67)).

Influenza A virus	Year	Outbreak location	Number of human cases
H5N6	2014	China	9
H10N8	2013	China	2
H6N1	2013	Taiwan	No reported cases
H7N9	2013	China	314
H1N2	2012	United States	No reported cases
H1N1	2011	United States	No reported cases
H3N2	2011	United States	1
H10N7	2010	Australia	No reported cases
H1N1 09 (Pandemic)	2009	Mexico, Canada, and the United States	Estimated >24% population in 19 countries
H7N3	2004	Canada	19

H7N2	2003	United States	16
H1N2	2000	Singapore	No global estimates
H7N7	1979	United States	94
H9N2	1999	Hong Kong	28
H5N1	1997	Hong Kong	850
H1N2	1998	China	No case estimates
H1N1	1977	China	Estimated 3–5 million cases (severe illness) per year
H3N2 (Pandemic)	1968	Hong Kong	No global estimates
H2N2 (Pandemic)	1957	China	No global estimates
H1N1 (Pandemic)	1918	North America, Europe, and Africa	Estimated 500 million cases

1.5 Influenza virion structure, genome organisation, and proteins

1.5.1 Virion structure

Influenza viruses are single-stranded, segmented RNA viruses that are enveloped in a lipid membrane (68). These viral RNA segments form a ribonucleoprotein complex (RNP), which exist in enveloped virions. These RNPs consist of an RNA-dependent RNA polymerase complex and copies of nucleoproteins (68). The lipid membrane, that encloses virions, originates from a host cellular membrane through budding. The virions of IAV display spherical or filamentous shapes with a diameter between 80 and 120nm. IAV, which have been laboratory adapted, tend to present a spherical or elliptical shape, while IAV, from clinical isolates, mostly present a filamentous shape. The process of adaptation of IAV in eggs, leads to the loss of their filamentous shape (68-70).

The role of the filamentous shape of the virion still remains unclear but is thought to be vital. In clinical isolates, influenza viruses still form filamentous phenotypes. This could suggest the importance of the filamentous shape for its survival in nature (68). The filamentous phenotype is considered to be a genetic trait and other proteins of the influenza virus play a part in determining this shape (71). These proteins include M1 and M2 proteins as important causes of the filamentous virion shape (72-74).

i.

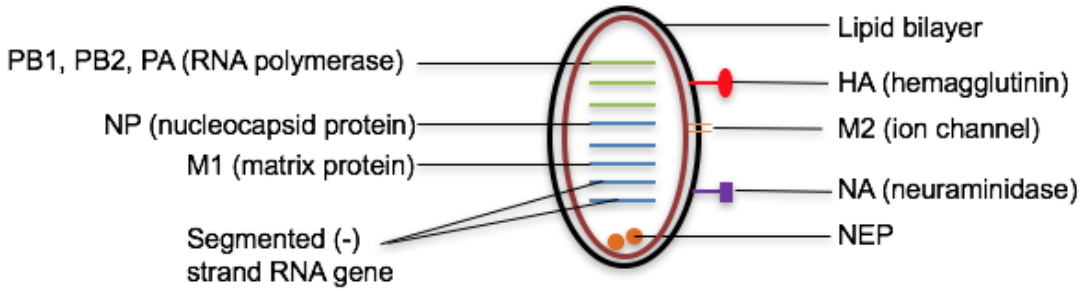

ii.

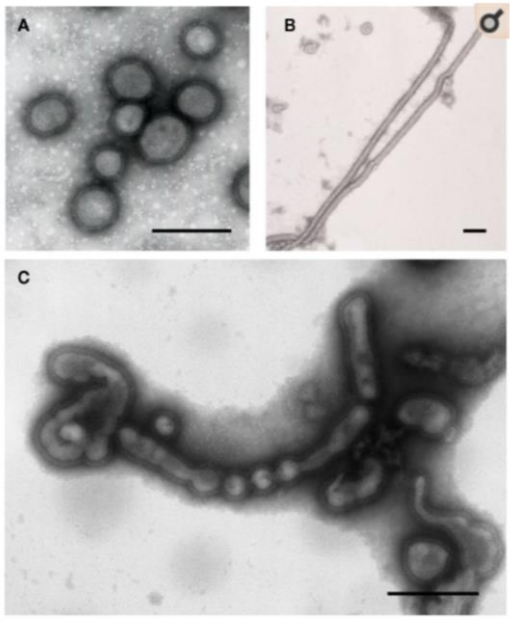

Figure 1.4: (i) Structure of the influenza virion (infectious particle). The virus is roughly spherical, enveloped with a lipid membrane on the outer layer obtained from the host cell in which the virus multiplies. The HA and NA, present on the lipid membrane, are glycoproteins, that contribute to determining the subtype of the influenza virus. The M1 protein forms a shell that strengthens and renders the lipid envelope rigid. The virions contain eight viral RNA segments for IAV that encode proteins shown in the diagram: PB1, PB2, PA, and NP (Table 1.4). (ii) Electron micrographs of influenza virions in different shapes: (A) spherical virions (A/WSN/33 [H1N1]); (B) filamentous

virions (A/Udorn/307/72 [H3N2]); and (C) irregular shaped virions (A/Puerto Rico 8/34). This image was taken from Noda et al., 2011 (68).

1.5.2 Genome structure, organisation, and viral proteins

Influenza A and B viruses differ in various ways, including their epidemiology and immunological specificity, but they also share numerous biochemical similarities (75). IAV and IBV are both negative-sense, single-stranded with eight viral RNA segments while ICV and IDV are both negative-sense, single-stranded with seven RNA segments (76). The genome of the influenza virus was initially thought to encode a single viral protein per genome segment. However, several novel IAV proteins have been identified (77). These proteins have different functions; some of these proteins play vital roles in efficient virus replication in cells and the formation of virions (68), while other proteins have unknown functions (Table 1.4). The full process of viral replication is explained in section 1.6 in the IAV replication cycle.

Table 1.4 Genomic segments and viral proteins of influenza A viruses adapted from (76, 78-80)

Segment	Encoded proteins	Segment length in nucleotides	Protein length in amino acids	Protein function	Reference
1	PB2	2341	759	Polymerase subunit; mRNA cap recognition, responsible for cap-binding, innate immunity antagonist	(81)
	PB2-S1		508	Putative interferon antagonist	(82)
2	PB1	2341	757	Polymerase subunit; RNA elongation, endonuclease activity	

	PB1-F2		87	Pro-apoptotic activity, virulence factor, and regulates apoptosis	(83)
	PB1-N40		718	Unknown function	(84)
3	PA	2233	716	Polymerase subunit; protease activity, endonucleolytic cap cleavage	
	PA-X		252	Endonuclease activity and regulates host immune response	(85)
	PA-N155		562	Unknown function	(77)
	PA-N128		535	Unknown function	(77)

4	HA	1778	566	Surface glycoprotein; facilitates virus receptor binding and fusion activities, virulence factor	(86)
5	NP	1565	498	RNA binding protein; nuclear import regulation, essential for transcription and replication	(87)
6	NA	1412	454	Surface glycoprotein; nuclear import regulation, cleaves sialic acid, and facilitates virus release	(88)
7	M1	1027	252	Matrix protein; vRNP interaction, RNA nuclear	(89)

				export regulation, viral budding, binds vRNP complexes, as well as HA and NA	
	M2		97	Acts as proton ion channel, acidifies the virion, facilitates vRNP release, virus uncoating, and assembly	(89)
	M3		9	Unknown function	(75)
	M4		54	Unknown function	(90)
	M42		99	Unknown function (present in Golgi compartment)	(91)

8	NS1	890	230	Interferon antagonist protein; regulation of host gene expression, inhibits polyadenylation of pre-mRNAs, binds to CPSF30 and PABPII	(87)
	NEP (often called NS2)		121	Regulates viral RNA transcription and replication, plays a crucial role in the nuclear export of vRNPs from the nucleus of the host (Figure 1.5 below)	(87, 92)
	NS3		188	Role in host adaptation	(93)
	NEG8		216	Unknown function	(94)

1.6 Influenza A virus replication cycle

IAV is an enveloped virus with its nucleic acid capsuled in a protein shell and a relatively simple structure, but the ability to obtain sophisticated mechanisms from their hosts to replicate, survive, and even thrive (95). Through each stage of the viral life cycle, it succeeds to integrate with, or disrupt, the host cell machinery for its replication (95). IAV is known to infect the epithelial cells in the upper respiratory tract, but also in alveolar macrophages and dendritic cells (96-98). In tissue culture, IAV replicates in 8–10 hours (95). After infection, several host-viral interactions occur to ensure viral pathogenesis and host an immune response (99). Figure 1.5 presents a schematic diagram of the IAV life cycle adapted from (100).

1.6.1 Virus attachment and entry to host cell surface receptors

For the virus to be present and replicate in the host cell, the life cycle starts with the virus binding to the host cell. The HA protein of the virus, as described above, plays a crucial role in ensuring the virus's attachment and entry into the host. HA proteins bind to sialic acids on glycoproteins or glycolipids present on the host's epithelial cells in the upper respiratory tract (99, 101-107). These sialic acids differ with each host. In humans, IAVs recognise sialic acid linked to galactose by an α2-6-linkage (Sia-α2,6-Gal). These are sialic acids linked from C2 of sialic acid to C6 of galactose (108-113). Contrarily, in avian species, IAV binds to Sia-α2,3-Gal. These are sialic acids linked from C2 of sialic acid to C3 of galactose. This is primarily present on epithelial cells in the duck intestine; various studies have shown that this is the site in which avian influenza replicates (110, 114-116). While humans and avian recognise only

one sialic acid linkage, swine recognise both. This has a factor to play in swine's ability to be a mixing vessel for both avian and human influenza, and produce pathogenic viral strains (117, 118).

Structurally, HA is a homotrimer that is found on the surface of the viral lipid membrane in a 'spike-like' shape. The HA precursor, HA0, contains two subunits with two distinct and essential functions that are linked by disulphide bonds: HA1 – receptor binding domain and HA2 – containing the fusion peptide (117, 119). Upon HA binding to the cell, IAV proceeds to enter the cell through receptor-mediated endocytosis. The primary, but not only, method of endocytosis is Clathrin-mediated endocytosis (120). Other mechanisms that IAV uses to enter the host cell; independent of Clathrin-mediated endocytosis to enter the cell, have been identified (121, 122), including micropinocytosis and micropinocytosis (123, 124). IAV therefore enters the cell in an endosome, which has a low pH of about five or six (117). The low pH in the endosome triggers various reactions; it causes the viral membrane to fuse with the endosomal membrane. It proceeds to induce a conformational change in the HA0 precursor, that reveals the HA2 fusion peptide. The fusion peptide closes the gap between the viral and endosomal membrane by inserting itself into the endosomal membrane (118, 119). It further causes the M2 ion to open and form a proton-selective ion channel (117, 125, 126), which then acidifies the viral core. This change in pH to an acidic setting causes the vRNP to be released from M1 into the host cell cytoplasm (117, 127). The vRNPs, by nature of the structure of IAV, contain viral proteins: NP, PA, PB1, and PB2. These proteins possess nuclear localisation signals (NLSs), that bind to

nuclear import factors: importin-α (Karyopherin-α) and importin-β (Karyopherin-β) (99, 117, 128-135). The M1 protein is transported separately into the nucleus (99, 136).

1.6.2 Replicating their genome

IAV is a negative-strand RNA that is first replicated by conversion into a positive-sense RNA, serving as a template for the production of viral RNA. The viral replication and transcription of IAV depends on the viral RNA dependent RNA polymerase (RdRp) that initiates RNA synthesis internally on viral RNA (137-140). The process of viral transcription cannot be completed solely by the virus due to its small coding capacity. As a result, the virus employs mechanisms using elements of the host cell to ensure its replication in the host (117).

Structurally, the host's mature cellular messenger RNAs (mRNA) has a 5' methylated cap and a poly(A) tail, while the vRNPs have poly(A) tails but no 5' caps (141, 142). During transcription, the virus employs a mechanism termed 'cap-snatching' which enables it to obtain the 5' cap from cellular mRNAs (143-150). The viral RdRp, which consists of three viral proteins – PB1, PB2, and PA plays a vital role in the 'cap-snatching' mechanism. It binds to the 5' methylated caps of cellular mRNAs and the protein PB2, which has endonuclease activity that cleaves the cellular mRNAs 10 to 15 nucleotides to the cap structure. This fragment is used by the viral RdRp to prime viral transcription (117, 151). Cellular transcription begins with the RNA Polymerase II (Pol II) binding to the DNA. The C-terminal repeat domain (CTD)

of the RNA Polymerase II contains a serine 5, which is phosphorylated during transcription initiation. This phosphorylation leads to the activation of the cellular cap synthesis complex. It has been demonstrated that this form of Pol II is the preferred binding site for influenza RdRp, and, therefore, is thought to be the point at which ‘cap snatching’ occurs (117, 152).

Once this is completed, the process of polyadenylation of the viral mRNA occurs through a mechanism called ‘stuttering’ (117). This process relies on the viral RdRp remaining bound to the 5’ end of the template viral RNA (153, 154). These viral segments have five to seven U residues, which are 17 nucleotides long at the 5’ end, upon which the polyadenylation signal is based. The RdRp, through the stuttering mechanism, moves back and forth over the U residues and this forms a poly(A) tail (155, 156).

1.6.3 vRNPs leaving the nucleus

Only negative sense vRNPs are exported from the nucleus (157). This process is thought to be carried out through the nuclear pores in a chromosomal maintenance 1 (CRM1), also known as Exportin 1 dependent pathway (117). CRM1 is a mammalian export protein that assists and eases the transport of molecules from the nuclear membrane to the cytoplasm. These molecules include RNA and protein (158). Other viral proteins within the virus are thought to play a role in interacting with CRM1 and enabling the vRNP export. NP interacts directly with CRM1. M1 also enables the export of the vRNPs by interacting directly with them through the C-terminal end of the protein and

binding of the N-terminal of the protein to NEP that subsequently binds to CRM1 (117, 159-161) (Figure 1.5).

1.6.4 Assembly and release

The viral particles are released from the cell's apical side (117, 162). This is the side in a polarised cell that faces the lumen. As a result, the protein segments HA, NA, and M2 are transported to this site within the cell. Through this process, M2 plays a crucial role in the viral formation and budding process (117). Upon budding, the IAV can be spherical (~ 100 nm diameter) and filamentous (~ 100 nm x 2 to 20 um) in shape (163). M2 plays a vital role in the shape of filament formation (163). These differences were observed in viruses in which the M2 tails were deleted or mutated: they formed elongated particles (117, 164). In addition to M2, M1 plays a crucial role in the process of closing and budding off the viruses from plasma membranes (117, 162, 165). Viral genomic segments are packaged into the virions in two hypothesised models: the random packaging model (117, 166, 167), in which, as the name suggests, the viral genomic segments are randomly packaged into virions, and the specific packaging model (52, 117), which is dictated by signals present in the viral segments (117). The specific packaging model is more widely adopted to be true as specific signals were identified in the 5' and 3' non-coding and coding regions of the viral segments (117, 120-123, 168). Finally, for the new viral particle to leave the plasma membrane, NA cleaves the sialic acid residue from glycoproteins and glycolipids. This is necessary for the total release of the viral particle from the plasma membrane (117, 124).

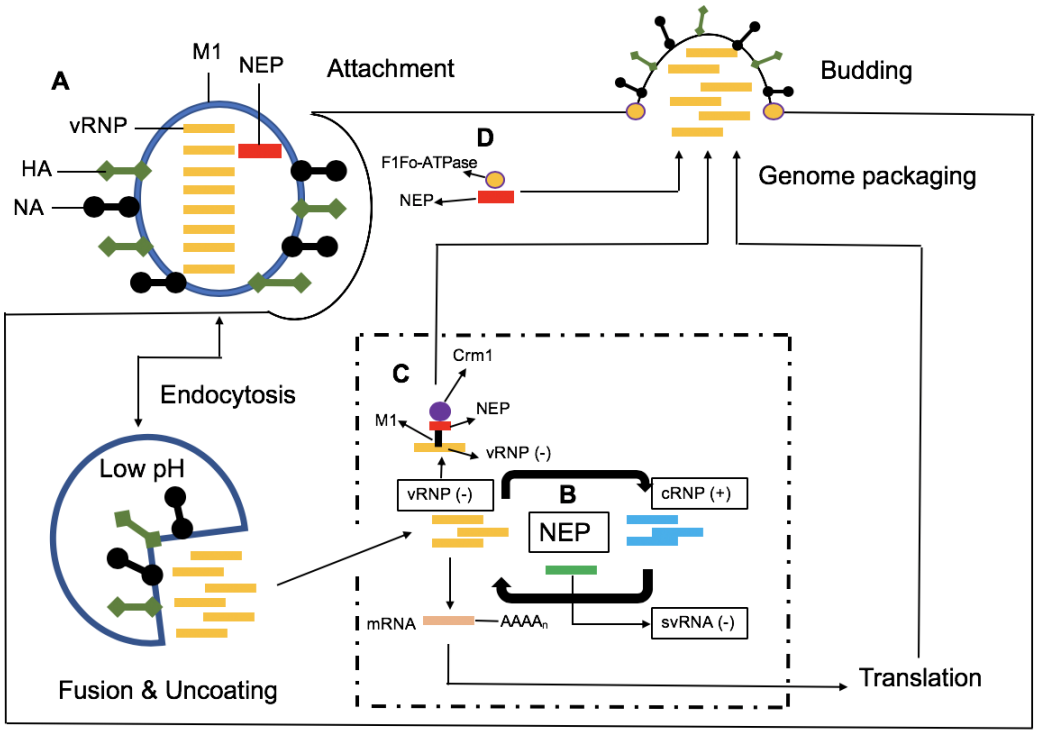

Figure 1.5: Adapted from Paterson et al., 2012 (100): A) Enveloped influenza virion containing hemagglutinin (HA), neuraminidase (NA), Matrix 1 (M1), Nuclear export protein (NEP), vRNPs, which contain PA, PB1 and PB2. B) NEP enables and triggers the synthesis of the viral cRNP. This results in increased vRNPs, which are packaged into progeny virions. NEP is thought to act with small viral RNAs (svRNAs). C) NEP acts as an adaptor protein and along with Crm1 and the viral protein M1, binds with vRNPs to export the vRNPs from the nucleus. D) NEP binds to and recruits F1Fo ATPase, which plays a part in the budding of progeny virions. E) vRNPs exported into new progeny virions.

1.7 Viral pathogenesis and host immune response

IAVs in the host are responsible for acute respiratory inflammation in humans. The symptoms observed in infected humans include a high fever, body aches, and fatigue (169). The incubation period for IAV, which is described as the time from infection to symptom onset, is between one and four days (170). Typically, the symptoms ameliorate after several days of the symptom's onset. However, this varies based on the IAV strain (169). The 2009 pandemic H1N1 influenza virus and the highly pathogenic H5N1 viruses have a higher pathogenicity than the seasonal IAV strains. The effect of their pathogenicity and virulence lead to severe pneumonia, and, as observed in the aftermath of the 1918 pandemic virus, it resulted in estimated 50 million deaths worldwide (169). The pathogenesis of the IAV is dependent both on host and viral contributions. The host's immune response and the virus's virulence factors play crucial roles in determining the pathogenicity of the IAV in the host (169, 171).

1.7.1 Host immune response

The immune system of the host protects it from infection with the IAV. IAV's entry into the host, through the respiratory epithelial cells or alveolar macrophages, is recognised by toll-like receptor (TLR) 7 and retinoic acid-inducible gene-I (RIG-I) (Figure 1.6) (172, 173). TLR7 and RIG-I induce type I interferons (IFNs) through their signalling pathways to activate antiviral host responses (174). Nonetheless, IAV has mechanisms to escape the host immune response. NS1 a viral protein enables IAV to escape this antiviral host response by interfering with the RIG-I signalling pathway. NS1 inhibits TRIM

25, which plays an essential role in the ubiquitination of RIG-I and subsequently the production of type I IFN response (169, 174). The effect of NS1 was observed in the 1918 pandemic, during which it efficiently suppressed the expression of IFN-regulated genes, controlled the antiviral innate immune response, and, thus, increased the viral pathogenesis in the host (169, 175). NS1 further binds to protein kinase R (PKR) inhibiting PKR's antiviral function (176). PKR is activated by the presence of dsRNA from viral replication or Type I IFN. PKR is ubiquitously present in the cells and is an intracellular receptor for dsRNA. PKR binds to dsRNA, which changes its conformation and is activated. Activated PKR goes on to phosphorylate the alpha-subunit of eukaryotic initiation factor 2 (eIF-2alpha). This impedes protein translation and subdues viral replication (177, 178) due to the efficiency of PKR IAV through the action of NS1-developed mechanisms to evade these anti-viral effects (169, 178). In addition to the type I IFN response, IAV upon entry into the host induces the production of numerous inflammatory cytokines and chemokines, including IL-1Beta, IL-6, IL-8, TNF alpha, CCL2, CCL3, CCL5, and CXCL10 (169, 179). Amongst these, CCL2 recruits' macrophages to the virus-infected lung. Macrophages with CCR2, a receptor of CCL2, express tumour necrosis factor-related, apoptosis-inducing ligand (TRAIL), which go on to induce apoptosis in alveolar epithelial cells. The effects of these is seen in IAV-infected hosts with CCR2 deficiency; macrophages are inhibited from migrating to the lung and thus play a crucial role in increasing pathogenesis in pulmonary inflammation (180, 181). In addition, neutrophils contribute to the pathogenesis of IAV as they are recruited to the inflamed lung of hosts infected with the 1918 virus or avian

H5N1 viruses (169, 182). In conclusion, the host's innate immune response is like a two-edged sword, playing different roles in the elucidation and pathogenesis of IAV. Contrarily, adaptive immunity is specific and efficient in eliminating virus-infected cells and enabling the host's recovery from viral infectious diseases.

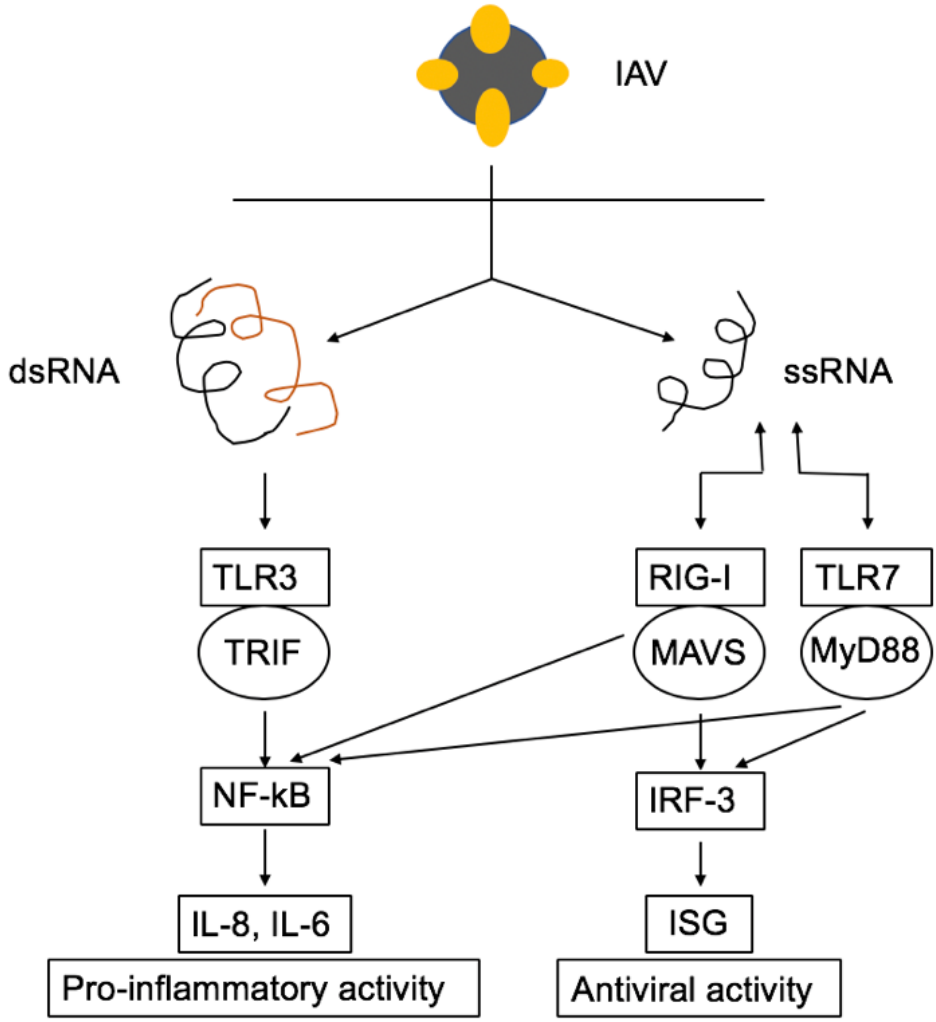

Figure 1.6: Pathways by which IAV and IAV-derived ribonucleic acids are recognised upon entry into the host. In infected hosts, sensing of IAV relies on the use of pattern-recognition receptors. These include toll-like receptor 7 (TLR7) and retinoic acid inducible gene-1 (RIG-I). Sensing IAV double stranded RNA (dsRNA) occurs through the TLR3 pathway, which subsequently activates the NFκB pathway. Single-stranded RNA (ssRNA) is

recognised through the RIG-I and TLR7. RIG-I interacts with mitochondrial antiviral-signalling (MAVS) and further activates the NFκB pathway as well as interferon regulated factor 3 (IRF3). TLR7 interacts with Myeloid differentiating factor 88 (MyD88), which is essential in signalling in the toll-like receptor pathway. TLR3 stimulates the proinflammatory response, while RIG-I and TLR7 stimulate the type 1 IFN-dependent antiviral signalling and interferon stimulated genes (ISG) (adapted from RIG-I & TLR3 from (183).

1.7.2 Virus factors that influence viral pathogenesis

Viral proteins and their functions have been described. These viral proteins have parts to play in the virulence of influenza A viral strains and thus influence its viral pathogenicity. Mutations in these viral proteins, which lead to viral pathogenicity, are elaborated in Table 1.5.

Table 1.5, from Fukuyama et al., 2011 (169), highlights mutations in viral proteins that influence viral pathogenicity

Protein	Virus	Mutation	Pathogenic effect	Reference
HA	H7N7	A143T	Increased attachment to bronchial epithelial cells and alveolar macrophages in humans	(184)
HA	1918 virus	D190E, D225G	From α2,6 to α2,3 (lost ability to transmit)	(185)
HA	Pandemic A (H1N1) 2009	D225G	From α2,6 to α2,3 infection of bronchial epithelial cells that are ciliated	(186)
NA	H3N2	R292K, E119V, N294S	Developed resistance to Oseltamivir, and, through R292K, lost ability to transmit	(187, 188)

NA	H5N1	H274Y	Developed resistance to Oseltamivir	(189)
PB1-F2	1918 virus	N66S	Delay in innate immune response	(190)
PB2	H5N1	T271A	Increased polymerase activity	(191)
PB2	H5N1, H7N7	E627K	Increased replication in respiratory tract	(192, 193)
PB2	H5N1	D701N	Increased replication in mice	(194)
PA	H5N2	T97I	Virus adapted in mice	(195)
NS1	H5N1	P42S	Increase in interferon antagonism	(196)
NS1	H5N1	Deletion from 85–94	Weakened inhibition of interferon production	(197)
NS1	H3N8 (duck), WSN	R127K, V205I, N209D	Increased replication and lethality in mice (R127K, loss of PKR binding)	(198, 199)

NS1	H5N1	D92E	Decrease in sensitivity to interferon and TNFα	(200)

1.8 Treatment and vaccines

The effects of an IAV infection on a population is continually felt through seasonal epidemics and pandemics. During these outbreaks, hospital admissions for respiratory diseases increase along with mortality from various causes (201, 202). Vaccinations and antivirals are two methods of preventing or treating IAV infections.

Vaccination is the foundation for influenza prevention (202). Influenza vaccines are traditionally trivalent (covering influenza A H3N2, H1N1, and the influenza B strain) or quadrivalent (to cover influenza A H3N2, H1N1, and two influenza B strains) (203). Due to the circulation of constantly changing strains of influenza, in February of each year, an expert panel, including the World Health Organisation (WHO) reviews data from the Northern and Southern hemisphere and decides which circulating strains should be included in the vaccines for the influenza season (203). This production begins in March in the hope that no antigenic changes occur – this is a limitation of this approach. The two main types of vaccines are 'parenteral inactivated vaccine' (the virus is killed) or 'intranasal live-attenuated' (the virus is weakened) (203). The inactivated vaccines contain virus antigens, specifically the surface glycoprotein; hemagglutinin, thus, stimulates the body to create antibodies against these specific strains. Antibodies to hemagglutinin and neuraminidase glycoproteins are known to protect against infection and enable quick recovery from infection (202). Live-attenuated vaccines (LAIV) produce a more complex, multifaceted, and broad immune response, which leads to longer periods of protection. Inactivated influenza vaccines are safe and effective and

are widely recommended for children from six months old, while live attenuated vaccines are recommended for children above the age of two years (203).

The use of anti-virals to combat IAV infections is dependent on two types of compounds: amantadine and rimantadine that are both M2 ion channel inhibitors and Zanamivir and Peramivir that are NA inhibitors (99). As the name suggests, M2 ion channel inhibitors inhibit the ion channel in the viral envelope formed by the M2 protein. These inhibitors block the process of pH changing in the endosome. This process is crucial for the release of vRNPs into the cytoplasm after IAV enters into the cell. These inhibitors stop the flow of hydrogen ions from the acidic late endosome to the interior of the virion (99). However, these compounds are no longer the preferred recommendation for human use as the IAV has gained resistance to the compounds (204). The NA inhibitors, again, as the name suggests, inhibit the enzymatic activity of the NA. This is essential in the release of the virus following viral replication (205-208). These compounds are the only antivirals to IAV currently recommended for human use worldwide. While resistance has been described to NA inhibitors, it is not common amongst IAV strains that are currently circulating (99, 209).

1.9 Quantitative proteomic techniques used to characterise viral-host interactions

The integration of virology and proteomics has led to a significant increase and contribution in understanding virology. Understanding viral evolution and

simultaneously understanding how the host responds to these changes has provided a platform to understand viral-host interaction. This is a crucial step in the search for novel biomarkers for the detection of the severity of disease and finding novel mechanisms of the host response to a viral infection.

1.9.1 Quantitative proteomics using two-dimensional gel electrophoresis (2D-DIGE)

The development of quantitative proteomics has provided global cellular proteome comparable studies (210). Quantitative proteomic analysis has seen evolution over the past decade with a multitude of strategies employed, originating with two-dimensional gel electrophoresis (2D-DIGE) and progressing to label-based strategies, including stable isotope labelling by amino acids in cell culture (SILAC) and label-free strategies coupled with mass spectrometry. Mass-spectrometry-based techniques have been employed for high-throughput, bio-analytical methods to understand cellular proteomes and interactions with various respiratory viruses and diseases (211-214). These have been used previously to characterise IAV infection *in vitro*. Quantitative mass spectrometry was introduced by 2D-DIGE in the mid-1970s. This was the first combination of two methods for separating proteins: isoelectric points and separation according to polypeptide sizes (215). While this was novel, the number of separated proteins remained low (in the lower hundreds) (216).

2D-DIGE coupled with mass spectrometry has been instrumental in detecting the mechanisms underlying the Hepatitis B-Virus (HBV) infection in a host cell and has demonstrated that proteomics could be used to map virus-host interactions. This gave rise to the creation of a hypothetical model containing

three major groups of the most varied proteins involved in retinol metabolism, calcium ion-binding, and protein-degradation pathways (217). Quantitative proteomics also played a vital role in obtaining host profile responses to the rabies virus (RBV). RBV affects the expression of proteins involved in ion homeostasis and also affects the movement of synaptic vesicles to merge with presynaptic membrane that leads to neuronal dysfunction (218).

While 2D-DIGE provided a global insight of cellular changes in response to viral infection, there were limitations. These included the identification of highly abundant proteins and the selection of proteins that could be resolved/separated by 2D-DIGE. IAV causes whole system changes, including low-abundance proteins. Therefore, this technique is not sensitive enough to highlight these changes. For example, changes in the cellular proteome of IAV-infected A549 and MDCK cell lines were observed using 2D-DIGE coupled with mass spectrometry. This revealed a total of 16 differentially abundant proteins (219). The use of subcellular fractionation as an enrichment method of A549 cells infected with H3N2 swine influenza virus, followed by 2D-DIGE and mass spectrometry, improved the number of proteins detected (220). Nuclear and cytoplasmic proteomic fractions were prepared and revealed a total of 47 differentially expressed proteins following IAV infection. Proteins involved in apoptosis, cell death, and the induction of the IFN pathway were differentially abundant. More proteins were recorded as differentially abundant when subcellular enrichment methods were used, thus improving the understanding of the cellular interactome. While it highlighted certain proteins, the limitations of the 2D-DIGE techniques can be observed, as only

proteins that registered a change in high abundance were identified (219). Subcellular fractionation, used to enhance 2D-DIGE, is time-consuming and can lead to the loss of proteins.

1.9.2 Quantitative proteomics using label-based techniques – SILAC and label-free techniques

Label-based techniques, including stable isotope labelling by amino acids in cell culture (SILAC) and label-free strategies coupled with mass spectrometry, also gained popularity in quantitative proteomics. Label-based methods entail metabolic, enzymatic, or chemical labelling, while label-free methods utilise spectral counting and ion intensity-based quantification (221). Despite having respective disadvantages, both methods are powerful tools to identify changes in the abundance of proteins (Table 1.6). Other limitations of label-based strategies include additional sample-processing steps, high cost of labelling reagents and human error, and variability in effective labelling (222).

Label-free liquid chromatography Mass Spectrometry (LC-MS) is a novel approach used to identify qualitative and quantitative information for the characterisation of components in a protein mixture (223). Label-free approaches have gained popularity due to the decrease in the number of chemistries required for a run as well as a wider range of application (224). This approach was used to compare the proteome of Hep 2 cells infected and uninfected with the respiratory syncytial virus (RSV). The cells were lysed, separated, and prepared using off-gel fractionation. The LC-MS run following tryptic digestion revealed a total of 1,352 cellular and seven viral differentially

abundant proteins. Proteins involved in the synthesis of interferon-induced proteins with tetratricopeptide repeats 3 (IFIT3) and 5'-3'-exoribonuclease 2 (XRN2) (225) were highlighted. Different proteomics methods were developed and used over the years. LC-MS has gained more popularity for high-throughput quantitative proteomics due to its simple and straightforward processing steps and can be used for a large sample size. These are particularly useful for biomarker discovery in clinical samples.

Table 1.6: Advantages and disadvantages of label-free LC MS/MS to identify novel biomarkers

	Advantages	Disadvantages
Label free LC-MS/MS	Highly reproducible and stable analysis workflow	Insufficient resolving power of previous generations of spectrometers
	Flexible technique	Uses two different quantification strategies – precursor-based and spectral counting. Spectral counting cannot resolve small abundance differences.
	Deep coverage of investigated proteome	Limited to samples undergoing active protein synthesis
	Quantification strategies; does not impose requirements about reference sample	
	Outperform SILAC in terms of both proteome coverage and dynamic range	
	Scalable to number of samples	

Reproducible samples and data are key elements to any successful biomarker study. Label-free approaches offer little or no technical variation, but may not automatically reduce systematic differences, such as bias.

A label-free LC-MS platform was used throughout this thesis to analyse the IAV-host interaction *in vitro* and *in vivo.* This maintained consistency in the data analysis and allowed the results obtained in each chapter to be compared to one another. Chapter 3 focused on the use of label-free LC-MS to understand the IAV-host interaction *in vitro* (A549 cells), Chapter 4 focused on the use of label-free LC-MS to understand the IAV-host interaction *in vivo* (samples from macaques), and Chapter 5 focused on the use of label free LC-MS to understand the IAV-host interaction in NAs from paediatric patients. This set the tone to evaluate IAV in different models and compare the data to that observed in human NAs.

1.10 Interferon-Induced proteins

The results detailed in this thesis from chapter 3 (*in vitro*), chapter 4 (*in vivo*) and chapter 5 in NAs from paediatric patients consistently highlighted proteins that form a major component of the antiviral host defense system; these are interferon induced proteins. The interferon-induced antiviral state is a powerful host's response to viral infection to limit the replication and spread of the virus (226) (227). Amongst these proteins are Interferon Induced Proteins with Tetratricopeptide repeats (IFITs) consisting of four members in humans and three in mice (227), Interferon-induced transmembrane proteins (IFITMs) consisting of five members in humans (228), interferon-induced murine *Mx1* (229) and interferon-induced human MxA (226).

1.10.1 Interferon Induced Proteins with Tetratricopeptide repeats (IFITs)

The human IFIT family comprises of IFIT1, IFIT2, IFIT3 and IFIT5. Upon bacterial and viral infection, IFITs are induced through type I IFNs (IFN-α/β). IFIT1s have the ability to bind to 5'-ppp-RNA whilst IFIT2 and IFIT3 enhance this biniding activity (227). Cells infected with IAV, showed restored replication with when IFIT1 was deficient. IFIT1 similarly to RIG-I and MDA5 recognise specific viral molecular patterns. IFIT1 specifically recognises and binds to viral mRNAs whose caps are deficient in 2'-O-methylation and subsequently blocks their translation (227). This goes on to inhibit the viral replication.

1.10.2 Interferon-induced transmembrane proteins (IFITMs)

IFITMs are small proteins located in plasma and endolysosomal membranes. IFITMs are part of the anti-viral innate response and prevent viral entry by halting the viral envelope and cellular membrane envelope fusion. In addition, they also reduce the number of infectious virions produced (228). A study in mice using a knockout model showed that IFITM3 was essential when defending the host against IAV. Mice that lack IFITM3 showed an explosive viral pneumonia and lung damage following IAV infection (230). Several studies that have examined patients with seasonal and pandemic H1N1 and H7N9 have reported an IFITM3 SNP of rs 12252 is associated with susceptibility and severity to these viral infections(228). This is the most studied SNP associated with altering IAV infection outcomes. IFITM3 SNP of rs 12252 is a nonsynonymous variation occurring in the first exon of IFITM3

(230). The major T allele is subsequently substituted with a C allele giving a CC allele and altering the IFITM3 mRNA spicing. The product of this is an N-terminally truncated variant of IFITM3 (21 amino acid residues deleted) (228). This has been a major difference between Europeans and East Asians. A study *in vitro* set out to explore the effect of the CC allele and found that these variants were more susceptible to infection and had lower levels of IFITM3 protein expression. This study also found that the truncated N terminal (21 amino acid residues deleted) were unable to restrict viral replication compared to wid type IFITM3 (230). This shows the importance of IFITM3 when restricting IAV infection.

1.10.3 Interferon-Induced Human MXA

The protein MxA is an Interferon Induced protein regulated by type I and type III interferon and frequently used as a biomarker for an Interferon Induced antiviral state in a host (226). In IAV infection, MxA specifically targets the nucleoprotein (NP) and is thought to be required to prevent the export of vRNP to the nucleus. Nonetheless, the exact mechanism of action has not been clearly defined (226). A similar effect was seen in mice cell line where human MxA was monitored and it blocked IAV replication after primary transcription (231).

1.10.4 Interferon-Induced Murine MX1

The Mx1 gene was discovered in the mouse over 50 years ago. It was thought to potently restrict IAV. Some studies in mice showed mice carrying functional Mx1 locus were resistant to IAV whilst mice that had a deletion of

Mx1 locus were susceptible to the virus (229). A study in mice showed that Mx1 inhibited the PB2-NP interaction and this correlated with a decrease in the virus' polymerase activity. A direct interaction was observed between Mx1, PB2 and NP. Active Mx1 was required for the inhibition process of NP-PB2. This therefore showed the role Mx1 played when interacting with the IAV ribonucleoprotein complex and subsequently interferes with its assembly by inhibiting the NP-PB2 interaction (229). These Interferon Induced proteins have significant functional roles in response to IAV infection *in vitro* and *in vivo* in mice in the literature. These proteins have also been identified in all the results chapters of this thesis therefore giving confidence to the methodology, data analysis and the results.

1.11 Thesis aims, objectives, and findings

My PhD aims were to investigate the interaction of IAV in hosts *in vitro* and *in vivo* as follows:

1- Establishing IAV infection *in vitro* over a time frame;
2- Establishing the potential of high-throughput techniques – label-free Mass Spectrometry and MinION sequencing to characterise IAV infection *in vitro* and *in vivo* and highlight potential biomarkers;
3- Find out if the dataset obtained from *in vitro* host-viral interactions are comparable to dataset from *in vivo* host-viral interactions;
4- Highlight the proteins connecting both *in vitro* and *in vivo* studies, ensuring proteins highlighted *in vitro* are of relevance and importance *in vivo*; and
5- Use bioinformatics tools (IPA) to further understand the data and highlight potential host biomarkers for diagnosis or therapeutics.

Chapter 3 formed the basis for IAV infection *in vitro*. It established IAV infection in A549 cells, quantified it using Avicel plaque assay, and validated by SDS-PAGE and immunofluorescence microscopy. It established the use of mass spectrometry for global proteome discovery and the use of MinION sequencing to obtain high-throughput data transcriptome, which validated the mass spectrometry data. The results from this chapter highlighted the importance of *in vitro* models to understand the cellular response to IAV infection and to highlight the proteins that contribute to the replication of the virus, its survival, and, therefore, its continuous pathogenesis within the host.

Chapter 4 focused on the use of Mass Spectrometry to explore an *in vivo* model, a non-human primate (NHP) macaque. NHP macaque is a commonly

used animal model for the study of human-infecting pathogens, due to their genetic closeness and immune response to humans. The results from this chapter highlight the importance of *in vivo* models, especially to understand respiratory infections such as IAV, which cause an exacerbated immune response.

Chapter 5 focused on the use of Mass Spectrometry to explore the global proteome of NA from IAV-infected paediatric patients, compared to IAV-negative patients. This chapter provided a global overview of the host's reaction to IAV: a combination of both cellular and immunological response. This chapter first validated the techniques used. Next, it highlighted the need for both *in vivo* and *in vitro* models, especially for the study of different aspects of the IAV pathogenesis. Finally, it highlighted potential protein biomarkers for the diagnosis of IAV in humans. The data in this chapter validated the data from chapter 3 – *in vitro* and that from Chapter 4 – *in vivo*.

This thesis set out to understand IAV pathogenesis and subsequently find a biomarker that could be used, clinically, in humans. Following this, the premise is that *in vitro* and *in vivo* studies are only essential and relevant if the results obtained can be reflected back to humans for this purpose. This was certainly the case in this PhD thesis.

PhD thesis contribution:

1- Several proteins were highlighted and associated with IAV infection, which have been published in the literature-confirming data;
2- New proteins were highlighted as potential biomarkers for diagnosis;
3- Different stages of IAV infection were observed and proteins that could be targets for different stages of infection were highlighted;
4- Proteins were identified that are drug targets currently used for other diseases. These drugs could be repurposed and potentially developed for therapeutic use against IAV infection; and
5- Use of new techniques – Mass spectrometry and MinION sequencing to identify these proteins and subsequent validation of the results *in vitro* and *in vivo*.

CHAPTER 2:
MATERIALS AND METHODS

2.1 Preparation of IAV strain

The IAV strain used in this study was kindly provided by Professor Paul Digard, from the Roslin Institute, at the University of Edinburgh. IAV X-31 is a mouse-adapted IAV H3N2. The X-31 strain undergoes productive infection in A549 and MDCK cells. The virus was grown in eggs and MDCK cells.

2.1.1 Growing IAV in MDCK cells and eggs

IAV can be grown in tissue culture in cells that are permissive to the virus (232) or in nine to 11-day-old embryonated chicken eggs (233). Chicken eggs usually produce high virus titres over a shorter time frame. This gives them the advantage over tissue culture. Furthermore, virus stocks from chicken eggs are free of mammalian pathogens (234). However, growing the influenza virus in chicken eggs for other purposes, such as vaccine production, has its limitations. The production is unable to meet the volume of required doses in scenarios of widespread epidemics and pandemics (235). To circumvent this limitation, a cell culture has been developed for the production of a seasonal vaccine and any shortages that may occur in pandemic situations (235). MDCK cell line is the preferred cell line for influenza virus propagation for vaccine production. This is because MDCK cells have the most suitable surface for primary isolates of influenza viruses to latch onto (236-241). This could be because the interferon (IFN)-induced myxovirus resistance protein 1 (MX1), produced by canine cells, cannot inhibit the IAV replication. In addition, trypsin is added to aid in virus entry during infection. This trypsin has an adverse effect on IFN-induced antiviral proteins (242-244). Therefore, the limited ability of the IFN system in the host allows viral replication and high

titres to be obtained (235). MDCK cells are, therefore, frequently used to grow IAV stocks *in vitro*.

2.1.2 Growing IAV in MDCK cells

MDCK cells were obtained from the Health Protection Agency Culture Collections (HPACC, UK) (232, 245). The cells were maintained according to the manufacturer's instructions. All cells were seeded at a density of $1x10^6$ cells/flask in two $25cm^2$ flasks, 48h prior to infection following the World Health Organisation (WHO) protocol and maintained at 37°C with 5% CO_2 (246). The Dulbecco's Modified Eagle Medium (DMEM) (Sigma [D6429]) supplemented with 10% (v/v) foetal bovine serum (FBS) (Invitrogen [10270]) and 1% (v/v) penicillin-streptomycin to 80–100% confluency.

For viral growth, DMEM was discarded from the flasks and cells were washed three times with Phosphate Buffered Saline (PBS). The X-31 strain (MOI 0.1) was diluted in 10ml serum-free DMEM media and TPCK trypsin in a 1/1000 dilution of 1mg/ml stock (245); 400µl was applied per flask and incubated for 1 hour at 37°C. The inoculum was then removed, and the cells were washed with PBS. DMEM media (supplemented with 0.14% BSA fraction V and TPCK Trypsin) was added to each flask (6 ml). Flasks were further incubated at 37°C. 3 days post infection (p.i.) the supernatant was collected and aliquoted into 1ml cryovials at 500µl/cryovial and stored at -80°C (246, 247). A hemagglutination test (described in section 2.2) was performed on the supernatant to test for the presence of the virus (248, 249). Following this, an avicel plaque assay was performed to quantify the virus and obtain a viral titre.

2.1.3 Growing IAV in eggs

As mentioned above, the influenza virus can be propagated in cell culture as well as in embryonated chicken eggs. To continuously study influenza *in vitro*, reliable and cost-effective methods, which produce high viral titres, are necessary (250). To achieve this, fertilised chicken eggs are incubated for 10–11 days at 37°C, 55–50% humidity. During this period, the embryo development is monitored using an egg candler. A needle is used to inject virus stock into the egg's allantoic fluid cavity. After this time, the eggshell is removed and the membrane containing the allantoic fluid opens. The allantoic fluid, which contains the virus, is harvested carefully using a syringe. This fluid is centrifuged to clear any debris and subsequently aliquoted. A total of 5–10 ml of allantoic is collected per egg (250). The eggs were infected following the WHO protocol (251) that has been widely used in the literature (250).

i) Candling of eggs

Fertile eggs at 9–10 days old were kindly provided by colleagues based in the School of Veterinary Science, at the University of Liverpool. The eggs were set in egg incubators at 37ºC, with a humidity of 61 and 0% CO_2. The eggs were incubated for nine days. On the ninth day, the eggs and the candler were wiped with 70% ethanol. They were candled one at a time in a dark room to ensure viability (250). The margin of air space and embryo location was marked using a pencil. Eggs lacking blood vessels were classed as non-viable while eggs with mobile embryos and blood vessels were viable and kept for infection (250-252).

ii) Preparation of virus inoculum and inoculation of eggs

The eggs were placed into egg trays with blunt end up, specifically labelled, and moved into a fume hood. The blunt end of each egg was wiped with 70% alcohol prior to injecting. Using an egg hole punch, a hole was drilled slightly above the airspace (following the pencil markings) slightly to the right or left of the embryo's location. The virus was diluted in a 1/1000 dilution with PBS. A needle was inserted into the hole in the shell at a 45° angle using a short stabbing motion. The chloroallantoic membrane was pierced and inoculated with 200 μl of the specimen. The hole was sealed using nail polish. The eggs were placed in an incubator at 35°C for 48 hours. At 48 hours post infection, the eggs were candled to ensure viability; 4 eggs were classed as non-viable and were discarded. The viable eggs were transferred to 4°C overnight (250-252).

iii) Harvesting virus from inoculated chicken eggs

After 48 hours, the eggs were inspected and taken out to harvest the allantoic fluid containing the IAV. The infected blunt end of each egg was cleaned with 70% ethanol and 15ml centrifuge tubes were labelled for each egg. Starting with the controls, the egg shells were broken over the air sac and the allantoic membrane was pushed to the side using sterile forceps. Using a 1ml pipette, the allantoic fluid was aspirated and placed in the corresponding 15ml centrifuge tubes. The tubes were centrifuged at 2000 rpm for 10 minutes to remove excess blood, tissue, and debris (Figure 2.1). A hemagglutination test was performed on the collected allantoic fluid (Figure 2.2) (249, 252).

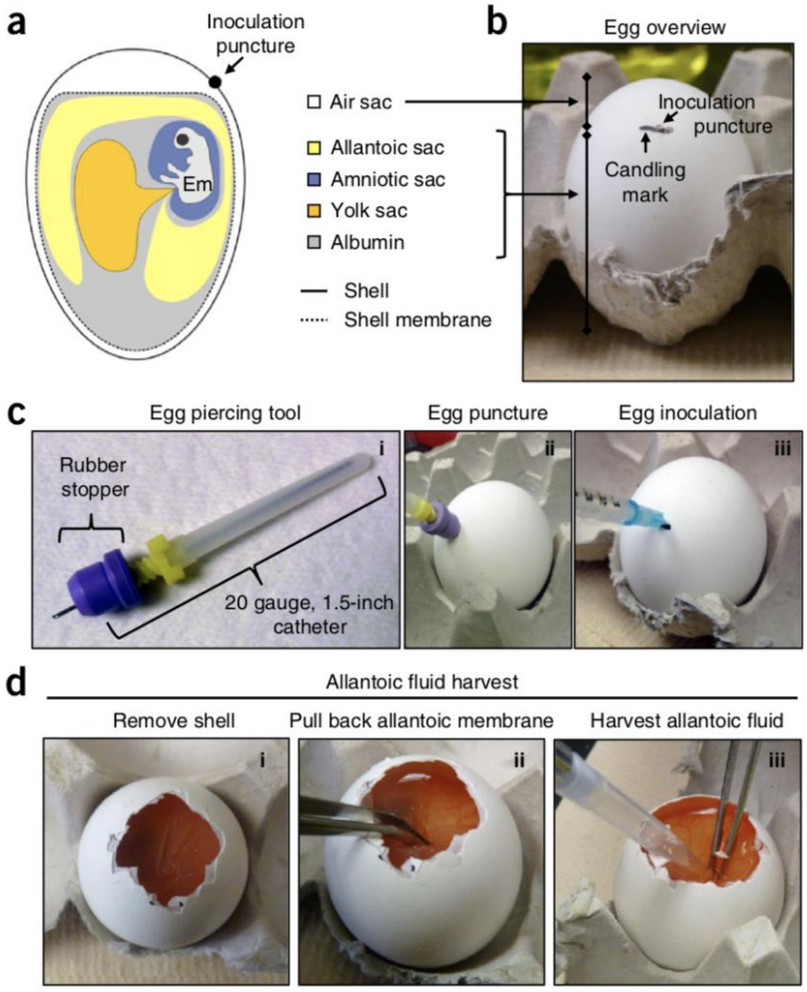

Figure 2.1: Taken from Eisfield et al., 2014 (252) – The process of IAV inoculation in eggs and harvesting allantoic fluid. A) Representation of a fertilized egg's interior B) an overview of the egg with the markings for candling and inoculation puncture hole. C) The egg piercing tool, puncturing the egg, and subsequent inoculation with IAV. D) 48 hours following inoculation, the eggs were removed to harvest the allantoic fluid containing the virus.

2.2 Identification of influenza isolates using hemagglutination inhibition (HAI) test

The hemagglutination assay is an economical and rapid assay used to detect the presence of the virus. The assay is based on the virus's ability to agglutinate and bind to red blood cells (RBCs). This occurs through the α2,3-linked and α2,6- linked sialic acid component present on the RBC surface. RBCs are mixed with virus-containing samples and the agglutination pattern is observed. The presence of the virus causes the RBCs to agglutinate and form a sheet, giving a cloudy appearance. Contrarily, the absence of the virus causes the RBCs to settle at the bottom of the well (252).

Using a multichannel pipette, 50µl of PBS was aliquoted into eight rows (a row/egg) of a 96-well round-bottom tissue culture plate. Exactly 50 µl of the virus and 50µl chicken adult red blood cells in Alsever's was added into the first column of each row. Using a multichannel pipette, the solution was mixed, and a serial dilution carried out by taking up 50µl, mixing three to five times and transferring it to the next well (A1 to A2; then A2 to A3; and continuously in the same order). The final 50µl after column 11 was discarded; column 12 was maintained as the negative control. The assay was incubated at room temperature for 45 minutes. The results were recorded and interpreted. The absence of hemagglutination represents the inability to recover virus from the specimen (253).

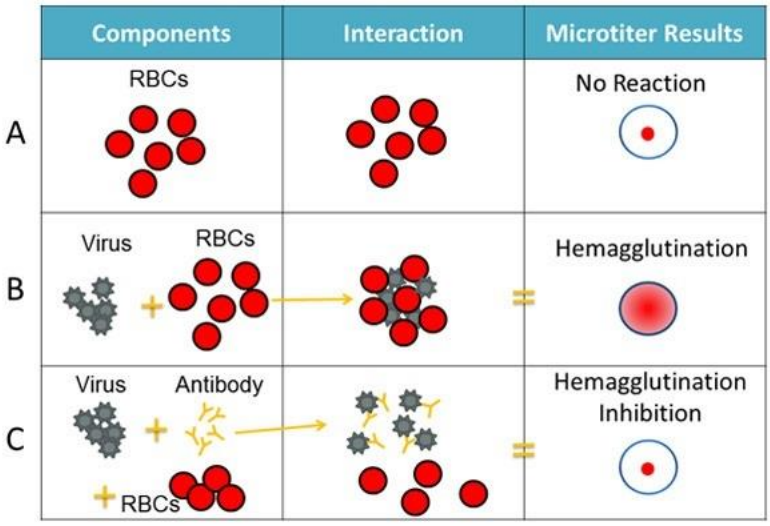

Figure 2.2: Taken from www.microbeonline.com showing the interpretation of the hemagglutination assay. A) The presence of just RBCs and no virus leads to no interaction and therefore no reaction. This give a clear appearance with cells settled at the bottom of the plate. B) In the presence of the virus and RBCs, an interaction occurs and leads to a hemagglutination reaction. This gives a cloudy appearance. C) The presence of the virus, antibody, and RBCs lead to interaction between the antibody and the virus. This gives a similar appearance as in A, where the RBCs settle at the bottom of the plate.

2.3 *In vitro* studies – maintaining continuous cell culture and preparing cells for different techniques

2.3.1 Maintaining continuous cell culture

Adenocarcinoma human alveolar basal epithelial cells (A549) and madin-darby canine kidney cells (MDCK) were obtained from the Health Protection Agency Culture Collections (HPACC, UK). All cells were maintained according to the manufacturer's recommendations.

i) Cell culture (MDCK cells) and plating for avicel plaque assay

The X-31 Strain titre was calculated using an avicel based plaque assay (254, 255). MDCK cells were found to be more suitable for plaque assay purposes. MDCK Cells were grown in a T75 flask in Dulbecco's modified Eagle's medium (DMEM) (Sigma [D6429]) supplemented with 10% (v/v) foetal bovine serum (FBS) (Invitrogen [10270]) and 1% (v/v) penicillin-streptomycin to 80–100% confluency. Twenty-four hours prior to infection for the plaque assay, the cells were obtained and seeded at $5x10^5$/mL suspension and 2mL added to each well of a six-well tissue culture plate (Table 3.1). This was to obtain 90–100% confluency when infecting cells.

Table 2.0: Plaque assay cell types and conditions

Viral strain	Influenza A
Cell type	MDCK
Infection period	1 hour
Incubation time	3 days
Plaque overlay	Avicel

ii) Cell culture (A549 cells) for immunofluorescence (IF)

For immunofluorescence experiments, 19 mm glass coverslips were dipped in 100% methanol, left to dry, and then washed in sterile PBS. These coverslips were transferred to six-well dishes, prior to seeding, using methanol sterilised forceps. Cells were grown in a six-well dish (1 x10^6/well). Cells were infected 24 hours after seeding. IF was performed after the infection time point had elapsed.

iii) Cell culture (A549 cells), plating for infection and preparation for SDS-PAGE

For infection, cells were seeded in a six-well dish (1x10^6/ well), 24h prior to infection, to achieve 70–80% confluency. For infection experiments, using the H3N2 lab-adapted X-31strain, cell lines were grown in Dulbecco's modified Eagle's medium (DMEM) (Sigma [D6429]) supplemented with 10% (v/v) foetal bovine serum (FBS) (Invitrogen [10270]), 1% (v/v) penicillin-streptomycin, and Glutamax. The cells were scraped using cell scrapers, resuspended in PBS, and transferred in Eppendorfs.

iv) Cell culture (A549 cells) plating for infection and preparation for RNA extraction and subsequent MinION sequencing

For infection and RNA extraction, cells were seeded in a six-well dish ($1x10^6$/ well) 24h prior to infection to achieve 70–80% confluency. For infection experiments using the H3N2 lab-adapted X-31strain, cell lines were grown in Dulbecco's modified Eagle's medium (DMEM) (Sigma [D6429]) supplemented with 10% (v/v) foetal bovine serum (FBS) (Invitrogen [10270]), 1% (v/v) penicillin-streptomycin, and Glutamax. RNA from the samples were extracted after the infection timepoint had elapsed. Total RNA was extracted from whole cell lysates using an RNeasy Mini Kit (Qiagen, Manchester, UK) following the manufacturer's instructions (Cell pellets [$5x10^5$ -10^6 cells]). RNA samples were subjected to MinION sequencing.

v) Cell culture and preparation of A549 samples for LC-MS/MS analysis

T75 flasks were seeded with $2x10^6$/ml A549 cells in 10ml of Dulbecco's Modified Eagles Medium/High Glucose (DMEM). Twenty-four hours later, the cells were infected with IAV at MOI 1. The virus was diluted in 5ml of serum-free media (SFM), 1% TPCK trypsin (1/1000 dilution of 1mg/ml stock), and 10% (v/v) penicillin-streptomycin. At the point of infection, the media was taken up and 3ml of virus stock was used to inoculate infected cells. Mock-treated cells were inoculated with a similar stock, without the virus. The inoculum was left to adsorb for one hour, after which the viral inoculum was aspirated from the wells and the wells washed with PBS. A post-inoculum solution was made; SFM, 1% TPCK trypsin (1/1000 dilution of 1mg/ml stock), 10% (v/v) penicillin-

streptomycin, and 0.14% BSA fraction V; 7ml of this solution was aliquoted into each flask and the flasks incubated at 37^{o}C with 5% CO_2 for 18 hours. After the incubation time had elapsed, the post-inoculum was aspirated, the cells were washed with PBS, and 2ml of PBS was aliquoted into both flasks. The cells were scraped using a cell scraper and transferred to an Eppendorf. The pellet samples were given to our colleagues for mass spectrometry analysis on the Q-Exactive.

2.4 Determining IAV X31 strain titre using avicel plaque assay

To determine the infectious virus titres, six-well tissue culture plates were seeded with 2x10^{6}/ml Madin-Darby Canine Kidney cells (MDCK) in 2ml Dulbecco's Modified Eagles Medium/High Glucose (DMEM). DMEM was supplemented with 10% foetal bovine serum, 1% L-glutamine, and 1% penicillin-streptomycin. Plates were incubated at 37^{o}C, 5% CO_2 overnight using the CO_2 incubator (SANYO, MCO175) to achieve 95–100% confluency. The next day, a 10-fold serial dilution of virus stock in ice-cold Dulbecco's Modified Eagles Medium/High Glucose (DMEM) only supplemented with 1µg/ml Tosylamido-Phenylethyl-Chloromethyl Ketone (TPCK)-trypsin (Worthington Biochemical Corporation, #3740) was carried out. A concentration of 1:1000 dilution of 1mg/ml stock was prepared in 7ml polystyrene Bijou containers. The dilutions 10^{-1} to 10^{-5} were used, and 1ml virus dilution from each dilution was used in duplicate (see Table 3.2).

Table 2.1: Viral dilutions for plaque assay (IAV)

10^{-1}	10 μl virus + 90 μl media (1:10)
10^{-2}	100 μl virus + 900 μl media (1:10)
10^{-3}	300 μl +2700 μl media
10^{-4}	300 μl +2700 μl media
10^{-5}	300 μl +2700 μl media
10^{-6}	300 μl +2700 μl media
10^{-7}	300 μl +2700 μl media

Discard 300 μl from last dilution. Add 1ml from each dilution to each well in duplicate. Plates were incubated for one hour at 37°C, 5% CO_2 using virus CO_2 incubator (SANYO, MCO-17AIC) and agitated every 10–15 minutes to ensure coverage. After one hour, the viral inoculums were removed and 2ml of overlay medium were added per well. The overlay medium was made up and contained immediately prior to overlaying cells (Table 3.3).

Table 2.2: Avicel overlay medium

Component
2.4% Avicel (FMC BioPolymer, RC-581)
20% of Dulbecco's Modified Eagles Medium 10% Low Glucose (Sigma D2429)
4% 1M HEPES Solution (Sigma, H0887)
2% L-glutamine
2% penicillin-streptomycin (Sigma P4333)
2% of 7.5% $NaHCO_3$ (Sigma, S5761)
70% of double-processed tissue culture water (Sigma, W3500)
TPCK-treated trypsin (1:1000 dilution of 1 mg/ml stock) (Worthington Biochemical Corporation, #3740)

The 2.4% Avicel and 20% of Dulbecco's Modified Eagles Medium 10% Low Glucose were added in a 1:1 ratio. Plates were incubated for three days (72 hours) and plaques were visible. The overlay was aspirated, and the wells were washed twice using PBS. Cells were fixed with ice-cold acetone: methanol (60:40) for 10 minutes at room temperature and left to completely air-dry. They were then stained with crystal violet for approximately 10 minutes. Plaques were counted macroscopically using a light microscope (MOTIC ST-30 SERIES) to determine the plaque-forming units (PFU) per sample. The PFU was the average PFU obtained in five different dilutions of

sample, each performed in duplicate. The infectious titre was the average result of two separate titrations and the titre was calculated using the formula:

$$\text{Titre (PFU/ml)} = \frac{\text{No. of plaques x dilution}}{\text{1 ml inoculum}}$$

2.5 Sodium-Dodecyl sulphate polyacrylamide gel electrophoresis (SDS-PAGE)

2.5.1 Preparation of whole cell lysate for SDS-PAGE

Cell pellets were re-suspended in radioimmunoprecipitation assay (RIPA) buffer (50 mM Tris, [pH 7.5], 150 mM NaCl, 1% (v/v) NP40 alternative, 0.5% (w/v) sodium deoxycholate, 0.1% sodium dodecyl-sulphate [SDS], supplemented with one EDTA free complete protease inhibitor mixture [Roche Applied Science] per 50 ml buffer) and incubated for 30 minutes at 4°C. Alternatively, the RIPA buffer was applied directly to the washed cell monolayer and incubated for 20 minutes before cell scraping. Both methods of lysis were followed by three minutes of incubation in a sonicating water bath at 4°C to ensure complete lysis. The supernatant that contained total protein was collected after centrifugation at 13,000 x g for 20 minutes at 4°C and stored at -80°C.

2.5.2 Determining protein concentration using a BCA Assay

The cellular fractions were obtained as detailed above. The total protein concentration was determined using the Micro Bicinchoninic Acid (BCA)

protein assay system (Pierce [23227]) according to the manufacture's 96-well plate protocol. Absorbance was measured at 570 nm on a F50 infinite plate reader (Tecan).

2.5.3 Preparation of SDS-PAGE Gel

Protein samples (8 µg) were resolved using a Bio-Rad Mini-Protein II minigel system. Resolving and stacking gels were made according to Sambrook and Russell (256). Acrylamide gels were made using 30% acrylamide. Standard gel recipes used are described in Table 2.0. Protein samples were prepared using 4 x LDS sample buffer (Invitrogen [NP0007]) supplemented with 50 mM DTT reducing agent and denatured at 70°C for 10 min. 7.5µl of Blue plus two pre-stained standard (Invitrogen: 250-4 kDa [LC5925]) or ColorPlus prestained protein ladder (NEB: 10-230 kDa [P7711S]) was loaded as a reference for molecular weight. SDS-PAGE gels were run at 150V in 1 x SDS-PAGE running buffer or until optimum resolution of the marker was achieved.

Table 2.3: SDS-PAGE resolving and stacking gel recipes. The acrylamide recipes used to cast two mini-gels for the Bio-Rad Mini-Protein II system. Acrylamide stock refers to 30% acrylamide. APS = ammonium persulphate. TEMED = Tetramethylethylenediamine

Resolving Gel (10ml)					**Stacking Gel (5ml)**	
% Gel	**15%**	**12%**	**10%**	**7.5%**	**% Gel**	**5%**
30% Acrylamide	5 ml	4 ml	3.3 ml	2.5 ml	30% Acrylamide	830µl
1.5M Tris-HCL pH 8.8	2.5ml				1M Tris-HCL pH6.8	630µl
H2O	2.3ml	3.3ml	4ml	4.8ml	H2O	3.4ml
10% (w/v) SDS	100µl				10% (w/v) SDS	50µl
10% (w/v)	100µl				10% (w/v)	50µl

APS					APS	
TEMED	5µl				TEMED	5µl
Resolution (Protein KDa)	10–40	20–100	30–100	25–200		

2.5.4 Immunoblot analysis

Poly-vinylidine fluoride (PVDF) membranes (Millipore [IPVH00010]) were primed in 100% methanol and equilibrated in SDS-PAGE transfer buffer (25 mM Tris-HCl [pH8.3], 192 mM glycine, 20% [v/v] methanol). Two thick pieces of filter paper were also soaked in the transfer buffer. Two pieces of thick filter paper soaked in Towbin and the PVDF membranes followed by the SDS-PAGE gel were placed in the semi-dry transfer apparatus. Transfers were performed according to the manufacturer's instructions, for 1h at 100 V. Following the transfer, the PVDF membranes were blocked in 10% (w/v) non-fat skimmed milk powder (Sigma) prepared in Tris-buffered saline (50 mM Tris-HCl [pH 8.3], 150 mM NaCl) containing 0.5% (v/v) Tween-20 (TBS-T). Antibodies were diluted in 5% (w/v) milk-TBST and applied overnight at 4˚C with rocking. Proteins, including IAV protein NP, were detected with the antibodies listed in Table 2.4. The primary antibodies were detected with the secondary antibodies listed in Table 2.4. The secondary antibodies were diluted in 5% (w/v) non-fat skimmed milk-TBST and applied for 1h at room temperature with rocking. The secondary antibodies were detected using Bio-Rad kit. Antibody-bound proteins were visualised on equipment (this is a Hiscox lab adapted protocol).

Table 2.4 Table of primary and secondary antibodies used in the detection of cellular and IAV proteins in protein samples

	Antigen	Cat n˚	Manufacturer	Species	Dilution
Primary	GAPDH	Ab8245	Abcam	Mouse monoclonal	1/5000
	NP	Ab20343	Abcam	Mouse monoclonal	1/1000
	SPLUNC1 (BPIFA1)	Ab1897	R&D systems	Mouse monoclonal	1/1000
	SCGB3A2	AF3545	R&D systems	Goat monoclonal	1/1000
	IL6	Ab9324	Abcam	Mouse monoclonal	1/1000
Secondary	Rabbit	Ab6741	Abcam	Goat	1/1000
	Mouse	A4116	Sigma	Goat	1/1000

Not all the data from the use of antibodies in Table 2.4 were reported in this thesis.

2.6 Immunofluorescence staining

DMEM Media was aspirated from a six-well plate and filled with 1ml of PBS. PBS was used to wash the cells three times and 4% paraformaldehyde was used to fix the cells at room temperature. 1ml of PBS was used to wash the cells, which were permeabilised using 0.1% of Triton and incubated for 10 minutes at room temperature. Cells were washed with PBS (and Tween 0.5%)

three times. A blocking step was used to reduce non-specific binding. Blocking was done using PBS + 10% FBS at room temperature. The primary antibody master mix was prepared following the dilutions in Table 2.5.

Table 2.5: Primary antibody master mix

	Dilution	**Volume**
Primary Antibody	1/50	2 μl
Foetal Bovine Serum (FBS)	1/50	2 μl
PBS with Tween 0.5%	Complete volume to 100 μl	96 μl
Final volume	100 μl	100 μl

100 μl of this master mix was placed on each coverslip and left in darkness for one hour at room temperature. These were washed three times with 1ml of PBS with Tween 0.5%. The second antibody master mix was prepared following the dilutions in Table 2.6.

Table 2.6: Secondary antibody master mix

	Dilution	**Volume**
Secondary Antibody	1/200	0.5 μl
Foetal Bovine Serum (FBS)	1/50	2 μl
PBS with Tween 0.5%	Complete volume to 100 μl	97.5 μl
Final volume	100 μl	100 μl

100 μl of this master mix was placed on each coverslip and left for one hour at room temperature in darkness. These were washed three times with 1ml of PBS with Tween 0.5%. The coverslips were dried and mounted on a slide using Prolong Gold® as a mounting media, with DAPI to stain the nucleus.

2.7 Label-free Liquid Chromatography Mass Spectrometry analysis on A549 cells

Sample preparation, mass spectrometry, and analysis were adapted from Dong et al., (2017) (257).

2.7.1 Homogenisation and protein digestion

Cell pellets were lysed in 1% w/v sodium deoxycholate (Sigma) in 50mM ammonium bicarbonate. This was followed by three cycles of sonication on ice (Vibra-cell 130PB sonicator, 20Hz, with microprobe, 10 seconds sonication alternating with 30 seconds incubation on ice). Samples were centrifuged at 13,000 x g for 10 minutes at 4°C. The supernatant was removed and retained. Samples were stored at -80°C until use. Protein concentrations of the samples

were determined using a Bradford protein assay (Thermo). Samples were heated at 80°C for 10 minutes followed by reduction with 3mM DTT (Sigma) at 60°C for 10 minutes, cooled, then alkylated with 9mM iodoacetamide (Sigma) at RT for 30 minutes in the dark; all steps were performed with intermittent vortex-mixing. Proteomic-grade trypsin (Sigma) was added at a protein-trypsin ratio of 50:1 and incubated at 37°C overnight. Sodium deoxycholate was removed by adding TFA to a final concentration of 0.5% (v/v). Peptide samples were centrifuged at 13,000 x g for 30 min to remove precipitate (258).

2.7.2 NanoLC MS ESI MS/MS analysis

Peptides were analysed by on-line nanoflow LC using the Ultimate 3000 nano system (Dionex/Thermo Fisher Scientific). Samples were loaded onto a trap column (Acclaim PepMap 100, 2 cm × 75 µm inner diameter, C18, 3 µm, 100 Å) at 9µl /min with an aqueous solution containing 0.1 %(v/v) TFA and 2% (v/v) acetonitrile. After 3 min, the trap column was set in-line with an analytical column (Easy-Spray PepMap® RSLC 50 cm × 75 µm inner diameter, C18, 2 µm, 100 Å) fused to a silica nano-electrospray emitter (Dionex). The column was operated at a constant temperature of 35°C and the LC system was coupled to a Q-Exactive mass spectrometer (Thermo Fisher Scientific). Chromatography was performed with a buffer system consisting of 0.1% formic acid (buffer A) and 80% acetonitrile in 0.1% formic acid (buffer B). The peptides were separated by a linear gradient of 3.8–50% buffer B over 90 minutes at a flow rate of 300 nl/min. The Q-Exactive was operated in data-dependent mode with survey scans acquired at a resolution of 70,000 at m/z

200. Scan range was 300 to 2000m/z. Up to the top 10 most abundant isotope patterns with charge states +2 to +5 from the survey scan were selected with an isolation window of 2.0Th and fragmented by higher energy collisional dissociation with normalised collision energies of 30. The maximum ion injection times for the survey scan and the MS/MS scans were 250 and 50ms, respectively, and the ion target value was set to 1E6 for survey scans and 1E4 for the MS/MS scans. MS/MS events were acquired at a resolution of 17,500. Repetitive sequencing of peptides was minimised through dynamic exclusion of the sequenced peptides for 20s (259).

2.7.3 Protein Identification and Quantification

Thermo RAW files were imported into Progenesis LC–MS (version 4.1, Nonlinear Dynamics. Peaks were picked by the software using default settings and filtered to include only peaks with a charge state between +2 and +7. Peptide intensities were normalised against the reference run by Progenesis LC-MS and these intensities were used to highlight differences in protein expression between control and treated samples with supporting statistical analysis (ANOVA p-values) calculated by the Progenesis LC-MS software. Spectral data were converted into .mgf files with Progenesis LC–MS and exported for peptide identification using the Mascot (version 2.3.02, Matrix Science) search engine. Tandem MS data were searched against a combined database, including translated ORFs from the Human genome (Uniprot, Feb 2017), Influenza H3N2 (Uniprot, Feb 2015) and a contaminant database (cRAP, GPMDB, 2012) (combined 25534 sequences; 13007852 residues). The search parameters were as follows: precursor mass tolerance was set to

10 ppm and fragment mass tolerance was set as 0.01 Da. Two missed tryptic cleavages were permitted. Carbamidomethylation (cysteine) was set as a fixed modification and oxidation (methionine) set as a variable modification. Mascot search results were further validated using the machine-learning algorithm Percolator, embedded within Mascot. The Mascot decoy database function was utilised, and the false discovery rate was <1%, while individual percolator ion scores >13 indicated identity or extensive homology ($p < 0.05$). Mascot search results were imported into Progenesis LC–MS as XML files (260).

2.8 The MinION sequencing protocol

2.8.1 Quantification of RNA samples using Qubit®3.0 fluorometer

RNA samples quantified using Qubit®3.0 fluorometer using the Qubit RNA HS Assay Kit (Thermo Fisher [Q328520]) following manufacturer's instructions. 260/280 and 260/230 ratios were established using NanoDrop One/OneC Microvolume UV-Vis Spectrophotometer (Thermo Scientific). The ideal ratios to be attained were 2.0. After that, each reaction concentration used was quantified on the Qubit®3.0 fluorometer.

2.8.2 Agarose gel electrophoresis

Agarose gel electrophoresis with cybersafe staining was used to visualise RNA. Electrophoresis grade agarose (AGTC Bioproducts) (1% [w/v]) was melted in TBE buffer (40 mM Tris-acetate, 1 mM EDTA, pH 8.0) by heating, and cybersafe was added to cooled molten agarose to a final concentration of 0.5 µg/ml. Molten agarose was poured into a gel-casting tray containing a

comb and allowed to set. The tray was transferred to a gel running tank and submerged in 1X TBE buffer. 5μl of samples was diluted in 2μl DNA loading buffer (Bioline) and loaded in the wells of the gel alongside Hyperladder I DNA ladder (Bioline). RNA was analysed on a 1% agarose gel by electrophoresis at 120V. 400mA for one hour. This was to observe the distinct 28S and 18S rRNA bands (with a ratio of band intensity ~2:1) (data not shown). RNA samples were stored at -80ºC. RNA samples were given to our colleagues at the centre for genomic research (CGR) to confirm the quality of RNA by visualising the 28S and 18S rRNA bands and RIN values.

2.8.3 Reverse transcription and strand-switching

200ng of total RNA was mixed with VN Primer (VNP) and 10mM dNTPs (NEB [N0447]) and incubated at 65°C for 5 minutes and snapped cooled. Superscript IV buffer and 100mM DTT (ThermoFisher Scientific [18090050]), RNaseOUT (Life technologies [10777019]) and SSP (ONT) were added to the reaction and incubated at 42°C for two minutes. 1μl of Superscipt IV (ThermoFisher Scientific [18090050]) was added to the reaction and incubated following the protocol, (50°C, 10 mins), (42°C, 10 mins), (80°C, 10 mins).

2.7.4 Selecting for full length transcripts by PCR

Reverse transcribed RNA was split into four separate reactions with the addition of 2x LongAmp Taq (NEB [M0287]) and cDNA PRM (cPRM [ONT]). Reverse transcribed RNA was amplified using the following cycling conditions (Table 2.7). The extension step was carried out for 10 minutes.

Table 2.7 Cycling conditions for full length transcripts by PCR

Cycle step	Temperature	Time	No. of cycles
Initial denaturation	95°C	30 secs	1
Denaturation	95°C	15 secs	11–18*
Annealing	62°C	15 secs	11–18*
Extension	65°C	50 secs per kb	11–18*
Final extension	65°C	6 mins	1
Hold	4°C	∞	

Exonucleases (NEB [M0293]) were added to each PCR reaction and were incubated at 37°C for 15 minutes, then 80°C for 15 minutes. The four separate reactions were then pooled before the addition of AMPure XP beads (Beckman Coulter [A63880]). The pooled reaction was then incubated for five minutes at room temperature on a Hula mixer. Reactions were then pelleted on a magnetic rack and washed twice with 70% ethanol. 21μl of Rapid Annealing Buffer (RAB [ONT]) was added to the reaction and incubated on a hula mixer for 10 minutes at room temperature. Reactions were pelleted on the magnetic rack and the eluate was retained for Qubit analysis.

2.8.5 Adapter ligation

2μl of cDNA Adapter Mix (cAMX [ONT]) was added to the amplified cDNA library and incubated on a Hula mixer for five minutes at room temperature.

2.8.6 AMPure XP bead binding

20μl of AMPure XP beads were added to the reaction and incubated on a hula mixer for five minutes at room temperature. Reactions were pelleted on the magnetic rack and supernatant was removed. AMPure XP beads were resuspended in 140μl of Adapter Bead Binding Buffer (ABB [ONT]), supernatant was removed once pelleted on the magnetic rack before resuspending the beads in ABB once again. Beads were resuspended in 13μl Elution Buffer (ELB [ONT]) and incubated on a hula mixer for 10 minutes at room temperature. Beads were pelleted on the magnetic rack and the eluate was transferred into a clean 1.5 ml Eppendorf DNA LoBind tube. 1μl of eluate was quantified using a Qubit fluorometer.

2.8.7 Priming and loading the flow cell

Approximately 20 μl of air was removed from the priming port of the flow cell 800 μl of priming mix containing Running Buffer with Fuel Mix (RBF [ONT]) and nuclease free water was added to the flow cell. After five minutes, the SpotON sample port cover was lifted and 200 μl of priming mix was added to the priming port. 12 μl of the cDNA library was mixed with 35 μl RBF (ONT), 25.5 μl of library loading beads (LLB [ONT]) and 2.5 μl of nuclease free water. 75μl of the prepared library was added, drop wise, to the flow cell via the SpotON sample port.

2.8.8 Data acquisition, transfer and Bioinformatic analysis

The specialist software MinKNOW was used for base calling and data acquisition. After the experiment was over (48 hours later), the data pass

FASTA files were downloaded on a 1TB external hard drive and transported for bioinformatic data analysis following the methods described in (261).

2.9 Infection of Cynomolgus NHP Macaque (*Macaca Fascicularis*) with IAV

All animal experiments in non-human primates (NHP) were conducted by our collaborators at Public Health England (PHE), at their facilities in Porton Down, UK. It was not possible for me to undertake the training and obtain a license to carry out the animal experiments for the duration of the project. The rest of the analysis and experiments were performed by me and my colleagues in the proteomics department at the University of Liverpool.

Cynomolgus NHP Macaque (*Macaca Fascicularis*) were infected via the inhaled aerosol (i.a.) route at a dose of 10^5 pfu. This i.a. dose was used because it was the maximum dose technically achievable for the A/Cal/04/09. These animals were culled at day five and day seven (262). Broncho-alveolar lavage fluid (BALF) from naïve NHP and i.a. challenged NHP-infected, culled at day five and day seven, were received. BALF samples were analysed by mass spectrometry as described below.

2.9.1 BALF sample preparation from NHP for Mass Spectrometry

Protein from Broncho-alveolar lavage fluid (BALF) after spinning out and discarding cells was dispensed into low protein-binding microcentrifuge tubes (Sarstedt, Leicester, UK) and made up to 160 µl with the addition of 25 mM ammonium bicarbonate. The proteins were denatured using 10 µl of 1% (w/v)

RapiGestTM (Waters MS Technologies, Manchester, UK) in 25 mM ammonium bicarbonate, followed by two cycles of 10-minute sonication in a water bath. A sample was then incubated at 80°C for 10 minutes, reduced (addition of 10µl of 60 mM DTT and incubation at 65 °C for 10 min), and alkylated (addition of 10µl of 180 mM iodoacetamide and incubation at room temperature for 30 min in the dark). Trypsin (Sigma-Aldrich) was reconstituted in 50 mM acetic acid to a concentration of 0.2 µg/µl. Digestion was performed by the addition of 10µl of trypsin to the sample followed by incubation at 37°C overnight. The RapiGestTM was removed from the sample by acidification (1 µl of trifluoroacetic acid and incubation at 37°C for 45 min) and centrifugation (15,000 × g for 15 min) (260).

Digests (2µl) were analysed on a 50cm Easy-Spray column with an internal diameter of 75µm, packed with 2µm C18 particles, fused to a silica nano-electrospray emitter (Thermo Fisher Scientific). Reversed phase liquid chromatography was performed using the Thermo EASY-nLC 1000 with a binary buffer system consisting of 0.1% formic acid (buffer A) and 80% acetonitrile in 0.1% formic acid (buffer B). The peptides were separated by a linear gradient of 5–40% buffer B over 110 min at a flow rate of 300nl/min. The column was operated at a constant temperature of 35°C and the LC system coupled to a Q-Exactive mass spectrometer (Thermo Fisher Scientific). The Q-Exactive was operated in data-dependent mode with survey scans acquired at a resolution of 70,000 at m/z 200. The top 10 most abundant isotope patterns with charge states +2, +3 and/or +4 from the survey scan were selected with an isolation window of 2.0Th and fragmented by higher energy

collisional dissociation with normalised collision energies of 30. The maximum ion injection times for the survey scan and the MS/MS scans were 250 and 100ms, respectively, and the ion target value was set to 1E6 for survey scans and 1E4 for the MS/MS scans. Repetitive sequencing of peptides was minimised through dynamic exclusion of the sequenced peptides for 20s (262).

2.10 Obtaining Nasopharyngeal aspirates (NA) from patients in Alderhey Children's Hospital (AHCH), Great Ormond Street Hospital (GOSH) and the Institute Pasteur, Dakar (IPD)

NAs (due for discard after routine diagnostic work) were obtained from the diagnostic laboratories at AHCH, GOSH, and IPD (Table 2.9). Samples were made anonymous and supplied only with the following information: respiratory virus status, influenza status, gender, and age in years. All samples from the different cohorts were sampled from paediatric patients between the ages of two and 13 years old. Five samples from those testing IAV-H3N2-positive, along with six samples testing negative, for a defined suite of respiratory viruses, including IAV, were provided by AHCH. Six samples from those testing IAV-H3N2-positive along with six samples testing negative for a defined suite of respiratory viruses, including IAV, were provided by GOSH. Ten samples from those testing IAV-H3N2-positive, 10 samples from those testing IAV-H1N1 (pdm2009)-positive, along with 10 samples from those testing negative for a defined suite of respiratory viruses and IAV-negative were provided by IPD. Upon completion of the project, the NA samples were destroyed.

Table 2.9 Patient sample data from Alder Hey Children's Hospital (AHCH), Great Ormond Street Hospital (GOSH) and Institute Pasteur Dakar (IPD)

	Age	Sex	Influenza Status	Ct value	Viral strain	Hospital/Location	Status used in experiment
1	3	M	Positive	16	Influenza a/H3N2	Great Ormond Street Hospital, London, UK	Positive sample
2	2	F	Positive	22	Influenza a/H3N2	Great Ormond Street Hospital, London, UK	Positive sample
3	4	M	Positive	25	Influenza a/H3N2	Great Ormond Street Hospital, London, UK	Positive sample

4	7	F	Positive	31	Influenza a/H3N2	Great Ormond Street Hospital, London, UK	Positive sample
5	6	F	Positive	33	Influenza a/H3N2	Great Ormond Street Hospital, London, UK	Positive sample
6	9	M	Positive	34	Influenza a/H3N2	Great Ormond Street Hospital, London, UK	Positive sample
7	4	M	Negative	0	-	Great Ormond Street Hospital, London, UK	Negative sample
8	2	F	Negative	0	-	Great Ormond Street Hospital, London, UK	Negative sample

9	3	F	Negative	0	-	Great Ormond Street Hospital, London, UK	Negative sample
10	7	M	Negative	0	-	Great Ormond Street Hospital, London, UK	Negative sample
11	6	F	Negative	0	-	Great Ormond Street Hospital, London, UK	Negative sample
12	9	M	Negative	0	-	Great Ormond Street Hospital, London, UK	Negative sample
13	9	M	Positive	26	Influenza a/H3N2	Institute Pasteur Dakar, Senegal	Positive sample
14	10	M	Positive	21	Influenza a/H3N2	Institute Pasteur Dakar, Senegal	Positive sample

15	2	M	Positive	22	Influenza a/H3N2	Institute Pasteur Dakar, Senegal	Positive sample
16	9	M	Positive	20	Influenza a/H3N2	Institute Pasteur Dakar, Senegal	Positive sample
17	4	M	Positive	26	Influenza a/H3N2	Institute Pasteur Dakar, Senegal	Positive sample
18	2	M	Positive	25	Influenza a/H3N2	Institute Pasteur Dakar, Senegal	Positive sample
19	10	M	Positive	28	Influenza a/H3N2	Institute Pasteur Dakar, Senegal	Positive sample
20	1	M	Positive	21	Influenza a/H3N2	Institute Pasteur Dakar, Senegal	Positive sample
21	5	F	Positive	21	Influenza a/H3N2	Institute Pasteur Dakar, Senegal	Positive sample
22	8	M	Positive	20	Influenza a/H3N2	Institute Pasteur Dakar, Senegal	Positive sample

23	2	M	Positive	20	H1N1 pandemic	Institute Pasteur Dakar, Senegal	Positive sample
24	6	M	Positive	25	H1N1 pandemic	Institute Pasteur Dakar, Senegal	Positive sample
25	4	F	Positive	32	H1N1 pandemic	Institute Pasteur Dakar, Senegal	Positive sample
26	4	M	Positive	30	H1N1 pandemic	Institute Pasteur Dakar, Senegal	Positive sample
27	12	M	Positive	21	H1N1 pandemic	Institute Pasteur Dakar, Senegal	Positive sample
28	4	F	Positive	34	H1N1 pandemic	Institute Pasteur Dakar, Senegal	Positive sample
29	6	F	Positive	26	H1N1 pandemic	Institute Pasteur Dakar, Senegal	Positive sample
30	9	F	Positive	27	H1N1 pandemic	Institute Pasteur Dakar, Senegal	Positive sample

31	4	F	Positive	37	H1N1 pandemic	Institute Pasteur Dakar, Senegal	Positive sample
32	6	F	Positive	22	H1N1 pandemic	Institute Pasteur Dakar, Senegal	Positive sample
33	6	F	Negative	0	-	Institute Pasteur Dakar, Senegal	Negative sample
34	2	M	Negative	0	-	Institute Pasteur Dakar, Senegal	Negative sample
35	7	M	Negative	0	-	Institute Pasteur Dakar, Senegal	Negative sample
36	8	F	Negative	0	-	Institute Pasteur Dakar, Senegal	Negative sample
37	3	M	Negative	0	-	Institute Pasteur Dakar, Senegal	Negative sample
38	4	M	Negative	0	-	Institute Pasteur Dakar, Senegal	Negative sample

39	7	M	Negative	0	-	Institute Pasteur Dakar, Senegal	Negative sample
40	3	F	Negative	0	-	Institute Pasteur Dakar, Senegal	Negative sample
41	5	M	Negative	0	-	Institute Pasteur Dakar, Senegal	Negative sample
42	3	M	Negative	0	-	Institute Pasteur Dakar, Senegal	Negative sample
43	2	-	Positive	-	Influenza a/H3N2	Alder Hey Children's Hospital, Liverpool, UK	Positive sample
44	1	-	Positive	-	Influenza a/H3N2	Alder Hey Children's Hospital, Liverpool, UK	Positive sample

45	11	-	Positive	-	Influenza a/H3N2	Alder Hey Children's Hospital, Liverpool, UK	Positive sample
46	1	-	Positive	-	Influenza a/H3N2	Alder Hey Children's Hospital, Liverpool, UK	Positive sample
47	12	-	Positive	-	Influenza a/H3N2	Alder Hey Children's Hospital, Liverpool, UK	Positive sample
48	-	-	Negative	0	-	Alder Hey Children's Hospital, Liverpool, UK	Negative sample

49	-	-	Negative	0	-	Alder Hey Children's Hospital, Liverpool, UK	Negative sample
50	-	-	Negative	0	-	Alder Hey Children's Hospital, Liverpool, UK	Negative sample
51	-	-	Negative	0	-	Alder Hey Children's Hospital, Liverpool, UK	Negative sample
52	-	-	Negative	0	-	Alder Hey Children's Hospital, Liverpool, UK	Negative sample

53	-	-	Negative	0	-	Alder Hey Children's Hospital, Liverpool, UK	Negative sample

*Sex and age unavailable for 6 IAV negative patients from Alder Hey Children's Hospital

*Sex unavailable for 5 IAV positive patients from Alder Hey Children's Hospital

Table 2.10 Summary Characteristics of patient samples from Great Ormond Street Hospital, Institut Pasteur Dakar and Alder Hey Children's Hospital

	Total No. of patients	No. of Males	No. of Females	Age bin (1-4)	Age bin (5-13)
GOSH (H3N2 Positive)	6	3	3	3	3
GOSH (H3N2Negative	6	3	3	3	3
IPD (H3N2 Positive)	10	9	1	4	6
IPD (H1N1 Positive)	10	4	6	5	5
IPD (H3N2 & H1N1 negative)	10	7	3	5	5
AHCH (H3N2 Positive)	5	-	-	3	2
AHCH (H3N2 & H1N1 Positive)	-	-	-	-	-

2.10.1 Ethics Statement

I used residual material that was from NHS diagnostic samples and was fully anonymised. These samples were held under the Human Tissue Authority (HTA) license. Similarly, residual material that was from diagnostic samples and was fully anonymised were obtained from Institut Pasteur Dakar, Senegal.

2.10.2 Film array and qRT-PCR analysis of influenza virus

The Film Array multiplex polymerase chain reaction (PCR) system respiratory panel by Biomerieux diagnostics was used to detect the presence of pathogens in the NA. This panel detects the 20 most common respiratory pathogens; adenovirus, coronavirus HKU1, coronavirus NL63, coronavirus OC43, human metapneumovirus, human rhinovirus/Enterovirus, influenza A, influenza A H1, influenza A H1-2009, influenza A/H3, influenza B, parainfluenza virus 1, parainfluenza virus 2, parainfluenza virus 3, parainfluenza virus 4, HRSV, *Bordetella pertussis*, *Chlamydophila pneumoniae* and *Mycoplasma pneumoniae*. IAV viral load was determined by qRT-PCR, where positive amplification controls were used with cDNA derived from plasmids that contained the amplicon sequences of each target. An internal positive control (IPC) of Phocine Distemper virus (PDV) was added to every sample. The PDV target was detected with a real-time RT-PCR assay that was run in a multiplex reaction with the IAV target. The targets for the IAV were HA, M1/M2, and NP segments. The limit of detection was 10 copies per reaction.

2.10.3 Sample preparation for proteomics

Protein pellets from nasal wash precipitation were re-solubilised in 50mM ammonium bicarbonate, 0.1% Rapigest (Waters). Protein concentration was determined using the Pierce Coomassie Plus bicinchoninic acid protein assay (Thermo Scientific) as instructed in the manufacturer's guide. Sample protein content and volume were normalised with 50mM ammonium bicarbonate. Samples were then heated at 80^0C for 10 minutes, reduced with 3mM dithiothreitol (Sigma) at 60^0C for 10 minutes, and then alkylated with 9mM iodoacetimde (Sigma) at room temperature for 30 minutes in darkness. Proteomic grade trypsin (Sigma) was added at a protein-trypsin ratio of 50:1 and samples incubated at 37^0C overnight. Rapigest was removed by adding TFA to a final concentration of 0.5% (v/v) and incubating at 37^0C for 2 h before centrifugation at 12,000g for 60 minutes (4^0C) to remove the precipitate (263) (257).

2.10.4 NanoLC MS ESI MS/MS analysis

Samples were re-analysed by on-line nanoflow LC using the Ultimate 3000 nano system (Dionex/Thermo Fisher Scientific) coupled with Q-Exactive mass spectrometer (Thermo Fisher Scientific). Samples were loaded on a 50cm Easy-Spray column with an internal diameter of 75µm, packed with 2µm C18 particles, fused to a silica nano-electrospray emitter (Thermo Fisher Scientific). The column was operated at a constant temperature of 35°C. Chromatography was performed with a buffer system consisting of 0.1% formic acid (buffer A) and 80% acetonitrile in 0.1% formic acid (buffer B). The peptides were separated by a linear gradient of 3.8–50% buffer B over 90 minutes at a flow

rate of 300nl/min. The Q-Exactive was operated in data-dependent mode with survey scans acquired at a resolution of 70,000. Up to the top 10 most abundant isotope patterns with charge states +2, +3 and/or +4 from the survey scan were selected with an isolation window of 2.0Th and fragmented by higher energy collisional dissociation with normalised collision energies of 30 (258). MS/MS scans were acquired at a resolution of 17,500. The maximum ion injection times for the survey scan and the MS/MS scans were 250 and 50 ms, respectively, and the ion target value was set to 1E6 for survey scans and 1E5 for the MS/MS scans. Repetitive sequencing of peptides was minimised through dynamic exclusion of the sequenced peptides for 20s.

2.10.5 Label-free analysis using Progenesis

Thermo RAW files were imported into Progenesis LC–MS (version 4.1, Nonlinear Dynamics). Runs were time aligned using default settings and using an auto-selected run as reference. Peaks were picked by the software and filtered to include only peaks with a charge state of between +2 and +6 (257). Peptide intensities were normalised against the reference run by Progenesis LC-MS and these intensities were used to highlight differences in protein expression between control and treated samples with supporting statistical analysis (ANOVA p-values) calculated by the Progenesis LC-MS software. Spectral data were transformed to .mgf files with Progenesis LC–MS and exported for peptide identification using the Mascot (version 2.3.02, Matrix Science) search engine (260). Tandem MS data were searched against a combined database including translated ORFs from the Human genome (Uniprot, Feb 2014), and a combined human respiratory virus database

(including Influenza (A), HRSV (A, B), Human adenovirus 14, Human mastadenovirus (A, B, C, D), Human parainfluenza virus (1, 2, 3), Human metapneumovirus, Human coronavirus (OC43,NL63, 229E), Human bocavirus, Rhinovirus (A, B14, C) all from NCBI, Aug 2014) and a contaminant database (cRAP, GPMDB, 2012) (combined 20896 sequences; 11589421 residues) (258). Mascot search parameters were as follows; precursor mass tolerance set to 10ppm and fragment mass tolerance set to 0.05 Da. One missed tryptic cleavage was permitted. Carbamidomethylation (cysteine) was set as a fixed modification and oxidation (methionine) set as a variable modification. Mascot search results were further processed using the machine-learning algorithm Percolator. The false discovery rate was <1%. Individual ion scores >13 indicated identity or extensive homology ($p<0.05$). Protein identification results were imported into Progenesis LC–MS as .xml files (264).

2.10.6 Label-free analysis using Progenesis

Thermo RAW files were imported into Progenesis LC–MS (version 4.1, Nonlinear Dynamics). Runs were time aligned using default settings and using an auto-selected run as reference. Peaks were picked by the software and filtered to include only peaks with a charge state of between +2 and +6 (257). Peptide intensities were normalised against the reference run by Progenesis LC-MS and these intensities were used to highlight differences in protein expression between control and treated samples with supporting statistical analysis (ANOVA p-values) calculated by the Progenesis LC-MS software. Spectral data were transformed to .mgf files with Progenesis LC–MS and exported for peptide identification using the Mascot (version 2.3.02, Matrix

Science) search engine. Tandem MS data were searched against the human (60,806 sequences, NCBI RefSeq release-2014_09). Mascot search parameters were as follows; precursor mass tolerance set to 10ppm and fragment mass tolerance set to 0.5 Da. One missed tryptic cleavage was permitted. Carbamidomethylation (cysteine) was set as a fixed modification and oxidation (methionine) set as a variable modification. Mascot search results were further processed using the machine-learning algorithm Percolator. The false discovery rate was <1%. Individual ion scores >13 indicated identity or extensive homology ($p<0.05$). Protein identification results were imported into Progenesis LC–MS as .xml files (259) (264).

CHAPTER 3: CHARACTERISING THE CELLULAR RESPONSE TO INFLUENZA A VIRUS INFECTION USING AN ALVEOLAR LUNG EPITHELIAL CELL LINE (A549 CELL LINE)

3.1 INTRODUCTION

The IAV possesses various mechanisms that enable it to enter, replicate, and exit host cells, as well as evade the host anti-viral response (117). The IAV has developed mechanisms for the production of more viruses, including 'cap-snatching' and preventing the host from expressing its own genes (117). The IAV has gained the ability to 'shut off the host'. This, in effect, means upon viral infection in infected cells, the virus has gained the capability to redirect cellular resources to enable viral gene expression. In addition, evading the host immune response. (265, 266). Some of the mechanisms used by the IAV to shut off the host, are described below.

NS1 is an IAV viral protein that plays a key role in inhibiting type I interferon (IFN) responses. This is crucial in evading the host innate immune response (266). Viruses in which the NS1 protein has been deleted, are proven to induce high levels of IFN. These viruses also replicated more efficiently in the absence of IFN-α/β in vero cells than in the presence of type 1 IFNs in MDCK cells (266-268). As stated above, 'cap-snatching' is another mechanism that IAV uses to 'shut off the host'. The RNA-dependent RNA polymerase RdRp complex from the IAV, binds to the host's RNA pol II. RdRp cleaves new transcripts close to the 5' end. These fragments are used as primers for viral mRNA transcription. The 5' caps intended for host messages are used for viral messages (146, 266). The RdRp-pol II association also leads to the ubiquitination and degradation of Pol II. Pol II plays a role in the expression of IFN-stimulated genes such as ISG15 (269). Therefore, the degradation of Pol II allows IAV to circumvent host antiviral response (266, 270). PA-X is a viral

protein produced after amino acid 191 of PA (85, 271). PA-X degrades host RNA by reducing reporter and endogenous gene expression and plays a role in circumventing host innate immune response. (85, 266, 272, 273).

Lung epithelial cells are the first line of the host defence from respiratory infections (2). Upon viral entry, the host interferon (IFN) response is one of the first barriers IAV overcomes to establish an infection (274, 275). Proteins from the IFN family play a major role in responding to the early stages of infections. Lung epithelial cells infected with respiratory viruses, and specifically IAV, produce IFN type I and III depending on the retinoic acid-inducible-gene-I protein and mitochondrial antiviral signalling protein (RIG-I/MAVS) pathway (276). Receptors that detect IAV affect the induction of IFN. The Toll-like receptor 7 (TLR7) on plasmacytoid dendritic cells (pDC) recognise the influenza virus, while RNA helicase retinoic acid-induced gene I (RIG-I) recognises RNA viral genomes (277). RNA binding to RIG-I caused interactions with mitochondrial adaptor protein MAVS. This leads to the activation of transcriptional factors, such as NFκB and expression of IFNβ and IFNα1 in humans and IFNα4 in mice (277-279). After IFNβ and IFNα1/ IFNα4 are secreted, receptor-associated tyrosine kinases JAK1 and Tyk2 are activated alongside transcription factors STAT1 and STAT2 (277, 280). These activated STATs go on to form complexes called interferon stimulator gene factor 3 (ISGF3), which induce hundreds of IFN-stimulated genes (ISGs). ISGs play a crucial role in establishing the antiviral state in the cell after infection (277). Type III IFNs are a novel class of IFNs and have three members: IFNλ1, IFNλ2 and IFNλ3, also called IL-29, IL-28A and IL-28B

respectively (281). IFN III are induced by similar mechanisms as IFN1 through RIG-I/MAVS/TBK1/IRF3 (277). IFN I and III therefore protect the host from IAV infection by upregulating interferon stimulated genes (ISGs) (277, 282).

The aim of this thesis was to understand host responses *in vitro* and *in vivo*. The first aim (and the subject of this chapter) was to characterise IAV H3N2 in a well-controlled *in vitro* cell culture system (A549 cells were used). This was established by infecting A549 cells with IAV and quantifying the virus at 3h.p.i, 6h.p.i, 9h.p.i, 12h.p.i, 18h.p.i, 24h.p.i, 36h.p.i, and 48h.p.i. The technique used for this was the avicel plaque assay (2.4%) (254). This was to assess the most suitable time point of infection before the cells arrived at cytopathic effect (CPE). Following this, an informed decision was made when choosing a time point (18h.p.i) that would be used for subsequent experiments. Immunofluorescence microscopy and SDS-PAGE were used to validate the data and confirm the cells were IAV infected prior to further experiments. Once this time point (18h.p.i) was selected, mass spectrometry was used to characterise the proteome of A549 cells infected with IAV compared to mock infected cells. MinION sequencing was further used to characterise the transcriptome of A549 cells infected with IAV compared to mock infected cells. The results from the *in vitro* experiment provided a high degree of confidence and allowed for a direct comparison between *in vitro* (chapter 3) and *in vivo* (Chapters 4 and 5) systems.

A549 cells used in this chapter are a model cell line derived from alveolar epithelial cells. These cells have been used extensively in the analysis of the

cellular response in other respiratory pathogens. Some of these respiratory pathogens include; respiratory syncytial virus (RSV) (283-286) and the measles virus (287). A comparison of the host cell proteome after infection of A549 cells with negative stranded viruses, such as HRSV, parainfluenza virus, measles virus, and HMPV was done. The results obtained revealed an induction of apoptosis upon infection. A two-dimensional gel electrophoresis (2D-DIGE) approach was used to identify the host proteome changes that are in concordance with these findings (287).

IAV, just like RSV and Porcine Reproductive and Respiratory Syndrome Virus (PRRSV) (288), is known to have a tropism for respiratory epithelial cells. Therefore, this cell line was selected as an appropriate model (289, 290). A549 cells have been used to understand the dynamics and complexity of virus-host cell interactions (219). A549 cells have been used for *in vitro* analysis of human surfactant synthesis (291). The cell line provides a robust IFN response as seen in humans during respiratory infection (226, 274). The IFN response has the potential to be used as a treatment against pandemic influenza virus infections (292, 293). The antiviral actions of type I and type III IFN were effective in suppressing the pandemic 2009 (H1N1) influenza virus infection (294).

However, there are caveats in using A549 cells. The A549 cell line is derived from a human alveolar cell carcinoma and has a modal chromosome number of 66 (295, 296). Consequently, the genes (and ultimately proteins) are maybe over or under represented compared to normal cells. Nonetheless, A549 cells

at both low and high passage numbers have properties typical of type II alveolar epithelial cells based on histochemical, electron microscopic, and biochemical data (297, 298).

In addition to A549 cells, MDCK cells are used in the study of influenza virus strains due to their high susceptibility to infection. As an alternative to egg-based vaccine production, MDCK cells have been used widely for these purposes (242). MDCK cell culture-derived influenza vaccine production has been approved by the European Medicines Agency (242, 299). MDCK cells are known to be more susceptible and robust to various strains of IAV and are, therefore, frequently used for viral growth *in vitro* and in the development of vaccines (300, 301). MDCK cells are used for the avicel plaque assay to quantify the virus over time. This is due to the MDCK cells robust nature and their ability to withstand being coated with 1μg/ml of trypsin over long periods of time. A549 cells do not have this ability.

To investigate the host response and identify biomarkers of viral infection, in this chapter, two independent approaches were used to investigate changes in protein and transcript abundance. A combination of these methods would give an insight into host changes. Quantitative proteomics was used to gain a global quantitative and qualitative overview of the cellular proteome changes. Label-free mass spectrometry was used because of its simpler biochemical workflows and the ability to use it in biomarker discovery in clinical samples. This was essential to ensure that all the data is collected and analysed from the same platform. This reduces technical variation and data comparison

between *in vitro* (chapter 3) and *in vivo* (Chapters 4 and 5). MinION sequencing was used to obtain a global transcriptome by sequencing samples from IAV-infected A549 cells and A549 mock-infected cells. Data from Mass Spectrometry and MinION revealed host proteome and transcriptome data that are comparable to further characterise IAV and identify potential biomarkers.

3.2 Next Generation Sequencing (NGS)

The benefits of having the ability to determine the order of nucleic acid residues in biological samples are numerous. This order gives information on biochemical and hereditary properties of a biological sample. Researchers have applied themselves over the last fifty years in the search of techniques and technologies to enable this. Sequencing has therefore encompassed sequencing DNA molecules, sequencing RNA molecules over increasingly shorter time frames (Figure 3.1) (302). Next Generation sequencing is the ability to use technologies to sequence DNA or RNA for high-throughput production of sequencing data. This is in comparison to the traditional sequencing method – Sanger first-generation sequencing. NGS is frequently used today to determine how an organism survives independently and within a host (Figure 3.1) (Table 3.1) (303).

NGS is a culmination of deep, high-throughput and in-parallel DNA sequencing technologies developed three decades after Sanger DNA sequencing. NGS technologies produce high-throughput data at a much-reduced cost, while undertaking parallel DNA analysis (303-306). First-

generation Sanger sequencing focused on the use of fragment-cloning methods to sequence DNA nucleotides (307). Second-generation sequencing focused on amplifying sequence libraries prior to sequencing amplified DNA clones (308). Third generation sequencing, on the other hand, can be completed without creating amplification libraries. This saves time and cost (309).

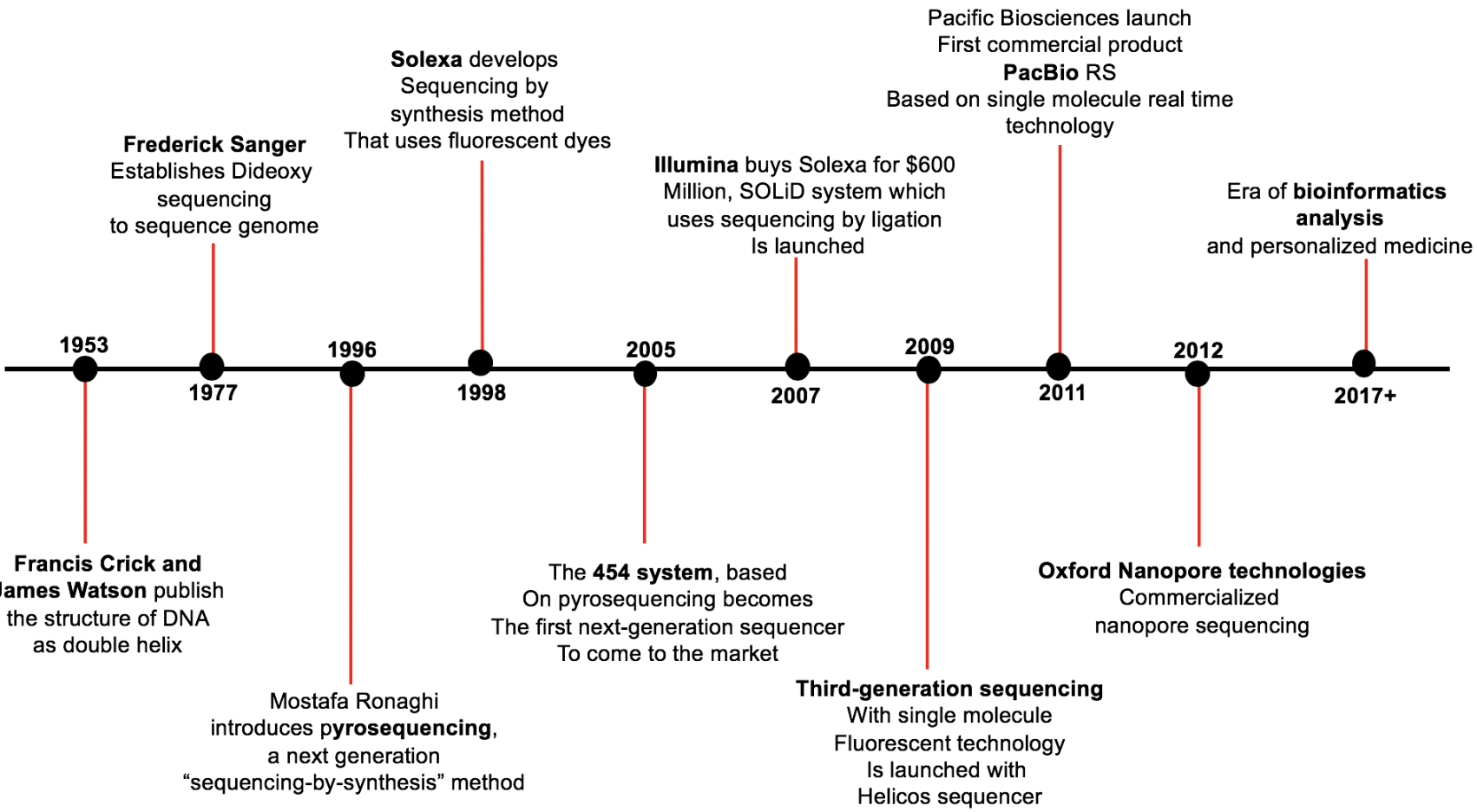
1953
Francis Crick and James Watson publish the structure of DNA as double helix
1977
Frederick Sanger Establishes Dideoxy sequencing to sequence genome
1996
Mostafa Ronaghi introduces p**yrosequencing**, a next generation "sequencing-by-synthesis" method
1998
Solexa develops Sequencing by synthesis method That uses fluorescent dyes
2005
The **454 system**, based On pyrosequencing becomes The first next-generation sequencer To come to the market
2007
Illumina buys Solexa for $600 Million, SOLiD system which uses sequencing by ligation Is launched
2009
Third-generation sequencing With single molecule Fluorescent technology Is launched with Helicos sequencer
2011
Pacific Biosciences launch First commercial product **PacBio** RS Based on single molecule real time technology
2012
Oxford Nanopore technologies Commercialized nanopore sequencing
2017+
Era of **bioinformatics analysis** and personalized medicine

Figure 3.1: A brief history DNA sequencing adapted from Eurofins GATC Biotech GmbH (www.eurofinsgenomics.eu) (310). It highlights the various well-known sequencing methods developed since the structure of the DNA double helix, which was published in 1953. The development of DNA sequencing methods from Sanger sequencing to pyrosequencing and the illumina buying Solexa. It highlights the start of Third-Generation Sequencing in 2009, the first PacBio commercialised in 2011m and the commercialisation of Oxford Nanopore Technologies in 2012. Finally, it highlights the era of bioinformatics analysis, which started in 2017.

Table 3.1: Features and performance of NGS platforms – First Generation Sequencing, Second Generation Sequencing and Third Generation Sequencing. For a better understanding of the NGS outputs, the human genome has $3x10^9$ bp or 3 Gb. (adapted from (303, 307, 311-313)

NGS platforms	Company	Maximum output per run	Read length per run (bp)	No. reads per run	Time (h or days)	Cost per 10^6 bases	Raw error rate (%)	Platform cost (USD approx.)	Chemistry
First Generation Sequencing									
Sanger	Life Technologies	84 kb	800	1	2 h	2400	0.3	95,000	Dideoxy terminator
Second Generation Sequencing									
454 GS FLX+	Roche	0.7Gb	700	$1x10^6$	24/48h	10	1	500,000	Pyrosequencing

GS Junior	Roche	70 Mb	500	$1x10^5$	18 h	9		100,000	Pyrosequencing
HiSeq	Illumina	1500 Gb	2x150	$5x10^9$	27/240 h	0.1	0.8	750,000	Reversible terminators
MiSeq	Illumina	15 Gb	2x300	$3x10^8$	27 h	0.13	0.8	125,000	Reversible terminators
SOLiD	Life Technologies	120 Gb	50	$1x10^9$	14 days	0.13	0.01	350,000	Ligation
Retrovolocity	BGI	3000 Gb	50	$1x10^9$	14 days	0.01	0.01	$12x10^6$	Nanoball/ligation
Ion Proton	Life Technologies	100 Gb	200	$6x10^7$	2-5 h	1	1.7	215,000	Proton detection
Ion PGM	Life Technologies	2 Gb	200	$5x10^6$	2-5 h	1	1.7	80,000	Proton detection
Third Generation Sequencing									
SMRT	Pac Bio	1 Gb	>10,000	$1x10^6$	1-2 h	2	12.9	750,000	Real-time SMS

Heliscope	Helicos	25 Gb	35	$7x10^9$	8 days	0.01	0.2	$1.35x10^6$	Real-time SMS
Electron microscopy	ZS		7200		14 h	<0.01		$1x10^6$	Real-time SMS
Nanopore	Oxford Nanopore Technologies	1 Gb	>5,000	$6x10^4$	48/72 h	<1	34	1000	Real-time SMS

3.3 MinION Sequencing (Oxford Nanopore technologies)

The MinION is the first commercial sequencer form Oxford Nanopore Technologies (ONT). The MinION has provided another leap in the revolution of genome sequencing. MinION sequencing uses electrical conductivity, which is generated as a DNA strand that passes through a biological pore to identify DNA bases. This is the first portable, affordable technology that can be used to produce real-time data (314). The MinION combats the caveat of short reads from previous genome sequencing technologies, by producing longer reads. This was a Sanger Generation Sequencing (SGS) shortfall as de novo genome assembly was relatively poor (314).

The MinION is a small sequencing device (Figure 3.2). It can be plugged into a standard USB3 port on a computer. The MinION produces a lot of data therefore devices with more than 128 GB of hard disk space are recommended. Software called MinKNOW is used to carry out data acquisition, real-time analysis and feedback, data streaming, sample identification, and tracking. This ensures the platform processes the samples correctly (314).

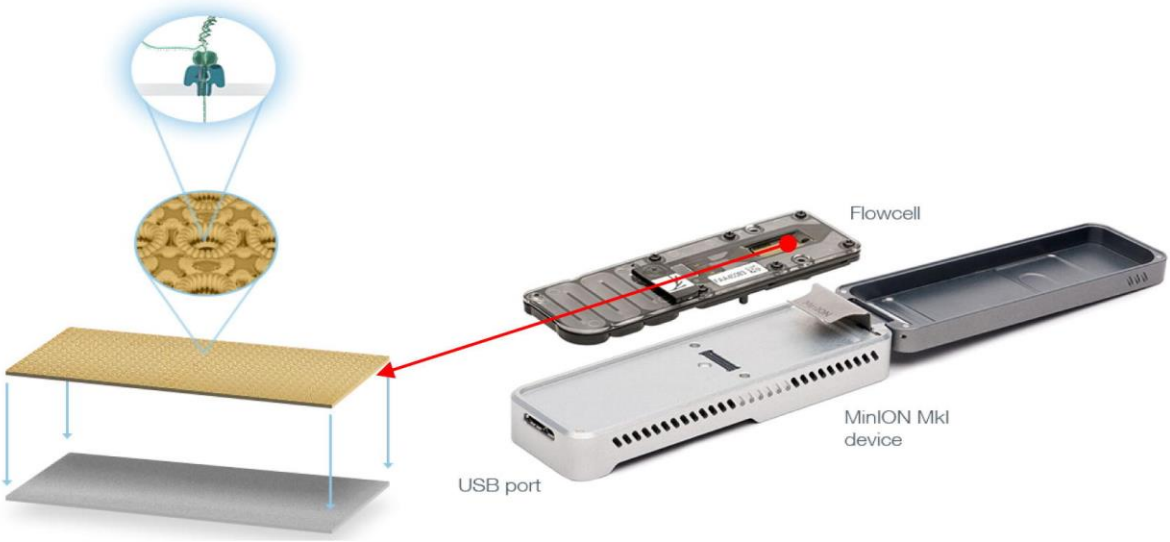

Figure 3.2: The MinION sequencing device taken from (314). The sample is added to the flow cell. Sequencing commences as the DNA molecules pass through the nanopore, a change in the magnitude of the current in the nanopore is measured and registered by the sensor. The data is collected by the software (MinKNOW) and processes it into two categories: 'pass' and 'fail'.

Once the sample was added to the flow cell, DNA sequencing began. When a DNA molecule passes through a nanopore, there is a change in magnitude of the current. This change in magnitude is measured by a sensor several thousand times a second (314). These data streams are passed to the MinKNOW, which generates the signal-level data, acquires the data, and conducts the analysis (314). The experiment runs for 48 – 72 hours. MinKNOW generates FASTA files while the experiment is running, and they are sorted into 'PASS' and 'FAIL'. For a file to 'PASS', the read had a mean Q-value >9. FASTA files that passed were downloaded to a hard drive and subjected to bioinformatics. A Q-value is described as minimum false discovery rate (FDR) (315). A Q-value is an adjusted P-value that uses the

FDR approach. Whilst the P-value takes into account all samples when discovering which are false prostives, Q-values take into account only tests with Q-values less than a specific threshold (in the case of this thesis Q-value of <0.05). This gives a far more accurate indication of the level of false positives (315).

The potential of the MinION sequencing was tested during the biggest Ebola outbreak in West Africa, which was responsible for over 28,599 cases and over 11,000 deaths (316). During an epidemic, genome sequencing is crucial as it provides information on the evolution of the pathogen and provides information to implement public health guide control measures (316). During an epidemic, genome surveillance has not been easily attained due to cost and practicality of the setting and equipment. The MinION sequencer provided a platform from which real-time genomic surveillance was implemented during an outbreak. Over one hundred positive Ebola samples were sequenced, and results were generated less than 24 hours after receipt of the positive sample. This showed the innovative potential of the MinION sequencer in resource-limited settings to monitor outbreaks. It was used to understand viral evolution, track and investigate transmission chains, and validate other diagnostic assays (314, 316-319).

3.4 RESULTS

As previously stated, the aim of this chapter was to characterise IAV H3N2 in a well-controlled *in vitro* cell culture system (A549 cells were used). Two independent approaches were used to investigate changes in protein and transcript abundance. A combination of these methods would give an overarching insight into host changes. Mass spectrometry was used to characterise the proteome of A549 cells infected with IAV compared to mock infected cells. MinION sequencing was used to characterise the global transcriptome. Finally, other techniques (immunofluorescence and SDS-PAGE) were used to validate the data and add to the findings from mass spectrometry and MinION sequencing. A549 cells were infected with IAV and the supernatant collected at the time points 3h.p.i, 6h.p.i, 9h.p.i, 12h.p.i, 18h.p.i, 24h.p.i, 36h.p.i, and 48h.p.i. The virus in the supernatant was quantified using avicel plaque assay (2.4%) (254). Following this, an informed decision was made when choosing a time point that would be used for subsequent proteomics and transcriptomics experiments. 18h.p.i was selected as the most suitable time point.

3.5 Characterisation and quantification of IAV in MDCK cells at time points post infection; 3h.p.i, 6h.p.i, 9h.p.i, 12h.p.i, 18h.p.i, 24h.p.i, 36h.p.i, 48h.p.i, and non-infected (mock)

Avicel plaque assay was used to characterise and quantify IAV at different time points. A549 cells were infected with IAV at MOI 1 and observed following figure 3.3. After the specified time points, the supernatants were collected and stored at -80°C. MDCK cells were then set up to quantify the IAV in these

supernatants using the avicel plaque assay. Two biological replicates were conducted, following the protocol described in the material and methods in Chapter 2 and following the workflow in Figure 3.3. After 72 hours, the plates were fixed with ice-cold acetone – methanol – and then stained with crystal violet (Figure 3.4). SDS-PAGE (Figure 3.5) and immunofluorescence staining (Figure 3.6) were used to confirm the presence of IAV in A549 cells at 6h.p.i, 12h.p.i, 18h.p.i, and 24h.p.i.

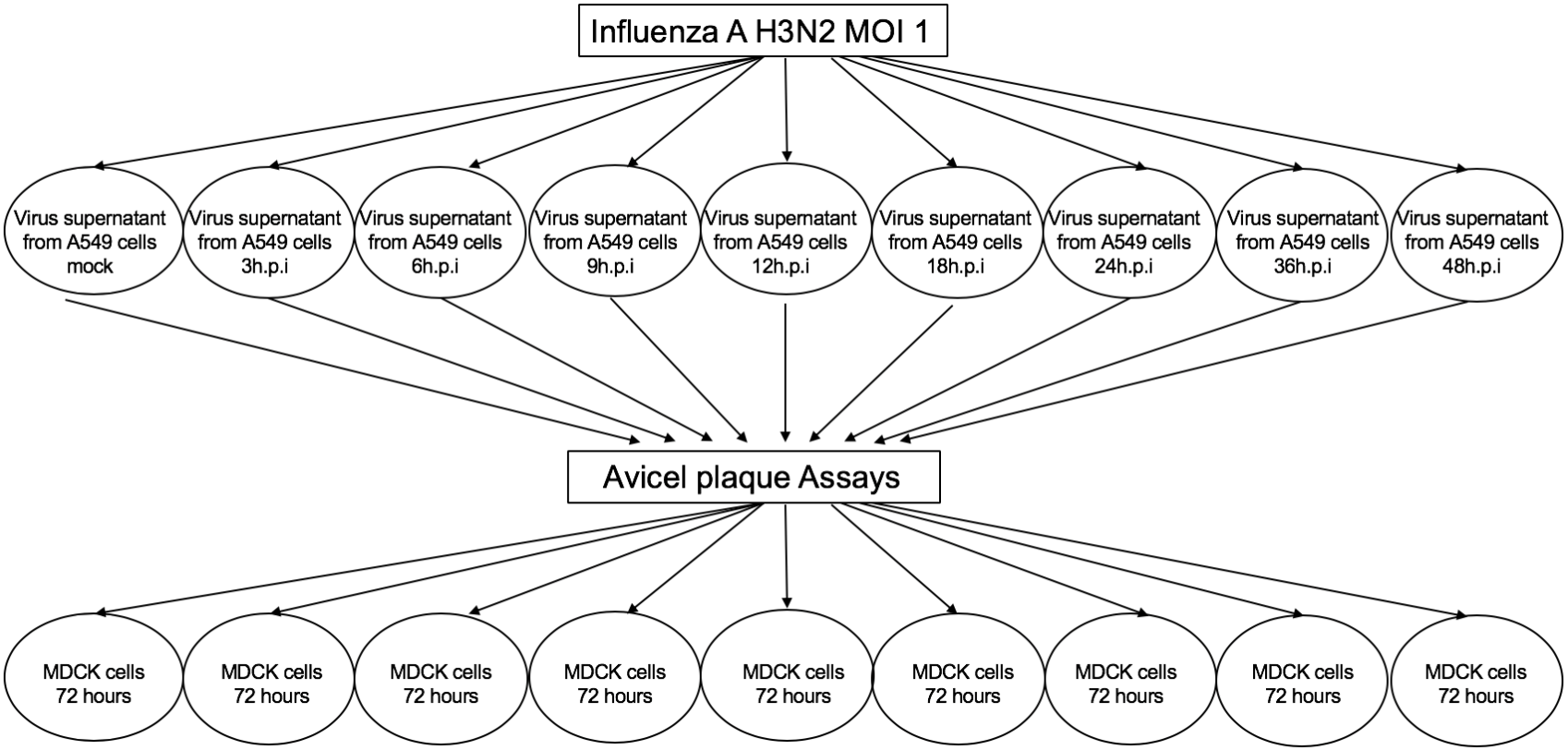
Influenza A H3N2 MOI 1
Virus supernatant from A549 cells mock
Virus supernatant from A549 cells 3h.p.i
Virus supernatant from A549 cells 6h.p.i
Virus supernatant from A549 cells 9h.p.i
Virus supernatant from A549 cells 12h.p.i
Virus supernatant from A549 cells 18h.p.i
Virus supernatant from A549 cells 24h.p.i
Virus supernatant from A549 cells 36h.p.i
Virus supernatant from A549 cells 48h.p.i
Avicel plaque Assays
MDCK cells 72 hours
MDCK cells 72 hours
MDCK cells 72 hours
MDCK cells 72 hours
MDCK cells 72 hours
MDCK cells 72 hours
MDCK cells 72 hours
MDCK cells 72 hours
MDCK cells 72 hours

Figure 3.3: Progression of workflow from obtaining IAV supernatant from A549 cells in six-well plates after infection 3h.p.i, 6h.p.i, 9h.p.i, 12h.p.i, 18h.p.i, 24h.p.i, 36h.p.i, 48h.p.i, and non-infected (mock). The virus in these supernatants were quantified via avicel plaque assay. MDCK cells were used for the avicel plaque assay and inoculated with the respective viral supernatants. This inoculum was adsorbed after one hour and the cells were covered with an avicel overlay for 72 hours.

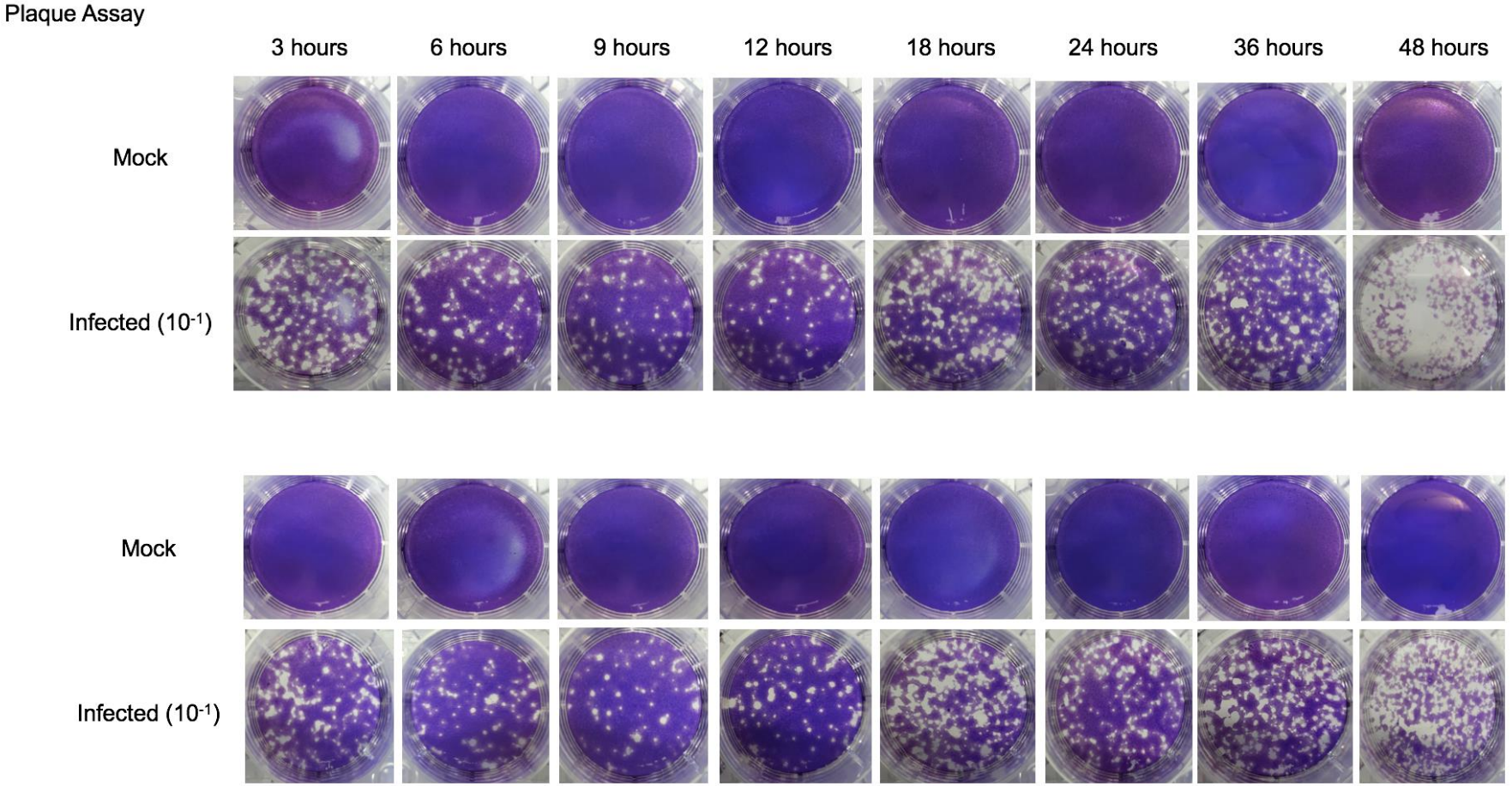
Plaque Assay
3 hours
6 hours
9 hours
12 hours
18 hours
24 hours
36 hours
48 hours
Mock
Infected (10^{-1})
Mock
Infected (10^{-1})

Figure 3.4: Avicel plaque assay of MDCK cells mock infected and infected with viral supernatant at 3h.p.i, 6h.p.i, 9h.p.i, 12h.p.i, 18h.p.i, 24h.p.i, 36h.p.i, and 48h.p.i. A virus dilution of 10^{-1} was used to infect the cells. After 72 hours, the cells were fixed with acetone – methanol – and stained with crystal violet. The plaques formed by the infectious viral particle are clearly visible at different time points in comparison to the mock-infected samples. This experiment was repeated twice for biological repeats.

3.6 Confirming and validating IAV in A549 cells infected at MOI 1 at 6h.p.i, 12h.p.i, 18h.p.i and 24h.p.i, compared to mock infected cells via SDS-PAGE

To assess virus-host cell interactions post infection, A549 cells were infected with the IAV X31 strain. The time points post infection 6h.p.i, 12h.p.i, 18h.p.i, and 24h.p.i were selected and compared to the mock-infected (M) cells, following the results from the plaque assay in Figure 3.4 and based on previous H3N2 swine influenza proteomics studies (219, 320). This allowed the viral infection process to be monitored by observing the NP viral protein and comparing it to the mock infected cells. MOI 1 was used to infect cells.

Proteins from these samples were extracted and the protein concentration was obtained using a BCA assay. The proteins extracted from the cells at different time points were separated by SDS-PAGE. Equal volumes and concentrations (8 μg/μl) of protein were loaded in each well. This allowed for visual comparison of relative abundance between these samples. Glyceraldehyde 3-phosphate dehydrogenase (GAPDH) was used as a

loading control. The influenza NP antibody, which is an IAV viral protein, is located within the nucleus of cells and used as a marker of infection (226) (Figure 3.5). The NP antibody (Chapter 2, Table 2.4) marker showed the NP protein abundance changed over the time post-infection. No viral protein was detected in the mock-infected cells. Cells collected at 24h.p.i showed a higher abundance of NP antibody markers compared to cells collected at 6h.p.i. There was a progressive increase in abundance of the viral protein NP from the times 6h.p.i, 12h.p.i, 18h.p.i, and 24h.p.i (Figure 3.6). Cells from which the cell lysate was collected 48 hours post infection showed visible signs of cell death and cytopathic effect (CPE) (data not shown).

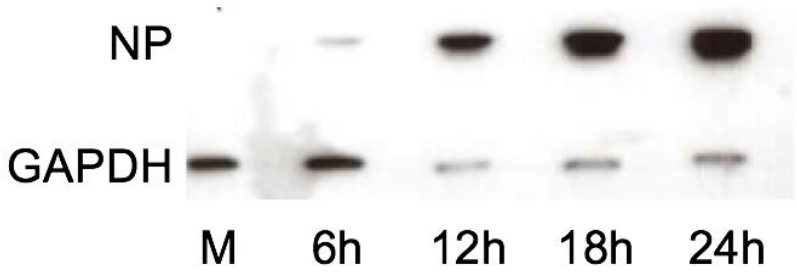

Figure 3.5: A549 cells were mock-treated (M) and infected with IAV X-31 at MOI 1. The cell lysates were strategically prepared and collected at 6h.p.i, 12h.p.i, 18h.p.i, 24h.p.i and compared to mock (M) infected cells. The NP antibody marker was used as an IAV marker and GAPDH antibody marker was used as a loading control.

3.7 Visualising IAV infection in A549 cells and mock-treated cells at MOI 1 and at 6 hours, 12 hours, 18 hours and 24 hours post infection via immunofluorescence staining

Immunofluorescence analysis was used to monitor the viral infection in A549 cells over the time frame – 6h.p.i, 12h.p.i, 18h.p.i, and 24h.p.i, and compared it to mock infected cells (Figure 3.6). The NP antibody was used as the marker of IAV infection in the immunofluorescence protocol. This protocol was elaborated in the materials and methods (Chapter 2).

Immunofluorescence
6 hours

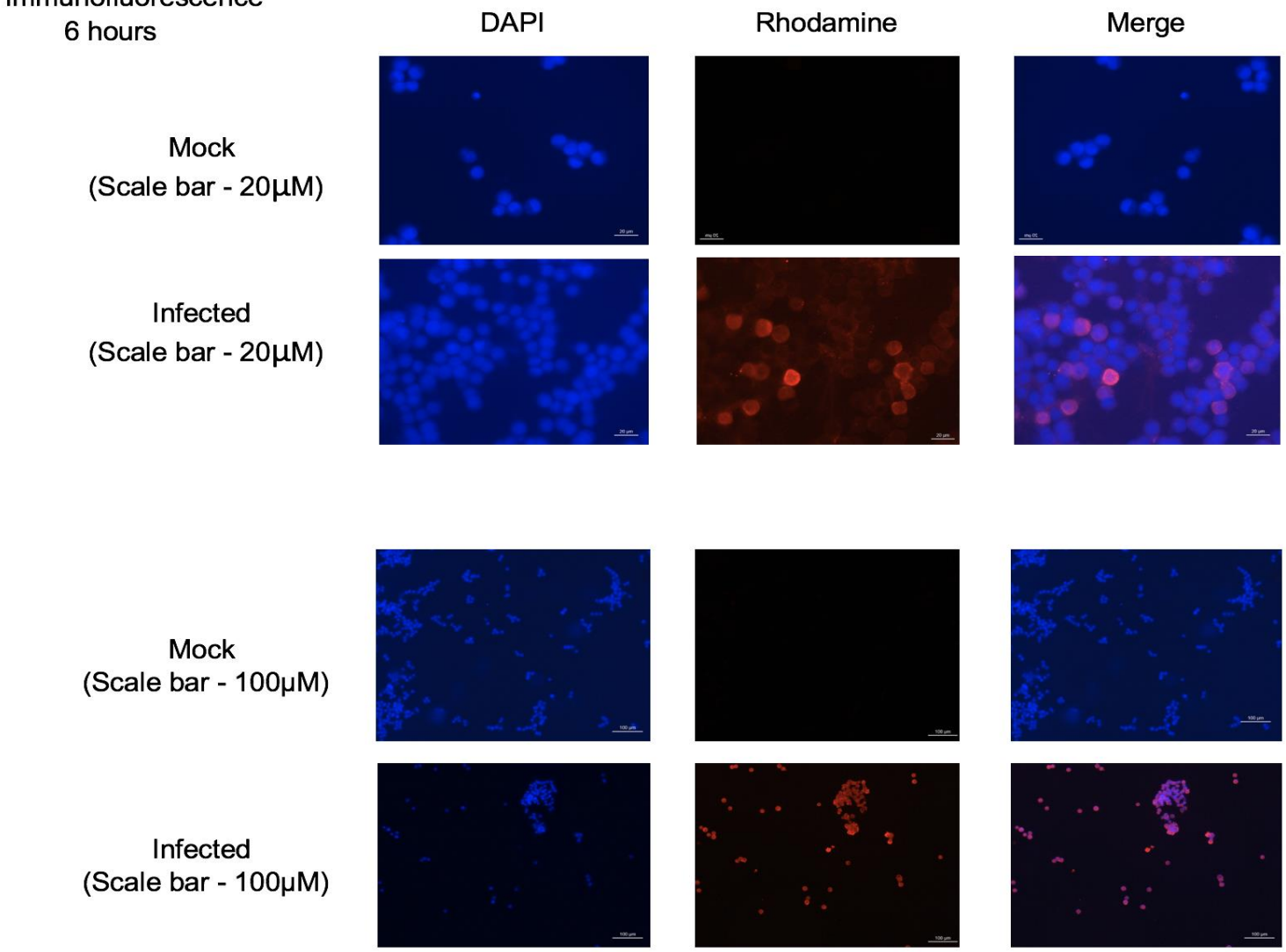

Immunofluorescence
12 hours

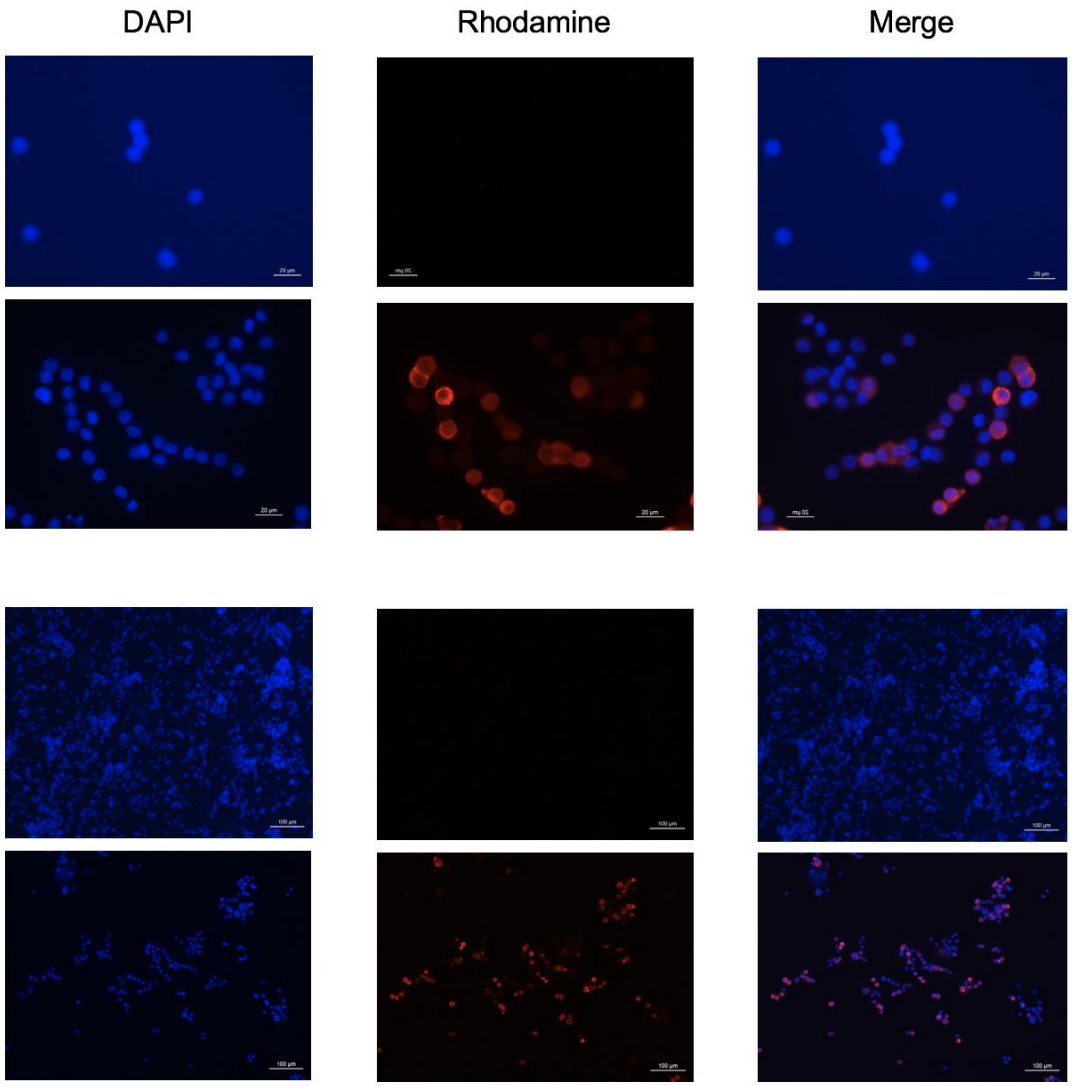

Immunofluorescence
18 hours

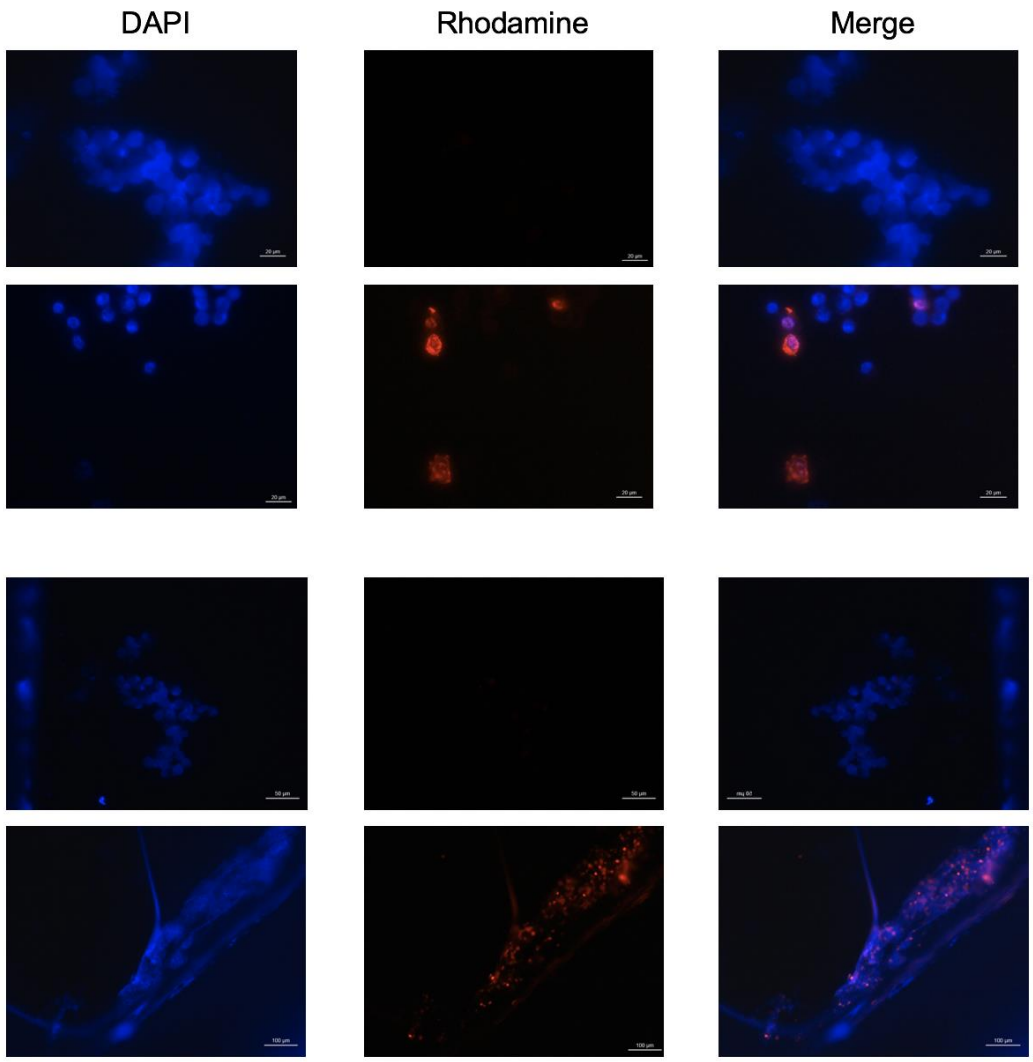

Immunofluorescence
24 hours

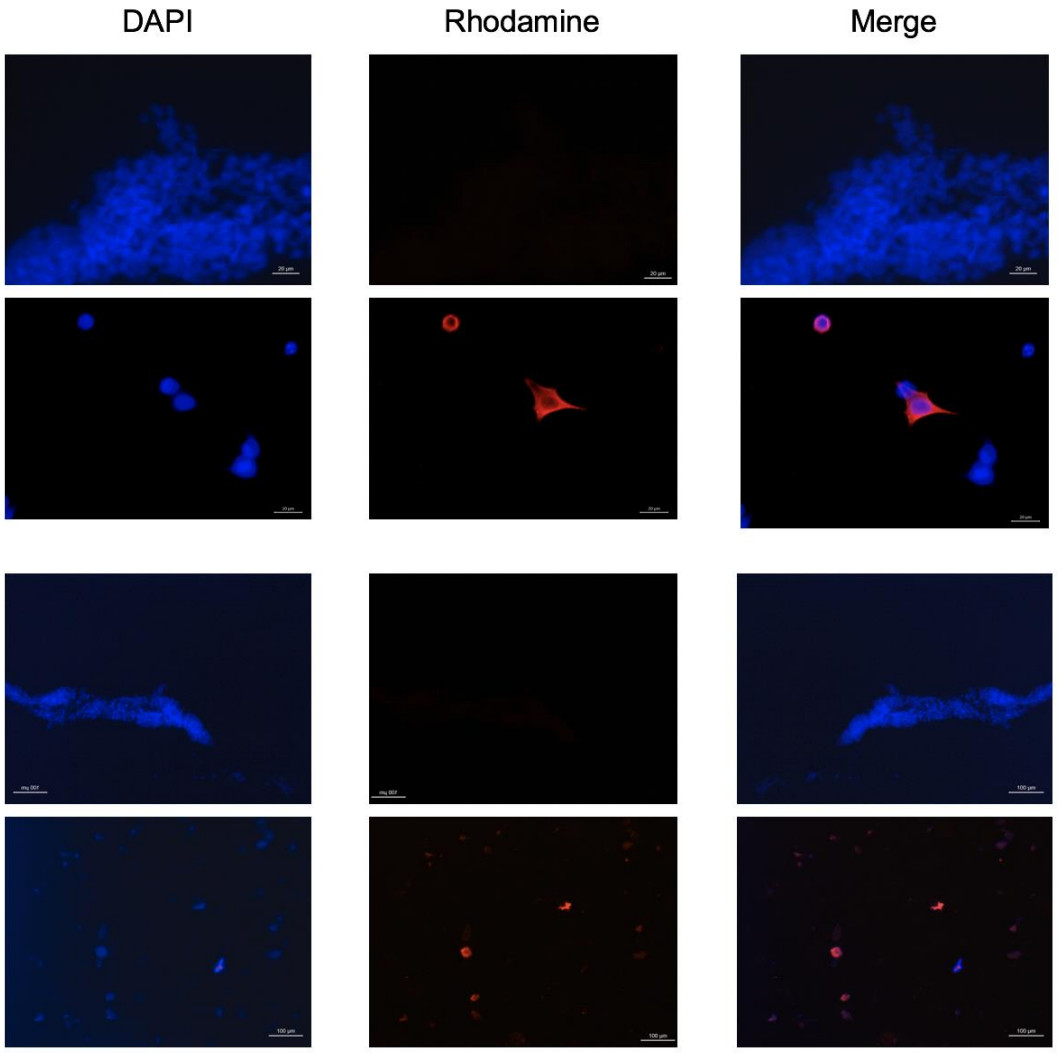

Figure 3.6: A549 cells mock-treated and IAV X-31 infected at MOI 1 at 6h.p.i, 12h.p.i, 18h.p.i, and 24h.p.i post infection. Cells were stained with the Influenza NP antibody (Table 2.4, Chapter 2), a marker protein located within the nucleus of the cells. The nucleus was stained blue with DAPI. The NP protein was stained red with Rhodamine. Both channels were merged and the NP in the nucleus was visible. The images of cells were taken from two different viewpoints providing; a far view (scale bar – 100μm) and a magnified view (scale bar – 20μm).

The results from these experiments outline IAV infection over time through the avicel plaque assay (Figure 3.4), validation via SDS-PAGE (Figure 3.5) and immunofluorescence staining (Figure 3.6) points towards 18h.p.i as the preferred time point for further analysis by label-free mass spectrometry and MinION sequencing.

3.8 Label-free mass spectrometry analysis and MinION sequencing on A549 cells infected with IAV X31 at MOI 1 and analysed 18 hours post infection

Label-free mass spectrometry was used to gain a global overview of the cellular proteome changes post IAV infection. The A549 cell line was mock-infected and IAV X31 infected at MOI 1 and analysed at 18h.p.i following the workflow in Figure 3.7. The results from these experiments were compared to understand the difference in cellular proteome between infected and non-infected cells. This dataset was further analysed by bioinformatics using the software, Ingenuity Pathway Analysis (IPA). To validate the data from these experiments, another technique was used. This was the MinION sequencing. A549 cells were mock infected and IAV X31 infected at MOI 1 and collected at 18h.p.i. The RNA was extracted from these samples and subjected to MinION sequencing. The data from the MinION sequencing was analysed using a differential gene expression analysis. The transcripts that were found to be differentially expressed in infected, compared to non-infected, cells confirmed the data from the label-free mass spectrometry. These datasets were further analysed using ingenuity pathway analysis (IPA). This analysis teased out and connected the proteins according to function and linked them to already identified proteins in the literature. These datasets gave high confidence to findings from mass spectrometry and when comparing them to similar studies in the literature and *in vivo* studies (Chapters 4 and 5).

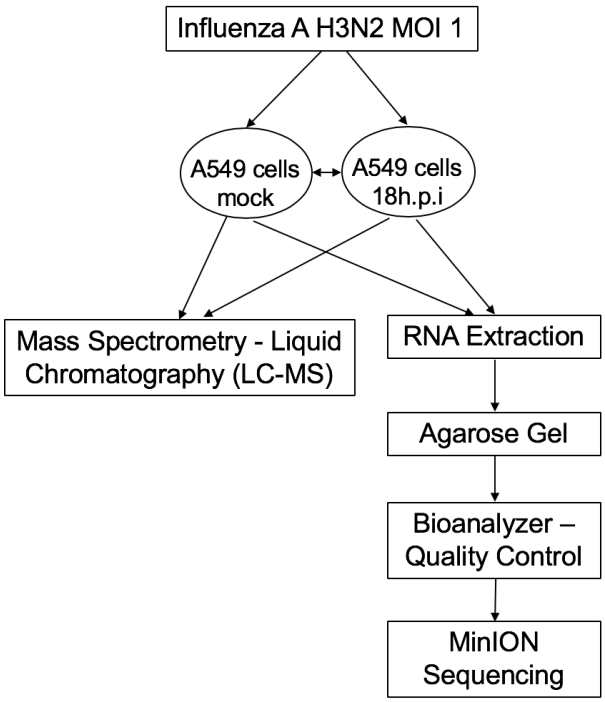

Figure 3.7: Progression of workflow and techniques for the processing of proteins and RNA from mock-infected and IAV X31-infected A549 samples at MOI 1 at 18h.p.i. Protein samples were subjected to the mass spectrometry platform; Q-Exactive for label-free proteomics and further data analysis was done via Bioinformatics – Ingenuity Pathway Analysis (IPA). RNA was extracted from cells and the concentration obtained via nanodrop and Qubit. RNA samples ran on an agarose gel to check for integrity by visualising 18S and 28S bands. These samples were then subjected to the Bioanalyser for further validation. After this, RNA samples were subjected to the MinION for sequencing.

3.9 Identification of cellular proteome of IAV infected A549 cells at MOI 1 and 18h.p.i via label-free mass spectrometry

Label-free proteomics was used to obtain an unbiased global view of the changes that occur in a host cell proteome after IAV X31 infection. The A549 cell line was mock-infected and IAV X31 infected at MOI 1, collected at 18h.p.i. The whole cell lysates were collected and subjected to the Q-Exactive LC-MS platform. This experiment was repeated twice (biological replicates). Data from biological replicates could be compared and also provide high confidence in this dataset. The dataset obtained from the first run produced over a thousand cellular and viral proteins that were detected and quantified. In the dataset from the second run, over three thousand cellular and viral proteins were detected and quantified.

3.10 Identification and quantification of cellular and viral proteins in host-viral interaction

The analysis of the dataset included several processing steps to increase confidence in the identified proteins. These processing steps included proteins with two or more peptides, proteins with a log two-fold change of +/- one or two and above, proteins with a p-value of <0.05 and proteins with a q-value of <0.05. A combination of these data-processing steps was used to process the data from the two biological repeats from the Q-Exactive. This increases the probability of correctly identifying proteins. These data-processing steps are widely used in the study of virus host interactions. However, many of the proteins identified by single peptides were also of interest and are included in the full data tables present in the appendices (321-

324).

In the first biological repeat, proteins identified with two or more peptides, proteins with a log two-fold change of +/- 2 and above and proteins with a p-value <0.05 were selected to be significantly different (325). In the second biological repeat, proteins identified with two or more peptides, proteins with a log two-fold change of +/- one and above and proteins with a q-value < 0.05 were selected to be significantly different. It is worth noting that these biological repeats were carried out three years apart. Similar proteins and the pathways involved were identified between the datasets from the two biological repeats. Nonetheless, slightly different data processing tools were utilised. This is as a result of advances in the data analysis processes when using high throughput techniques, such as mass spectrometry.

The quantitative proteomic analysis of the first biological repeat identified up to 1283 cellular and viral proteins. These proteins were obtained by comparing mock-infected samples to IAV X31 infected samples. This data set was quantified, analysed and provided the protein abundance changes which occurred following IAV X31 infection. The degree of change in abundance was represented by log two-fold change per protein. To increase confidence in the datasets, the data processing steps highlighted above were implemented. To reiterate, these steps were: proteins identified with two or more peptides, proteins with a log 2-fold change of +/- 2 and above, proteins with a p-value $<$ 0.05. The results after these data processing steps are detailed in Tables 3.2 and 3.3.

The quantitative proteomic analysis of the second biological repeat identified up to 3,361 cellular and viral proteins. These proteins were obtained by comparing mock-infected samples to IAV X31-infected samples. This data set was quantified, analysed and provided the protein abundance changes, which occurred following IAV X31 infection. The degree of change in abundance was represented by log two-fold change per protein. To increase confidence in the datasets, the data processing steps highlighted above were implemented. To reiterate, these steps were: proteins identified with two or more peptides, proteins with a log two-fold change of +/- 1 and above, and proteins with a q-value $<$ 0.05 to be significantly different. The results after these data processing steps are detailed in Tables 3.4 and 3.5.

3.11 Identification and quantification of proteins that were differentially abundant in the first biological repeat

The dataset was analysed on MaxQuant software and the data processing steps described above were used to increase confidence in the highlighted data. Proteins were grouped based on their increase or decrease in abundance when comparing the mock-infected to the IAV X31-infected cells. The dataset revealed 33 proteins, which significantly increased in abundance and 58 proteins, which significantly decreased in abundance. These proteins are presented in Table 3.2 and 3.3.

Table 3.2: 33 proteins identified in the first biological replicate by Q-Exactive Mass Spectrometry, followed by data processing steps, have significantly increased in abundance when comparing mock-infected cells to IAV X31-infected cells. The log two-fold change, the number of peptides (Pep.), and the proteins biological process are shown below using GO via uniprot: http://www.uniprot.org and (326).

33 proteins that significantly increased in abundance when comparing IAV X31 infected cells to mock-infected cells						
Uniprot Accession ID	**Gene ID**	**Protein Name**	**Function**	**Peptides for Quantification**	**Fold Change (Log 2)**	**Peptide Count**
O14879	IFIT3_HUMAN	Interferon- induced protein with tetratricopeptide repeats 3	Interferon-induced antiviral protein. Inhibitor of cellular and viral processes, cell migration, proliferation, signalling and viral replication	5	10.1	5
P20591	MXI_HUMAN	Myxovirus host protein (MX1)	Interferon-induced dynamin-like GTPase. Antiviral activity against RNA and DNA viruses	9	7.8	9
P20592	MX2_HUMAN	Myxovirus host protein (MX2)	Interferon-induced dynamin-like GTPase. Effective antiviral activity	9	7.8	9

			against human immunodeficiency virus type I.			
P09913	IFIT2_HUMAN	Interferon-induced protein with tetratricopeptide repeats 2	Interferon-induced antiviral protein. Inhibits expression of viral messenger RNAs lacking 2'-methylation of the 5' cap.	3	7.1	3
Q08945	SSRP1_HUMAN	Structure specific recognition protein 1	Component of FACT complex. General chromatin factor acting in reorganising nucleosomes	2	3.7	2
P31944	CASPE_HUMAN	Caspase-14	Non-apoptotic caspase involved in epidermal differentiation	2	3.5	2
Q86YZ3	HORN_HUMAN	Ig mu chain C region, secreted splice from - human	Transcription	9	3.4	9
P05089	ARGI1_HUMAN	Arginase	Arginase Activity	2	2.9	2
P29590	PML_HUMAN	Promyelocytic leukaemia protein	Functions in tumour suppression, transcription regulation, apoptosis,	2	2.9	3

			senescence, DNA damage response and viral mechanism			
P31689	DNJA1_HUMAN	DnaJ-like protein subfamily A member 1	Interacts with Hsp70. Stimulate ATPase activity.	2	2.7	3
Q01130	SRSF2_HUMAN	Serine/arginine-rich splicing factor 2	Necessary for splicing of pre-mRNA	3	2.5	3
Q9BRL6	SRSF8_HUMAN	Serine/arginine-rich splicing factor 8	Involved in pre-mRNA alternative splicing	3	2.5	3
P84103	SRSF3_HUMAN	Serine/arginine-rich splicing factor 3	Splicing factor	4	2.5	5
P49773	HINT1_HUMAN	Histidine triad nucleotide-binding protein 1	Modulates p53/TP53 levels	2	2.5	2
P63167	DYL1_HUMAN	Dynein light chain 1, cytoplasmic	Plays a role in the nuclear localisation of ESR1	2	2.3	2
Q02413	DSG1_HUMAN	Desmoglein-1	Component of intercellular desmosome junctions	2	2.3	2

Q07000	1C15_HUMAN	HLA class I histocompatibility antigen, cw-15 alpha chain	Involved in the presentation of foreign antigens to the immune system	3	2.2	3
P01892	1A02_HUMAN	HLA class 1 histocompatibility antigen, A-2 alpha chain	Involved in the presentation of foreign antigens to the immune system	3	2.2	3
P01893	HLAH_HUMAN	Putative HLA class I histocompatibility antigen, alpha chain H	Involved in the presentation of foreign antigens to the immune system	3	2.2	3
P05534	1A24_HUMAN	HLA class I histocompatibility antigen, A-24 alpha chain	Involved in the presentation of foreign antigens to the immune system Involved in the presentation of foreign antigens to the immune system	3	2.2	3
P10321	1C07_HUMAN	HLA class I histocompatibility antigen, Cw-7 alpha chain	Involved in the presentation of foreign antigens to the immune system	3	2.2	3
P13746	1A11_HUMAN	HLA class I histocompatibility antigen, A-11 alpha chain	Involved in the presentation of foreign antigens to the immune system	3	2.2	3
P18463	1B37_HUMAN	HLA class I histocompatibility antigen, B-37 alpha chain	Involved in the presentation of foreign antigens to the immune system	3	2.2	3

P30447	1A23_HUMAN	HLA class I histocompatibility antigen, A-23 alpha chain	Involved in the presentation of foreign antigens to the immune system	3	2.2	3
P30460	1B08_HUMAN	HLA class I histocompatibility antigen, B-8 alpha chain	Involved in the presentation of foreign antigens to the immune system	3	2.2	3
P30499	1C01_HUMAN	HLA class I histocompatibility antigen, Cw-1 alpha chain	Involved in the presentation of foreign antigens to the immune system	3	2.2	3
Q29718	1B82_HUMAN	HLA class I histocompatibility antigen, B-82 alpha chain	Involved in the presentation of foreign antigens to the immune system	3	2.2	3
Q29940	1B59_HUMAN	HLA class I histocompatibility antigen, B-59 alpha chain	Involved in the presentation of foreign antigens to the immune system	3	2.2	3
P30046	DOPD_HUMAN	D-dopachrome decarboxylase	Tautomerization of D-dopachrome with decarboxylation to give 5,6-dihydroxyindole	2	2.1	2
P18124	RL7_HUMAN	60S ribosomal protein L7	Binds to G-rich structures in 28S rRNA and in mRNAs	9	2.1	9
P81605	DCD_HUMAN	Dermcidin	Displays antimicrobial activity	2	2.0	2

Q86VP6	CAND1_HUMAN	Cullin-associated NEDD8-dissociated protein 1	Cell differentiation	2	2.0	2
O75874	IDHC_HUMAN	Isocitrate dehydrogenase (NADP) cytoplasmic	Response to oxidative stress	2	2.0	2

Table 3.3: 58 proteins identified in the first biological replicate by Q-Exactive Mass Spectrometry, followed by data processing steps have significantly decreased in abundance when comparing mock-infected cells to IAV X31-infected cells. The log two-fold change, the number of peptides (Pep.), and the proteins' biological process are shown below using GO via uniprot: http://www.uniprot.org and (326).

58 proteins that significantly decreased in abundance when comparing IAV X31 infected cells to mock-infected cells						
Uniprot accession ID	**Gene ID**	**Protein Name**	**Function**	**Peptides for Quantification**	**Fold Change (Log 2)**	**Peptide Count**
P16144	ITB4_HUMAN	Integrin Beta 4	Critical structural role in the hemidesmosome of epithelial cells	2	8.3	3
Q14116	IL18_HUMAN	Interleukin 18	Increases natural killer cell activity in spleen cells. Stimulates interferon gamma	2	5.5	2

			production in T-helper type cells			
Q96PK6	RBM14_HUMAN	RNA binding motif protein 14	Nuclear receptor coactivator and enhancing transcription	2	5.3	2
Q13740	CD166_HUMAN	CD166 antigen homolog	Cell adhesion molecule that binds to CD6	7	3.7	7
O00468	AGRIN_HUMAN	Agrin	Basal lamina glycoprotein plays a central role in formation and maintenance of neuromuscular junction (NMJ)	2	3.6	2
Q43570	CAH12_HUMAN	Carbonic anhydrase 12	Hydration of carbon dioxide (Reversible)	2	3.2	2
Q8NFJ5	RAI3_HUMAN	Retinoic acid induced 3	Modulating differentiation and maintaining homeostasis in epithelial cells	3	3.2	3
Q00341	VIGLN_HUMAN	Vigilin	Cell protection from over-accumulation of cholesterol	2	3.1	2

Q12860	CNTN1_HUMQN	Contactin 1	Mediate cell surface interactions during nervous system development	11	2.9	11
Q15056	IF4H_HUMAN	Eukaryotic translation initiation factor 4H	Stimulates the RNA helicase activity of EIF4A in the translation initiation complex	4	2.9	4
Q8NBJ4	GOLM1_HUMAN	Golgi membrane protein 1	Cellular response protein to viral infection	5	2.9	5
P98179	RBM3_HUMAN	RNA-binding protein 3	Reduces the relative abundance of microRNAs	4	2.9	4
Q9C005	DPY30_HUMAN	Protein dpy-30 homolog	May play some role in histone H3 acetylation	2	2.8	2
Q9HC84	MUC5B_HUMAN	Mucin – 5B	Gel forming mucin rich, contributes to lubricating and viscoelastic properties of saliva and cervical mucus	16	2.8	18

O15230	LAMA5_HUMAN	Laminin subunit alpha - 5	Binding to cells via high affinity receptor, mediates attachment, migration and organisation of cells	3	2.7	3
P62633	CNBP_HUMAN	Cellular nucleic acid-binding protein	Single-stranded DNA binding protein	4	2.7	4
P04844	RPN2_HUMAN	Dolichyl-diphosphooligosaccharide-protein glycosyltransferase subunit 2	Essential subunit of the N-oligosaccharyl transferase (OST) complex	4	2.6	6
P49756	RBM25_HUMAN	RNA-binding protein 25	RNA – binding protein that acts as a regulator of alternative pre-mRNA splicing	2	2.5	2
Q71DI3	H32_HUMAN	Histone H3.2	Core component of nucleosome	2	2.5	5

Q96PD2	DCBD2_HUMAN	Discoidin, CUB and LCCL domain-containing protein 2	Intracellular receptor signalling pathway	3	2.5	3
Q9BWF3	RBM4_HUMAN	RNA-binding protein 4	RNA-binding factor involved in multiple aspects of cellular processes like alternative splicing of pre-mRNA and translation regulation	3	2.4	3
Q9BVJ6	UT14A_HUMAN	U3 small nucleolar RNA-associated protein 14 homolog A	May be required for ribosome biogenesis	6	2.4	6
Q5TAP6	UT14C_HUMAN	U3 small nucleolar RNa-associated protein 14 homolog C	Essential for spermatogenesis	6	2.4	6
P30049	ATPD_HUMAN	ATP synthase subunit delta, mitochondrial	Proton-transporting ATP synthase activity, rotational mechanism	2	2.4	2

Q68CZ2	TENS3_HUMAN	Tensin-3	May play a role in actin remodelling	3	2.4	4
P23246	SFPQ_HUMAN	Splicing factor, proline and glutamine rich	DNA and RNA binding protein involved in several nuclear processes	9	2.4	10
O60763	USO1_HUMAN	General vesicular transport factor p115	Act as a vesicular anchor	4	2.3	5
Q5JTJ3	COA6_HUMAN	Cytochrome C oxidase assembly factor 6 homolog	Involved in the maturation of the mitochondrial respiratory chain complex IV subunit	5	2.3	5
P98088	MUC5A_HUMAN	Mucin 5AC	Gel forming glycoprotein of gastric and respiratory tract epithelia that protects the mucosa from infection	9	2.3	9
P20290	BTF3_HUMAN	Transcription factor BTF3	When associated with NACA prevents inappropriate targeting of non-secretory	4	2.3	5

			polypeptides to the endoplasmic reticulum (ER)			
Q13242	SRSF9_HUMAN	Serine/arginine-rich splicing factor 9	Plays a role in constitutive splicing and can modulate the selection of alternative splice sites	3	2.3	3
Q00325	MPCP_HUMAN	Phosphate carrier protein, mitochondrial	Transport of phosphate groups from the cytosol to the mitochondrial matrix	2	2.3	2
Q9Y2W2	WBP11_HUMAN	WW domain-binding protein 11	Activates pre-mRNA splicing	3	2.3	3
Q03701	CEBPZ_HUMAN	CCAAT/enhancer-binding protein zeta	Stimulates transcription from the HSP70 promoter	3	2.3	3
O60869	EDF1_HUMAN	Endothelial differentiation-related factor 1	Regulates nitric oxid synthase activity	2	2.3	2
P60866	RS20_HUMAN	40S ribosomal protein S20	Poly (A) RNA binding	2	2.2	2

P28799	GRN_HUMAN	Granulins	Granulins have possible cytokine-like activity	7	2.2	8
Q14247	SRC8_HUMAN	Src substrate cortactin	Contributes to the organization of the actin cytoskeleton and cell shape	10	2.2	11
Q9UKV3	ACINU_HUMAN	Apoptotic chromatin condensation inducer in the nucleus	Auxiliary component of the splicing-dependent multiprotein exon junction complex (EJC)	7	2.1	8
Q14061	COX17_HUMAN	Cytochrome c oxidase copper chaperone	Copper chaperone for cytochrome c oxidase (COX)	2	2.1	2
Q9ULD2	MTUS1_HUMAN	Microtubule-associated tumour suppressor 1	Cooperates with AGTR2 to inhibit ERK2 activation and cell proliferation	3	2.1	3
P05067	A4_HUMAN	Amyloid beta A4 protein	Cell surface receptor	6	2.1	6
Q9P0K7	RAI14_HUMAN	Ankycorbin	Actin cytoskeleton	3	2.0	6

Q15233	NONO_HUMAN	Non-Pou domain-containing octamer-binding protein	DNA and RNA binding protein involved in several nuclear processes	5	2.0	6
Q6UN15	FIP1_HUMAN	Pre-mRNA 3' end processing factor FIP1	Component of the cleavage and polyadenylation specificity factor (CPSF)	3	2.0	4
Q16891	IMMT_HUMAN	MICOS complex subunit MIC60	Plays an important role in the maintenance of the MICOS complex	21	2.0	22
Q9HC35	EMAL4_HUMAN	Echinoderm microtubule-associated protein-like 4	May modify the assembly dynamics of microtubules	2	2.0	2
P46976	GLYG_HUMAN	Glycogenin-1	Self-glucosylates	3	2.0	3
O75976	CBPD_HUMAN	Carboxypeptidase D	Metallocarboxypeptidase activity	9	2.0	9
Q9GZU8	F192A_HUMAN	Protein FAM192A	Post translation modification	2	2.0	2

P16070	CD44_HUMAN	CD44 antigen	Receptor for hyaluronic acid (HA)	7	2.0	7
P68431	H31_HUMAN	Histone H3.1	Core component of nucleosome	2	2.0	5
P11940	PABP1_HUMAN	Polyadenylate-binding protein 1	Binds the poly (A) tail of mRNA	6	2.0	7
Q13310	PABP4_HUMAN	Polyadenylate-binding protein 4	Binds the poly (A) tail of mRNA	6	2.0	7
Q9H361	PABP3_HUMAN	Polyadenylate-binding protein 3	Binds the poly (A) tail of mRNA	6	2.0	7
P20073	ANXA7_HUMAN	Annexin A7	Calcium/phospholipid binding protein which promotes membrane fusion and is involved in exocytosis	3	2.0	3
P33240	CSTF2_HUMAN	Cleavage stimulation factor subunit 2	One of the multiple factors required for polyadenylation	4	2.0	4

			and 3’end cleavage of mammalian pre-mRNA			
Q9H0L4	CSTFT_HUMAN	Cleavage stimulation factor subunit 2 tau variant	Significant role in AAUAAA-independent mRNA polyadenylation in germ cells	4	2.0	4

3.12 Identification and quantification of viral and host proteins that were differentially abundant in the second biological repeat

Table 3.4: 2 Influenza A viral proteins identified in the second biological replicate by Q-Exactive Mass Spectrometry followed by data processing steps, have significantly increased in abundance when comparing mock-infected cells to IAV X31-infected cells. The log two-fold change, the number of peptides (Pep.), and the proteins' biological function are shown below using GO via uniprot http://www.uniprot.org and (326).

2 Influenza A viral proteins identified by Mass Spectrometry when comparing IAV X31 infected cells to mock-infected cells						
Uniprot accession ID	**Gene ID**	**Protein Name**	**Function**	**Peptides for Quantification**	**Fold Change (Log 2)**	**Peptide Count**
Q91UL1	Q91UL1_I000X	Nucleoprotein – Influenza A virus (strain A/X31 H3N2)	RNA binding and essential in viral penetration into host nucleus	3	9.7	3
Q0PDM0	NS1_I000X	Non-structural protein 1 (NS1A) – Influenza A virus (strain A/X31 H3N2)	Prevents establishment of the cellular antiviral state by inhibiting TRIM25-mediated DDX58 (innate immune receptor sensing viral infection) ubiquitination	2	2.6	2

Table 3.5: Nine cellular proteins identified in the second biological replicate by Q-Exactive Mass Spectrometry, followed by data processing steps, have significantly increased and decreased in abundance when comparing mock-infected cells to IAV X31-infected cells. The log 2-fold change, the number of peptides (Pep.), and the proteins' biological function are shown below using GO via uniprot http://www.uniprot.org and (326).

9 cellular proteins that significantly increased and decreased in abundance when comparing IAV X31 infected cells to mock-infected cells						
Uniprot accession ID	**Gene ID**	**Protein Name**	**Function**	**Peptides for Quantification**	**Fold Change (Log 2)**	**Peptide Count**
P20591	MX1_HUMAN	Interferon-induced GTP-binding protein Mx1	Antiviral activity against some RNA and DNA viruses. Targets negative-stranded RNA viruses through binding and inactivation of their ribonucleocapsid	3	3.1	3
Q9Y6D9	MD1L1_HUMAN	Mitotic spindle assembly checkpoint protein MAD1	Part of the spindle-assembly checkpoint that prevents onset of anaphase until	2	1.8	2

			chromosomes are aligned at metaphase			
P29317	EPHA2_HUMAN	Ephrin type-A receptor 2	Regulates migration, integrin-mediated adhesion, proliferation and differentiation of cells. Also acts as a receptor for hepatitis C virus (HCV) and facilitates its entry into cells5	4	3.3	5
P23229	ITGA6_HUMAN	Integrin alpha-6	Integrin alpha-6/beta-1 is a receptor for laminin on platelets	9	1.6	10
Q13740	CD166_HUMAN	CD166 antigen	Contributes to formation and maturation of immunological synapse through interaction with CD6	7	1.4	7

P54289	CA2D1_HUMAN	Voltage-dependent calcium channel subunit alpha-2/delta-1	Metal ion binding and voltage-gated calcium channel activity	4	1.4	4
P49916	DNLI3_HUMAN	DNA ligase 3	Isoform 3 – heterodimer with DNA-repair protein XRCC1 in nucleus. Isoform 1 –functions as DNA ligase in mitochondrial base-excision DNA repair	2	1.1	2
P26006	ITA3_HUMAN	Integrin alpha-3	Receptor for fibronectin, laminin, collagen, epiligrin participate in adhesion, matrix degradation processes, promoting cell invasion	14	1.1	14
Q53EL6	PDCD4_HUMAN	Programmed cell death protein 4	Inhibits translation initiation and cap-dependent translation. Down regulates expression of	4	-1	4

			MAP4K1, inhibiting events that drive invasion			

3.13 Bioinformatics Analysis- Ingenuity Pathway Analysis (IPA)

The datasets obtained from the Q-Exactive platform were analysed using Ingenuity Pathway Analysis (IPA) (QIAGEN Inc., https://www.qiagenbioinformatics.com/products/ingenuity-pathway-analysis). The proteins highlighted were connected and categorised based on function. Different expression networks were generated using IPA. The data sets contained accession gene identifiers, corresponding maximum fold change values, P-values, and q-values, which were uploaded into the application. This analysis provided a deeper understanding of the dataset. Proteins were visualised from a perspective of their function in the host in response to IAV infection. Through this analysis, all proteins, which were involved in the 'replication of IAV', were highlighted (Table 3.6). Among these proteins in Table 3.6, the proteins in bold are those that were also highlighted when the data from MinION sequencing was subjected to IPA.

Table. 3.6: 131 proteins identified by Q – Exactive Mass Spectrometry and highlighted by the IPA in the category – Replication of IAV (the proteins in bold are those that were highlighted when data from MinION sequencing was subjected to IPA)

Uniprot accession ID	Gene ID	Protein name	Function	Log-2-fold change
P05161	ISG15_HUMAN	Ubiquitin-like protein ISG15	Key role in innate immune response to viral infection	6.046
P20591	MX1_HUMAN	Interferon-induced GTP-binding protein Mx1	Antiviral activity against some RNA and DNA viruses. Targets negative-stranded RNA viruses through binding and inactivation of their ribonucleocapsid	3.051
P26006	ITGA3_HUMAN	Integrin alpha-3	Receptor for fibronectin, laminin, collagen, epiligrin, thrombospondin and CSPG4	1.099
P17612	PRKACA_HUMAN	cAMP-dependent protein kinase catalytic subunit alpha	Phosphorylates a large substrate in the cytoplasm and nucleus	1.011
Q9H269	VPS16_HUMAN	Vacuolar protein sorting-associated protein 16 homolog	Role in vesicle-mediated protein trafficking to the lysosomal compartments	0.833
Q9Y6K5	OAS3_HUMAN	2’-5’-oligoadenylate synthase 3	Activated by dsRNA and plays a role in innate antiviral response (Interferon-induced)	0.808
P42224	STAT1_HUMAN	Signal transducer and activator of transcription 1-alpha/beta	Mediates cellular responses to interferons (IFN)	0.704
Q13287	NMI_HUMAN	N-myc-interactor	Augments cytokine-mediated STAT transcription	0.498

Q8WUK0	PTPMT1_HUMAN	Phosphatidylglycerophosphatase and protein-tyrosine phosphatase 1	Lipid phosphatase	0.484
P55265	ADAR_HUMAN	Double-stranded RNA-specific adenosine deaminase	Catalyzes hydrolytic deamination of adenosine to inosine	0.464
Q13190	STX5_HUMAN	Syntaxin-5	Mediates endoplasmic reticulum to Golgi transport	0.449
Q9UBU9	NXF1_HUMAN	Nuclear RNA export factor 1	Nuclear export of mRNA species from nucleus to cytoplasm	0.421
P19525	EIF2AK2_HUMAN	Interferon-induced, double stranded RNA-activated protein kinase	Key role in innate immune response to viral infection	0.384
Q9ULT8	HECTD1_HUMAN	E3 ubiquitin-protein ligase HECTD1	E3 ubiquitin-protein ligase	0.332
P62875	POLR2L_HUMAN	DNA-directed RNA polymerases I, II and III subunit RPABC5	Catalyses the transcription of DNA into RNA	0.314
P14324	FDPS_HUMAN			0.312
Q12788	TBL3_HUMAN	Transducin beta-like protein 3	RNA binding	0.25
P08865	RPSA_HUMAN	40S ribosomal protein SA	Assembly and/or stability of the 40S ribosomal subunit	0.249
P52434	POLR2H_HUMAN	DNA-directed RNA polymerases I, II and III subunit RPABC3	Catalyses transcription of DNA to RNA	0.234
P62263	RPS14_HUMAN	40S ribosomal protein S14	mRNA 5’-UTR binding	0.228

P49790	NUP153_HUMAN	Nuclear pore complex protein Nup153	Required for trafficking across the nuclear envelope	0.214
Q14152	EIF3A_HUMAN	Eukaryotic translation initiation factor 3 subunit A	RNA-binding component of eukaryotic translation initiation factor 3 and required for initiation of protein synthesis	0.214
Q96CW1	AP2M1_HUMAN	AP-2 complex subunit mu	Protein transport via transport vesicles	0.213
P07437	TUBB_HUMAN	Tubulin beta chain	Major constituent of microtubules	0.204
O75821	EIF3G_HUMAN	Eukaryotic translation initiation factor 3 subunit G	RNA-binding component of eukaryotic translation initiation factor 3 (eIF-3) complex	0.201
Q7Z3B4	**NUP54_HUMAN**	**Nucleoporin p54**	**Component of nuclear pore complex needed for trafficking across the nuclear membrane**	**0.19**
P31749	AKT1_HUMAN	RAC-alpha serine/threonine-protein kinase	Regulates processes including; metabolism, proliferation cell survival, growth, and angiogenesis	0.186
Q9BTD8	**RBM42_HUMAN**	**RNA-binding protein 42**	**Binds 3'-untranslated region (UTR) of CDKN1A mRNA**	**0.182**
Q9Y3B4	SF3B6_HUMAN	Splicing factor 3B subunit 6	Involved in pre-mRNA splicing	0.181
P68104	EEF1A1_HUMAN	Elongation factor 1-alpha 1	GTPase activity	0.171
O95470	SGPL1_HUMAN	Sphingosine-1-phosphate lyase 1	Involved in the pathway sphingolipid metabolism	0.162
Q2TAY7	SMU1_HUMAN	WD40 repeat-containing protein SMU1	Involved in pre-mRNA splicing	0.149
Q9Y224	RTRAF_HUMAN	RNA transcription, translation and	RNA binding protein involved in mRNA transcription by	0.146

		transport factor protein	Polymerase II	
P62979	RPS27A_HUMAN	Ubiquitin-40S ribosomal protein S27a	Ubiquitin – covalently bound to another protein or free	0.145
Q99720	SIGMAR1_HUMAN	Sigma non-opioid intracellular receptor 1	Lipid transport from the endoplasmic reticulum	0.138
O75153	CLUH_HUMAN	Clustered mitochondria protein homolog	Regulates transport or translation of transcripts close to mitochondria	0.136
P15428	**HPGD_HUMAN**	**15-hydroxyprostaglandin dehydrogenase**	**Prostaglandin inactivation**	**0.135**
P07900	HSP90AA1_HUMAN	Heat shock protein HSP 90-alpha	Molecular chaperone promoting maturation of specific target proteins	0.134
Q13200	PSMD2_HUMAN	26S proteasome non-ATPase regulatory subunit 2	Role in maintaining protein homeostasis	0.132
Q14974	KPNB1_HUMAN	Importin subunit beta-1	Function in nuclear protein import	0.131
Q9UHY1	NRBP1_HUMAN	Nuclear receptor-binding protein	Role in subcellular trafficking between endoplasmic reticulum and Golgi apparatus	0.129
P49841	GSK3B_HUMAN	Glycogen synthase kinase-3 beta	ATP binding	0.128
P53621	COPA_HUMAN	Coatomer subunit alpha	Hormone activity	0.125
Q15424	SAFB_HUMAN	Scaffold attachment factor B1	Allows formation of ‘transcriptional’ complex containing SR	0.119

			proteins and RNA polymerase II	
P27708	CAD_HUMAN	CAD protein	Fusion protein	0.119
Q9Y678	COPG1_HUMAN	Coatomer subunit gamma-1	Mediates biosynthetic protein transport form the ER	0.108
Q12906	ILF3_HUMAN	Interleukin enhancer-binding factor 3	Essential role in biogenesis of circular RNAs	0.107
Q9UQ35	SRRM2_HUMAN	Serine/arginine repetitive matrix protein 2	Involved in pre-mRNA splicing	0.105
Q16658	FSCN1_HUMAN	Fascin	Role in organization of actin filament	0.093
Q6P2Q9	PRPF8_HUMAN	Pre-mRNA-processing splicing factor 8	RNA binding	0.092
P60953	CDC42_HUMAN	Cell division control protein 42 homolog	Apolipoprotein A-I receptor binding	0.091
Q15907	RAB11B_HUMAN	Ras-related protein Rab-11B	Key regulators of intracellular membrane trafficking	0.09
O95747	OXSR1_HUMAN	Serine/threonine-protein kinase OSR1	ATP binding	0.09
	RPS5_HUMAN	40S ribosomal protein S5	mRNA binding	0.087
P18583	SON_HUMAN	Protein SON	RNA-binding protein	0.087
P35658	NUP214_HUMAN	Nuclear pore complex protein Nup214	Serves as a docking site for substrates in nuclear pore complex	0.086
P48444	ARCN1_HUMAN	Coatomer subunit delta	RNA binding	0.082
P36507	MAP2K2_HUMAN	Dual specificity mitogen-activated protein kinase kinase 2	Activates ERK1 and ERK2 MAP Kinases	0.072

O75533	SF3B1_HUMAN	Splicing factor 3B subunit 1	Involved in pre-mRNA splicing as a component of splicing factor SF3B complex	0.067
P62249	RPS16_HUMAN	40S ribosomal protein S16	RNA binding	0.064
P48506	**GCLC_HUMAN**	**Glutamate cysteine ligase catalytic subunit**	**ADP binding**	**0.06**
Q01628	IFITM3_HUMAN	Interferon-induced transmembrane protein 3	IFN-induced antiviral protein	0.06
Q99613	EIF3C_HUMAN	Eukaryotic translation initiation factor 3 subunit C	Component of eukaryotic translation initiation factor 3 complex	0.059
Q96KB5	PBK_HUMAN	Lymphokine-activated killer T-cell-originated protein kinase	Phosphorylates MAP kinase p38	0.056
P23246	SFPQ_HUMAN	Splicing factor, proline and glutamine rich	DNA and RNA binding protein	0.041
Q9UNH7	SNX6_HUMAN	Sorting nexin-6	Involved in intracellular trafficking	0.038
O00487	PSMD14_HUMAN	26S proteasome non-ATPase regulatory subunit 14	Component of 26S proteasome	0.038
P08133	ANXA6_HUMAN	Annexin A6	Regulates release of Ca^{2+} from intracellular stores	0.038
P55060	CSE1L_HUMAN	Exportin-2	Export receptor for importin-alpha	0.033

P53618	COPB1_HUMAN	Coatomer subunit beta	Vesicle mediated transport from endoplasmic reticulum to Golgi apparatus	0.029
Q9UBE0	SAE1_HUMAN	SUMO-activating enzyme subunit 1	Involved in the pathway for protein sumoylation	0.029
P15144	**ANPEP_HUMAN**	**Aminopeptidase N**	**Aminopeptidase activity**	**0.022**
Q13526	PIN1_HUMAN	Peptidyl-prolyl cis-trans isomerase NIMA-interacting 1	Involved in cell cycle and beta-catenin binding	0.019
Q9UEW8	STK39_HUMAN	STE20/SPS1-related proline-alanine-rich protein kinase	Mediator of stress-activated signals	0.018
P60033	CD81_HUMAN	CD81 antigen	Involved in integrin binding and have a role in activation of MAPK activity	0.007
Q12802	**AKAP13_HUMAN**	**A-kinase anchor protein 13**	**cAMP-dependent protein kinase activity**	**0.005**
Q0JRZ9	FCHO2_HUMAN	F-BAR domain only protein 2	Has a role in early step clathrin-mediated endocytosis	0.005
Q9NQW7	XPNPEP1_HUMAN	Xaa-Pro aminopeptidase 1	Has a role in degradation of bradykinin	0.004
P25786	PSMA1_HUMAN	Proteasome subunit alpha type-1	Component of the 20S core proteasome complex	-0.003
P21281	ATP6V1B2_HUMAN	V-type proton ATPase subunit B	ATP binding	-0.015
P61956	SUMO2_HUMAN	Small ubiquitin-related modifier 2	Ubiquitin like protein– covalently bound to another protein or free	-0.016

Q6RW13	AGTRAP_HUMAN	Type-1 angiotensin II receptor-associated protein	Angiotensin type II receptor activity	-0.02
P38919	EIF4A3_HUMAN	Eukaryotic initiation factor 4A-III	ATP-dependent RNA helicase	-0.021
Q96FX7	TRMT61A_HUMAN	tRNA-methyltransferase catalytic subunit TRMT61A	mRNA-methyltransferase activity	-0.028
Q9Y696	CLIC4_HUMAN	Chloride intracellular channel protein 4	Chloride channel activity	-0.029
Q9Y230	RUVBL2_HUMAN	RuvB-like 2	ADP binding	-0.031
P10809	HSPD1_HUMAN	60 kDa heat shock protein	Apolipoprotein A-I binding	-0.031
P36776	LONP1_HUMAN	Lon protease homolog	ADP binding	-0.032
P38606	ATP6V1A_HUMAN	V-type proton ATPase catalytic subunit A	Catalytic subunit of peripheral V1 complex of vacuolar ATPase	-0.059
Q6PKG0	LARP1_HUMAN	La-related protein 1	RNA-binding protein that promotes translation of mRNAs downstream of the mTORC1 complex	-0.062
P46783	RPS10_HUMAN	40S ribosomal protein S10	Component of 40S ribosomal subunit	-0.078
Q13573	SNW1_HUMAN	SNW domain-containing protein 1	Involved in pre-mRNA splicing	-0.078
Q9Y5S2	CDC42BPB_HUMAN	Serine/threonine-protein kinase MRCK	Important component of CDC42 and role in cell migration	-0.081

		beta		
O14980	XPO1_HUMAN	Exportin-1	Mediates nuclear export of cellular proteins	-0.083
Q15459	SF3A1_HUMAN	Splicing factor 3A subunit 1	RNA binding	-0.086
Q7KZ85	SUPT6H_HUMAN	Transcription elongation factor SPT6	Transcription elongation factor	-0.089
P62306	SNRPF_HUMAN	Small nuclear ribonucleoprotein F	Has a role in pre-mRNA splicing	-0.089
Q9Y5X1	SNX9_HUMAN	Sorting nexin-9	Involved in endocytosis and intracellular vesicle trafficking	-0.09
P24928	POLR2A_HUMAN	DNA-directed RNA polymerase II subunit RPB1	DNA binding	-0.093
P60891	PRPS1_HUMAN	Ribose-phosphate pyrophosphokinase 1	Catalyses the synthesis of phosphoribosyl pyrophosphate (PRPP) needed for nucleotide synthesis	-0.1
Q92905	COPS5_HUMAN	COP9 signalosome complex subunit 5	Part of the CSN complex which is essential in ubiquitin conjugation pathway	-0.101
P51452	DUSP3_HUMAN	Dual specificity protein phosphatase 3	Cytoskeletal protein binding	-0.102
P40429	RPL13A_HUMAN	60S ribosomal protein L13a	mRNA binding	-0.103
Q9H0H5	**RACGAP1_HUMAN**	**Rac GTPase-activating protein 1**	**Alpha-tubulin binding**	**-0.105**
P16220	**CREB1_HUMAN**	**Cyclic AMP-responsive element-binding protein 1**	**Phosphorylation-dependent transcription that stimulates transcription**	**-0.105**

P78406	RAE1_HUMAN	mRNA export factor	Binds mRNA, and has a role in mitotic bipolar spindle formation	-0.106
P61421	ATP6V0D1_HUMAN	V-type proton ATPase subunit d 1	Protein-containing complex binding	-0.108
O75348	ATP6V1G1_HUMAN	V-type proton ATPase subunit G1	ATPase binding	-0.109
Q04206	RELA_HUMAN	Transcription factor p65	Involved in the NF-kappa-B complex such as inflammation, immunity, differentiation, cell growth	-0.11
O43865	AHCYL1_HUMAN	S-adenosylhomocysteine hydrolase-like protein 1	RNA binding and identical protein binding	-0.127
P08621	SNRNP70_HUMAN	U1 small nuclear ribonucleoprotein 70 kDa	mRNA binding	-0.134
Q7L7X3	TAOK1_HUMAN	Serine/threonine-protein kinase TAO1	Involved in p38/MAPK14 stress-activated MAPK cascade	-0.144
P11182	DBT_HUMAN	Lipoamide acyltransferase component of branched-chain alpha-keto acid dehydrogenase complex	Acetyltransferase activity	-0.161
P42766	RPL35_HUMAN	60S ribosomal protein L35	Component of large ribosomal subunit	-0.161
P28482	MAPK1_HUMAN	Mitogen-activated protein kinase 1	Essential component of the MAP kinase signal transduction pathway	-0.165

P68032	ACTC1_HUMAN	Actin, alpha cardiac muscle 1	Involved in cell motility	-0.165
O00754	**MAN2B1_HUMAN**	**Lysosomal alpha-mannosidase**	**Alpha-mannosidase activity**	**-0.169**
P62861	FAU_HUMAN	40S ribosomal protein S30	RNA binding	-0.171
P35606	COPB2_HUMAN	Coatomer subunit beta	Mediates biosynthetic protein transport from endoplasmic reticulum	-0.198
Q9NRR5	UBQLN4_HUMAN	Ubiquilin-4	Role in regulation of protein degradation	-0.208
Q13177	PAK2_HUMAN	Serine/threonine-protein kinase PAK 2	Role in signalling pathways including cytoskeleton regulation, cell motility cell cycle progression, apoptosis or proliferation	-0.225
P41743	**PRKCI_HUMAN**	**Protein kinase C iota type**	**Role in protective role against apoptotic stimuli involved in NF-Kappa-B**	**-0.24**
P98194	ATP2C1_HUMAN	Calcium-transporting ATPase type 2C member 1	Transport of calcium	-0.253
P63165	SUMO1_HUMAN	Small ubiquitin-related modifier 1	Ubiquitin – covalently bound to another protein or free	-0.334
P61769	B2M_HUMAN	Beta-2-microglobulin	It's a component of class I major histocompatibility complex (MHC)	-0.363
Q8TD19	NEK9_HUMAN	Serine/threonine-protein kinase Nek9	Regulates mitotic progression	-0.413
Q8NBM4	UBAC2_HUMAN	Ubiquitin-associated domain-containing	Restricts trafficking of FAF2 from endoplasmic reticulum to	-0.445

		protein 2	lipid droplets	
Q92621	NUP205_HUMAN	Nuclear pore complex protein Nup205	Role in nuclear pore complex (NPC) assembly	-0.525

The IAV proteins highlighted in Table 3.4 and the IAV transcripts in Table 3.6 confirm the presence of IAV infection in the cells and the ongoing process of viral replication *in vitro.* The host proteins highlighted in Tables 3.5, 3.6, and 3.8 show the potential of the Q-Exactive Mass Spectrometry in combination with bioinformatic analysis to categorise and highlight host proteins involved in IAV pathogenesis. The IPA further connects the proteins identified into networks based on their function. These pathways are a visual representation of the changes occurring in the host cell after IAV infection. The pathways below (Figure 3.8) highlight the proteins involved in the immune response and activation of proteins known to exacerbate the IAV pathogenesis.

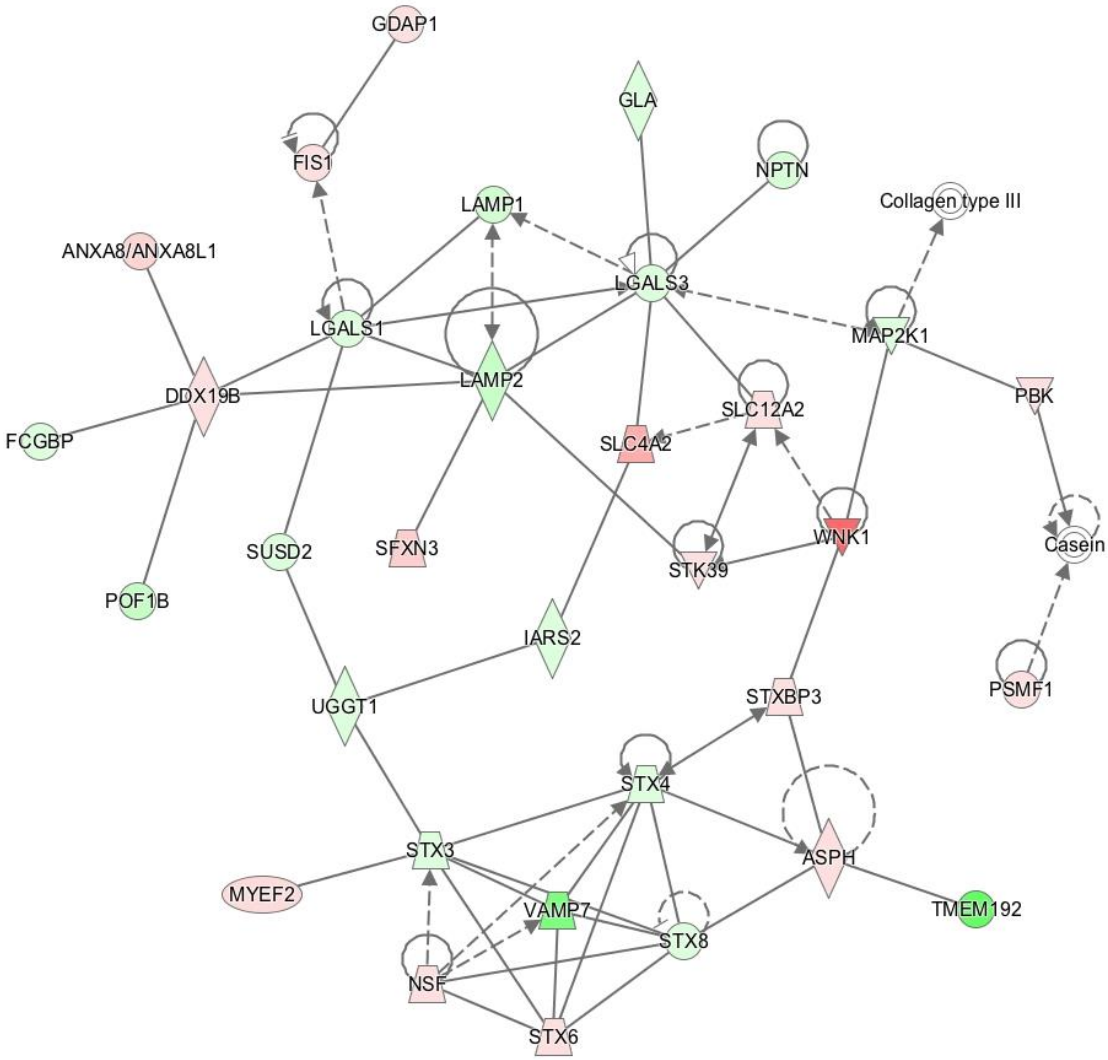

Figure 3.8: Network pathway analysis of proteins identified in A549 cells infected with IAV compared to mock-infected cells. The network highlights proteins increased or decreased in protein abundance. Proteins in red highlight a two-fold or more increase in abundance, while proteins in green highlight a two-fold or more decrease in abundance when comparing the IAV infected samples to mock-infected samples. The lines with solid arrows represent a direct molecular interaction with one protein initiating the other and the dashed arrows an indirect molecular interaction with one protein potentially initiating the other. Strong lines without an arrow show a relationship between two protein molecules and dashed lines without an arrow

show an assumed relationship between two protein molecules. Strong lines or dashed lines with a dash at the end are inhibitory to that protein. The proteins that were not highlighted were not identified in the dataset but are indirectly involved in these pathways.

3.14 Identification of the transcriptome in IAV infected A549 cells compared to mock-infected cells at MOI 1 at 18h.p.i by MinION sequencing

A549 cells were infected with IAV X31 and compared to mock-infected cells. The RNA was extracted and subjected to the MinION for sequencing (Chapter 2, section 2.8). Differential gene expression (DEG) analysis was used to process the data obtained from these experiments. To the best of our knowledge, this is the first study to explore the viral (IAV) host (A549 cells – *in vitro*) interaction using MinION sequencing and analysed for DEG. To the best of our knowledge, DEG following MinION sequencing has been conducted in only one published paper. The same data analysis method was used in this chapter (261). 139 IAV transcripts pertaining to five segments of the IAV genome were identified (Table 3.7). The presence of these transcripts from IAV segments confirm the cells were infected with IAV.

Table 3.7: 139 Influenza A viral transcripts from five segments identified by MinION sequencing (327)

	Influenza A viral transcripts
1	Influenza A virus (A/reassortant/NYMC X-203A (A/Puerto Rico/8/1934 x A/Minnesota/11/2010) (H3N2)) segment 1 polymerase PB2 (PB2) gene
2	Influenza A virus (A/Tehran/Sm03/2015[H1N1]) segment 1 polymerase PB2 (PB2) gene, complete cds
3	Influenza A virus (A/white-rumped sandpiper/Lagoa do Peixe/RS1167/2012[H6N1]) segment 1 polymerase PB2 (PB2) gene, complete cds
4	Influenza A virus (A/white-rumped sandpiper/Lagoa do Peixe/RS1167/2012[H6N1]) segment 1 polymerase PB2 (PB2) gene, complete cds
5	Influenza A virus (A/Netherlands/M1/1957[H2N2]) segment 1 polymerase PB2 (PB2) gene, complete cds
6	Influenza A virus (A/reassortant/X-139[X-31B x New Caledonia/20/1999] [H1N1]) segment 1 polymerase PB2 (PB2) gene, complete cds
7	Influenza A virus (A/white-rumped sandpiper/Lagoa do Peixe/RS1167/2012(H6N1)) segment 1 polymerase PB2 (PB2) gene, complete cds
8	Influenza A virus (A/white-rumped sandpiper/Lagoa do Peixe/RS1167/2012[H6N1]) segment 1 polymerase PB2 (PB2) gene, complete cds
9	Influenza A/Puerto Rico/8/34 (H1N1), subgenomic RNA 4 (from seg 1), in defective interfering virus
10	Influenza A virus (A/guineafowl/Hong Kong/WF10_CIP046_RGAO032/1999[H9N1]) clone AO03_S21 segment 1 polymerase PB2 (PB2) gene, complete cds
11	Influenza A virus (A/white-rumped sandpiper/Lagoa do Peixe/RS1167/2012[H6N1]) segment 1 polymerase PB2 (PB2) gene, complete cds
12	Influenza A virus (A/white-rumped sandpiper/Lagoa do Peixe/RS1167/2012[H6N1]) segment 1 polymerase PB2 (PB2) gene, complete cds
13	Influenza A virus (A/Puerto Rico/8/1934(H1N1)) RNA, segment 1, complete sequence
14	Influenza A virus (A/white-rumped sandpiper/Lagoa do Peixe/RS1167/2012[H6N1]) segment 1 polymerase PB2 (PB2) gene, complete cds
15	Influenza A virus (A/white-rumped sandpiper/Lagoa do Peixe/RS1167/2012[H6N1]) segment 1 polymerase PB2 (PB2) gene, complete cds

16	Influenza A virus (A/white-rumped sandpiper/Lagoa do Peixe/RS1167/2012[H6N1]) segment 1 polymerase PB2 (PB2) gene, complete cds
17	Influenza A/Puerto Rico/8/34 (H1N1), subgenomic RNA 4 (from seg 1), in defective interfering virus
18	Influenza A virus (A/white-rumped sandpiper/Lagoa do Peixe/RS1167/2012[H6N1]) segment 1 polymerase PB2 (PB2) gene, complete cds
19	Influenza A virus (A/Puerto Rico/8/1934[H1N1]) RNA, segment 1, complete sequence
20	Influenza A virus (A/white-rumped sandpiper/Lagoa do Peixe/RS1167/2012[H6N1]) segment 1 polymerase PB2 (PB2) gene, complete cds
21	Influenza A virus (A/PR/8/34[H1N1]) mRNA for hypothetical protein, strain A/PR/8/34
22	Influenza A virus (A/Puerto Rico/8/1934[H1N1]) polymerase PB2 (PB2) gene, complete cds
23	Influenza A virus (A/reassortant/X-139[X-31B x New Caledonia/20/1999] [H1N1]) segment 1 polymerase PB2 (PB2) gene, complete cds
24	Influenza A virus (A/Puerto Rico/8-SV7/1934[H1N1]) polymerase PB2 (PB2) gene, complete cds
25	Influenza A virus (A/lvPR8/34[H1N1]) segment 1, complete sequence
26	Influenza A virus (A/guineafowl/Hong Kong/WF10_CIP046_RGAO032/1999[H9N1]) clone AO03_S21 segment 1 polymerase PB2 (PB2) gene, complete cds
27	Influenza A virus (A/guineafowl/Hong Kong/WF10_CIP046_RGAO032/1999[H9N1]) clone AO03_S21 segment 1 polymerase PB2 (PB2) gene, complete cds
28	Influenza A virus (A/reassortant/X-175C (Uruguay/716/2007 x Puerto Rico/8/1934) [H3N2]) segment 1 polymerase PB2 (PB2) gene, complete cds
29	Influenza A virus (A/lvPR8/34[H1N1]) segment 1, complete sequence
30	Influenza A virus (A/swine/IL/00685/2005[H1N1]) segment 1 polymerase PB2 (PB2) gene, complete cds

31	Influenza A virus (A/Tehran/Sm03/2015[H1N1]) segment 1 polymerase PB2 (PB2) gene, complete cds
32	Influenza A virus (A/Tehran/Sm03/2015[H1N1]) segment 1 polymerase PB2 (PB2) gene, complete cds
33	Influenza A virus (A/Puerto Rico/8/34[H1N1]) segment 1, complete sequence
34	Influenza A virus (A/guineafowl/Hong Kong/WF10_CIP046_RGAO032/1999[H9N1]) clone AO03_S21 segment 1 polymerase PB2 (PB2) gene, complete cds
35	Influenza A/Puerto Rico/8/34 (H1N1), subgenomic RNA 4 (from seg 1), in defective interfering virus
36	Influenza A/Puerto Rico/8/34 (H1N1), subgenomic RNA 4 (from seg 1), in defective interfering virus
37	Influenza A virus (A/chicken/Henan/nd/1998[H9N2]) non-functional polymerase basic protein 2 (PB2) gene, partial sequence
38	Influenza A virus (A/guineafowl/Hong Kong/WF10_CIP046_RGAO032/1999[H9N1]) clone AO03_S21 segment 1 polymerase PB2 (PB2) gene, complete cds
39	Influenza A virus (A/guineafowl/Hong Kong/WF10_CIP046_RGAO032/1999[H9N1]) clone AO03_S21 segment 1 polymerase PB2 (PB2) gene, complete cds
40	Influenza A/Puerto Rico/8/34 (H1N1), subgenomic RNA 4 (from seg 1), in defective interfering virus
41	Influenza A virus (A/Tehran/Sm03/2015[H1N1]) segment 1 polymerase PB2 (PB2) gene, complete cds
42	Influenza A Virus (A/Fiji/15899/83[H1N1]) mRNA for PB2 protein
43	Influenza A virus (A/guineafowl/Hong Kong/WF10_CIP046_RGAO032/1999[H9N1]) clone AO03_S21 segment 1 polymerase PB2 (PB2) gene, complete cds

44	Influenza A virus (A/guineafowl/Hong Kong/WF10_CIP046_RGAO032/1999[H9N1]) clone AO03_S21 segment 1 polymerase PB2 (PB2) gene, complete cds
45	Influenza A virus (A/guineafowl/Hong Kong/WF10_CIP046_RGAO032/1999[H9N1]) clone AO03_S21 segment 1 polymerase PB2 (PB2) gene, complete cds
46	Influenza A/Puerto Rico/8/34 (H1N1), subgenomic RNA 4 (from seg 1), in defective interfering virus
47	Influenza A/Puerto Rico/8/34 (H1N1), subgenomic RNA 4 (from seg 1), in defective interfering virus
48	Influenza A/Puerto Rico/8/34 (H1N1), subgenomic RNA 4 (from seg 1), in defective interfering virus
49	Influenza A/Puerto Rico/8/34 (H1N1), subgenomic RNA 4 (from seg 1), in defective interfering virus
50	Influenza A/Puerto Rico/8/34 (H1N1), subgenomic RNA 4 (from seg 1), in defective interfering virus
51	Influenza A/Puerto Rico/8/34 (H1N1), subgenomic RNA 4 (from seg 1), in defective interfering virus
52	Influenza A/Puerto Rico/8/34 (H1N1), subgenomic RNA 4 (from seg 1), in defective interfering virus
53	Influenza A/Puerto Rico/8/34 (H1N1), subgenomic RNA 4 (from seg 1), in defective interfering virus
54	Influenza A/Puerto Rico/8/34 (H1N1), subgenomic RNA 4 (from seg 1), in defective interfering virus
55	Influenza A/Puerto Rico/8/34 (H1N1), subgenomic RNA 4 (from seg 1), in defective interfering virus
56	Influenza A virus (A/reassortant/NYMC X-211B (NYMC X-157 x St. Petersburg/100/2011)[H1N1]) polymerase PB2 (PB2) gene, complete cds
57	Influenza A virus (A/swine/QC/382/2009[H3N2]) segment 1 polymerase PB2 (PB2) gene, complete cds
58	Influenza A virus (A/mink/Shandong/F10/2013[H9N2]) segment 1 polymerase PB2 (PB2) gene, complete cds

59	Influenza A virus (A/mallard/Wisconsin/1107/1982[H11N9]) polymerase PB2 (PB2) gene, complete cds
60	Influenza A virus (A/lvPR8/34[H1N1]) segment 1, complete sequence
61	Influenza A virus (A/Tehran/Sm03/2015[H1N1]) segment 1 polymerase PB2 (PB2) gene, complete cds
62	Influenza A virus (A/white-rumped sandpiper/Lagoa do Peixe/RS1167/2012[H6N1]) segment 2 polymerase PB1 (PB1) gene, complete cds
63	Influenza A virus (A/Puerto Rico/8HY/1934[H1N1]) segment 2 polymerase PB1 (PB1) gene, complete cds
64	Influenza A virus (A/NYMC X-157B (Puerto Rico/8/1934-New York/55/2004) [H3N2]) segment 2, complete sequence
65	Influenza A virus (A/Puerto Rico/8/1934[H1N1]) RNA, segment 2, complete sequence
66	Influenza A virus (A/guineafowl/Hong Kong/WF10_CIP046_RGAO032/1999[H9N1]) clone AO09_S3 segment 2 polymerase PB1 (PB1) gene, complete cds
67	Influenza A virus (A/reassortant/NYMC X-153A (Texas/40/2003 x Puerto Rico/8/1934) [H3N2]) polymerase PB1 (PB1) and PB1-F2 protein (PB1-F2) genes, complete cds
68	Influenza A virus (A/guineafowl/Hong Kong/WF10_CIP046_RGAO032/1999[H9N1]) clone AO09_S3 segment 2 polymerase PB1 (PB1) gene, complete cds
69	Influenza A virus (A/guineafowl/Hong Kong/WF10_CIP046_RGAO032/1999[H9N1]) clone AO09_S3 segment 2 polymerase PB1 (PB1) gene, complete cds
70	Influenza A virus (A/turkey/OH/313053_CIP046_RGJS71/2004[H3N2]) clone JS71_S17 segment 3 polymerase PA (PA) and PA-X protein (PA-X) genes, complete cds

71	Influenza A virus (A/Puerto Rico/8-CV9/1934[H1N1]) polymerase PA (PA) gene, complete cds
72	Influenza A virus (A/Beijing/1/1968[H3N2]) hemagglutinin (HA) gene, complete cds
73	Influenza A virus (A/Bilthoven/908/1969[H3N2]) hemagglutinin (HA) gene, complete cds
74	Influenza A virus (A/Puerto Rico/8/1934[H1N1]) gene for nucleoprotein, genomic RNA
75	Influenza A virus (A/Puerto Rico/8/1934[H1N1]) gene for nucleoprotein, genomic RNA
76	Influenza A virus (A/Puerto Rico/8/1934[H1N1]) gene for nucleoprotein, genomic RNA
77	Influenza A virus (A/Puerto Rico/8-1-MA/1934[H1N1]) segment 5, complete sequence
78	Influenza A virus (A/Bel/1942[H1N1]) segment 5, complete sequence
79	Influenza A virus (X-31[H3N2]) RNA segment 5 for NP, complete sequence
80	Influenza A virus (X-31[H3N2]) RNA segment 5 for NP, complete sequence
81	Influenza A virus (X-31[H3N2]) RNA segment 5 for NP, complete sequence
82	Influenza A virus (A/reassortant/X-139(X-31B x New Caledonia/20/1999) [H1N1]) segment 5 nucleocapsid protein (NP) gene, complete cds
83	Influenza A virus (X-31[H3N2]) RNA segment 5 for NP, complete sequence
84	Influenza A virus (A/Puerto Rico/8/1934[H1N1]) gene for nucleoprotein, genomic RNA
85	Influenza A virus (A/Puerto Rico/8HY/1934[H1N1]) segment 5 nucleoprotein (NP) gene, complete cds
86	Influenza A virus (A/guineafowl/Hong Kong/WF10_CIP046_RGAO032/1999[H9N1]) clone AO09_S3 segment 5 nucleocapsid protein (NP) gene, complete cds

87	Influenza A virus (X-31[H3N2]) RNA segment 5 for NP, complete sequence
88	Influenza A virus (A/Puerto Rico/8/1934[H1N1]) nucleocapsid protein (NP) gene, complete cds
89	Influenza A virus (X-31[H3N2]) RNA segment 5 for NP, complete sequence
90	Influenza A virus (A/reassortant/NYMC X-223(A/Puerto Rico/8/1934 x A/Texas/50/2012) [H3N2]) segment 5 nucleocapsid protein (NP) gene, complete cds
91	Influenza A virus (A/Puerto Rico/8-1-MA/1934[H1N1]) segment 5, complete sequence
92	Influenza A virus (A/white-rumped sandpiper/Lagoa do Peixe/RS1167/2012[H6N1]) segment 7 matrix protein 2 (M2) and matrix protein 1 (M1) genes, complete cds
93	Influenza A virus (A/NanChang/08/2010[H1N1]) segment 7 matrix protein 2 (M2) and matrix protein 1 (M1) genes, complete cds
94	Influenza A virus (A/Puerto Rico/8/34/Mount Sinai/Wi[H1N1]) matrix protein 2 mRNA, partial cds
95	Influenza A virus (A/Puerto Rico/8/34/Mount Sinai/Wi-M2-P10L[H1N1]) matrix protein 2 mRNA, partial cds
96	Influenza A virus (A/Puerto Rico/8/34/Mount Sinai/Wi[H1N1]) matrix protein 2 mRNA, partial cds
97	Influenza A virus (A/Puerto Rico/8/34/Mount Sinai/Wi[H1N1]) matrix protein 2 mRNA, partial cds
98	Influenza A virus (A/Sofia/1250/2006[H3N2]) matrix protein 2 (M2) gene, partial cds; and matrix protein 1 (M1) gene, complete cds
100	Influenza A virus (A/reassortant/X-139(X-31B x New Caledonia/20/1999) [H1N1]) segment 8 nuclear export protein (NEP) and non-structural protein 1 (NS1) genes, complete cds
101	Influenza A virus (A/Leningrad/1954/1[H1N1]) gene for non-structural protein, genomic RNA

102	Influenza A virus (A/Leningrad/1954/1[H1N1]) gene for non-structural protein, genomic RNA
103	Influenza A virus (A/Puerto Rico/8HY/1934[H1N1]) segment 8 nuclear export protein (NEP) and non-structural protein (NS1) genes, complete cds
104	Influenza A virus (A/reassortant/X147(Wyoming/3/2003 x Puerto Rico/8/1934)[H3N2]) segment 8 sequence
105	Influenza A virus (A/Puerto Rico/8HY/1934[H1N1]) segment 8 nuclear export protein (NEP) and non-structural protein (NS1) genes, complete cds
106	Influenza A virus (A/Puerto Rico/8HY/1934[H1N1]) segment 8 nuclear export protein (NEP) and non-structural protein (NS1) genes, complete cds
107	Influenza A virus (A/Brevig_Mission/1/18[H1N1]) non-structural protein NS1 and non-structural protein NS2 genes, complete cds
108	Influenza A virus (A/Puerto Rico/8HY/1934(H1N1)) segment 8 nuclear export protein (NEP) and non-structural protein (NS1) genes, complete cds
109	Influenza A virus (A/reassortant/X147[Wyoming/3/2003 x Puerto Rico/8/1934] [H3N2]) segment 8 sequence
110	Influenza A virus (A/reassortant/X147[Wyoming/3/2003 x Puerto Rico/8/1934][H3N2]) segment 8 sequence
111	Influenza A virus (A/turkey/OH/313053_CIP046_RGJS71/2004[H3N2]) clone JS71_S17 segment 8 nuclear export protein (NEP) and non-structural protein 1 (NS1) genes, complete cds
112	Influenza A virus (A/reassortant/X147(Wyoming/3/2003 x Puerto Rico/8/1934) [H3N2]) segment 8 sequence
113	Influenza A virus (A/reassortant/NYMC X-197(Brisbane/11/2010 x Puerto Rico/8/1934) [H3N2]) segment 8 nuclear export protein (NEP) and non-structural protein 1 (NS1) genes, complete cds
114	Influenza A virus (A/Puerto Rico/8HY/1934[H1N1]) segment 8 nuclear export protein (NEP) and non-structural protein (NS1) genes, complete cds
115	Influenza A virus (A/Puerto Rico/8/1934[H1N1]) RNA, segment 8, complete sequence
116	Influenza A virus (A/reassortant/X147(Wyoming/3/2003 x Puerto Rico/8/1934) [H3N2]) segment 8 sequence

117	Influenza A virus (A/reassortant/X147(Wyoming/3/2003 x Puerto Rico/8/1934) [H3N2]) segment 8 sequence
118	Influenza A virus (A/reassortant/X147(Wyoming/3/2003 x Puerto Rico/8/1934) [H3N2]) segment 8 sequence
119	Influenza A virus (A/reassortant/X147(Wyoming/3/2003 x Puerto Rico/8/1934) [H3N2]) segment 8 sequence
120	Influenza A virus (A/Puerto Rico/8HY/1934[H1N1]) segment 8 nuclear export protein (NEP) and non-structural protein (NS1) genes, complete cds
121	Influenza A virus (A/reassortant/X147(Wyoming/3/2003 x Puerto Rico/8/1934) [H3N2]) segment 8 sequence
122	Influenza A virus (A/reassortant/X147(Wyoming/3/2003 x Puerto Rico/8/1934) [H3N2]) segment 8 sequence
123	Influenza A virus (A/Puerto Rico/8/1934[H1N1]) non-structural protein 2 (NS2) and non-structural protein 1 (NS1) genes, complete cds
124	Influenza A virus [A/reassortant/X147(Wyoming/3/2003 x Puerto Rico/8/1934] [H3N2]) segment 8 sequence
125	Influenza A virus (A/lvPR8/34[H1N1]) segment 8, complete sequence
126	Influenza A virus (A/Henry/1936[H1N1]) segment 8, complete sequence
127	Influenza A virus (A/reassortant/X147(Wyoming/3/2003 x Puerto Rico/8/1934) [H3N2]) segment 8 sequence
128	Influenza A virus (A/Puerto Rico/8HY/1934(H1N1)) segment 8 nuclear export protein (NEP) and non-structural protein (NS1) genes, complete cds
129	Influenza A virus (A/lvPR8/34[H1N1]) segment 8, complete sequence
130	Influenza A virus (A/reassortant/NYMC X-197(Brisbane/11/2010 x Puerto Rico/8/1934) [H3N2]) segment 8 nuclear export protein (NEP) and non-structural protein 1 (NS1) genes, complete cds
131	Influenza A virus (A/NanChang/08/2010[H1N1]) segment 8 nuclear export protein (NEP) and non-structural protein 1 (NS1) genes, complete cds
132	Influenza A virus (A/reassortant/X147(Wyoming/3/2003 x Puerto Rico/8/1934) [H3N2]) segment 8 sequence

133	Influenza A virus (A/reassortant/X147(Wyoming/3/2003 x Puerto Rico/8/1934) [H3N2]) segment 8 sequence
134	Influenza A virus (A/NanChang/08/2010[H1N1]) segment 8 nuclear export protein (NEP) and non-structural protein 1 (NS1) genes, complete cds
135	Influenza A virus (A/Puerto Rico/8HY/1934[H1N1]) segment 8 nuclear export protein (NEP) and non-structural protein (NS1) genes, complete cds
136	Influenza A virus (A/reassortant/NYMC X-197[Brisbane/11/2010 x Puerto Rico/8/1934] [H3N2]) segment 8 nuclear export protein (NEP) and non-structural protein 1 (NS1) genes, complete cds
137	Influenza A virus (A/reassortant/X147[Wyoming/3/2003 x Puerto Rico/8/1934] [H3N2]) segment 8 sequence
138	Influenza A virus (A/reassortant/X147[Wyoming/3/2003 x Puerto Rico/8/1934] [H3N2]) segment 8 sequence
139	Influenza A virus (A/Puerto Rico/8HY/1934[H1N1]) segment 8 nuclear export protein (NEP) and non-structural protein (NS1) genes, complete cds

In addition to the IAV transcripts, a total of 1,878 host transcripts were identified to be differentially expressed when comparing IAV infected cells to mock-infected cells (data not shown). Amongst the transcripts highlighted were interferon stimulated genes, such as IFI27, IFI44, and genes from the integrin family. These datasets were subjected to bioinformatic analysis – IPA for further analysis.

3.15 Bioinformatics Analysis - Ingenuity Pathway Analysis (IPA)

The datasets obtained from MinION sequencing were analysed using Ingenuity Pathway Analysis (IPA) (QIAGEN Inc., https://www.qiagenbioinformatics.com/products/ingenuity-pathway-analysis). The highlighted transcripts were connected and categorised based on function, and different expression networks were generated using IPA. The data sets used contained accession gene identifiers, corresponding maximum fold change, and p-values and q-values were uploaded into the application. This analysis provided a deeper understanding of the dataset. This was to visualise the transcripts from the perspective of their function in the host, in response to the viral infection.

IPA analysis of the datasets from MinION sequencing revealed 18 transcripts that have direct interactions with IAV replication (Table 3.8). Ten of these 18 transcripts had their complementary protein identified by Mass Spectrometry (Table 3.9). These proteins were highlighted in bold. These results are consistent between both techniques (MinION sequencing and Mass Spectrometry). Therefore, this increases confidence in the experiments and

techniques. Of these 10 transcripts, five transcripts were identified in a study using genome-wide RNA interference screening to identify cellular factors that play functional roles in the early replication of IAV in A549 cells infected with IAV (328). In addition, RABEP1, CBLL1, and MDM2 were identified by MinION sequencing, but not by Mass Spectrometry, and were grouped under the functional category – replication of IAV by IPA. These transcripts were also identified in a study using genome-wide RNA interference screening to identify cellular factors that play functional roles in the early replication of IAV in A549 cells infected with IAV (328). This shows consistency and reliability in the experiments, techniques, and the results obtained in this chapter.

Table 3.8: 18 transcriptomes highlighted by the MinION sequencing and connected through Ingenuity Pathway Analysis were in the category – Replication of Influenza A virus (the proteins in bold are those that were also highlighted when the data from Mass Spectrometry was subjected to IPA)

ENSEMBL ID	Gene ID	Gene name	Function	Expression Log-two-fold change
ENST00000493583	TFE3	Transcription factor E3	DNA-binding transcription factor activity	9.072
ENST00000407540	MATN3	Matrilin-3	Role of extracellular filamentous networks	8.737
ENST00000558740	**ANPEP**	**Aminopeptidase N**	**Aminopeptidase activity**	**8.918**
ENST00000442489	CDKN1B -203	Cyclin-dependent kinase inhibitor 1B	An important regulator in the cell cycle progression	9.079
ENST00000549342	**RACGAP1**	**Rac GTPase-activating protein 1**	**Alpha-tubulin binding**	**9.072**
ENST00000492398	PLK3	Serine/threonine-protein kinase PLK3	Involved in cell cycle regulation	9.072
ENST00000560185	**AKAP13**	**A-kinase anchor protein**	**cAMP-dependent protein kinase**	**9.087**

		13	**activity**	
ENST00000494092	DMAP1	DNA methyltransferase 1-associated protein 1	Involved in transcription repression and activation	8.737
ENST00000341923	RABEP1	Rab GTPase-binding effector protein 1	Effector protein acting as a linker between gamma-adaptin, RAB4A and RAB5A	9.072
ENST00000505197	**GCLC**	**Glutamate cysteine ligase catalytic subunit**	**ADP binding**	**8.918**
ENST00000222597	CBLL1			9.087
ENST00000421139	**CREB1**	**Cyclic AMP-responsive element-binding protein 1**	**Phosphorylation-dependent transcription that stimulates transcription**	**9.072**
ENST00000485837	**PRKCI**	**Protein kinase C iota type**	**Role in protective role against apoptotic stimuli involved in NF-**	**8.942**

			Kappa-B	
ENST00000422112	**HPGD**	**15-hydroxyprostaglandin dehydrogenase**	**Prostaglandin inactivation**	**2.836**
ENST00000544561	MDM2	E3 ubiquitin-protein ligase Mdm2	Mediates ubiquitination of p53/TP53 following degradation by proteasome	8.974
ENST00000592202	**RBM42**	**RNA-binding protein 42**	**Binds 3'-untranslated region (UTR) of CDKN1A mRNA**	**9.079**
ENST00000515460	**NUP54**	**Nucleoporin p54**	**Component of nuclear pore complex needed for trafficking across the nuclear membrane**	**8.818**
ENST00000596591	**MAN2B1**	**Lysosomal alpha-mannosidase**	**Alpha-mannosidase activity**	**9.057**

To analyse the datasets further, IPA was used to identify pathways that are affected by IAV infection in the host. This has a potential of highlighting pathways that are triggered to respond to IAV infection. IPA connects the transcripts identified into networks based on their function. These pathways are a visual representation of the changes occurring in the host cell. Two pathways were highlighted as the transcripts identified were involved in the immune response (Figure 3.8) and the activation of other transcripts known to have anti-viral roles in the host following IAV infection (Figure 3.9).

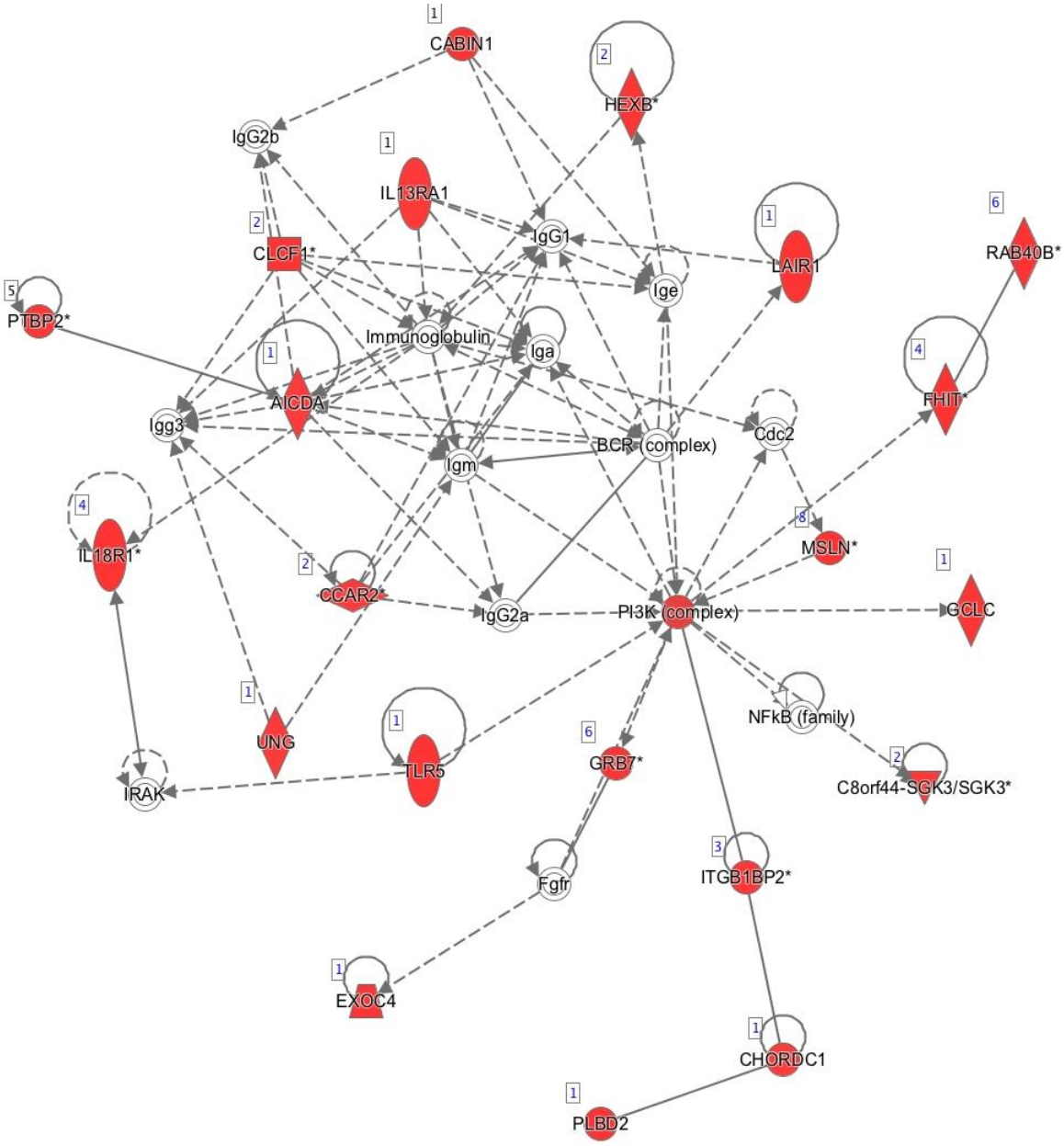

Figure 3.9: Network pathway analysis of transcripts identified in A549 cells infected with IAV compared to mock-infected cells. The network highlights transcripts with an increase in Log two-fold change involved in the immune response. Transcripts in red highlight a two-fold or more increase in transcript abundance when comparing the IAV infected samples to mock-infected samples. The lines with solid arrows represent a direct molecular interaction with one transcript initiating the other and the dashed arrows an indirect

molecular interaction with one transcript potentially initiating the other. Strong lines without an arrow show a relationship between two transcripts and dashed lines without an arrow show an assumed relationship between two transcripts molecules. Strong lines or dashed lines with a dash at the end are inhibitory to that transcript. The transcripts that were not highlighted were not identified in the dataset but are indirectly involved in these pathways.

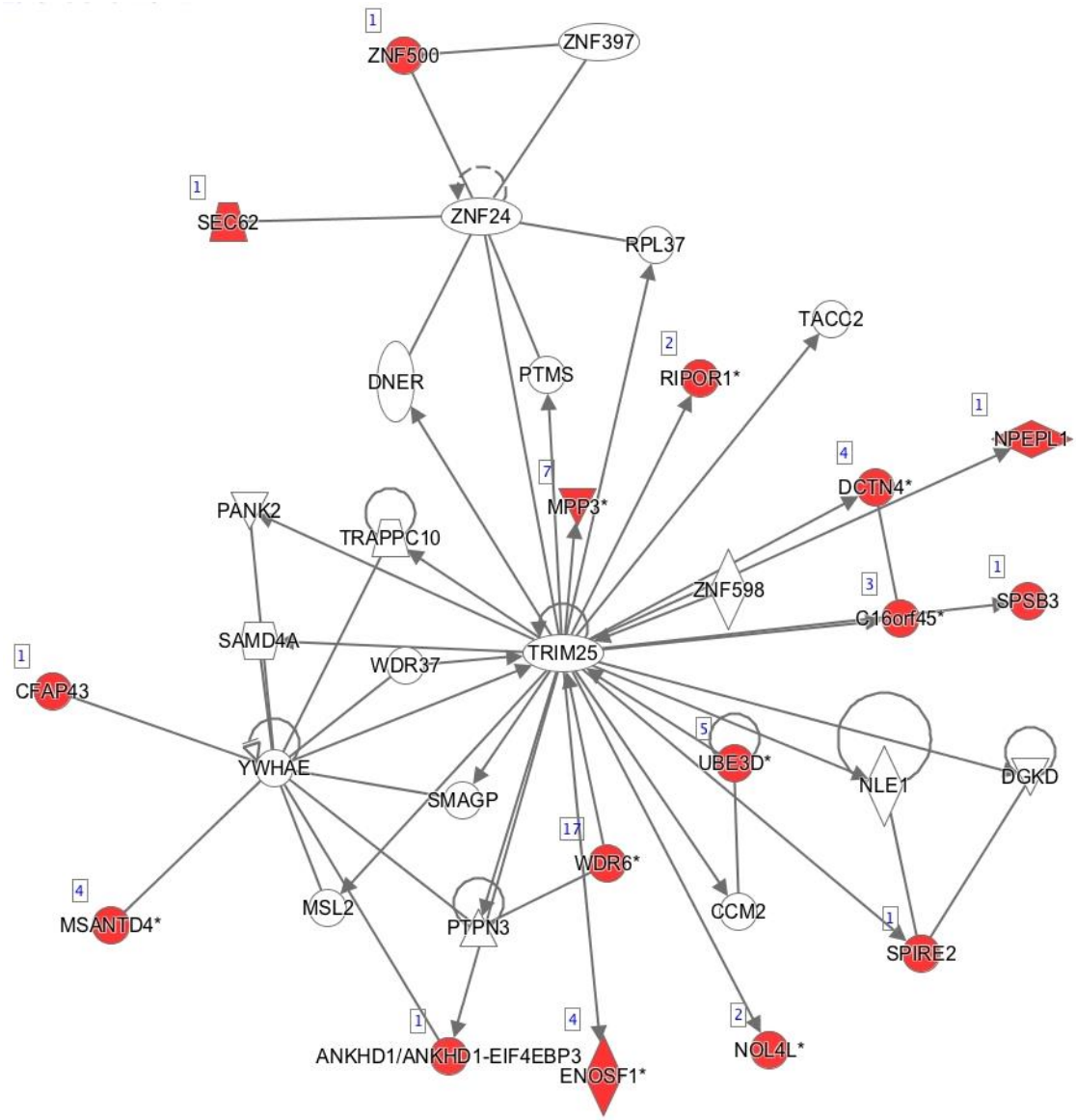

Figure 3.10: Network pathway analysis of transcripts identified in A549 cells infected with IAV compared to mock-infected cells. The network highlights transcripts with an increase in Log two-fold change and directly or indirectly affect, or are affected by, Trim25. Trim 25 is known to have a crucial anti-viral role in IAV infection. Transcripts in red highlight a two-fold or more increase in abundance when comparing the IAV infected samples with mock-infected samples.

The lines with solid arrows represent a direct molecular interaction with one transcript initiating the other and the dashed arrows an indirect molecular interaction with one transcript potentially initiating the other. Strong lines without an arrow show a relationship between two transcripts and dashed lines without an arrow show an assumed relationship between two transcripts molecules. Strong lines or dashed lines with a dash at the end are inhibitory to that transcript. The transcripts that were not highlighted were not identified in the dataset but are indirectly involved in these pathways.

3.16 Transcripts and proteins identified by Mass Spectrometry and MinION sequencing, respectively, when comparing IAV infected A549 cells with mock-infected cells

As mentioned above, after the data was obtained from the Mass Spectrometry, they were analysed through IPA. Through this analysis, the data were categorised into proteins and transcripts involved in the 'replication of IAV'. The comparison of these datasets revealed 10 proteins identified by Mass Spectrometry also identified in the transcripts from the MinION sequencing data. These are highlighted in Table 3.9.

Table 3.9: 10 proteins highlighted by Mass Spectrometry and 10 transcripts highlighted by the MinION sequencing categorised by IPA under 'replication of IAV'

Mass Spectrometry			MinION sequencing			
Uniprot accession ID	**Gene ID**	**Expression Log two-Fold change**	**Ensembl ID**	**Gene name**	**Expression Log 2-Fold change**	**Function**
Q7Z3B4	NUP54_HUMAN	1.14	ENST00000515460	NUP54	8.81794297	Component of the nuclear pore complex needed for trafficking across the membrane
Q9BTD8	RBM42_HUMAN	1.13	ENST00000592202	RBM42	9.07895134	Binds to 3' untranslated region of CDKN1A mRNA
P15428	HPGD_HUMAN	1.2	ENST00000422112	HPGD	2.82781902	Prostaglandin inactivation
P48506	GCLC_HUMAN	1.04	ENST00000505197	GCLC	8.89996107	Synthesises glutathione

P15144	ANPEP_HUMAN	1.01	ENST00000558740	ANPEP	8.91796873	Broad spectrum with roles in processing digestion peptides, neuropeptides, and chemokines
Q12802	AKAP13_HUMAN	1.003	ENST00000560185	AKAP13	9.08693234	Role in activation of several G-protein coupled receptors activating other Rho family members and pathways, such as NFκB complex and MAP kinases
Q9H0H5	RACGAP1_HUMAN	1.895	ENST00000549342	RACGAP1	9.07199858	Key role in cell cycle cytokinesis
P16220	CREB1_HUMAN	1.895	ENST00000421139	CREB1	9.07199858	Stimulates transcription by binding to DNA cAMP

						response element (CRE), present in many viral and cellular promoters
O00754	MAN2B1_HUMAN	1.831	ENST00000596591	MAN2B1	9.05690862	Cellular protein modification process
P41743	PRKCI_HUMAN	1.76	ENST00000485837	PRKCI	8.94192792	Involved in NFκB activation, cell survival and differentiation and polarity

3.17 DISCUSSION

The study of viruses has moved beyond the need to understand their pathology and association to disease, but more ultimately to identify important cellular, regulatory proteins, transcripts, and pathways involved in the elucidation, survival, and transmission of viruses in the host. The era of proteomics and transcriptomics has revolutionised the understanding of the host-viral pathogenesis, by providing important insights into the interaction between host cellular and viral proteins. This chapter focused on understanding host-viral interaction, *in vitro* by using two independent approaches: proteomics by Mass Spectrometry and transcriptomics by MinION sequencing after using other techniques – avicel plaque assay, immunofluorescence staining, and SDS-PAGE to confirm IAV infection and select the most appropriate time point for infection. Figures 3.4, 3.5, and 3.6 show IAV infected cells (stained with NP) in comparison with mock-infected cells at different time points. Based on this data, 18h.p.i was selected for the proteomics and transcriptomics experiments. Samples were run on the Q-Exactive in two biological replicates three years apart. Samples were run on the MinION sequencer in two biological replicates two weeks apart.

Proteomic approaches, specifically label-free methodologies, has allowed the exploration of changes in the cellular proteome during IAV infection. The use of label-free Liquid Chromatography Mass Spectrometry (LC – MS) is not restricted to cells *in vitro*, but can be replicated in a wider range of samples, including clinical samples. Similarly, MinION sequencing has provided the ability to sequence RNA from samples *in vitro* and obtain a host transcriptome,

while comparing mock-infected samples to IAV-infected samples. A combination of the two-independent approaches provides information on a cell's transcriptome and proteome. This provides another dimension in the understanding of the host following infection. MinION sequencing has eased the process of observing the transcriptomics of host-viral interaction efficiently with high reliability and at a lower cost. This is the first study that has used the MinION Sequencer to observe differential gene expressions of the global transcriptome to compare IAV-infected with mock-infected A549 cells.

The experiments in this chapter followed an assumption of a correlation (positive or negative) between transcriptomics and proteomics data. The results in this chapter showed a positive correlation as can be seen in Table 3.9 with 10 proteins identified by Mass Spectrometry and their corresponding transcripts identified by MinION sequencing. However, the change in expression by the log two-fold change, identified by these techniques, are significantly different. Although they both registered an increase in expression, MinION sequencing identified about a 300-fold increase in Log two-fold change compared to Mass Spectrometry. This suggests that the changes identified in the transcripts have reduced, in translation to proteins. This could be a result of post-transcription machinery and different half-lives (329). These include ubiquitination, phosphorylation, and localisation of proteins post-transcriptionally. In addition to this, mRNA transcripts in eukaryotic cells have a reported half-life of 10–20h, while proteins' half-life are 48–72h. The degradation of different proteins affects their half-lives and expression levels albeit their correlation to the mRNA transcript (329). In addition to this, external

factors, such as experimental and technical differences in the process of sample collection and data extraction could affect these expression differences.

3.17.1 Analysing proteomic data from the Q-Exactive platform and bioinformatic analysis via IPA

Data from the first biological run of samples on the Q-Exactive revealed a data set of 1,283 cellular and viral proteins. These proteins were differentially abundant when comparing mock-infected A549 cells to IAV X31 infected A549 cells. This data set was analysed by focusing on proteins represented by two or more peptides to increase reliability in the dataset. Identified proteins without a maximum fold change, as well as keratins, were removed from the dataset. Keratins are considered common contaminants of LC-MS experiments (330). The differentially abundant proteins were segregated into proteins with increased abundance and proteins with decreased abundance. The dataset revealed a total of 33 proteins showing an increase in abundance (Table 3.2) and 58 proteins showing a decrease in abundance (Table 3.3).

To increase accuracy and focus on the proteins showing the maximum fold change, the top 10 proteins significantly increase or decrease in abundance will be discussed. Myxovirus resistance host proteins (MX1 and MX2) had an increase in expression by Log two-fold change of 7.8. Interferon-induced protein with tetratricopeptide repeats three (IFIT3) and interferon-induced protein with tetratricopeptide repeats two (IFIT2) had an increase in expression by log two-fold change of 10.1 and 7.1 respectively. These

proteins are all part of the interferon (IFN)-induced pathway; this pathway is stimulated as a response to pathogen (bacteria or viral) entry (331, 332). The IFN-induced pathway serves as a means of communication between cells, thereby triggering protective defences of the immune system. Promyelocytic leukaemia (PML) had an increase in expression by Log two-fold change of 2.9. PML located in the nucleoplasm and matrix-associated protein complexes responds to IAV infection by inhibiting viral replication (320, 333). The direct pathway by which PML acts is not known but it is thought to occur indirectly by modifying other cellular proteins (333). Other proteins present within this dataset are immunoglobulins (Ig), this suggests the activation of the immune system to combat foreign bodies – viruses.

Contrarily, Interleukin-18 (IL18) had a decrease in expression by a Log two-fold change of 5.5 and Integrin Beta 4 (ITB4) had a decrease in expression by Log two-fold change of 8.3. IL18 acts as a pro-inflammatory cytokine, induces IFN-gamma, and activates natural killer cells, as well as proliferates T lymphocytes. This is a main role in protective immunity (334). Mice, deficient in IL-18, produced a poor immune response (335). The decrease in abundance of IL-18 following IAV infection cannot be confirmed without further independent assays to validate the results.

The quantitative proteomic analysis of the second biological repeat identified up to 3361 cellular and viral proteins. These proteins were obtained by comparing mock-infected A549 cells to IAV X31-infected A549 cells. This data set was quantified, analysed, and provided the protein abundance changes

which occurred following IAV X31 infection. The degree of change in abundance was represented by Log two-fold change per protein. Two IAV proteins were identified; NP and NS1A. NP had an increase in expression log two-fold change of 9.7 and NS1 had an increase in expression log two-fold change of 2.6. This proves that the A549 cells were infected and shows the high abundance viral proteins reach in host cells. Nine host cellular proteins were identified with differentially significant abundances. Similar to the first biological run, the Myxovirus resistance host protein (MX1) was highlighted and had an increase expression log two-fold change of 3.1. Integrin subunit alpha 6 (ITGA6) had an increase in expression log two-fold change of 1.6. IAV infection increases ITGA6 leading to epithelial cell apoptosis and an increase in collagen deposition (336, 337). These changes go on to cause pulmonary fibrosis and lead a host to acute lung injury and emphysema (338).

Bioinformatics analysis was performed on these datasets using the software IPA. IPA further categorised these proteins based on function; 131 proteins highlighted were involved in the 'replication of IAV' (Table 3.6). Some of these proteins were highlighted on a transcript level by MinION sequencing. These were highlighted in bold in Table 3.8 and also reported in Table 3.9. The concordance of the dataset identified in both Q-Exactive and MinION sequencing brings confidence in the techniques and experiments used in this chapter. Further network analysis highlighted proteins, such as galectin 3 (LGALS3) and galectin 1 (LGALS1) (Figure 3.8). Galectin 1 inhibits viral infectivity by binding to IAV. Galectin 1 has been used as a potential treatment

for IAV (H7N9) and experiments in mice showed a decrease in viral load, reduced lung inflammation, and increased mouse survival (339).

3.17.2 Analysing transcriptomic data from the MinION sequencing platform and bioinformatic analysis via IPA

MinION sequencing was used as an independent approach alongside proteomics to obtain the transcriptome of the host and observe transcriptomic changes in the host following IAV infection. This was also to explore whether the transcriptomic data compliments the proteomics data from Mass spectrometry, thus giving a deeper understanding of the host changes. This established the first *in vitro* study exploring the transcriptome of IAV-infected A549 cells compared with mock-infected cells using DEG analysis to discover quantitative changes in expression levels of identified transcripts. This dataset only contained transcripts that increased in log two-fold change when comparing IAV infected samples to mock-infected samples; 139 IAV transcripts pertaining to five IAV segments were identified (Table 3.7). The five IAV segments identified were 2, 3, 5, 7, and 8. A total of 1,878 host cellular transcripts were identified to have significantly different expression levels (Data not shown). Of these 1,878 transcripts, 18 of them were classified by IPA to be involved in replication of IAV and 10 of these 18 transcripts had their complementary protein identified by Mass Spectrometry (Table 3.9). Five of the 10 transcripts were identified in a study using genome-wide RNA interference screening, to identify cellular factors that play functional roles in the early replication of IAV in A549 cells infected with IAV (328, 340). The

functional role of these transcripts identified by genome-wide RNA interference in IAV replication were as follows:

ANPEP with a role in actin organisation and functions in intracellular transport and implicated in NP functions, such as transcription, replication, and genome-trafficking; AKAP13, RACGAP1, PRKCI with signalling roles in the IP3-PKC pathway; the binding and the presence of IAV HA protein to the cell is thought to activate the PKC pathway (340); PKC is thought to play a crucial role in the IAV entry into the cell; the use of a PKC inhibitor has shown an inhibition of the IAV entry into the cell (340); CREB1 has a signalling role in the MAPK pathway; the MAPK family has four subgroups that have been well studied; extracellular signal regulated kinases (ERKs), the p38 MAPK, c-jun N-terminal (JNK/SAPK) and ERK5/Big MAP kinase (BMK1) (340); influenza infection has been shown to activate all of these four subgroups – this promotes viral production and vRNP traffic; the activation of p38, JNK, and ERK lead to increased expression of inflammatory response (340-342). The activation of JNK goes further to activate the transcription factor activator protein -1 (AP1); AP1 is essential for the expression of IFNβ and other antiviral cytokines; through its different subgroups, the MAPK pathway plays a crucial role in viral survival as well as inflammatory response to IAV infection (328, 340); CREB1 plays a role in calcium regulation and signalling (328). This is essential in the entry of IAV into the cells via clathrin-mediated and clathrin-independent pathways and the calcium levels have a role to play in the regulation of these pathways (343); NUP54 is another protein that was identified by Mass Spectrometry and the corresponding transcript identified by MinION sequencing (Table 3.9). NUP54 has a role in nuclear transport and is

also an influenza polymerase interacting protein. These proteins are essential for the viral replication and subsequently survival in the host (344).

Some of the transcripts identified by MinION sequencing (Table 3.8) without complementary proteins highlighted by Mass Spectrometry have been identified to have roles in influenza replication in the host. RABEP1, CBLL1, and MDM3 were identified in genome-wide RNA interference screening to identify cellular factors that play functional roles in the early replication of IAV in A549 cells infected with IAV (328). TFE3, MATN3, PLK3, and DMAP1 were also identified in another genome-wide study, which focused on host cell factors needed for IAV infection (345). MDM2 was identified by MinION sequencing and is involved in the PI3-AKT pathway (328). IAV activates the PI3-AKT pathway through NS1 protein to maintain efficient viral replication (340). Out of the other 1,360 host transcripts, identified by MinION sequencing, some of them have known crucial roles in IAV infection in the host. Interferon stimulated transcripts, such as IFI27, IFI44 were highlighted with an increase in expression of log two-fold change of 9.1. Transcripts from the Integrin family: ITGB4, ITGB1, and ITGB7, were also highlighted with an increase in expression of log two-fold change of 9.1. The role ITGBA6 plays in IAV infection was highlighted above. Integrins are a large family primarily known to maintain cell adhesion and tissue integrity. However, they are also known to have essential roles in cell survival, differentiation, proliferation, and migration, and are potential therapeutic targets for respiratory diseases (338).

Figure 3.8 highlights several immunoglobulins present with an increase in log two-fold change in IAV infected cells compared to mock-infected cells in the

MinION sequencing data. This confirms data observed from the Mass Spectrometry (Table 3.2). Figure 3.10 highlights various transcripts with an increase in log two-fold change, which form a network and directly or indirectly affect TRIM25. TRIM25 induces ubiquitination of RIG-I that leads to increased signalling of RIG-I (346, 347). In addition, TRIM25 is essential for RIG-I mediated IFNβ production and therefore anti-viral response to RNA viral infection (346). TRIM25 binds to influenza ribonucleoproteins, inhibits viral RNA chain elongation, and stops the RNA's movement into the polymerase. The Influenza NS1 protein avidly acts against TRIM25 activity (347). Although TRIM25 was not highlighted in the MinION data, the data highlighted directly or indirectly affects it. TRIM25 was highlighted in the data from the first biological replicate on the Mass Spectrometry platform (data not shown). TRIM28 was highlighted in the MinION sequencing data (data not shown) with an increase in expression log two-fold change of 8.9. TRIM28 negatively regulates interferons (348). Excessive IFN-induced response could negatively affect the host, so this is regulated by interferon regulatory factor 7 (IRF7). IRF7 is essential in the regulation of Type 1 IFN-dependent response to viral infection. Overexpression of TRIM28 inhibits IRF7 and knockdown of TRIM28, enhances IFN production as well as antiviral responses (349). The TRIM family have roles in regulating innate immunity. These are induced by type I and II interferons, necessary for the host resistance to pathogen infection (350, 351).

3.18 Conclusion

This chapter forms the basis of the study of IAV in host *in vitro.* The results from this chapter established the reliability of quantitative label-free LC-MS Mass Spectrometry and MinION sequencing in the study of IAV *in vitro*. These results are concordant with the results seen by other studies and highlight proteins and transcripts that are observed *in vivo* and have the potential for biomarker studies. This is essential, as it gives room for high throughput, and rapid, controlled, and reliable research *in vitro.* The results in this chapter are phenomenal and reliable as they identify proteins and transcripts involved in the activation of four out of five well-known cell signalling pathways (MAPK pathway, PI3/AKT pathway, RIG-I/TLR pathway, and the IP3/PKC pathway) triggered by IAV infection (340). This highlights their importance for the continuous pathogenesis of the virus *in vitro*. Furthermore, these results give confidence in the techniques used. However, the bioinformatic analysis performed on these datasets were based on already existing data in the literature. Whilst this further validates the results in this chapter, to find novel biomarkers, targets that have not been highlighted need to be further explored using independent assays.

RESULTS CHAPTER 4:

ELUCIDATING THE HOST RESPONSE TO INFLUENZA A VIRUS INFECTION *IN VIVO* in Non-Human Primates (NHP)

4.1 INTRODUCTION

The aim of this thesis was to use proteomics to characterise IAV in three different hosts; *in vitro* – cell culture model (Chapter 3), *in vivo* – animal model (macaques - non-human primates [NHP]) (Chapter 4) and *in vivo* – humans through nasopharyngeal aspirates (NAs) (Chapter 5). This current chapter focused on examining the host response to IAV in macaques using NHP as a model. This chapter first reviewed studies in which *in vivo* models were infected with IAV and analysed using high-throughput methods. Focus was placed on studies that used proteomics as a high-throughput method. However, exceptions were made and some studies that used transcriptomics as a high-throughput method were also reviewed. This was to provide a literature review aligning with the high throughput methods used throughout this thesis.

IAV infection can be distinguished into three forms: zoonotic, pandemic, and seasonal influenza. Each of these bear a differing severity of disease in humans: mild to severe morbidity and mortality burdens (352). The IAV is classed as a zoonotic infection, due to the ability of IAV in animals to infect humans. The zoonotic IAVs are generally not transmissible among humans via air droplets (352). If the IAV gains this ability, this could lead to a novel influenza pandemic (353). Examples of other viruses with these properties include Ebola and hanta viruses). IAV has the ability to reside in avian and swine, which poses the threat of a potential pandemic in humans. Using death toll as a criterion, the four major IAV pandemics that have occurred include: 1918 (30–50 million deaths worldwide), 1957 ‘Asian Flu’ (0.3–2 million

deaths), 1968 ‘Hong Kong Flu’ (0.3–2 million deaths), and the 2009 ‘Mexican flu’ (0.3–2 million deaths) (352). Through several waves of circulation globally, IAV pandemics eventually became seasonal IAV epidemics leading to 3–5 million severe cases and 290,000–650,000 deaths yearly (64, 352, 354, 355). Consequently, influenza viruses that have the potential to cause pandemics are thought to be zoonotic influenza viruses that have gained the ability through mutation, re-assortment, or both to be effectively air-borne transmissible (352). Understanding and characterising of IAV *in vivo* is therefore essential to anticipate potential changes in IAV-host interactions, which may lead to a pandemic. This is also important in the search of potential biomarkers to increase the efficiency of diagnostics. This may provide a blueprint towards what may be expected to occur in humans.

1) IAV infection in birds

Proteomic analysis was carried out on chickens infected with avian influenza virus H9 subtype. This virus caused major economic losses and severe respiratory tract diseases (356). The tracheal epitheliums of chickens, which was the primary target organ of avian influenza viruses, was infected with influenza virus H9 subtype. These samples were subjected to 2D-DIGE analyses followed by MALDI-TOF/TOF MS and bioinformatics analyses. In comparison to the control, 48 proteins were identified to be differentially expressed. Most of these proteins had roles in oxidative stress response as well as activating secretion of pro-inflammatory cytokines by interactions with other proteins such as TLR4. These proteins include ANXA1, PRDX1, ANXA2, and HSPB1 (356). These proteins provide insight into the host – viral

interactions and may serve as targets for further work – therapeutics and viral pathogenesis. Another study focused on understanding the central nervous system dysfunction in poultry caused by the H5N1 avian influenza virus (AIV). Proteomics – 2D-DIGE coupled with MALDI-TOF MS/MS was used to analyse the infection in chicken brain tissue. Eighteen proteins that increased in abundance and were differentially expressed were identified. In addition, 13 proteins that decreased in abundance and were differentially expressed were also identified. These proteins gave insight into viral-host interaction in the brain tissue (357). The proteomic approaches provided insight into viral-host interaction and highlighted proteins of interest. However, this method is still fairly new, and, as a result, there are limited studies using this methodology.

Sun et al. (2014) used proteomics – 2D-DIGE followed by MALDI-TOF/TOF-MS to better understand the molecular pathogenesis and replication features of the AIV with H9 subtype in chickens (356). A total of 48 proteins, which had significantly changed in abundance, were identified. Following bioinformatics, protein expression changes associated with biosynthetic, immune and inflammatory response, signal transduction, and cell death were highlighted. ANXA1 is an example of a protein that was differentially expressed and involved in the inflammatory process. ANXA1 was reduced in abundance in AIV H9 infected groups. This may suggest its association with the inflammatory phenotype. The ubiquitin-proteasome pathway (UPP) was highlighted and it has been reported to influence the replication of several viruses, IAV included. Inhibition of the UPP affects viral replication (356, 358). In AIV infected group, proteasomel subunit alpha type six was upregulated.

This suggests a mechanism via which the virus facilitates replication and infection through distinct proteasomal subunits (356).

2) IAV infection in ferrets

The domestic ferret (*Mustela putorius furo*) has frequently been utilised as a model to study the pathogenesis and transmission of influenza. This is mainly due to its natural susceptibility to the human influenza virus and its ability to portray clinical symptoms in a similar manner to humans. LC/MS analysis was used to analyse samples from the lung and trachea of ferrets infected with either 1918 or 2009 human pandemic H1N1 influenza viruses; 4811 and 4060 proteins were respectively identified. Proteins associated with innate immune and antiviral responses were highlighted. These proteins included Trim25, Stat1, and Mx1. Trim25 is part of the TRIM superfamily, which regulates viral RNA sensing pathways through the activation of RIG-I (359, 360).

3) IAV infection in mice

To understand the pathogenesis of IAV, several *in vivo* models have been used. To analyse the samples, high throughput methods, including, but not limited to, proteomics were used. Some studies have used the mouse (*Mus musculus*) as an *in vivo* model. This is mainly due to practical reasons: cost, size, husbandry requirements, species specific reagents, and ability to manipulate mice genetically (361). Tchitchek et al. (2013) used proteomics and transcriptomics (both high-throughput methodologies) to analyse mice infected with A/California/04/2009 (H1N1) (362). A total of 230 transcriptomic and 198 proteomic profiles were collected. Following analysis, the data profiles

revealed specific biological functions that were over represented in the infected cohort. These included the role of pattern recognition receptors in recognition of bacteria and viruses, death receptor signalling, and a protein ubiquitination pathway (363). There were 29 signalling pathways that overlapped and were highlighted in both transcript and protein sets. This dataset showed and confirmed that the transcriptomic and proteomic profiles complement each other (362).

Still, in a bid to understand the pathogenesis of IAV in mice further, Shen et al. (2016) (364) used shot-gun proteomic profiling to analyse samples from mice infected with IAV H3N2 A/Hong Kong/X31 at four and 10 days. The results from this study were concurrent with various studies in the literature and highlighted within this thesis. For example, proteins with significant change in abundance included interferon stimulate genes (ISGs) ISG15, proteins relevant to interferon signalling, members of the IFIT family (IFIT1, IFIT2, IFIT3). These proteins play vital roles in inhibiting translation of uncapped viral RNA, thus suggesting the activation and stimulation of the antiviral pathway. IFITM3 is another protein that increased in abundance. IFITM3 plays a specific role in inhibiting IAV (364).

4) IAV infection in macaques

Rodent (mice and ferrets) model systems have frequently been used to study IAV, as seen above (365). However, the genetic and physiological differences

when comparing the datasets to humans have led to the use of more physiologically relevant models (366). Therefore, research has turned to several macaque species to study IAV. This includes *Macaca mulatta, Macaca nemestrina*, and *Macaca fascicularis*. These macaque species are currently used to study other viruses, such as HIV, Ebola, variola major, and IAV (367, 368). Understanding the pathogenesis of IAV, and the host response to IAV, is important, especially if the virus has the potential to cause a pandemic. Baas et al. (2006) combined both high-throughput methods – proteomic and genomics – to analyse *Macaca nemestrina* infected with H1N1 A/New Cal/20/99, H3N2 A/Panama/2007/99 and H3N2 A/New Mexico/17/2003. Samples were collected at two, four, and seven days (367). The proteins that were differentially abundant in infected samples included GBP1, HMOX1, IFI44, IFIT1, IFIT2, IFIT3, LAMB1, MX1, SFTPD, and STAT1. Most of these proteins, especially those from the interferon family – IFIT1, IFIT2 and IFIT3 – have antiviral roles (367). These proteins may be potential biomarkers and indicators of IAV. The data obtained from this study concurred with data from human studies challenged with IAV. For example, IL-6 and TNF-α were highlighted in this study and have an increased abundance in nasal lavage fluid. IL-6 and IFN-γ also increased in abundance in volunteers infected with influenza A/Texas/36/91/virus (369, 370). A subset of the proteome results overlapped with parallel transcriptomic results (371), especially when focusing on interferon-mediated and anti-virus responsive factors (367).

Brown et al. (2010) (372) built on the findings of Baas et al. (2006) (367) described above, and further analysed the *in vivo* host proteome response to

IAV infection (372). Cynomolgus macaque (*Macaca fascicularis*) were infected with high pathogen avian influenza (HPAI) and observed over seven days; 35,239 peptides (about 4,250 proteins) were identified, while Baas et al. (2006) identified 15,322 peptides (3,098 proteins). 10,156 peptides (2,287 proteins) were found in both studies (372). Data analysis by ingenuity pathway analysis identified the following biological processes: inflammatory response, complement system, role of pattern receptors in recognition of bacteria and viruses, replication of virus, and immune response (372). Extensive datasets have been obtained in previous studies that used high-throughput methods to evaluate IAV-host interaction.

The findings presented in this chapter used high throughput proteomic methods on clinical left-over material of NHP macaques infected with IAV. Samples were collected at two and seven days, post infection. These samples were kindly provided by our collaborators at Public Health England (PHE) (studies headed by Prof Miles Carroll and Dr Catherine Whittaker). Table 4.0 highlights the different samples, location, personnel in charge, and techniques used.

Table 4.0 Compilation of the samples used in this study, their location, personnel in charge, routes of infection, MOI of infection and the techniques used for analysis

Samples	Location	Personnel in charge	Routes of Infection	Plaque Forming Units (Measure of the number of infectious particles)	Techniques
Cynomolgus NHP Macaque (*Macaca Fascicularis*) – Broncho alveolar fluid (BALF)	Public Health England (PHE)	Prof Miles Carroll Dr. Tony Marriott	Inhaled aerosol (i.a), intra-nasal (i.n) and intra-tracheal (i.t)	Inhaled aerosol – 10^5 pfu	Infection then mass spectrometry

Only animals infected via inhaled aerosol (i.a) showed signs of disease throughout the body. For this reason, samples from NHP infected via i.a were used in this study; other routes of infection showed a confinement of the disease within a section of the body. The infected and non-infected (mock) samples were used for the analysis presented in this chapter.

The samples obtained from the NHP macaques were subjected to proteomic analysis on the label-free mass spectrometry Q-Exactive platform.

Data from this chapter contributed towards the following publication:

Marriott AC, Dennis M, Kane JA, Gooch KE, Hatch G, Sharpe S, Prevosto C, Leeming G, **Zekeng EG**, Staples KJ, Hall G, Ryan KA, Bate S, Moyo N, Whittaker CJ, Hallis B, Silman NJ, Lalvani A, Wilkinson TM, Hiscox JA, Stewart JP, Carroll MW. 2016. Influenza A Virus Challenge Models in Cynomolgus Macaques Using the Authentic Inhaled Aerosol and Intra-Nasal Routes of Infection. *PLoS One.* 11(6): e0157887. doi: 10.1371/journal.pone.0157887.

The general bioinformatics approaches developed were also used in the following publication:

Liu X, Speranza E, Muñoz-Fontela C, Haldenby S, Rickett NY, Garcia-Dorival I, Fang Y, Hall Y, **Zekeng EG**, Lüdtke A, Xia D, Kerber R, Krumkamp R, Duraffour S, Sissoko D, Kenny J, Rockliffe N, Williamson ED, Laws TR, N'Faly M, Matthews DA, Günther S, Cossins AR, Sprecher A, Connor JH, Carroll MW,

Hiscox JA. 2017. Transcriptomic signatures differentiate survival from fatal outcomes in humans infected with Ebola virus. *Genome Biology*. 18(1):4. doi: 10.1186/s13059-016-1137-3.

4.2 RESULTS

4.2.1 Host – viral cellular overview from BALF from NHP cynomolgus macaques infected with influenza A H1N1 pandemic virus via an i.a challenged route

To obtain an overview of the cellular interactome upon infection with IAV, BALF from NHP cynomolgus macaques was collected and analysed by label-free mass spectrometry. NHPs were i.a challenged with IAV H1N1 2009 pandemic virus at a dose of 10^5 pfu. The proteins from these samples, alongside proteins from BALF of naïve NHP cynomolgus macaques, were extracted and subjected to proteomic analysis using label-free mass spectrometry and the results were compared. Figure 4.1 illustrates the work flow from infection to analysis.

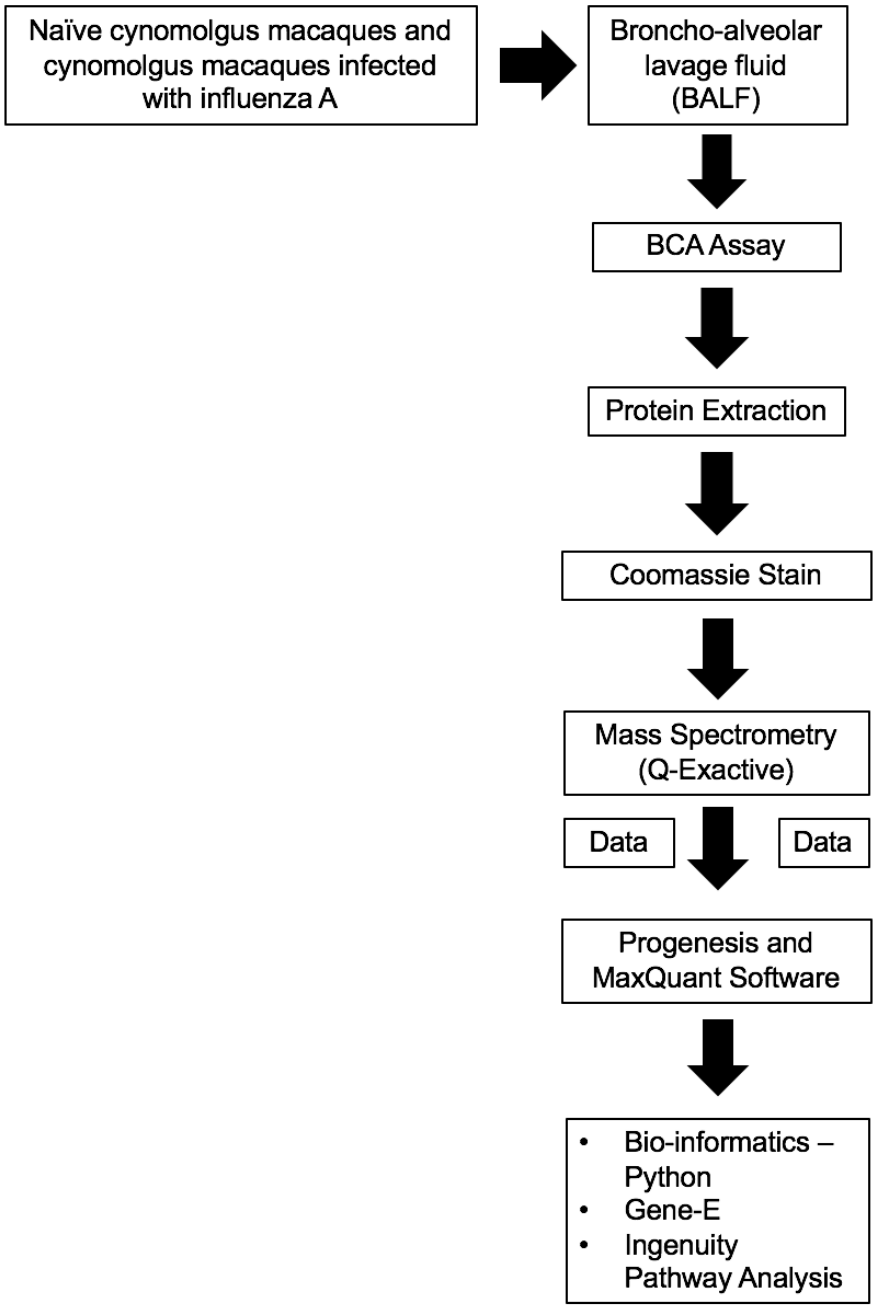
Naïve cynomolgus macaques and cynomolgus macaques infected with influenza A
Broncho-alveolar lavage fluid (BALF)
BCA Assay
Protein Extraction
Coomassie Stain
Mass Spectrometry (Q-Exactive)
Data
Data
Progenesis and MaxQuant Software
• Bio-informatics – Python
• Gene-E
• Ingenuity Pathway Analysis

Figure 4.1: Schematic workflow for the processing of broncho-alveolar fluid (BALF) samples from NHP cynomolgus macaques infected with IAV 2009 pandemic infection. Protein concentration was measured via the BCA assay and proteins were extracted from the samples. The samples were subjected to Coomassie staining followed by analysis on the mass spectrometry platform: Q-Exactive for label-free proteomics and subsequent data analysis. The data from the samples were analysed via Progenesis and Maxquant software. Further data analysis was done via bio-informatic python, Gene E, and Ingenuity pathway analysis (IPA).

Proteins from BALF obtained from cynomolgus macaques, naïve and infected, were extracted and subjected to Coomassie staining as described in Figure 4.1. This was to ensure the presence of protein in all samples prior to the proteomic analysis on the label-free mass spectrometry platform (Q-Exactive) (Figure 4.3).

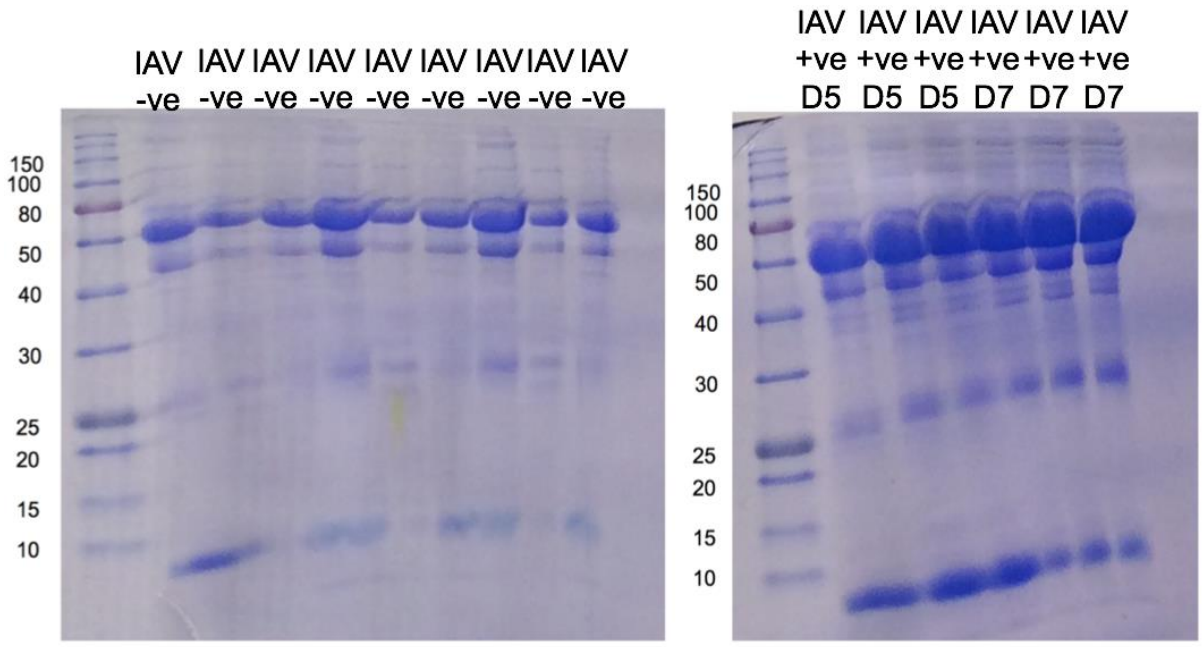

Figure 4.2: Coomassie staining of proteins obtained from BALF from naïve cynomolgus macaques and cynomolgus macaques infected with IAV H1N1 2009 pandemic via inhaled aerosol at a dose of 10^5 pfu culled five days post infection and seven days post infection. Equal protein concentration of each sample was loaded onto each well and stained to confirm the visual presence of protein in each sample. This figure confirms the presence of protein in each sample. The unequal band size seen shows the protein variation in each sample.

4.2.2 Defining the proteome of BALF taken from naïve and influenza A 2009 pandemic cynomolgus NHP at day five and day seven post-infection.

To carry out this study, BALF samples were obtained from naïve NHPs, NHPs infected and culled at five days post infection and NHPs infected and culled at seven days post infection. The BALF proteome from three naïve NHPs (mock), three IAV-positive NHPs (culled at five days post infection) and three IAV-positive NHPs (culled at seven days post infection) were compared. A label-free quantitative proteomic approach was used to identify and quantify proteins from these samples. Each sample was simultaneously run in triplicate on the Q-Exactive platform to ensure reliability, reduce technical variation, and ensure the statistical relevance of the obtained data. Several data-processing steps were used to increase precision when highlighting proteins, which have significantly increased, decreased in abundance, or stayed the same. These steps included the removal of proteins identified with low confidence, including proteins identified by a single peptide, the p-value was set at 0.05 and proteins with an abundance difference of two-fold or more were recorded as being differentially abundant. This ensured that the final proteins selected were significantly differentially abundant when comparing the data set from naïve samples (mock) to IAV-positive samples. The data obtained from the mass spectrometry was analysed in three comparable sets (Table 4.1).

Table 4.1 Data comparisons of proteome from BALF from NHP and the proteome data observed and obtained from the comparisons and analysis

Comparisons	Total number of proteins (including single peptides)	Proteins after data processing steps	Number of proteins significantly increased in abundance	Number of proteins significantly decreased in abundance	Figures
Naïve NHP vs i.a infected NHP (5 Day's post infection)	1038	509	49	76	4.3

Naïve NHP vs i.a infected NHP (7 Day's post infection)	714	509	67	77	4.4
i.a infected NHP (5 Day's post infection) vs i.a infected NHP (7 day's post infection)	1149	721	58	83	4.5

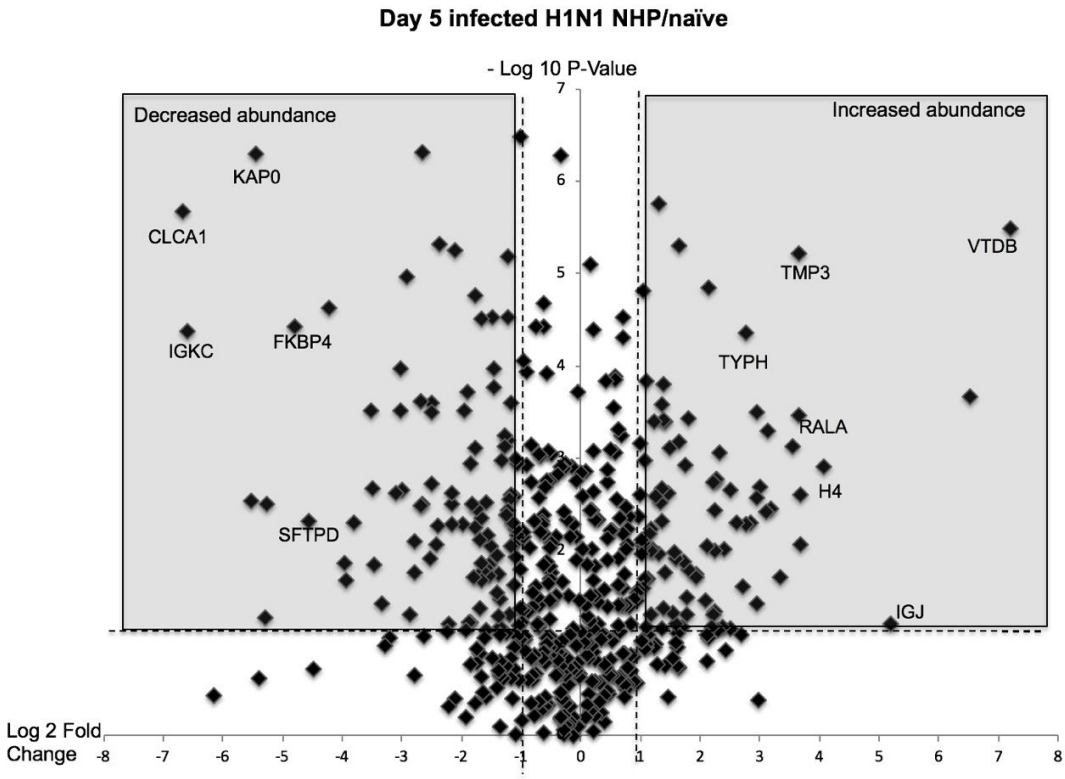

Figure 4.3: The volcano plot of proteins increased and decreased in abundance in individual broncho-alveolar lavage fluid (BALF) samples from inhaled aerosol (i.a) IAV-H1N1 2009 pandemic-infected NHP cynomolgus macaques (n=3) culled five days post-infection, compared to samples from naïve cynomolgus macaques (n=3). The vertical dashed lines indicate a cut-off of two-fold change between infected and naïve, while the horizontal dashed line indicates a p-value of <0.05 to define cohorts of polypeptides (shaded areas) with significantly increased (right-hand side) or decreased (left-hand side) abundance in infected samples.

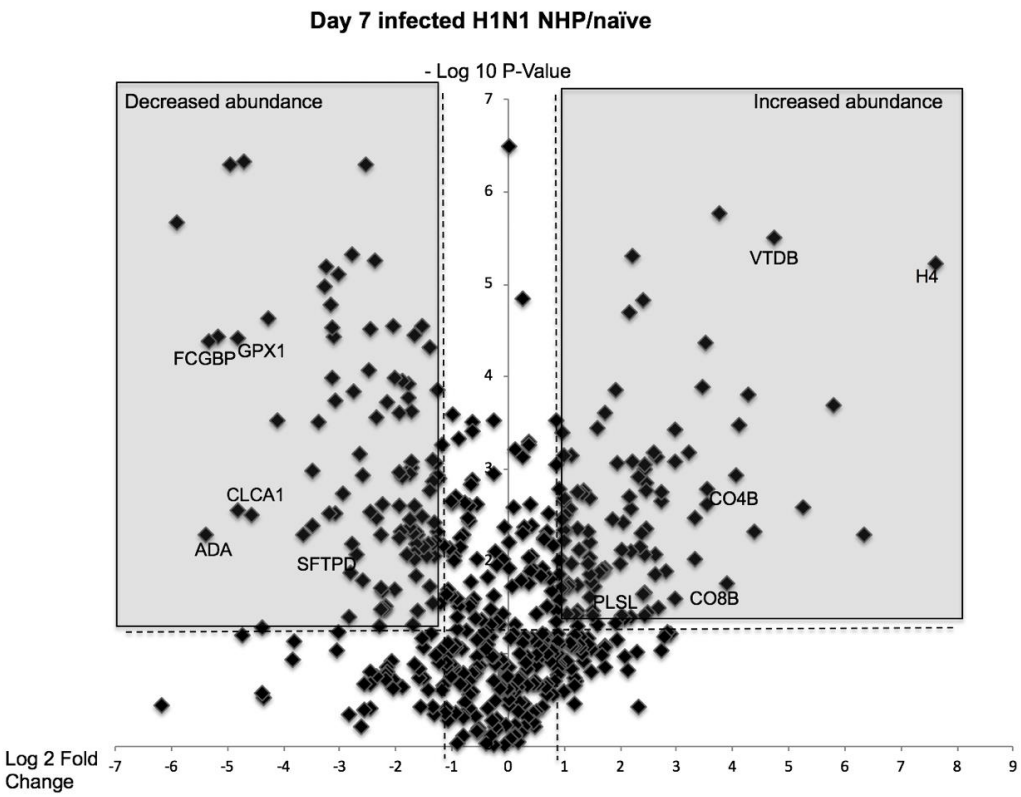

Figure 4.4: The volcano plot of proteins increased and decreased in abundance in individual broncho-alveolar lavage fluid (BALF) samples from inhaled aerosol (i.a) IAV-H1N1 2009 pandemic-infected NHP cynomolgus macaques (n=3) culled seven days post-infection compared to samples from naïve cynomolgus macaques (n=3). Vertical dashed lines indicate a cut-off of two-fold change between infected and naïve, while the horizontal dashed line indicates a p value of <0.05 to define cohorts of polypeptides (shaded areas) with significantly increased (right-hand side) or decreased (left-hand side) abundance in infected samples.

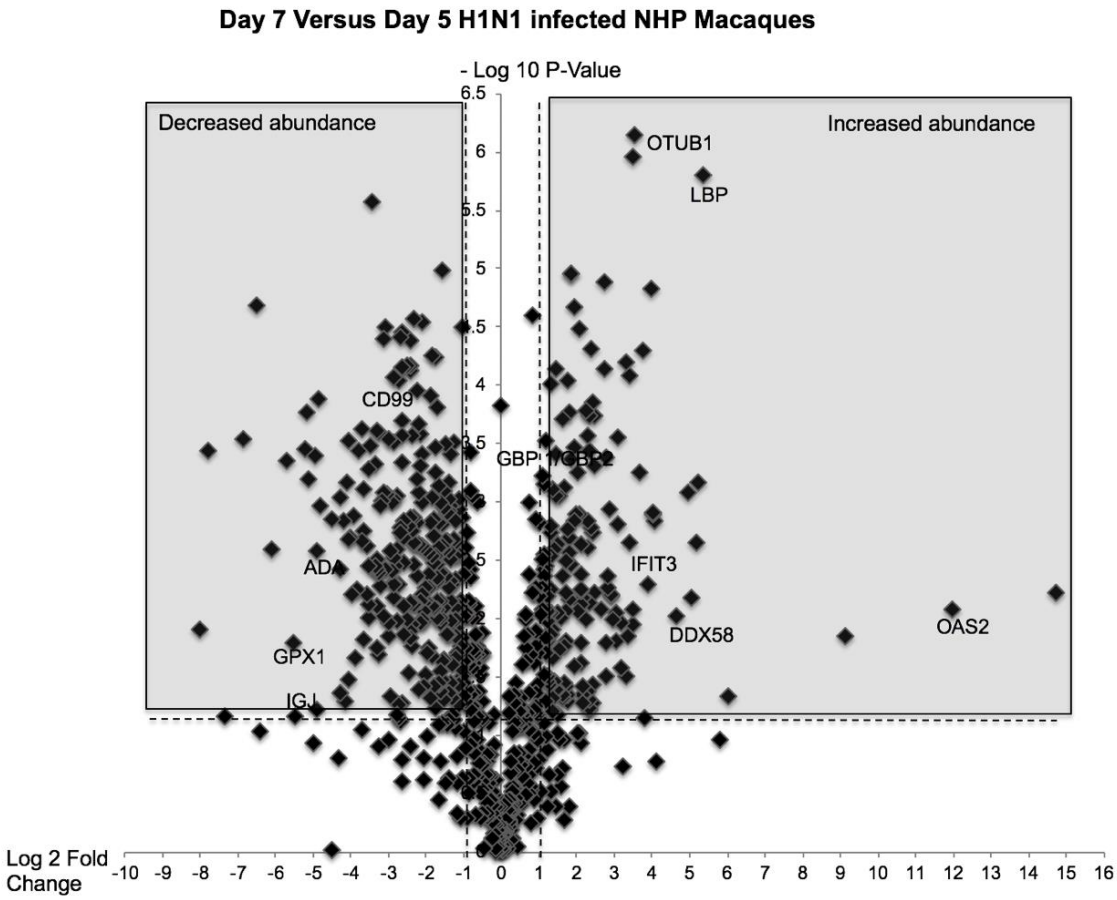

Figure 4.5: The volcano plot of proteins increased and decreased in abundance in individual broncho-alveolar lavage fluid (BALF) samples from inhaled aerosol (i.a) IAV-H1N1 2009 pandemic-infected NHP cynomolgus macaques (n=3) culled seven days post-infection compared to samples from IAV-H1N1 2009 pandemic infected NHP cynomolgus macaques (n=3) culled five days post-infection naïve cynomolgus macaques (n=3). Vertical dashed lines indicate a cut-off of two-fold change between infected and naïve, while the horizontal dashed line indicates a p-value of <0.05 to define cohorts of polypeptides (shaded areas) with significantly increased (right-hand side) or decreased (left-hand side) abundance in infected samples.

4.2.3 Identification and quantification of cellular proteins in BALF

Thermo RAW files were imported into Progenesis QI (version 2.0, Nonlinear Dynamics). Replicate runs were time-aligned using default settings and an auto-selected run as a reference. Peaks were selected by the software using default settings and filtered to include only peaks with a charge state of between +2 and +6. Spectral data were transformed to .mgf files with Progenesis QI and exported for peptide identification using the Mascot (Matrix Science) search engine against a custom database that contained the common contamination and internal standards, H1N1_CA_2009_Mar15, and UniProt Homo sapiens reviewed proteins (373) (February 2015). The search parameters were as follows: precursor mass tolerance was set to 10ppm and fragment mass tolerance was set to 0.01 Da. One missed tryptic cleavage was permitted. Carbamidomethylation was set as a fixed modification and oxidation (M) was set as a variable modification (374). The false discovery rates were set at below 1% using Mascot Percolator and the search results were imported back to Progenesis. Raw abundances of replicates from Progenesis QI output of Naïve, day five and day seven samples were compared first where matching identifications with >=2 unique peptides were selected for normalisation using the Loess Global normalisation method provided by Normalyzer (375). The reported abundance is the mean of the biological replicates.

4.2.4 Bioinformatics Analysis – Protein Pathway Analysis

Data were analysed through the use of Ingenuity Pathway Analysis (IPA) (QIAGEN Inc., https://www.qiagenbioinformatics.com/products/ingenuity-

pathway-analysis). Networks linking differentially abundant proteins and their effects were generated using Ingenuity Pathway Analysis (IPA) (QIAGEN Inc., https://www.qiagenbioinformatics.com/products/ingenuity-pathway-analysis).

The data sets used contained accession gene identifiers, corresponding maximum fold-change values, and P-values, which were uploaded into the application. To select for genes which expressions were significantly differentially regulated, a cut-off of 1.0 was set. The application contains a global molecular network onto which these genes were overlaid. These genes were connected based on proven studies supported by references in the literature, or known canonical pathways present in the application knowledge base.

4.2.5 Protein Pathway Analysis

The analysis of these data revealed proteins already identified *in vitro* (cells) Chapter 3. In addition to this, a focus on immune response highlighted various aspects similar to those observed in IAV-infected humans: i.a. induced a transient lymphopenia and virus-specific cellular immune responses. There was a significant increase in the activation of lung macrophages and innate immune response at five to seven days post-infection. The kinetics of infection, virological and immunological were broadly in line with human IAV infections.

Analysis of cellular proteins in BALF – Focus on Immune response

These data indicated that at day five and day seven post-infection proteins associated with the innate and adaptive immune responses had differential abundance when compared between these time points as well as to BALF

taken from the naïve animals. At day seven post-infection, there was an increase in type I interferons including interferon α (IFNα) and its variants, compared to day five post-infection. These specific proteins were not identified by mass spectrometry (this may be a result of low abundance compared to other proteins) and therefore their presence is inferred due to the known activation of the highlighted proteins in Table 4.2. The abundances of interferon induced gene products, such as IFN-induced proteins with tetratricopeptide repeats (IFITs) 1, 2 and 3 (Figure 4.3, 4.4 and 4.5) (262) are significantly higher at day seven then at day five (p-values of 0.014, 0.0054 and 0.0049 respectively). IFN-inducible guanylate binding protein (GBP) 1 and 2, also known to be regulated by interferon (376) were also significantly different (as determined by Progenesis) between day seven post-infection and day five post-infection (Figure 4.5).

Table 4.2; Analysis of proteins identified in the BALF of samples from i.a. challenged NHP seven days post-infection, compared to samples from i.a. challenged NHP 5 days post- infection involved in immune response.

	Protein accession significantly increased in abundance	Protein name	Fold change	Proteins significantly decreased in abundance	Protein name	Fold change	Proteins affected by association but not identified in the mass spectrometry data
1	IFIT3	Interferon-induced protein with	14.6	SGTA	Small glutamine-rich tetratricopeptide repeat-	-4.1	IFN alpha/beta

		tetratricopeptide repeats 3			containing protein alpha		
2	IFIT1	Interferon-induced protein with tetratricopeptide repeats 1	10.1	SODE	Extracellular superoxide dismutase	-7.3	IFN type 1
4	EIF3	Eukaryotic translation initiation factor 3	9.95	DDAH2	Dimethylarginine dimethylamino hydrolase 2	-1.6	JAK

5	MX1	Myxovirus 1	6.9	POSTN	Periostin	-1.6	IFN Beta
6	ISG20	Inteferon-stimulated gene 20 KDa	8.5	FHL1	Four and a half LIM domains protein 1	-1.7	Collagen type II
7	DDX58	Probable ATP-dependent RNA helicase	31.4	DHX8	Facilitates nuclear export of spliced mRNA by releasing the RNA from the spliceosome	-1.6	MTORC2
8	IDO1	Indoleamine 2,3-dioxygenase 1	3.5				Cpla2

9	C1QC	Complement C1q subcomponent subunit C	3.5				Collagen II
10	C1q	Complement C1q subcomponent	2.3				IFN
11	C1QB	Complement C1q subcomponent subunit B	4.1				
12	C1QA	Complement C1q	2.2				

		subcomponent subunit A					
13	SFTPD	Pulmonary surfactant-associated protein D	2.7				
14	IgG	Immunoglobulin G					

A significant increase was observed at day seven, compared to day five, post-infection in the abundance of interleukins (IL), including IL1B, IL2, IL4, IL5, IL6, IL10, and IL13. In addition, CXCL7 also increased in abundance at day seven compared to day five post-infection. Proteins associated with the activation of lymphocytes were identified at day five post-infection, but not at day seven post-infection.

Proteins associated with the activation of macrophages were more abundant in BALF from NHP collected at five and seven days post-infection compared to BALF from naïve animals (Figure 4.3 and 4.4). However, at day seven post-infection, proteins associated with inhibiting the activation of macrophages were increased in abundance compared to day five post-infection. At both day five and day seven post-infection, there was an increase in proteins associated with the activation of neutrophils, with more neutrophils present at day five. Proteins associated with the activation of lymphocytes were identified at day five post-infection but not at day seven post-infection. There was a further increase in viral replication in NHP seven days post infection in comparison to five days post infection (Figure 4.5).

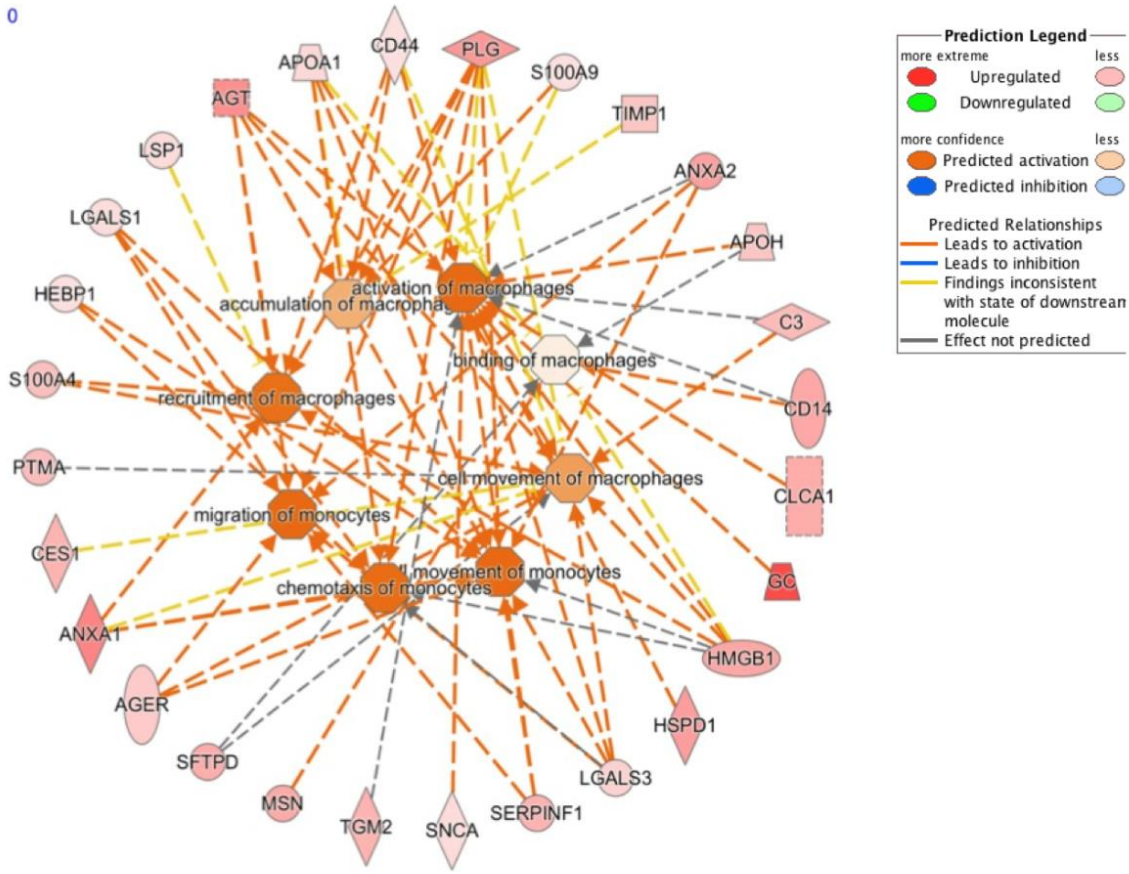

Figure 4.6: Network pathway analysis of proteins identified in the BALF of samples from i.a. challenged NHP five days post-infection, compared to samples from naïve NHP samples. The network highlights proteins increased in protein abundance involved in activation of macrophages in samples five days post-infection compared to naive NHP samples. Proteins in green highlight a two-fold or more decrease in abundance in the NHP five days post-infection compared to naïve NHP samples. Proteins in red highlight a two-fold or more increase in abundance. The shapes separate the different molecular classes. The lines with solid arrows represent a direct molecular interaction with one transcript initiating the other and the dashed arrows an indirect molecular interaction with one transcript potentially initiating the other. Strong

lines without an arrow show a relationship between two transcripts and dashed lines without an arrow show an assumed relationship between two transcripts molecules. Strong lines or dashed lines with a dash at the end are inhibitory to that transcript. The transcripts that were not highlighted were not identified in the dataset but are indirectly involved in these pathways.

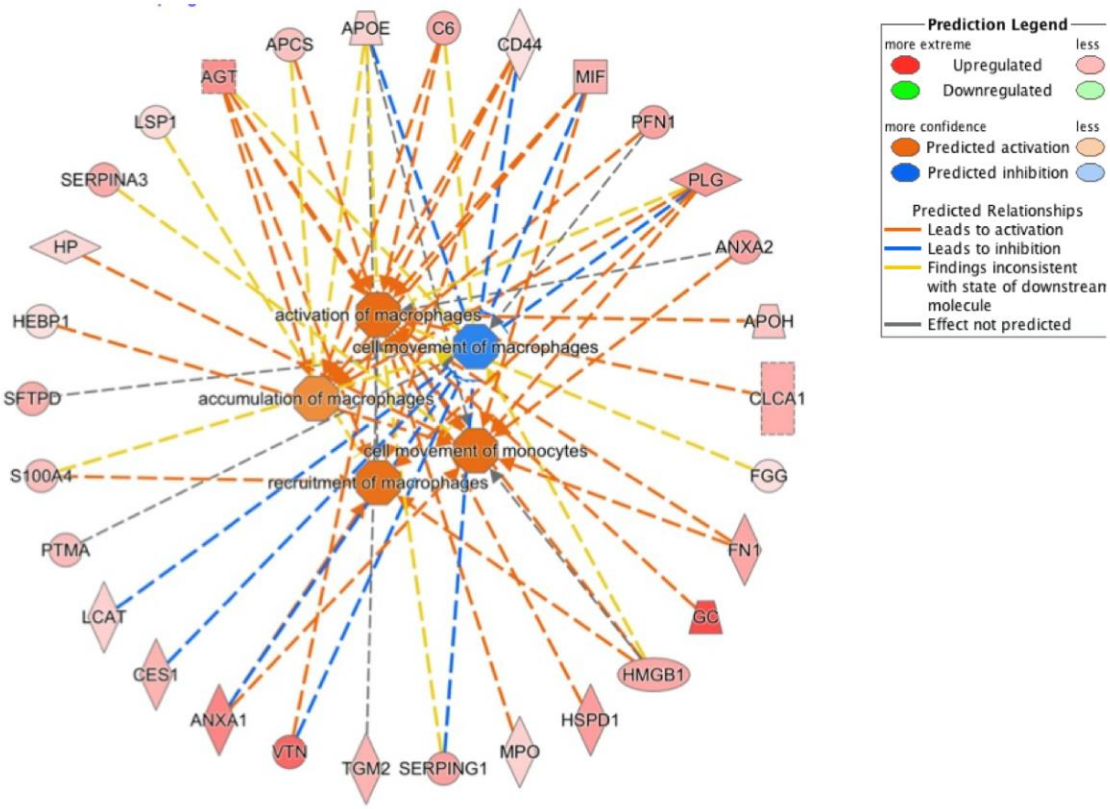

Figure 4.7: Network pathway analysis of proteins identified in the BAL fluids of samples from i.a. challenged NHP seven days post-infection, compared to samples from naïve NHP samples. The network highlights the proteins increased in the protein abundance involved in activation of macrophages in samples seven days post infection, compared to naive NHP samples. Proteins in green highlight a two-fold or more decrease in abundance in the NHP five days post-infection compared to naïve NHP samples. Proteins in red highlight a two-fold or more increase in abundance. The shapes separate the different molecular classes. The lines with solid arrows represent a direct molecular interaction with one transcript initiating the other and the dashed arrows an indirect molecular interaction with one transcript potentially initiating the other. Strong lines without an arrow show a relationship between two transcripts and dashed lines without an arrow show an assumed relationship between two

transcripts molecules. Strong lines or dashed lines with a dash at the end are inhibitory to that transcript. The transcripts that were not highlighted were not identified in the dataset but are indirectly involved in these pathways.

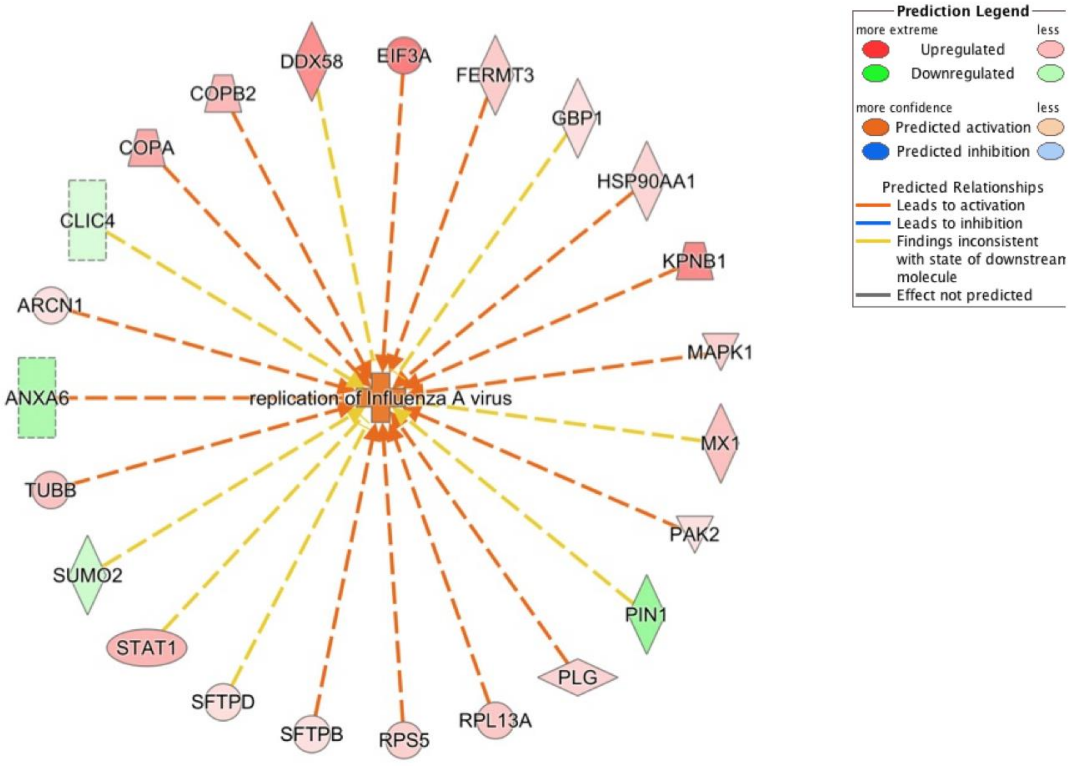

Figure 4.8: Network pathway analysis of proteins identified in the BALF of samples from i.a. challenged NHP seven days post-infection, compared to samples from i.a. challenged NHP five days post- infection. The network highlights proteins necessary to activate the replication of IAV. Proteins in green highlight a two-fold or more decrease in abundance in the NHP seven days post-infection compared to samples from NHP five days post-infection. Proteins in red highlight a two-fold or more increase in abundance. The shapes

separate the different molecular classes. The lines with solid arrows represent a direct molecular interaction with one transcript initiating the other and the dashed arrows an indirect molecular interaction with one transcript potentially initiating the other. Strong lines without an arrow show a relationship between two transcripts and dashed lines without an arrow show an assumed relationship between two transcripts molecules. Strong lines or dashed lines with a dash at the end are inhibitory to that transcript. The transcripts that were not highlighted were not identified in the dataset but are indirectly involved in these pathways.

4.3 DISCUSSION

The first aim of this thesis was to characterise IAV *in vitro* using a common cell culture model of A549 cells (Chapter 3) and observe the host proteome response to IAV infection. The results obtained from *in vitro* studies are limited to cellular responses and frequently omit an adaptive immune response. In addition, the multiple cell types present in the human/animal airway affect the response observed *in vivo* compared to *in vitro*. This chapter focused on examining the host response to IAV in a cynomolgus NHP macaque (*Macaca Fascicularis*) commonly used to study IAV. This data was subsequently compared to data from an *in vitro* cell culture model (Chapter 3). The data from the cynomolgus NHP macaque (*Macaca Fascicularis*) in this chapter was compared to the data obtained from the analysis of NAs in IAV positive and IAV-negative paediatric patients (Chapter 5). The data from the viral-host interactome in Chapters 3 and 4 reveals and suggests different stages of

infection, host interaction, and immune response. The cynomolgus NHP macaque (*Macaca Fascicularis*) is advantageous due to the semblance of the immune system to the human host.

The aim of this chapter was to understand the *in vivo* proteome host response post-IAV infection in the cynomolgus NHP macaque (*Macaca Fascicularis*). In the NHP macaques, emphasis was laid on the immune response due to the similarity observed in human response to IAV infection. In addition to the immune response, host proteins, which were significantly differentially abundant when comparing the IAV-positive and IAV-negative conditions that were highlighted. Some of these proteins include IFN-induced proteins with tetratricopeptide repeats (IFITs) 1, 2 and 3 (Figure 4.3, 4.4 and 4.5), which had a significant increase in abundance at day seven compared to day five. An increase and activation of alveolar macrophages, monocytes, and replication of IAV was observed. Samples from IAV positive NHP culled five- and seven-days post infection were compared between themselves and to samples from IAV-negative NHPs.

The analysis of the proteome of BALF taken from IAV-positive and IAV-negative NHP macaques revealed a vast dataset of results. Some of these results included protein changes that have been previously described in other experimental model systems and in the macaque model. The novel data this comparison provided was analysed and contributed to a publication (262). The data analysis revealed an increased and sustained expression of type I interferons, which are associated with infection of a highly pathogenic influenza virus (H5N1) (371). Studies in mice showed a correlation between

an increase in infectious viral load and macrophage and neutrophil depletion, highlighting the significance of macrophage and neutrophils in controlling IAV viral replication and spread (377). Another study in mice infected with a recombinant IAV strain, which had HA and NA from the 1918 pandemic, showed an increase in mortality rate along with an increase in viral replication, greater influx of neutrophils in the lungs, increased number of alveolar macrophages (AM), and increased protein expression of cytokines and chemokines (378, 379). These are concordant with findings within this study: an increase in viral replication, activation of macrophage, and influx of cytokines and chemokines.

Investigating the reason for the virulence of the 1918 pandemic has led various scientists to several suggestions. Some of these suggestions include severe lung pathology caused by the influx of AM, neutrophils, and cytokines. These responses have a part to play in exacerbating the mortality of the disease on the host. Macrophages and neutrophils have a central part to play in the host defence as they respond quickly to viral infection. The proteome analysis of the BALF from NHP culled five- and seven-days post infection showed a much-elevated level of AMs in comparison to naïve NHP. Furthermore, in NHP culled seven days post infection, there was activation for inhibition of AMs. This potentially demonstrates that, at this point, the presence of AMs is causing more lung pathology (380, 381). An interesting study that could be further carried out would be exploring the maximum number of AMs required to induce lung pathology, at which point, could be a defining marker for the prediction of disease outcomes in the host.

IFNβ was not highlighted as differentially abundant but was activated in the immune response pathway by other significantly differentially abundant proteins. Studies in mice showed the effects of various host responses on one another, including vascular margination of T lymphocytes induced by direct interaction with type I interferons (382). The data in this study is in concordance with our findings. The innate immune response observed in this study aligns with previously published studies carried out in ferrets, mice, and other NHPs infected with IAV. The host immune response to the viral infection plays a role in exacerbating the severity of the disease. The convergence of host responses with one another further affects the overall host response to viral infection.

This chapter provides information on the proteome from BALF highlighting proteins differentially abundant in NHP infected with IAV. The findings in this study are concordant with various findings in the literature. Most importantly, it provides information about different stages of infection and the change in the proteome in BALF when comparing IAV-positive NHP to IAV-negative NHPs.

It is important to note there were proteins concurrent throughout the chapters – interferon-induced proteins alongside other proteins involved in the replication of IAV present *in vitro* (Chapter 3), now *in vivo* in the NHP, and subsequently, the human nasopharyngeal aspirates (Chapter 5). The reoccurrence of these proteins suggests they have essential roles in an IAV-infected host. These proteins could serve as potential biomarkers for the severity of the disease. The state of the immune response, if further analysed,

could provide specific information on the disease progression in hosts. Considering IAV is a respiratory infection that affects the immune system, immune system biomarkers could be the turning point of an indication for IAV disease progression.

RESULTS CHAPTER 5:
CHARACTERISING THE HOST RESPONSE TO INFLUENZA A VIRUS INFECTION *IN VIVO* IN HUMANS BY ANALYSING NASOPHARYNGEAL ASPIRATES (NA) FROM PAEDIATRIC PATIENTS (2–13 YEAR OLDS)

5.1 INTRODUCTION

The IAV has caused millions of deaths over the years since the 1918 pandemic. Seasonal IAV infection globally infects 5–10% of adults and 20–30% of children. Deaths are mainly associated with high-risk groups including children, the elderly, and patients who are chronically ill. Annual infections account for 3–5 million cases of severe illness and about 250,000 to 500,000 deaths worldwide (353). Clinical signs and symptoms are frequently used to detect IAV in emergency departments. This follows the Centre for Disease Control (CDC) guidelines. Clinical diagnoses done in these settings and following these guidelines had a low sensitivity of 36% and specificity of 78% (383). To improve sensitivity and specificity, improved methods of diagnosis to guide management in clinical settings are required. The response of the host to IAV infection is not just restricted to the cellular environment. Infection influences several biological processes, particularly in the respiratory tract and airway secretions. Understanding the biological processes behind a host response provides an opportunity to determine a sensitive diagnostic biomarker linking to a predictive outcome. This creates a diagnostic strategy, which is not totally reliant on the pathogen, but enables IAV infection to be categorised based on the host response (384-386). Host gene expression profiling was used in the early diagnosis of IAV-H1N1 and IAV-H3N2 (387). Human volunteers (aged between 20 and 41 years) were inoculated with both H1N1 and H3N2 strains and their gene profile monitored over seven days. This dataset was converted into a gene signature with the ability to detect 94% of IAV infected cases. This dataset was used in an emergency setting to differentiate between infected and non-infected patients. It was 92% accurate

(387). The top 50 genes identified in this dataset were mostly related to the host antiviral response (387). Some of these genes included multiple interferon response elements, STAT-1, RIG-I, the myxovirus-resistance gene MX1, and the OAS family (387) (388-390). In addition, some of the genes identified within this dataset could be combined into networks responsible for the development or amplification of the immune response. Whilst the effects of IAV infection on the host are largely indicated by the immune response (387), the entirety of the host expression on a cellular level still needs to be determined. Clusters of symptoms and certain criteria (vaccination and age) observed in clinical settings have allowed medical personnel to distinguish between IAV-H3N2 and IAV-H1N1 positive (391). Vaccinated patients developed pneumonia, while non-vaccinated patients had IAV. Age played a factor, as patients above 54.5 years had H3N2, while patients below this age had H1N1 (391). Whilst these findings are insightful, the population most vulnerable to IAV are children. Children under five (1.9/1000) have the highest influenza admission rate. Admission rate increases 5.7-fold for 5–24-year olds. Patients above 65 have the majority (72%) of influenza-related deaths in hospital with co-morbidities (392). The host response to IAV, particularly in humans, still requires extensive characterisation. This will provide data that informs the search of biomarkers for increased diagnostic efficiency or to further understand the aetiology of the virus.

Respiratory disease can be predicted to alter the function of the airway and this would manifest in changes in the protein composition of the nasopharyngeal aspirates (NAs). One way to assess this is by characterising

the proteome of the NAs between infected and non-infected individuals. Several factors, such as a small sample size and non-high throughput methods, have limited the research on NA proteome changes infected with IAV (393). Other respiratory diseases, such as asthma, chronic obstructive pulmonary disease (COPD), and cystic fibrosis (394-396) have been comparatively more researched.

The advancement in high resolution approaches, such as sequencing and proteomics, allows for a more in-depth analysis of the host response to IAV infection. Accordingly, this study used a label-free quantitative proteomic approach to identify proteins that were differentially abundant in the proteome of NAs from laboratory confirmed paediatric IAV cases. To increase robustness, samples from three separate geographical locations (Alder Hey Children's Hospital (AHCH), Liverpool, UK; Great Ormond Street Hospital (GOSH), London, UK; and Institute Pasteur (IPD), Dakar were chosen. Samples from laboratory-confirmed IAV-positive patients were compared to matched samples from patients that tested negative for IAV and other common respiratory pathogens. The data indicated that both representation of virus abundance (Ct value) and strain (H3N2 versus H1N1) had a direct effect on the composition of the NAs proteome compared to IAV-negative samples. Furthermore, a set of proteins were identified with differing abundance that distinguished an infected sample from a non-infected sample and could therefore be used towards biomarker selection.

Data from this chapter mainly contributed towards the following publication:

Elsa G Zekeng, Dong Xia, Stuart Armstrong…Julian A Hiscox. '**The application of nasopharyngeal aspirates to evaluate proteomic changes in airway secretions during influenza virus infection in paediatric cases**'

The main aim of this chapter was to characterise the pathogenesis of IAV in humans through the analysis of NA samples taken from patients. The data was mined for the presence of potential biomarkers, which could be used to delineate an IAV-positive sample from an IAV-negative sample. The data was subsequently compared (in general discussion in Chapter 6) to data obtained from *in vitro* studies (Chapter 3) and *in vivo* studies (NHP macaques – Chapter 4). This was with an aim to evaluate and understand IAV pathogenesis in each model system.

5.2 RESULTS

The aim of this study was to investigate how the protein compositions of airway secretions in paediatric cases were altered following IAV infection. The data from this study primarily provided a deeper understanding of IAV pathogenesis in the host. Subsequently, it highlighted the proteomic differences between IAV-H3N2-positive, IAV-H1N1-positive, and IAV-negative samples. Finally, it identified potential host-protein biomarkers as a sign of infection and explored the part that viral load has to play in increasing these proteomic differences. NAs from three different sites: AHCH, GOSH, and IPD, were obtained from paediatric patients and were confirmed as IAV positive or negative by RT-PCR. The workflow used to analyse NA samples in this study are shown in Figure 5.1. Proteins were extracted from NAs; identified and quantified via LC-MS/MS to compare the proteomes in the various samples, followed by bioinformatics analyses on Ingenuity Pathway Analysis (IPA). The results showed that similar proteins were significantly differentially abundant across the sample cohorts, but had varying amounts of proteins within each cohort. In parallel, SDS-PAGE and ELISA were applied to selected examples to validate the LC-MS/MS data. To confirm protein extraction from the NAs, equal volumes of samples were separated by 1D SDS-PAGE and stained with Coomassie blue. Downstream sample analysis by western blot and ELISA were standardised to protein concentration.

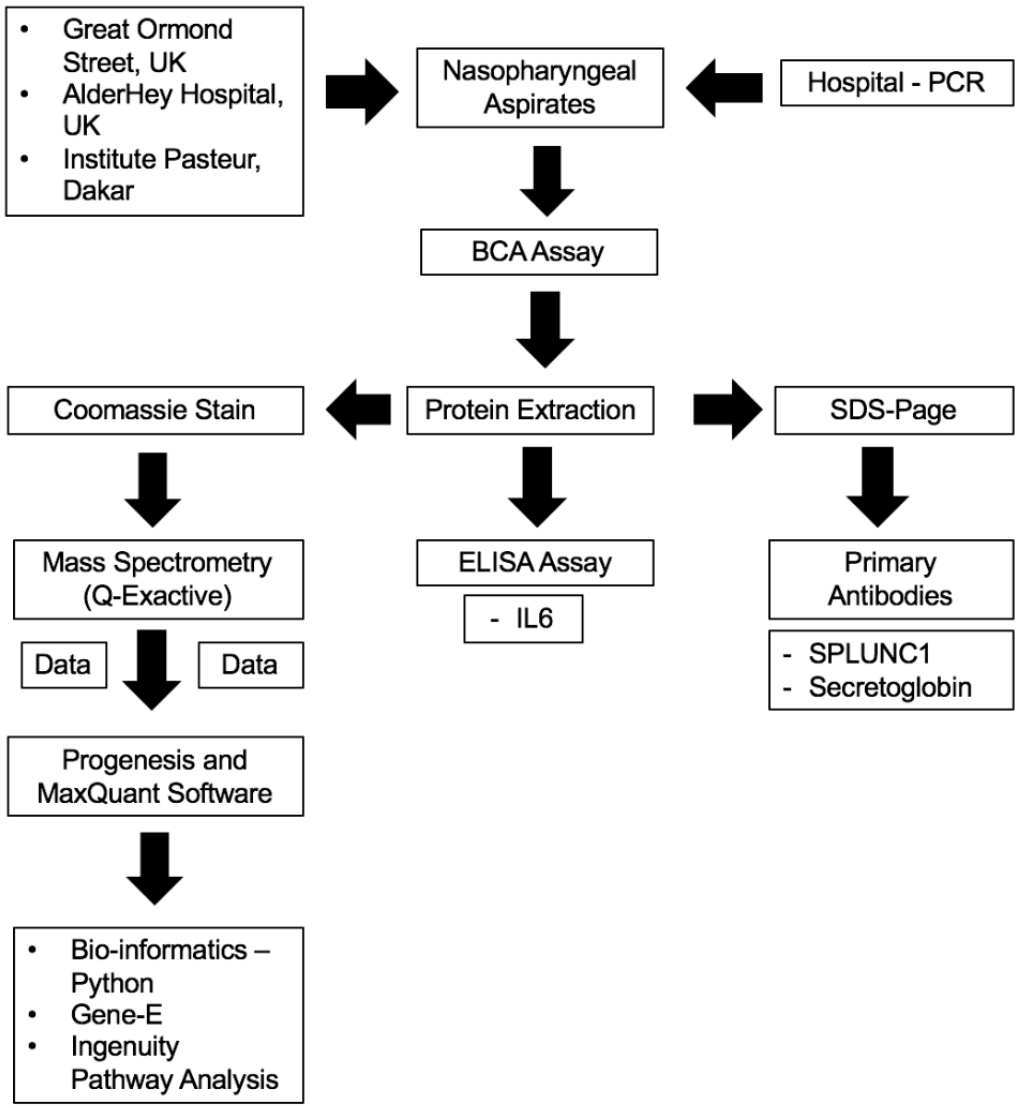

Figure 5.1: Schematic workflow for the processing of proteins from nasopharyngeal aspirate (NA) samples. Protein concentration was measured via the BCA assay and proteins were extracted from the samples. The sample was split and a portion subjected to Coomassie staining followed by analysis on the mass spectrometry platform: Q-Exactive for label-free proteomics and subsequent data analysis. The other portion was analysed by SDS-PAGE and western blot for BPIFA1 and SCGB3A2 as validation of the LC-MS.

5.2.1 Statistical significance of age and sex ratio of patient samples from all cohorts for comparison

Age and sex are associated with a host's immune response to infection at large (397) and specifically IAV infection (398). For the datasets from IAV negative samples to be comparable to IAV positive samples across all cohorts, it is essential that there is no statistically significant difference between the age and sex ratio of the patients within these cohorts. A two-sample t-test and Chi-squared test was performed using Minitab 17 (399) to determine whether there was any statistically significant difference between the age and sex ratio within the sample cohorts, albeit the numerical difference of patients' age and sex. A two-sample t-test was performed on the ages and then a Chi-squared test on the gender of patients' samples from each cohort (399, 400). A two-sample t-test was performed to determine the association of age within the sample cohorts (Table 5.2). A Chi-squared test was performed to determine the association of gender within the sample cohorts (Table 5.3). A p-value cut off range was set at 0.05. A p-value below this value was said to be statistically significantly different. The datasets revealed in association to age, there was no statistically significant difference within each cohort (Table 5.2). The datasets revealed in association to gender, there was no statistically significant difference within all but one of the cohort comparisons (Table 5.3). The chi-squared test revealed the cohorts – IAV-H3N2 positive cohort and IAV-H1N1 positive cohort from IPD had a statistically significant difference in the patients' gender. This indicates that the difference in gender between the two cohorts could affect the results obtained. Although the data between the

two cohorts has been compared, this is worth noting.

Table 5.2: Two sample t-test on sample comparison (IAV positive and IAV negative) between cohorts - Great Ormond Street Hospital (GOSH), Institute Pasteur Dakar (IPD) and Alder Hey Children's Hospital (AHCH)

Geographical location	Sample cohort	Sample Cohort	P-Value	Result Interpretation
Great Ormond Street Hospital (GOSH)	IAV negative	IAV H3N2 positive	1.00	Non-statistically significant
Institute Pasteur Dakar (IPD)	IAV negative	IAV H3N2 positive	0.377	Non-statistically significant
Institute Pasteur Dakar (IPD)	IAV negative	IAV H1N1 positive	0.840	Non-statistically significant
Institute Pasteur Dakar (IPD)	IAV H3N2 positive	IAV H1N1 positive	0.439	Non-statistically significant
Alder Hey Children's Hospital (AHCH)	IAV negative	IAV H3N2 positive	-	-

Table 5.3: Chi-squared test on sample comparison (IAV positive and IAV negative) between cohorts - Great Ormond Street Hospital (GOSH), Institute Pasteur Dakar (IPD) and Alder Hey Children's Hospital (AHCH)

Geographical location	Sample cohort	Sample cohort	P-value	Result Interpretation
Great Ormond Street Hospital (GOSH)	IAV negative	IAV H3N2 positive	1.00	Non-statistically significant
Institute Pasteur Dakar (IPD)	IAV negative	IAV H3N2 positive	0.255	Non-statistically significant
Institute Pasteur Dakar (IPD)	IAV negative	IAV H1N1 positive	0.174	Non-statistically significant
Institute Pasteur Dakar (IPD)	IAV H3N2 positive	IAV H1N1 positive	0.015**	Statistically significant
Alder Hey Children's Hospital (AHCH)	IAV negative	IAV H3N2 positive	-	-

5.2.2 Determining the proteome of nasopharyngeal aspirates taken from paediatric patients either influenza virus positive or influenza virus negative

To identify and quantify proteins in NAs and compare potential changes in the airway secretion between IAV-negative and IAV-positive paediatric cases, a label-free quantitative proteomic approach was used. This simultaneously provided information on protein identification and quantity. Samples were analysed on the Q–Exactive MS platform using longer gradients and an

Orbitrap to acquire both MS and MS/MS spectra. To accurately identify and quantify proteins present in the NAs, several data processing steps were used, including the removal of proteins identified with low confidence and proteins identified by a single peptide (262). An overall p-value for confidence in identification was set at 0.05. Using these criteria, the analysis of IAV positive and IAV negative patients from all three cohorts, AHCH (Appendix 1, Table 1), GOSH (Appendix 1, Table 2), IPD IAV-H3N2 positive versus IAV negative (Appendix 1, Table 3), and IPD IAV-H1N1 positive versus IAV negative (Appendix 1, Table 4) identified proteins that increased in abundance, decreased in abundance, or remained unchanged. Note that proteins identified by single peptides are also included in these tables for interest.

Each site was treated as a separate dataset. For AHCH, samples were analysed by LC-MS/MS individually, and for GOSH and IPD the IAV-H3N2 positive samples and the IAV negative samples were pooled separately. This is because for GOSH and IPD, initial LC-MS/MS analysis of individual samples suggested poor sample quality. The overall number of proteins identified in each cohort was different, with 1,623, 489, and 360 proteins identified in all samples for AHCH, GOSH, and IPD, respectively. In this study, proteins whose abundance changed by two-fold or more, giving a p-value less than 0.05 were considered to have a significant difference in abundance. This revealed that in the samples from AHCH, 25 proteins had significantly increased in abundance and 88 proteins had significantly decreased in abundance, in samples from IAV-H3N2-positive patients compared to IAV-negative patients. In the samples from GOSH, 33 proteins significantly

increased in abundance, while 50 significantly decreased in abundance. In the samples from IPD, IAV-H3N2-positive compared to IAV-negative, 22 proteins significantly increased in abundance and 41 proteins significantly decreased in abundance. In the samples from IPD, IAV-H1N1-positive compared to IAV-negative, 28 proteins significantly increased in abundance and 33 proteins significantly decreased in abundance. To identify changes in these large replicate datasets, volcano plots were used to highlight proteins that were reproducibly altered in abundance in IAV-H3N2-positive patients. Volcano plots are a type of scatterplot that aid in graphic visual representation of large datasets. These volcano plots contain the logarithmic ratio of protein intensities labelled as log two-fold change (x-axis) plotted against the negative logarithmic 10 p-values (y-axis). The proteins that significantly increased in abundance are represented by dots in the top right-hand quadrant. The proteins that significantly decreased in abundance are represented by dots in the top left-hand quadrant. Each dot below the dotted lines represent a protein that did not significantly change in abundance but was highlighted by the technique. The volcano plots were plotted for each dataset sampled and analysed; IAV-H3N2-positive compared to IAV-negative; AHCH (Figure 5.2A), GOSH (Figure 5.2B), IPD (Figure 5.2C) and IAV-H1N1-positive compared to IAV-negative – IPD (Figure 5.2D).

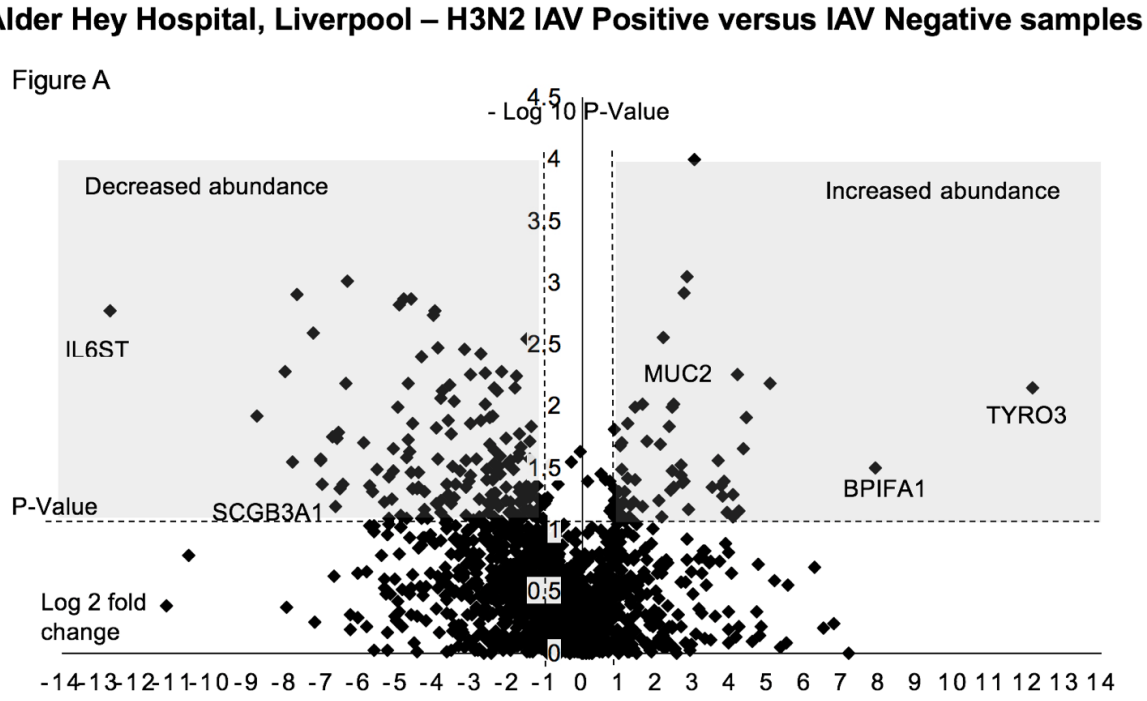

Figure 5.2A: The volcano plot of proteins increased and decreased in abundance in individual nasopharyngeal aspirate (NA) samples from IAV-H3N2-positive samples, compared to IAV-negative samples from Alder Hey hospital, Liverpool. Vertical dashed lines indicate a cut-off of two-fold change between IAV-positive and IAV-negative, while the horizontal dashed line indicates a p-value of <0.05 to define cohorts of polypeptides (shaded areas) with significantly increased (right-hand side) or decreased (left-hand side) abundance in infected patient samples.

Great Ormond Street, London – H3N2 IAV Positive versus IAV Negative samples

Figure B

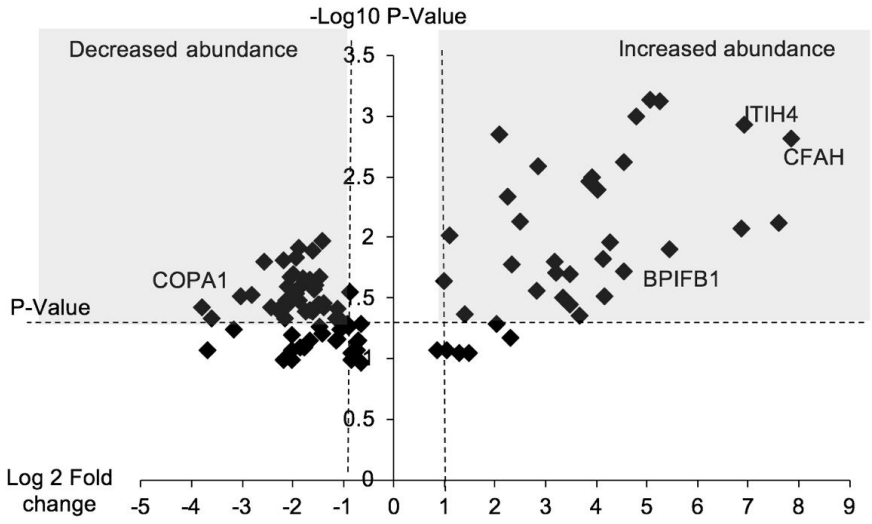

Figure 5.2B: The volcano plot of proteins increased and decreased in abundance in individual nasopharyngeal aspirate (NA) samples from IAV-H3N2-positive samples, compared to IAV-negative samples from Great Ormond Street Hospital. Vertical dashed lines indicate a cut-off of two-fold change between IAV-positive and IAV-negative, while the horizontal dashed line indicates a p-value of <0.05 to define cohorts of polypeptides (shaded areas) with significantly increased (right-hand side) or decreased (left-hand side) abundance in infected patient samples.

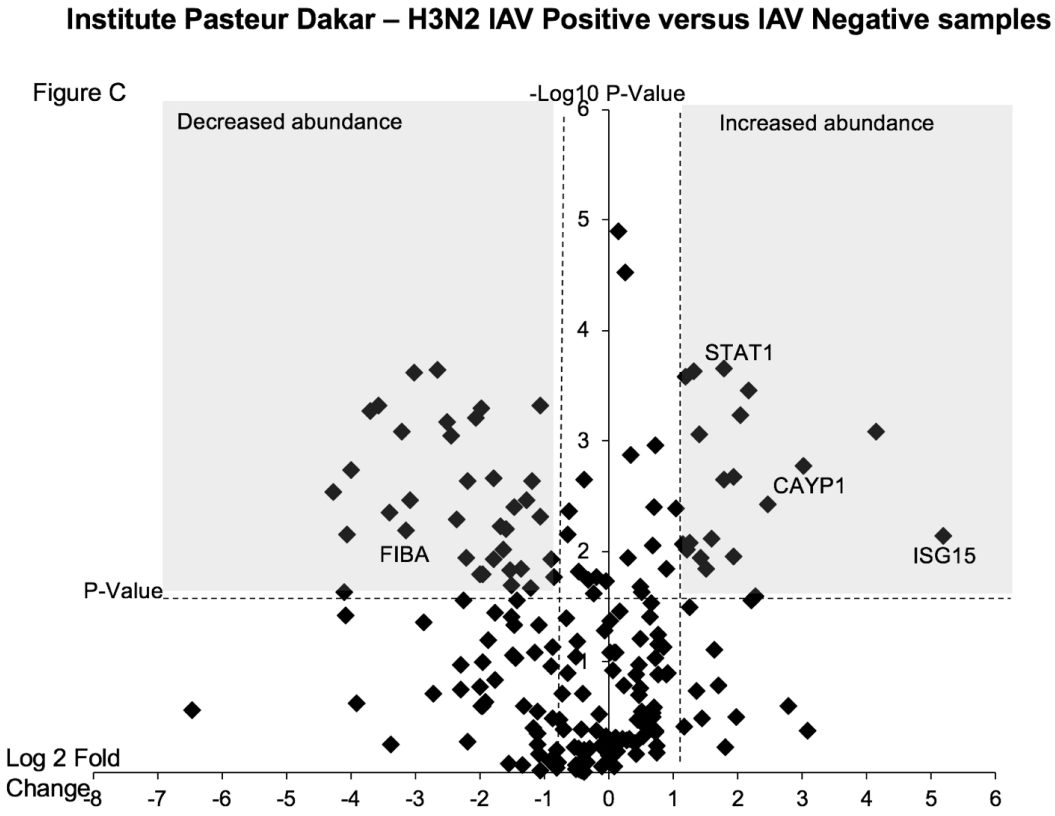

Figure 5.2C: The volcano plot of proteins increased and decreased in abundance in individual nasopharyngeal aspirate (NA) samples from IAV-H3N2-positive samples, compared to IAV-negative samples from Institute Pasteur, Dakar, Senegal. Vertical dashed lines indicate a cut-off of two-fold change between IAV-positive and IAV-negative, while the horizontal dashed line indicates a p-value of <0.05 to define cohorts of polypeptides (shaded areas) with significantly increased (right-hand side) or decreased (left-hand side) abundance in infected patient samples.

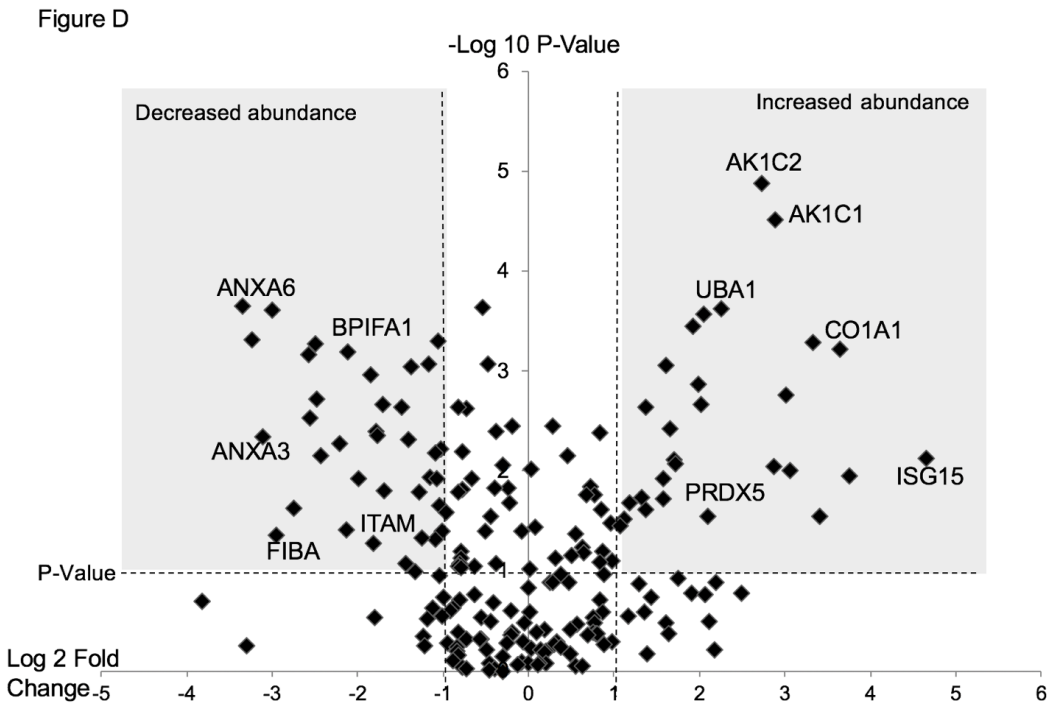

Figure 5.2D: The volcano plot of proteins increased and decreased in abundance in individual nasopharyngeal aspirate (NA) samples from IAV-H1N1-positive samples compared to IAV-negative samples from Institute Pasteur Dakar, Senegal. Vertical dashed lines indicate a cut-off of two-fold change between IAV-positive and IAV-negative, while the horizontal dashed line indicates a p-value of <0.05 to define cohorts of polypeptides (shaded areas) with significantly increased (right-hand side) or decreased (left-hand side) abundance in infected patient samples.

MUC2 and BPIFA1 are examples of proteins highlighted in Figure 5.2A (samples from AHCH) to have significantly increased in abundance in IAV-H3N2-positive samples, compared to IAV-negative samples. MUC2 functions in creating a mucus barrier to inhibit pathogen entry (401). BPIFA1 (a member of the BPI-fold containing family) is another protein involved in the host defence mechanism from viral entry. BPIFA1 was seen to increase post IAV infection in mice (402). Figure 5.2B (samples from GOSH) highlights BPIFB1, which increased in IAV-positive samples in comparison to IAV-negative samples. BPIFB1 is from the same family of proteins as BPIFA1. BPIFB1 is expressed in the upper respiratory tract and functions in host defence (403). These are examples of proteins, which increased in IAV-positive samples in comparison to IAV-negative samples. This suggests host response and defence against viral entry as two pathways that are potentially activated in IAV-infected paediatric cases. Figure 5.2C (samples from IPD) highlights a significant increase in the proteins STAT1 and ISG15 in IAV-positive samples, compared to IAV-negative samples. These are proteins involved in the anti-viral response via the JAK/STAT signalling pathway induced by interferon. The JAK/STAT pathway induction by interferon leads to the up regulation of interferon stimulated genes (ISGs), such as ISG15 (31). This anti-viral pathway is thought to be the earliest and most potent of innate responses (404).

The analysis of the datasets revealed proteins combined through different pathways responding to viral infection. These can be seen by the different proteins significantly increasing and decreasing in abundance in Figures 5.2A,

5.2B, 5.2C, and 5.2D, showing a response to viral infection through different pathways. The proteins highlighted in Figure 5.2C suggest early stages of viral infection, while the secretory proteins highlighted in Figures 5.2B and 5.2C suggest a later response to viral infection. In mice, BPIFA1 was decreased at seven days post-infection but increased at 14 days post-infection (402).

5.2.3 Sample analysis via western blot

When antibody availability was permitted, the abundance of selected proteins identified and quantified by the mass spectrometry was examined by western blot. In the first instance, the abundance of BPIFA1 was investigated in samples pooled from AHCH, GOSH, and IPD. This protein was identified in all sample sets and showed significant changes in abundance in response to infection in all cases, albeit evidence of opposing directions in some cohorts (Figure 5.2A, 5.2B, 5.2C, and 5.2D). For IPD samples, this also allowed comparison between IAV-H3N2-positive and IAV-H1N1-positive. For consistency, pooled samples were used, and equal amounts of protein was loaded (8 μg). The western blot analysis from IAV-H3N2-positive samples compared to IAV-negative samples from AHCH and GOSH, reflected the LC-MS/MS analysis. The abundance of BPIFA1 was greater in the IAV-H3N2 positive pooled samples than the IAV-negative pooled samples (Figure 5.3A). Contrarily, in the IPD cohort, BPIFA1 was less abundant in the pooled IAV-H3N2-positive and IAV-H1N1-positive NA samples compared to pooled IAV-negative NA samples. This is in accordance with the LC-MS/MS data. In samples from AHCH, SCGB3A2 was identified, quantified and found to be more abundant in IAV-negative samples than IAV-positive samples.

SCGB3A2 comes from the Clara cell secretory protein (CCSP) family. This family of proteins are known to function as lung surfactants and has been reported to protect the lung epithelia (405, 406). Western blot analysis was used to investigate and compare the abundance of SCGB3A2 in individual samples from IAV positive and negative patients (Figure 5.3) (8 μg of total protein from each patient). The data again reflected the LC-MS/MS result, in that the abundance of SCGB3A2 was greater in the samples taken from IAV-negative patients compared to IAV-positive patients.

Figure A

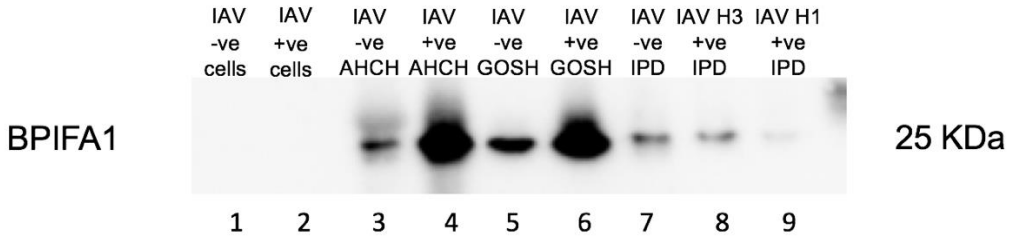

Figure B

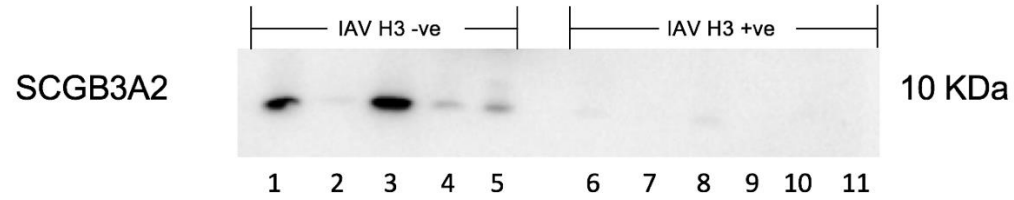

Figure 5.3: (A) Western blot analysis of the abundance of BPIFA1 in pooled nasopharyngeal aspirates samples from; IAV negative A549 cells (Lane 1), IAV positive A549 cells (Lane 2), IAV-negative patients (Lane 3) and IAV-positive patients (Lane 4) from AHCH; IAV-negative patients (Lane 5) and IAV-positive patients (Lane 6) from GOSH; IAV-negative patients (Lane 7) and IAV-H3N2-positive (Lane 8) and IAV-H1N1-positive (Lane 9) from IPD. (B) Western blot analysis of the abundance of SCGB3A2 from individual nasopharyngeal aspirates taken from IAV-negative patients (Lanes 1 to 5, corresponding to individual patients) and IAV-positive patients (lanes 6 to 11, corresponding to individual patients) from AHCH.

5.2.4 Data analysis on IPD sample cohort – comparing H1N1 strain with H3N2 strain

The samples obtained from the IPD cohort provided the potential to compare airway secretions from IAV-H1N1, IAV-H3N2-positive, and IAV-negative patients. Figure 5.2D shows the comparison between IAV-H1N1-positive and IAV-negative samples. Plotting the fold change in abundance between IAV-H3N2-positive samples and IAV-H1N1-positive-samples showed that, globally, the responses from IAV-H1N1-positive and IAV-H3N2-positive cohorts were similar (Figure 5.4A; Pearson R score of 0.65, $P < 0.0001$). However, there was a slight, but statistically significant ($P<0.001$) tendency for proteins in the IAV-H1N1-positive samples to be present at a greater abundance than in the H3N2 cohort (Figure 5.4B).

Figure A

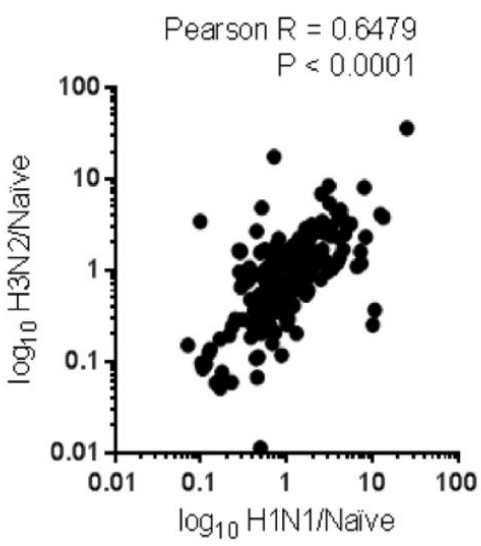

Figure B

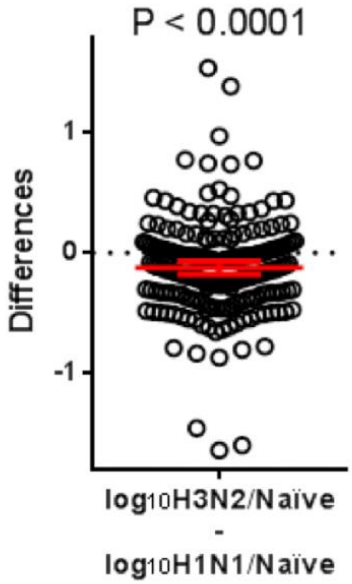

Figure 5.4:A comparison of proteomics data obtained from the Mass spectrometry (Q-Exactive) platform from pooled Nasopharyngeal aspirates samples from H3N2 IAV positive samples (n=10), IAV H1N1 positive samples (n=10), and IAV negative samples (n=10) obtained from Institute Pasteur Dakar-Senegal. Data was graphed and analysed using the software GraphPad PRISM V6.0. Figure 5.4A shows a positive correlation between the abundance of the 200 selected proteins by our bioinformatic data analysis in IAV H3N2 positive samples in comparison to IAV H1N1 positive samples. Data was analysed by Pearson correlation and an R value of 0.6479 and P value of <0.0001 were obtained. Figure 5.4B shows the differential protein abundance of the 200 proteins selected by our bioinformatic data analysis in H3N2 IAV positive samples in comparison to H1N1 IAV positive samples. Using a paired t-test, we determined a significantly higher general abundance of the 200 host proteins selected by our bioinformatics data analysis in the presence of H1N1 IAV (P<0.0001).

Many of the proteins were identified in the samples from IPD as significantly differentially abundant between IAV-positive and IAV-negative patients and there were similar abundance changes in the other two cohorts. However, the abundance of some proteins was different between the three cohorts. To provide a visual display of the differences between IAV-negative and patients positive for either IAV-H1N1 or IAV-H3N2, the protein abundance data were plotted as a heat map (Figure 5.5).

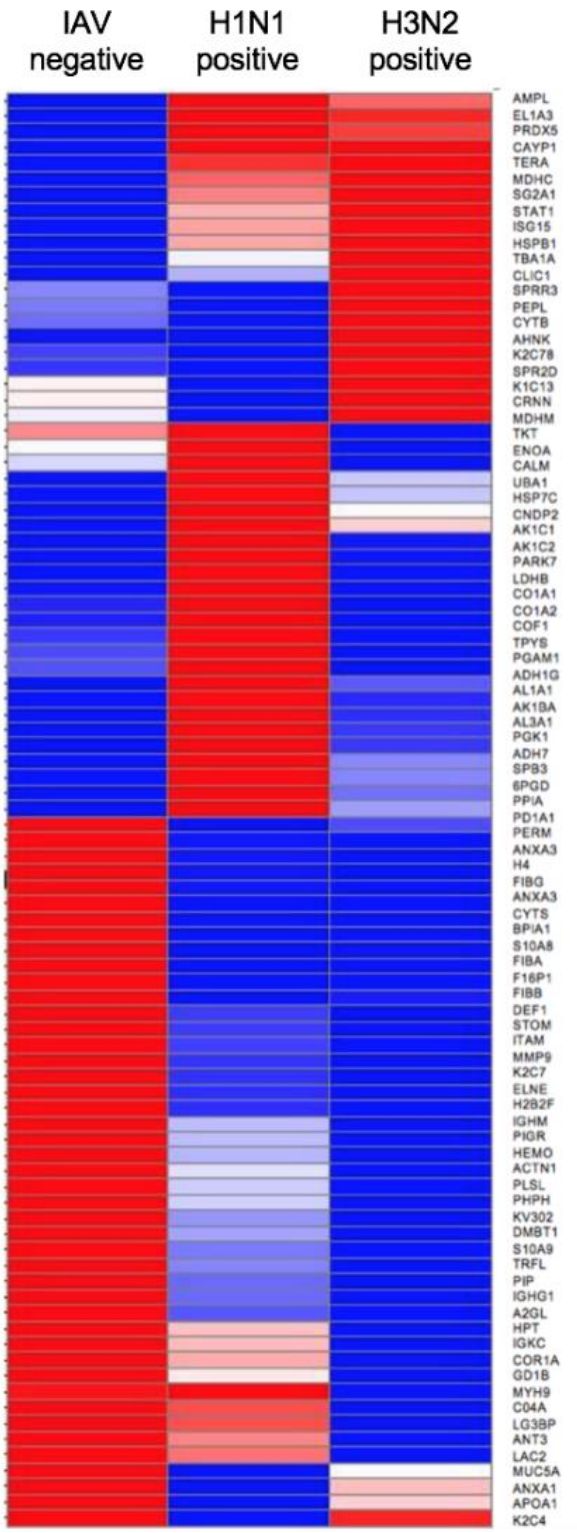

Figure 5.5: The proteomics data obtained from Mass spectrometry (Q-Exactive) platform from pooled aspirates samples from H3N2 IAV positive samples (n=10), H1N1 IAV positive samples (n=10) and IAV negative samples (n=10) obtained from Institute Pasteur Dakar-Senegal were subjected to

Gene-E program. The Gene-E program clusters proteins based on relative abundance within all three conditions. This allows for a better relative representation and comparison of protein abundance per cohort compared with proteins interacting together within/across each cohort. Red represents high protein abundance, blue represents a low protein abundance, and white indicates an intermediary transition within the various cohorts.

Figure 5.5 presents the comparison of different sample cohorts: IAV negative, IAV-H1N1-positive, and IAV-H3N2-positive. This figure combines proteins that are significantly different in abundance and are common across all three cohorts. It allows for a visual comparison of protein levels across all three cohorts. The different proteins and their abundance give insight into the host response to IAV-H1N1-infection and IAV-H3N2 infection. STAT1, SG2A1, and ISG15 are examples of some of the proteins highlighted to be significantly increased in abundance in the IAV-H3N2-positive cohort as well as IAV-H1N1-positive. However, these proteins are at a higher abundance in IAV-H3N2-positive compared to IAV-H1N1-positive and IAV-negative. SCG2A1 is a protein from the secretoglobin family, which has immune-regulatory functions. This is a function also shared by Clara cell secretory protein (CCSP). In neonatal human lungs with bronchopulmonary dysplasia, these proteins decreased in abundance (405). The host's primary response to viral infection is the innate response most frequently induced by interferons. Interferons respond by triggering the host immune response through various pathways (407). The upregulation of these specific proteins have the ability to rapidly inhibit virus replication (404). While the differential abundance of these specific

proteins is seen with various viral infections, studies in mice infected with the influenza A H3N2 X31 strain show the importance of STAT1 in ISG induction and subsequently inhibiting mice from the influenza A infection (408). This confirms the importance of these proteins in IAV-H3N2-positive and IAV-H1N1-positive cohorts and their increase in abundance as the host responds to the IAV infection. Another protein that significantly increased in abundance across the cohorts is cornulin (CRNN). CRNN showed an increase in abundance in IAV-H3N2-cohort, a comparatively lower abundance in IAV-H1N1-positive cohort, and a slight increase in IAV-negative samples. CRNN is categorised as part of the newly identified stress protein family in mammals. These proteins defend the host against different forms of environmental stresses, whilst maintaining tissue integrity (409). UBA1, which is a ubiquitin-like modifier-activating enzyme 1, significantly increased in IAV-H1N1-positive samples in comparison to IAV-H3N2-positive and IAV-negative samples. UBA1 plays a role in catalysing the first step in marking cellular proteins for degradation (410, 411). UBA1 is at the centre of the ubiquitin proteasome pathway (UPP) and is a logical target to disrupt downstream ubiquitination reactions (412). The UPP has been associated with the viral infection cycle as well as virus-host interactions (413) although the mechanism has not yet been elucidated. The effects of inhibiting the UPP reportedly affects replication of several viruses, including influenza viruses (358). No known study has directly linked UBA1 as part of a host response to IAV, but a study by Sun et al. (2014) highlighted proteasomal subunit alpha type 6 to be upregulated in an avian influenza virus H9 infected group. This suggests that different viruses find different strategies to utilise UPP to their advantage (356). Another study by

Byk and colleagues showed that the Dengue virus needs ubiquitination to uncoat its genome (414). In this study, when UBA1 was silenced, there was a four-fold inhibition of viral translation. This suggests the role UBA1 has to play in the viral process. Whilst the mechanism of the action of UBA1 and the role it plays in IAV infection has not been tested, UBA1 is a protein of great interest to potentially differentiate between IAV-H3N2-positive and IAV-H1N1-positive. Another protein that significantly increased in abundance in IAV-H1N1-positive samples in comparison to the IAV-H3N2-positive samples is CNDP2; this is a cytosolic non-specific dipeptidase that acts to suppress the growth of gastric cancer through the mitogen-activation protein kinase (MAPK) pathway. No known study has linked CNDP2 as a host response to IAV infection. However, Increased levels of CNDP2 were associated with apoptosis whilst decreased levels were associated with cell proliferation (415). This is another protein of interest to monitor and observe the trends in IAV-infected cells as in cancerous cells.

Cofilin (COF1) was highlighted in Figure 5.5 to have an increased abundance in the IAV-H1N1-positive cohort compared to the IAV-H3N2-positive and IAV-negative cohort. COF1 is essential for the normal progress of cells through mitosis and cytokinesis and has been found to interact with the Matrix (M) protein structure in RSV-infected cells. The M protein in RSV inhibits viral transcription (416) and through its interaction with COF1, is a potential antiviral target (417). COF1 was identified in human bronchial epithelial cells from different donors infected with IAV-H1N1 (418). COF1 could be further studied

to understand the viral pathogenesis as well as being a potential diagnostic biomarker.

To further analyse the data from Figure 5.5, and the proteins that increased in abundance in the IAV-negative cohort in comparison to the IAV-H3N2 positive and IAV-H1N1 positive cohort, BPIFA1, FIBA, FIBB, and lactotransferrin (LTF) were highlighted across all three cohorts. These proteins were processed through the program – protein interaction network viewer (PINV) – for further data analysis. PINV is a web-based protein interaction network visualiser and was used to visualise these proteins within the context of proteins associated with IAV infection (419). Using PINV, the protein-protein interaction of FIBA, FIBB, FIBG, LTF, and BPIFA1 identified were examined in relation to the PABP-binding protein (an influenza host-binding protein) and influenza virus NS1A-binding protein (IVNS1ABP). On PINV, these proteins act as hubs as they connect to several other proteins. What is interesting to note is that each one of these proteins is linked by intermediary proteins to proteins involved in transcription regulation of IAV. This linkage forms an interactome of LTF, PABP-binding protein, and NS1A (Figure 5.6). A similar interactome is observed with proteins FIBA, FIBB, FIBG, and BPIFA1. A more detailed representation of the protein interactome and the intermediary proteins involved in these interactions can be seen in Figure 5.6A (FIBA, FIBB, FIBG interaction), Figure 5.6B (LTF interaction), and Figure 5.6C (BPIFA1 interaction). The interactions between these proteins highlighted in AHCH, GOSH, and IPD, with PABP-binding protein and IVNS1ABP demonstrate a possible involvement of IAV binding to the host. This suggests these proteins

may be involved in the survival of the virus in the host and should be further investigated. This could be done through gene knockout and then confirmed by PCR (DNA), RT-PCR (RNA), and western blot (protein expression). These proteins have the potential to be further studied as diagnostic biomarkers due to the central role they play in enabling IAV to bind to the host. An increase in abundance of these proteins could suggest the presence of IAV infection.

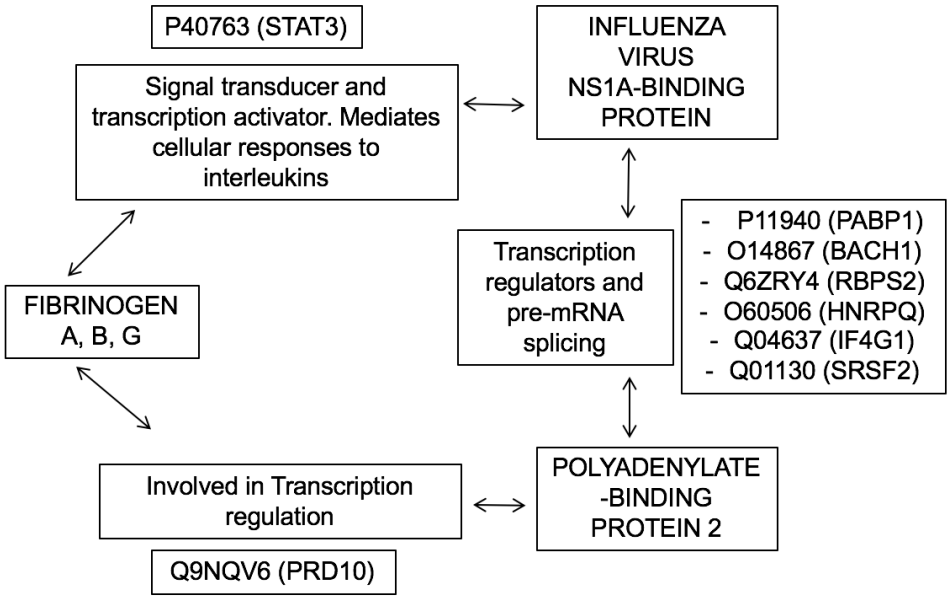

Figure 5.6A: Significantly differentially abundant proteins from datasets from AHCH, GOSH, and IPD, which were highlighted by the mass spectrometry (Q-Exactive) platform, were further analysed and visualised using the Protein Interaction Network Viewer (PINV). This highlights the interaction between Fibrinogen Alpha, Fibrinogen Beta, Fibrinogen Gamma, and the influenza virus NS1A binding protein (IVNS1ABP) and Polyadenylate – binding protein 2 (PABP2). These proteins are linked by transcription regulators also highlighted in the data from Mass spectrometry.

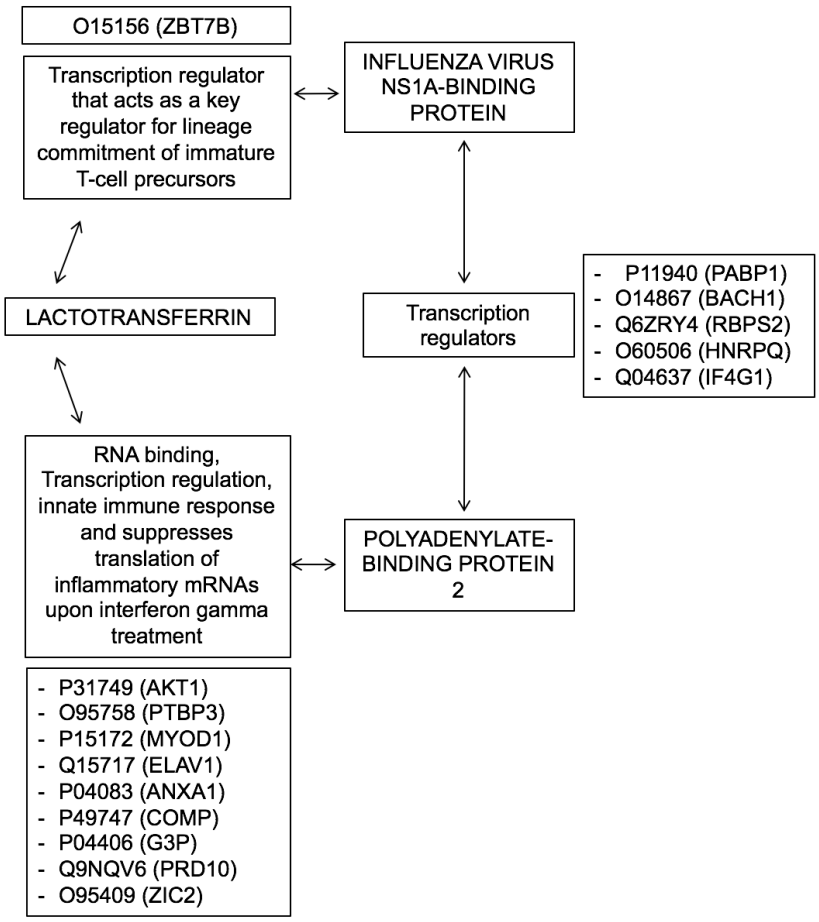

Figure 5.6B: Significantly differentially abundant proteins from datasets from AHCH, GOSH, and IPD, which were highlighted by the Mass spectrometry (Q-Exactive) platform, were further analysed and visualised using the Protein Interaction Network Viewer (PINV). This highlights the interaction between Lactotransferrin, Influenza virus NS1A – binding protein (IVNS1ABP) and Polyadenylate – binding protein 2 (PABP2). These proteins are linked by proteins involved in RNA binding and transcription regulators, also highlighted in the data from Mass spectrometry.

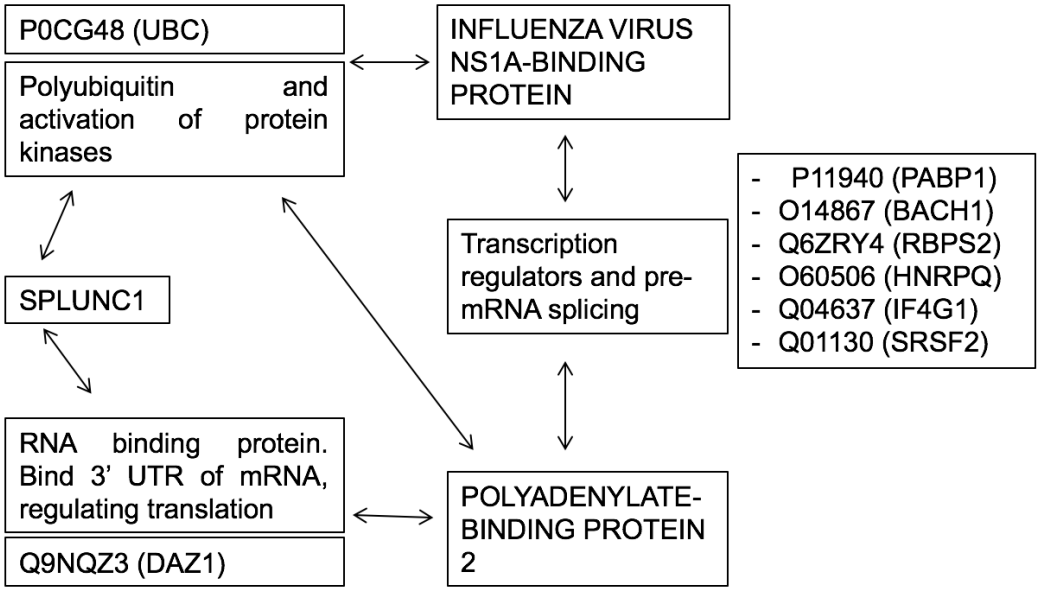

Figure 5.6C: Significantly differentially abundant proteins from datasets from AHCH, GOSH, and IPD, which were highlighted by the Mass spectrometry (Q-Exactive) platform were further analysed and visualised using the Protein Interaction Network Viewer (PINV). This highlights the interaction between BPIFA1, Influenza virus NS1A – binding protein (IVNS1ABP) and polyadenylate – binding protein 2 (PABP2). These proteins are linked by proteins involved in RNA binding, highlighted in the data from Mass spectrometry.

Examining the pattern of protein abundance between the different strains led to potential strain-specific differences in IL-6 signalling. Interleukin 6 signal transducer (IL6ST) was highlighted to be significantly decreased in Figure 5.2A. IL6ST is a signal transducer molecule and receptor for IL6. This led to the hypothesis that IL6 was differentially abundant. To test this, ELISA was used to measure the concentration of IL-6 in NAs from IPD cases either positive for H1N1 or H3N2 or negative for common respiratory pathogens. These data showed that while the level of IL-6 in H3N2-positive samples was

not significantly different from the uninfected controls, there was a statistically significant increase in the abundance of IL6 in the IAV-H1N1-positive cohort (Figure 5.7).

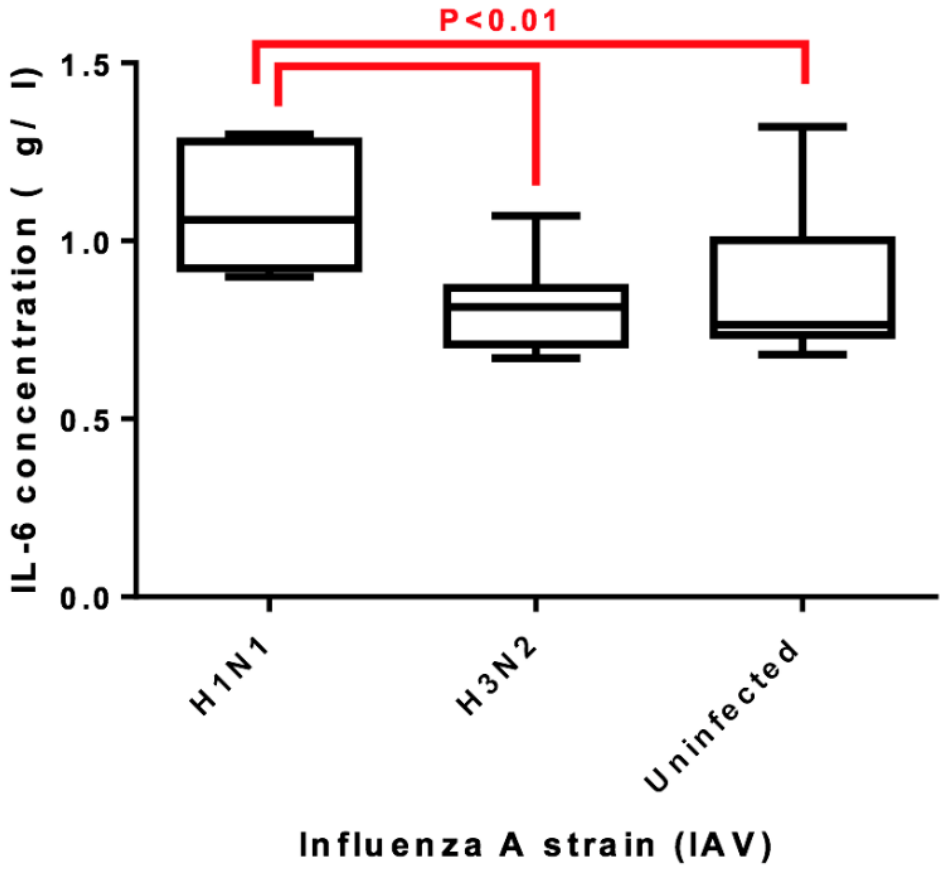

Figure 5.7: Relative interleukin-6 (IL-6) in individual nasopharyngeal aspirates (NA) samples from H1N1 IAV positive samples (n=10), H3N2 IAV positive samples (n=10), and IAV negative samples (n=10) from Institute Pasteur. IL-6 concentration was determined by ELISA and comparison to standard curve (data not shown). The software GraphPad PRISM was used to plot the Tukey's plot shown and for Bonferroni's post-test comparisons to the control. We found reduced IL-6 in both H1N1 IAV positive samples and H3N2 IAV positive samples when compared to the control ($P<0.01$, in both cases).

5.2.5 The influence of viral load on airway secretions

The amount of virus (viral load) per patient may influence the airway secretome and subsequently disease severity. In some respiratory viruses such as adenoviruses, human metapneumovirus and parainfluenza virus, Ct values of NAs are correlated to clinical severity (420). To investigate whether IAV viral load influenced the proteome component of the airway secretome, protein abundance profiles were further analysed according to viral load (measured by Ct value) as determined at the time of diagnosis and sampling of NAs. Samples were separated according to Ct values between 20–25 reflecting a higher viral load or Ct values between 26–30 reflecting a lower viral load, as well as into H3N2-positive (Figure 5.8A) or H1N1-positive (Figure 5.8B) categories. It is worth noting that the samples were not all tested on the same day and time using the same equipment. These inconsistencies could affect or skew the dataset. The comparative data indicated that the abundance of certain proteins may or may not be affected by viral load. This was observed in both IAV-H3N2 and IAV-H1N1 strains. CATG (cathepsin G) is a protein involved in tissue remodelling at sites of inflammation, and DEF1 (defensin, alpha 1) is found at the epithelia of mucosal surfaces. These proteins decreased in abundance in patients IAV-H3N2 and IAV-H1N1 positive at both low and high viral loads.

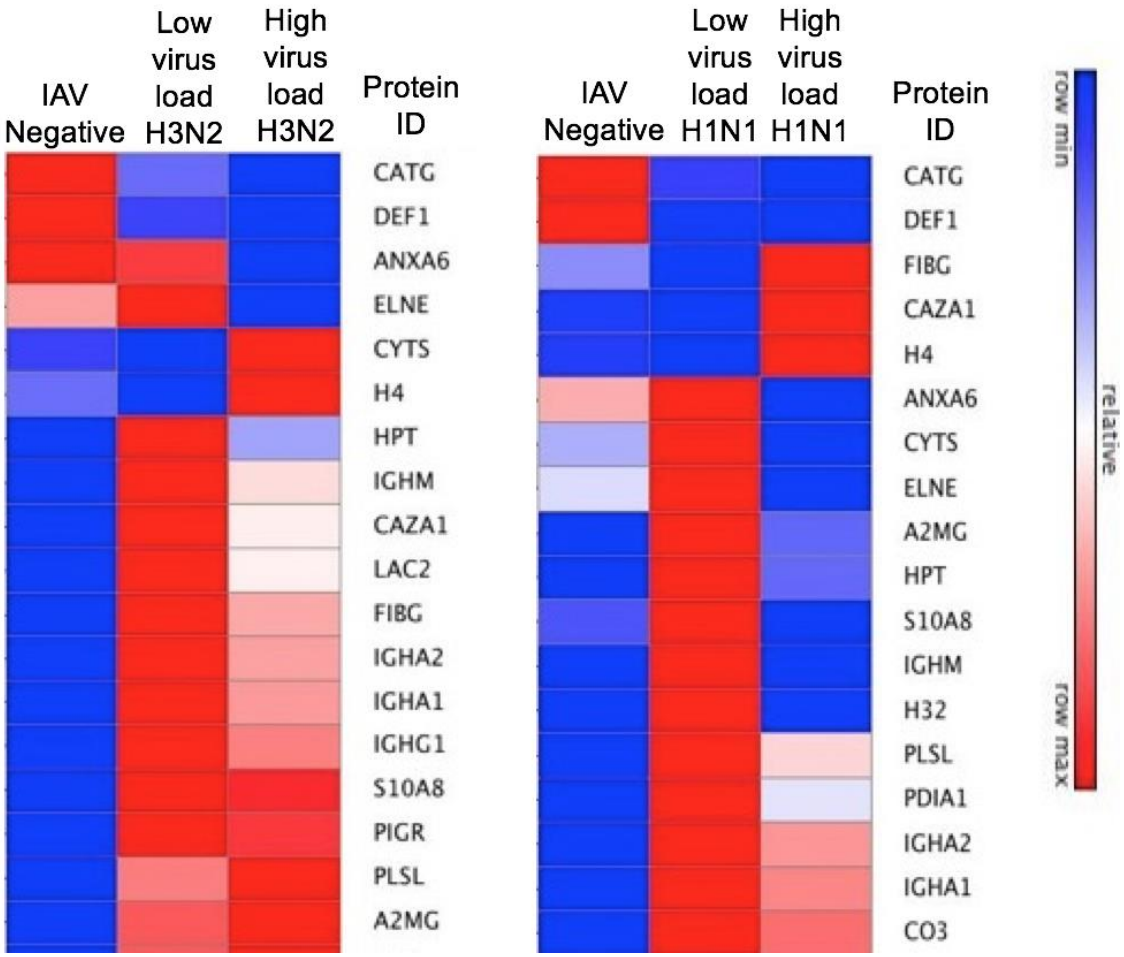

Figure 5.8: The proteomics data obtained from Mass spectrometry (Q-Exactive) platform from pooled Nasopharyngeal aspirates samples from IAV-H3N2 positive samples (n=10) (A), IAV-H1N1 positive samples (n=10) and IAV negative samples (n=10) (B) obtained from Institute Pasteur Dakar-Senegal were separated based on viral titres. Low viral titre was a Ct value of 26 and above and high viral titre was Ct value of 20-25. After filtering for proteins common in all datasets they were subjected to Gene-E program. The Gene-E program clusters proteins based on relative abundance within all three conditions. This allows for a better relative representation and comparison of protein abundance for each cohort compared – proteins interacting together within/across each cohort. Red represents high protein abundance, blue low

protein abundance, and white, an intermediary transition within the various cohorts. Figure 5.8A represents proteins of differential abundance in different viral titres of IAV-H1N1-positive samples and Figure 5.8B represents proteins of differential abundance in different viral titres of IAV-H3N2-positive samples.

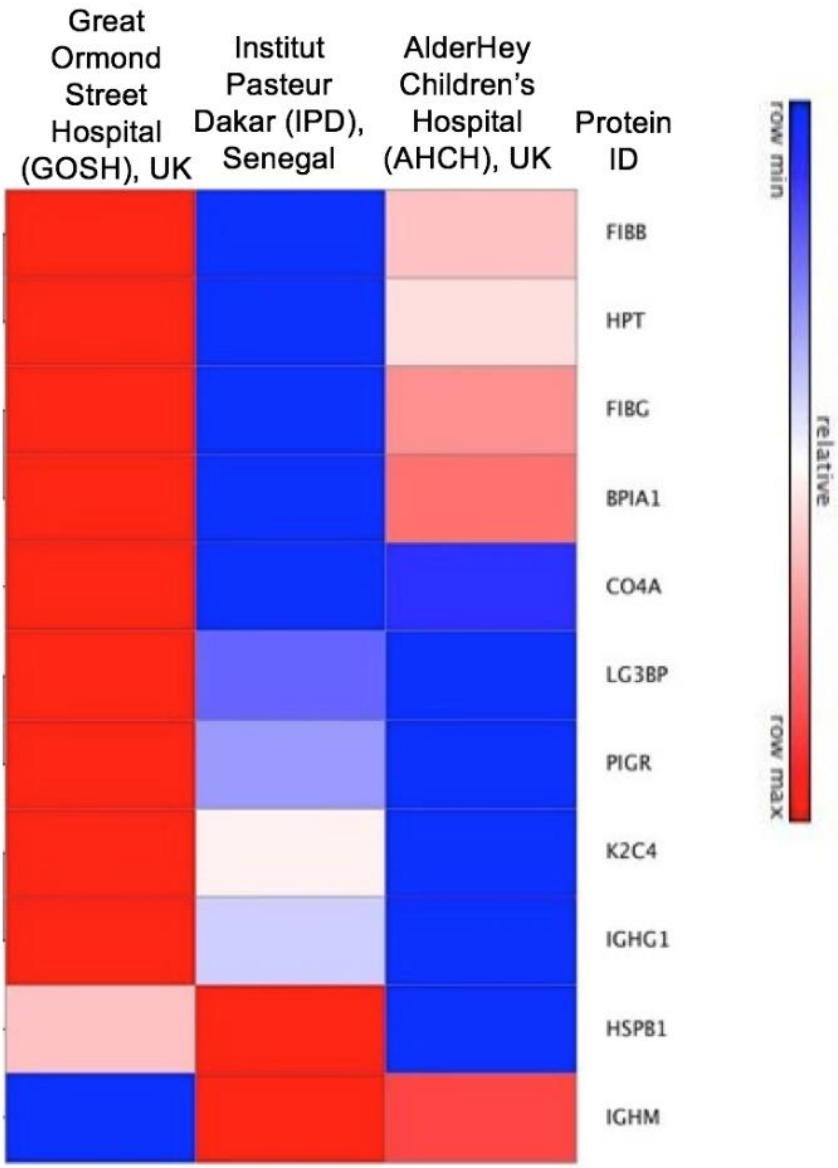

Figure 5.9: The proteomics data obtained from all three cohorts that were IAV-H3N2-positive: Alder Hey Children's Hospital (AHCH), Great Ormond Street Hospital (GOSH), and Institute Pasteur Dakar (IPD) were compared to IAV-negative samples. Following various data analysis steps via bioinformatics,

proteins present in AHCH, GOSH, and IPD that were significantly differentially abundant were highlighted. These proteins were subjected to Gene-E program. The Gene-E program clusters proteins based on relative abundance within all three conditions. This allows for a better relative representation and comparison of protein abundance per cohort compared – proteins interacting together within/across each cohort. Red represents high protein abundance, blue low protein abundance, and white an intermediary transition within the various cohorts.

Figure 5.9 shows the proteins identified in all three sites - Great Ormond Street, Institut Paster Dakar and AlderHey Hospital. This figure allows for the visual comparison in the protein abundance between these three sites. Whilst these proteins can be considered potential biomarkers as there is an obvious difference in protein abundance between these sites, it is worth noting that there was a lack of information on the stage of IAV infection. As a result, no direct correlation can be made between these differences and the stage of IAV infection or if geographical location affects IAV infection and therefore protein abundance in these samples.

5.2.6 Identifying correlates of infection using machine learning

Machine learning, based on a panel of differentially abundant proteins in IAV negative versus IAV positive samples, potentially offered a means of identifying proteins that could differentiate IAV-positive from IAV-negative samples, based on an analysis of NAs. To ensure that the outcome was robust for variations between clinical centres in clinical and analytical procedures, the protein abundance data were collated for NAs from the three independent

cohort studies to identify protein biomarkers with consistent responses to infection. For data normalisation to be processed, measurements were required on all entities. This step was limited by the different protocols used. To circumvent this, two measurements of a sample on a protein pair were centred to zero. This allowed us to explore all the pair-wise combinations of normalised proteins and identify those providing the greatest discrimination between control and infected status. Subsequently, these were combined to provide averaged and individual profiles across the selected protein, as illustrated in Figure 5.10, which illustrates the outcomes for control uninfected and patients infected either with H1N1 or H3N2. This is indicated by a 'correlation difference' defined as cor (sample profile, controls profile) – cor(sample profile, infected profile), which naturally falls between -2 (for infected) and 2 (for uninfected). Usually, the zero line can be used to separate the controls and infected in a prediction. If a control sample has a negative value in correlation difference, it will be predicted. This shows that all control samples, and all but two infected samples, were predicted correctly. The accuracy was 91.7% (22 out of 24 being correct). The two incorrect samples were from the IAV-H3N2-positive infection from the AHCH cohort. Albeit this, the two other samples were correctly predicted. The correlation difference values for the control samples from AHCH were also distinctly different to the other two sites. The IPD data allowed comparison of the predictive power for H1N1 with H3N2, and infected individuals were determined with equal success.

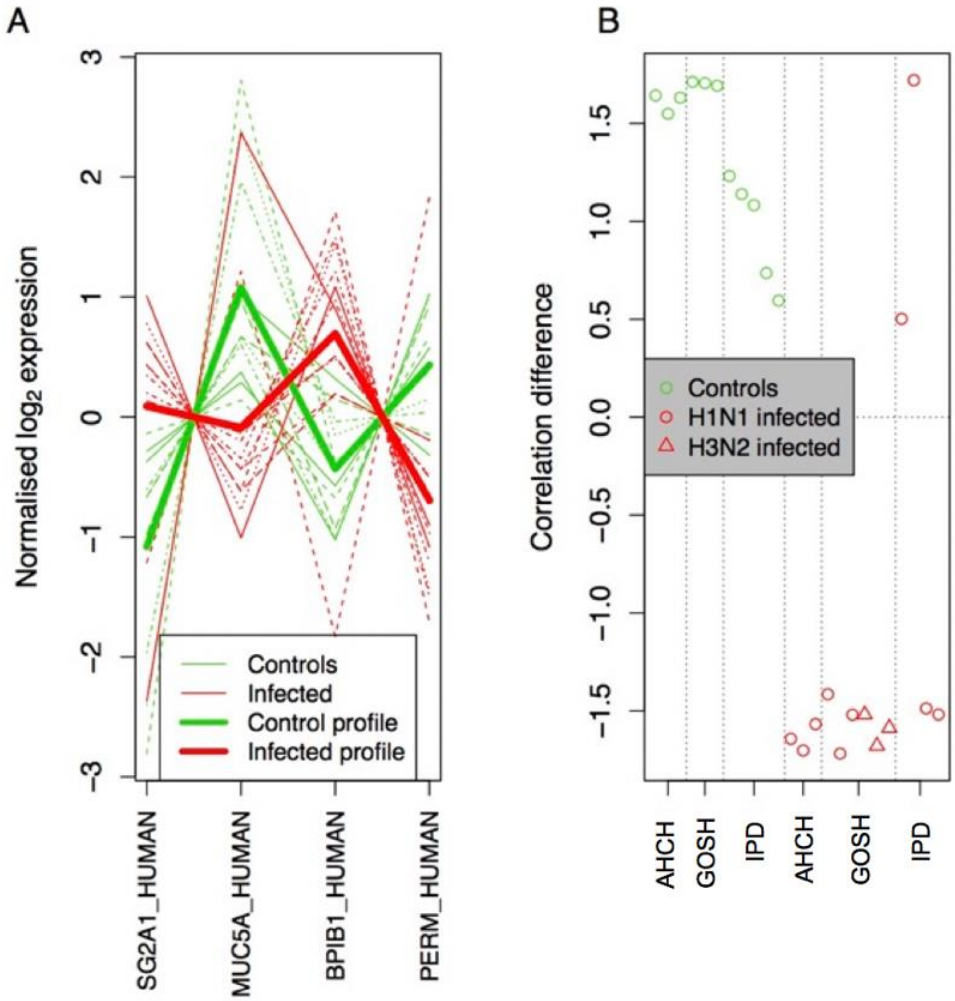

Figure 5.10: Predicting the IAV status of patients based on proteomic analysis. Data from independent proteomic analyses in three different clinical sites (Alder Hey Children's Hospital (AHCH), Liverpool, Great Ormond Street Hospital (GOSH), London, and Institute Pasteur Dakar (IPD)) was collated to identify differentially expressed (DE) proteins between control and infected patients. Figure 5.10A displays normalised-by-centering profiles for a set of 4 DE human proteins that conspicuously separated the profile of control (uninfected) from infected conditions. These proteins have a crucial role to play in innate immunity and are seen to be inversely abundant between the infected and non-infected cohorts. The thick solid lines represent the average profile across all patients from each of the two groups, whilst the thin lines

represent data from individual patients. Figure 5.10B displays replicate control and infected patients, across the three sampling sites (AHCH, GOSH and IPD). This shows the difference between the infected samples (red circles and triangles) and the uninfected samples (green circles). This gives confidence in the ability for this data, methodology and analysis to be used to predict proteins that can be potential differentiators between the infected and uninfected (control). These proteins can be used as potential biomarkers.

5.3 DISCUSSION

The effects of IAV have been studied in various animal models and cell systems using high throughput techniques (219, 421-423). These studies have revealed extensive modification of the host transcriptome and proteome due to infection. To investigate the effect of IAV infection on airways in paediatric patients, quantitative proteomics was used to define the proteome of NAs. These samples were compared to samples from paediatric patients that were IAV negative. To our knowledge, no study has applied label-free Mass spectrometry on NAs taken from IAV-positive paediatric patients in comparison to samples from IAV-negative paediatric patients. These samples were taken from different cohorts to evaluate and understand the proteome changes involved in airway secretions upon influenza infection, and whether any changes were common to all three patient groups. This chapter highlights the benefits of label-free Mass spectrometry by providing an in-depth list of proteins differentially abundant in these samples, allowing for a comparison between IAV-negative samples, IAV-H3N2-positive, and IAV-H1N1-positive samples. In addition, the results in this chapter provide an in-depth understanding of the proteins identified with significant abundance through functional links and networks. These proteins were further analysed for commonality across cohorts and some of them narrowed down with the potential of biomarkers for diagnosis.

In the search for proteome changes in airway secretions due to IAV infection, the list of statistically differentially abundant proteins was mined by looking for common proteins across all patient cohorts (AHCH, GOSH and IPD). This

revealed FIBA, FIBG, FIGG, BPIFA1, and LTF, which differed in abundance. This group of proteins increased in abundance in the AHCH and GOSH cohort but decreased in abundance in the IPD cohort (Figure 5.2). This may be because of the different stages of the disease progression at the time of infection or disease onset prior to sample collection. A similar analysis was observed with BPIFA1 abundance in the different cohort. Fibrinogen levels may be a useful marker of disease progression and severity. Fibrinogen has been shown to aid the binding of *streptococcus pneumoniae* to IAV-infected cells (424) during opportunistic co-infections. Studies in mice have linked the activation of an antifungal pathway, possibly driving allergic airway inflammation through fibrinogen (425). These various studies indicated the potential of FIBA, FIBB, and FIBG as markers for possible disease severity and progression through different pathways. This difference between clinical samples, in this case airway secretion, and cell culture model, is reflected in our observation that fibrinogen decreases in abundance in the NAs from paediatric patients infected with IAV. In contrast, in Madin-Darby canine kidney cells (MDCK) infected with IAV, fibrinogen was shown to increase in abundance (426). However, this may reflect differences in the sample type. This work illustrated the advantage of working with clinical material compared to commonly used cell culture systems (such as A549 cells – a human lung respiratory epithelial cell line), as not all the proteins affected by IAV will be expressed in cell culture – such as BPIFA1 (Figure 5.2).

BPIFA1 has been proposed to abrogate IAV infection and possibly act as a novel target for antiviral treatment (427). The role of BPIFA1 and SCGBA1 as

innate defence mediators during respiratory infection have been elucidated (402). LTF was shown to decrease in two out of the three patient cohorts. This protein has been used as an experimental therapy against IAV infection. Studies in mice, infected with IAV and orally administered LTF, showed less lung damage compared to control mice. LTF has also been shown to have inhibitory activity against viruses such as; cytomegalovirus, herpes simplex virus-1 (HSV1), HIV, hepatitis B and C, poliovirus and respiratory syncytial virus (RSV). This shows LTF has roles in inhibiting other viruses including IAV (428). However, in a similar manner as BPIFA1 and FIBA, FIBB, and FIBG, LTF could be used as a marker for disease progression and severity.

The cohort of samples obtained from IPD allowed for inter-strain comparison as well as IAV-positive versus IAV-negative. This comparison revealed sets of proteins common to IAV-H3N2-positive, IAV-H1N1-positive and IAV-negative. These proteins were all present in differing quantities thereby emphasising the effects of infectivity on the host response. Proteins such as STAT1, ISG15, and SG2A1 increased in abundance when compared to an IAV-negative cohort, regardless of the IAV-strain. These proteins have roles in transcription regulation of interferon pathways as well as play key roles innate immune response to viral infection. STAT1 and ISG15 are commonly increased in volume and upregulated during virus infection. The increase in abundance of these proteins confirms the IAV-positive infection of the samples and on-going viral replication. The presence of these proteins in the interactome between FIBA, FIBB, FIBG, LTF, SPLUNC1, PABP-binding, and IVNS1ABP suggest the importance and possible function of the proteins common in all three

cohorts in viral replication and viral survival in the host. The interaction seen in Figure 5.6A, 5.6B, and 5.6C between these proteins, highlights the potential of these proteins as biomarkers for disease severity. Alongside LTF, other proteins, such as LDHB, involved in the sub pathway synthesis of lactate from pyruvate, were particularly elevated in IAV-H1N1-positive patients. This is also observed in bacterial infection (429). *In vitro* studies in MDCK cells, which compared IAV-infected cells to IAV negative cells observed the increase in lactate release in the cell culture supernatant in H1N1-PR8 (430).

The differential abundance of cellular proteins in NAs from IAV-infected patients may reflect both time post-infection as well as viral load. The limitation of this study was the inability to know when the patients were infected with IAV. The only information we are confident of is the symptoms they presented when admitted to hospital with acute illness. In this respect, it illustrates how animal models provide a more controlled environment to study IAV infection over time. However, data associated with the samples from the IPD did allow us to evaluate the potential role of viral load in changes in cellular protein levels. In IAV-H3N2-positive samples, FIBG increased in abundance in comparison to IAV-negative samples regardless of viral load (Figure 5.8A). In IAV-H1N1-positive samples, FIBG increased with a low viral load in IAV-H1N1-positive in comparison to IAV-negative and high viral load in IAV-H1N1-positive patients (Figure 5.8B). This further confirms the potential use of fibrinogen as a marker for disease progression and severity. IL6 is a well-known and documented marker of infection with IAV-H1N1 having been studied in both animal models of infection and in serum from human patients

(431-433). Our study highlights a significant difference in the abundance of IL6 in IAV-H1N1-infection compared to IAV-H3N2-infection. This suggests a difference in trajectory of host response between the two different viral strains, which has also been described in a mouse mode examining the level of IL6 between IAV-H1N1 and IAV-H3N2-infected mice (434).

In the search for Biomarkers, biomarkers can be divided into various groups including “prognostic biomarkers”. Prognostic biomarkers aim to aid with IAV diagnosis, facilititate this process and provide more information on the overall outcome of patients following infection (435). This study focused on the search for prognostic biomarkers. Following further studies and validation, this is to enhance clinicians’ ability to make decisions on treatment. This process is rather tedious due to the effect of IAV infection to the host’s immune system. However, this study was hypothesis generating and provides a good foundation for potential prognostic biomarkers in IAV infection.

5.4 CONCLUSION

This study analysed the proteome of airway secretions using NAs taken from paediatric patients admitted to hospital and confirmed positive (or negative) for IAV-infection in three different cohorts – AHCH, GOSH, and IPD. These samples provided a window on the *in vivo* effects of IAV on the airway. Mass spectrometry, data analysis, and confirmation via a second technique across all three cohorts revealed the proteins FIBA, FIBB, FIBG, and BPIFA1 to be differentially abundant between infected and non-infected patients. These proteins have been identified in various models of IAV-infection and our data suggests the relevance of these models to the study of human airways, but, more importantly, the potential for these proteins to be used in the search of potential biomarkers. This study also allowed for a comparison between IAV-H3N2, IAV-H1N1, and IAV-negative samples using data from Mass spectrometry. This comparison revealed proteins such as STAT1, SG2A1, ISG15, CRNN, and COF1 as potential discriminatory biomarkers between the two IAV strains and IAV-negative samples. In addition, the machine learning conducted in this study confirmed the ability to differentiate and predict between IAV-H3N2 and IAV-H1N1 by highlighting certain proteins – SG2A1, MUC5A, BPIB1, and PERM. The importance of the UPP in IAV survival was further highlighted and the potential role UBA1 has to play in achieving this. Finally, this study illustrates how proteomic analysis of biological samples can be used to identify markers that may serve as potential diagnostic indicators for infection with IAV, despite potential problems of inconsistent protocols and different instrumentation between centres.

CHAPTER 6:

GENERAL DISCUSSION

The overarching aim of this study was to investigate the global proteomic and transcriptomic response to IAV infection *in vitro* (A549 cells) and *in vivo* (NHP macaques and humans). This study characterised, the proteome of the host (A549 cells) *in vitro* following IAV infection using label-free Mass spectrometry for the first time and the transcriptome of the host (A549 cells) following IAV infection using a MinION sequencer-based approach (Chapter 3). The results obtained resembled previously established proteomes of the host (A549 cells) *in vitro* following IAV infection using other techniques (210, 219, 436-438). The data obtained from sequencing on a MinION sequencer were in concordance with data obtained from a previously established study that used genome-wide RNAi screening of IAV-infected A549 cells (328, 345). IAV infection was characterised by infecting A549 cells with IAV at MOI 1 and collected over a time frame of 3h.p.i–48h.p.i. The Avicel plaque assay (254) was used to quantify the virus titer at different time points after which 18h.p.i was selected as the time point for further experiments. 18h.p.i was selected because this time point showed peak viral load and less Cytopathic effect (CPE) in the cells. IAV infection in A549 cells was further validated by SDS-PAGE and immunofluorescence microscopy. A549 cells were then infected at MOI 1, collected at 18h.p.i and subjected to mass spectrometry. RNA was extracted from A549 cells infected at MOI 1, 18h.p.i and subjected to MinION sequencing. The datasets obtained were further analysed using IPA analysis and categorised based on function. One of the pathways/categories highlighted was a ‘replication of IAV’. Ten proteins and transcripts identified by Mass spectrometry and MinION sequencing were highlighted under this category. These ten targets had been published in the literature as host

proteins essential for IAV replication, they include; NUP54, RBM42, HPGD, GCLC ANPEP, AKAP13, RACGAP1, CREB1, MAN2B1, and PRKCI (328). Gaining knowledge of these host cell target's roles in IAV replication provides information on the pathways IAV uses but also are potential antiviral drug targets. This validates and confirms the dataset highlighted in chapter 3 (in this thesis) and more importantly gives confidence in the technique and experiments used and so the targets identified should be explored further. In addition, these targets are potential antiviral drug targets or reveal new molecular pathways the IAV exploits to survive in the host. Although this study wasn't aimed at conducting a full functional validation for the highlighted targets, these could be validated further in future work. A limited amount of time and financial resources for this study prevented further experiments to explore these targets. However, general analysis of the data via IPA highlighted proteins in the Trim family – TRIM25, as well as immunoglobulins, which were affected following IAV infection. TRIM25 induces ubiquitination of RIG-I that leads to increased signalling of RIG-I (346, 347). RIG-I sits upstream as an activator of an antiviral pathway, which induces type I IFN host protective innate immunity (346). Proteins and transcripts involved in major cell signalling pathways triggered by IAV infection (340) in the host were highlighted. This includes MAPK1 in the MAPK pathway (328, 340), MDM2 in the PI3/AKT pathway (340), all type 1-IFN induced proteins (IFIT2, IFIT3 and MX1), interferon stimulated genes (ISG15), and TRIM25 in the RIG-I/TLR pathway (276, 277, 340); finally, AKAP13, RACGAP1, PRKCI in the IP3/PKC pathway (340). The two techniques used; one being protein based and the other RNA based, show the potential of the platforms used to obtain these results. The

other targets should therefore be analysed further for pathways and anti-viral drug targets.

This study allowed for the possibility to analyse and compare samples from *in vitro* and *in vivo* models, analyse them on the same platform, and explore whether there was coherence in the protein targets identified and highlighted in different hosts following IAV infection. This was the first of its kind using the above-mentioned techniques. IAV infection observed in an *in vivo* model - NHPs, used an infection route that modelled natural human infection. This was the natural inhaled aerosol route of infection (262). This is essential to ensure concordance with human IAV infections as they are valuable for testing and identifying anti-influenza targets. To understand the host response of NHP macaques to IAV infection and identify protein targets essential in host-IAV interaction; Broncho alveolar fluid (BALF) was obtained from IAV-infected NHP and compared to naïve NHP macaques using proteomics. The NHP model is useful and informative in the study of IAV and other respiratory pathogens. This is mainly due to its high similarity to the human immune system, susceptibility to non-adapted human strains, similarity to the respiratory tract anatomy of humans, and the broad availability of immunology reagents in this study (439). BALF samples were used from NHPs due to their similarity to NAs from humans (Chapter 5). This was essential as the data from both chapters would be compared; this increased confidence when comparing data. The main reason as stated above for using NHP as a model for the study of IAV was due to the robustness of its immune system and similarity to humans. The data obtained from BALF proteome associated with the immune system were a) similar to some cellular proteins (IFIT3 and MX1) highlighted

in vitro in A549 cells (Chapter 3) and b) had a high percentage of proteins involved in the immune system from NAs from humans (Chapter 5). In addition, STAT1 was identified and highlighted to have a significant differential abundance in this study following IAV infection. IAV is thought to interrupt the IFN γ - pathway by disrupting the JAK/STAT pathway. It does this by inhibiting the nuclear translocation of STAT1 gamma activated by interferon gamma (440). Some of the pathways highlighted in the BALF proteome of NHPs are known to be associated in the IAV-immune response in humans were pathways involving type 1 IFN proteins and also the JAK/STAT pathway (404, 440). The proteome of BALF from NHP, five days post-infection in comparison to naïve samples highlighted an extensive increase in proteins associated with macrophage activation, accumulation, and cell movement. These proteins include AGT, APOA1, PLG, CD44, ANXA2, ANXA1, S100A4 and S100A9 (Chapter 4 figure 4.6). Neutrophils and macrophages are known to play a key role in the phagocytosis of IAV-infected cells. There is a direct correlation between the changes in the level of phagocytosis and the amount of IAV in lung tissue (441). The NHP model therefore supports the results from the *in vitro* model and also supports the changes observed in the immune response in the host proteome in humans. Chapter 4, figure 4.8 highlighted proteins involved in the replication of IAV when comparing samples from NHP seven days post-infection to samples from NHP five days post-infection. The proteins highlighted in this figure were also uncovered by Mass spectrometry in A549 cells and categorised under 'replication of Influenza A virus' by Ingenuity Pathway Analysis (Table 3.9). The proteins common across these two datasets are highlighted in Table 6.0.

Table 6.0: Proteins highlighted as involved in "replication of influenza A virus" by Mass spectrometry when comparing A549 cells infected with IAV compared to IAV negative cells and in samples from IAV infected NHP at 7 days post infection compared to 5 days post infection

Uniprot accession ID	Protein name	Protein function in relation to IAV
DDX58_HUMAN	Probable ATP-dependent RNA helicase DDX58	Encodes cytosolic RNA receptor RIG-I. RIG-I plays an essential role in IAV recognition. Defects in the RIG-I encoding gene DDX58 impairs signalling of RIG-I (442)
EIF3A_HUMAN	Eukaryotic translation initiation factor 3 subunit A	eIF3A is one of many proteins that interact with IAV proteins (PA-N155 and PA-N182) in the host (443)
HSP90AA1_HUMAN	Heat shock protein HSP 90-alpha	HSP90 is a host chaperone thought to interact extensively with influenza virus

		enabling the folding of defective NP(444) variants
KPNB1_HUMAN	Importin subunit beta-1	Involved in nuclear trafficking of viral factors. Cells with a low abundance of KPNB1 show a significant decrease of NP in the cytoplasm (328, 445)
MAPK1_HUMAN	Mitogen-activated protein kinase 1	Part of a pathway affected by influenza infection. MAPKs regulate the overproduction of IL-6 during influenza virus infection (446) (447)
MX1_HUMAN	Interferon-induced GTP-binding protein Mx1	Part of the antiviral response induced by type I and III interferons. Responsible for inhibiting infection by blocking viral transcription and replication (229)

PAK2_HUMAN	Serine/threonine-protein kinase PAK 2	Essential role in viral entry and blocking viral RNA replication (328)
PIN1_HUMAN	Peptidyl-propyl cis-trans isomerase NIMA-interacting 1	Regulates NF-κB signalling through ubiquitin proteasome system (UPS. UPS is necessary for the entry of influenza virus into cells (448)
RPL13A_HUMAN	60S ribosomal protein L13a	Pro-viral host factor that Interacts with NS1 and NS2 IAV proteins (449)
RPS5_HUMAN	40S ribosomal protein S5	Host factors influenza depends on (345)
STAT1_HUMAN	Signal transducer and activator of transcription 1-alpha/beta	Involved in IFN signalling, STAT1 is suppressed in IAV infected cells (450)
SUMO2_HUMAN	Small ubiquitin-related modifier 2	IAV infection causes an increase in proteins modified by SUMO2 (451)

TUBB_HUMAN	Tubulin beta chain	Has a role in intracellular viral transport (328)
ARCN1_HUMAN	Coatomer subunit delta	Role in inhibiting replication of influenza strains (452)
CLIC4_HUMAN	Chloride intracellular channel protein 4	Host factors essential for influenza infection (345)
COPA_HUMAN	Coatomer subunit alpha	Involved in endosomal trafficking and early secretory pathway (328, 445)
COPB2_HUMAN	Coatomer subunit beta	Part of the complex essential for the formation of transport vesicles between early and late endosomes (328)

Some of the proteins highlighted in Table 6.0 above were also identified to have significant difference in abundance when human NA samples were analysed using proteomics (Chapter 5). These proteins include; HSPB1 (a heat shock protein), COPA, and TUBB, were all identified in the dataset from GOSH when comparing IAV H3N2 infected samples to non-infected samples (Appendix 1, Table 2). STAT1, CLIC1 and HSPB1 were also identified in the dataset from IPD when comparing IAV H3N2 infected samples to non-infected samples (Appendix 1, Table 3). TUBB, STAT1 and HSPB1 were all identified in the dataset from IPD when comparing IAV H1N1 infected samples to non-infected samples (Appendix 1, Table 4). In addition to these, proteins involved in pathways such as MAPK pathway and in the PKR signalling pathway were identified in the dataset from AHCH when comparing IAV H3N2 infected samples to non-infected samples (Appendix 1, Table 1). These proteins are therefore consistent across all three hosts – A549 cells, NHPs and humans. These proteins could additionally be potential biomarkers to identify disease progression and severity of IAV infection. Each of these proteins have been identified in studies in the literature to have roles in IAV infection and survival in the host. It is interesting to note that some of these proteins (Table 6.0) were not identified by MinION sequencing in Chapter 3. This highlights the importance of further experiments to explore individual targets as a potential biomarker after downstream analysis. It also shows the importance of using independent approaches and validation across species. However, when considering *in vivo* models, it is worth noting the NHP models incur a high amount of cost, require very skilled personnel to carry out these

experiments and are ethically controversial (453, 454). Chapter 4 brings in another dimension of the model for the study of IAV infection in comparison to the *in vitro* model. While the *in vitro* model provides information on host, cellular proteins found in human NAs and confirmed *in vivo* NHPs, NHPs give the opportunity to study other aspects, such as the immune response. It is essential that the findings observed *in vitro* and *in vivo* are compared to studies in humans. This is to ensure that when searching for potential anti-viral drug targets, the techniques and findings are efficient in IAV-infected humans. Proteomes of NAs from IAV-infected patients in comparison to non-infected patients were analysed. Samples with a wide range of C(t) values were obtained from three cohorts: AHCH, Liverpool, GOSH, London, and IPD, Senegal. Samples were taken from these cohorts to explore if any changes observed were a result of the geographical location. In the search for a model most reflective of the occurrences in humans following IAV infection, Chapter 5 highlighted already illustrated similarities and differences from Chapters 3 and 4 as well as novel potential biomarkers. Chapter 5 of this thesis established the use of Mass spectrometry as a technique to identify a global host proteome in NAs. The results from Mass spectrometry were validated by SDS-PAGE using the antibodies BPIFA1 and SCGB3A2. BPIFA1/SPLUNC1 has been identified as a potential biomarker for the diagnosis or severity of IAV (455). In Chapter 5, the abundance of BPIFA1 is seen to increase in some cohorts post infection (AHCH and GOSH) (Figure 5.3A) but seen to decrease in IPD post infection (Figure 5.3A). The reason for this is unknown but could be an indication of disease progression in different cohorts.

The Mass spectrometry data was further validated by ELISA. IL6 concentration was measured in IAV-H1N1 positive, IAV-H3N2 positive and IAV negative samples and it validated the data from Mass spectrometry. Further bioinformatic analysis identified proteins as potential biomarkers. Three proteins were highlighted during the data analysis of Chapter 5, which could play crucial roles as biomarkers. The host proteins: lactotransferrin, Fibrinogen A, B, and G, and BPIFA1/SPLUNC1 were all found to be directly associated with the influenza virus NS1A binding protein and polyadenylate binding protein 2. These proteins were also present across all three cohorts, regardless of geographical location. Lactotransferrin and BPIFA1/SPLUNC1 were identified with a significant difference in abundance in a study using 2DE proteomics to compare NA from IAV-infected H3N2 to mock samples (393). Lactotransferrin has natural immunity properties with an antiviral role and inhibits influenza infection via induced apoptosis (456-458). Fibrinogen in humans binds to glycoprotein on the surface of IAV-infected cells. Bound fibrinogen further acts as a receptor for group A Streptococcus (424). BPIFA1 plays a significant role in defence against IAV infection in the mucous. Mice deficient in BPIFA1/SPLUNC1 had lost more weight after infection as well as a higher viral load (455). These proteins play crucial roles in IAV infection and host defence. Lactoferrin's innate immune role could limit its potential as a biomarker. However, Fibrinogen A, B and G and BPIFA1/SPLUNC1 could be potential IAV biomarkers. This study presents the first time these proteins have been highlighted using label-free Mass spectrometry in human NAs across three cohorts from different geographical locations. This illustrates how

label free proteomic analysis of biological samples can be used to identify markers that may serve as potential diagnostic indicators for IAV infection. For research into host cellular response to IAV infection, a specific target or experimenting a potential drug, an *in vitro* A549 cellular model is recommended. For research into host cellular response and immune response, *in viv*o NHP macaque is the recommended model.

In **summary**, this thesis presented an in-depth analysis of IAV infection in three different models by proteomic analysis. It identified and highlighted several proteins associated with IAV infection, which have been published in the literature, confirming the data. Host proteins, which play essential roles in the replication of IAV were identified *in vitro* (Chapter 3) via two independent approaches; Mass spectrometry and MinION sequencing, and across species *in vitro* (Chapter 3) and *in vivo* (Chapter 4). These proteins could serve as potential biomarkers for disease progression or even drug targets. Other proteins that were highlighted to play a role in the replication of IAV have the potential to be biomarkers and should be explored further for full functional validation.

In addition, IAV infection was observed at different stages (Chapter 4) and proteins that could be targets for different stages of infection were highlighted (proteins involved in IAV replication). Data from *in vivo* and *in vitro* models were compared to data from human NA samples from patients aged 2–13 years old. From this data, three proteins (Chapter 5) were highlighted that could be used as

potential biomarkers for diagnosis of severity and predictability of outcome. Overall, this thesis presented the use and benefits of Mass spectrometry and MinION sequencing to identify a host's global proteome and transcriptome *in vitro* and *in vivo*. This thesis showed the potential of a new sequencing technique using the MinION sequencer to observe host response to IAV infection.

The main caveat faced in this thesis was limited information was provided on the NAs samples obtained from humans. This limited a definitive interpretation of the results obtained thereby focusing on comparing these results with findings in other studies for example mice models. When studying IAV in different models, we know that due to the differences in the hosts, there is an expected difference when observing the host proteome. Therefore, we can expect a level of change and difference after IAV infection only up to the capacity of the host being studied. Studies *in vitro* and *in vivo* have to be relatable back to humans; thus, embracing various facets of the host's response to IAV infection. As a result, there is no one size fits all model in the study of IAV, but rather, models that can be used based on what is being researched.

CHAPTER 7:

BIBLIOGRAPHY

1. Pappas G, Kiriaze IJ, Falagas ME. Insights into infectious disease in the era of Hippocrates. Int J Infect Dis. 2008;12(4):347-50.
2. Chen Y, Mo YN, Zhou HB, Wei ZZ, Wang GJ, Yu QX, et al. Emergence of human-like H3N2 influenza viruses in pet dogs in Guangxi, China. Virol J. 2015;12:10.
3. Short KR, Richard M, Verhagen JH, van Riel D, Schrauwen EJ, van den Brand JM, et al. One health, multiple challenges: The inter-species transmission of influenza A virus. One Health. 2015;1:1-13.
4. Nelson MI, Holmes EC. The evolution of epidemic influenza. Nat Rev Genet. 2007;8(3):196-205.
5. Ferguson L, Olivier AK, Genova S, Epperson WB, Smith DR, Schneider L, et al. Pathogenesis of Influenza D Virus in Cattle. J Virol. 2016;90(12):5636-42.
6. Taubenberger JK, Morens DM. The pathology of influenza virus infections. Annu Rev Pathol. 2008;3:499-522.
7. Taubenberger JK, Morens DM. Influenza viruses: breaking all the rules. MBio. 2013;4(4).
8. Zhao M, Wang L, Li S. Influenza A Virus-Host Protein Interactions Control Viral Pathogenesis. Int J Mol Sci. 2017;18(8).
9. Patzina C, Botting CH, Garcia-Sastre A, Randall RE, Hale BG. Human interactome of the influenza B virus NS1 protein. J Gen Virol. 2017;98(9):2267-73.
10. Su S, Fu X, Li G, Kerlin F, Veit M. Novel Influenza D virus: Epidemiology, pathology, evolution and biological characteristics. Virulence. 2017;8(8):1580-91.
11. Chowell G, Echevarria-Zuno S, Viboud C, Simonsen L, Tamerius J, Miller MA, et al. Characterizing the epidemiology of the 2009 influenza A/H1N1 pandemic in Mexico. PLoS Med. 2011;8(5):e1000436.
12. Zimmer SM, Burke DS. Historical perspective--Emergence of influenza A (H1N1) viruses. N Engl J Med. 2009;361(3):279-85.
13. Smith WH. The Report of the Committee on the Cost of Medical Care. Can Med Assoc J. 1933;28(2):198-9.
14. Krystal M, Young JF, Palese P, Wilson IA, Skehel JJ, Wiley DC. Sequential mutations in hemagglutinins of influenza B virus isolates: definition of antigenic domains. Proc Natl Acad Sci U S A. 1983;80(14):4527-31.
15. Greenbaum E, Morag A, Zakay-Rones Z. Isolation of influenza C virus during an outbreak of influenza A and B viruses. J Clin Microbiol. 1998;36(5):1441-2.
16. Potter CW. A history of influenza. J Appl Microbiol. 2001;91(4):572-9.
17. (ICTV) ICoToV. Orthomyxoviridae, virus taxonomy: 2017 release 2017, July [Available from: https://talk.ictvonline.org/ictv-reports/ictv_9th_report/negative-sense-rna-viruses-2011/w/negrna_viruses/209/orthomyxoviridae.
18. viruses ICoTo. Family: Orthomyxoviridae 2009 [Available from: https://talk.ictvonline.org/ictv-reports/ictv_9th_report/negative-sense-rna-viruses-2011/w/negrna_viruses/209/orthomyxoviridae.
19. Peng R, Zhang S, Cui Y, Shi Y, Gao GF, Qi J. Structures of human-infecting Thogotovirus fusogens support a common ancestor with insect baculovirus. Proc Natl Acad Sci U S A. 2017;114(42):E8905-E12.
20. Anderson CR, Casals J. Dhori virus, a new agent isolated from Hyalomma dromedarii in India. Indian J Med Res. 1973;61(10):1416-20.

21. Haig DA, Woodall JP, Danskin D. Thogoto Virus: A Hitherto Underscribed Agent Isolated from Ticks in Kenya. J Gen Microbiol. 1965;38:389-94.
22. Hubalek Z, Rudolf I. Tick-borne viruses in Europe. Parasitol Res. 2012;111(1):9-36.
23. Moore DL, Causey OR, Carey DE, Reddy S, Cooke AR, Akinkugbe FM, et al. Arthropod-borne viral infections of man in Nigeria, 1964-1970. Ann Trop Med Parasitol. 1975;69(1):49-64.
24. Butenko AM, Leshchinskaia EV, Semashko IV, Donets MA, Mart'ianova LI. [Dhori virus--a causative agent of human disease. 5 cases of laboratory infection]. Vopr Virusol. 1987;32(6):724-9.
25. Kosoy OI, Lambert AJ, Hawkinson DJ, Pastula DM, Goldsmith CS, Hunt DC, et al. Novel thogotovirus associated with febrile illness and death, United States, 2014. Emerg Infect Dis. 2015;21(5):760-4.
26. Portela A, Jones LD, Nuttall P. Identification of viral structural polypeptides of Thogoto virus (a tick-borne orthomyxo-like virus) and functions associated with the glycoprotein. J Gen Virol. 1992;73 (Pt 11):2823-30.
27. Presti RM, Zhao G, Beatty WL, Mihindukulasuriya KA, da Rosa AP, Popov VL, et al. Quaranfil, Johnston Atoll, and Lake Chad viruses are novel members of the family Orthomyxoviridae. J Virol. 2009;83(22):11599-606.
28. Clifford CM, Thomas LA, Hughes LE, Kohls GM, Philip CB. Identification and comparison of two viruses isolated from ticks of the genus Ornithodoros. Am J Trop Med Hyg. 1968;17(6):881-5.
29. Taylor RM, Hurlbut HS, Work TH, Kingston JR, Hoogstraal H. Arboviruses isolated from ARGAS TICKS IN Egypt: Quaranfil, Chenuda, and Nyamanini. Am J Trop Med Hyg. 1966;15(1):76-86.
30. Wang TT, Palese P. Unraveling the mystery of swine influenza virus. Cell. 2009;137(6):983-5.
31. Capua I, Alexander DJ. Avian influenza: recent developments. Avian Pathol. 2004;33(4):393-404.
32. Shaw ML, Stone KL, Colangelo CM, Gulcicek EE, Palese P. Cellular proteins in influenza virus particles. PLoS Pathog. 2008;4(6):e1000085.
33. Banks J, Speidel ES, Moore E, Plowright L, Piccirillo A, Capua I, et al. Changes in the haemagglutinin and the neuraminidase genes prior to the emergence of highly pathogenic H7N1 avian influenza viruses in Italy. Arch Virol. 2001;146(5):963-73.
34. Tong S, Li Y, Rivailler P, Conrardy C, Castillo DA, Chen LM, et al. A distinct lineage of influenza A virus from bats. Proc Natl Acad Sci U S A. 2012;109(11):4269-74.
35. Tong S, Zhu X, Li Y, Shi M, Zhang J, Bourgeois M, et al. New world bats harbor diverse influenza A viruses. PLoS Pathog. 2013;9(10):e1003657.
36. Sanjay Kapoor KD. Insight into Influenza Viruses of Animals and Humans. Switzerland: Springer International Publishing Switzerland; 2014.
37. Dadonaite B, Vijayakrishnan S, Fodor E, Bhella D, Hutchinson EC. Filamentous influenza viruses. J Gen Virol. 2016;97(8):1755-64.
38. White MC, Lowen AC. Implications of segment mismatch for influenza A virus evolution. J Gen Virol. 2018;99(1):3-16.

39. Webster RG, Bean WJ, Gorman OT, Chambers TM, Kawaoka Y. Evolution and ecology of influenza A viruses. Microbiol Rev. 1992;56(1):152-79.
40. Shao W, Li X, Goraya MU, Wang S, Chen JL. Evolution of Influenza A Virus by Mutation and Re-Assortment. Int J Mol Sci. 2017;18(8).
41. Holmes EC, Ghedin E, Miller N, Taylor J, Bao Y, St George K, et al. Whole-genome analysis of human influenza A virus reveals multiple persistent lineages and reassortment among recent H3N2 viruses. PLoS Biol. 2005;3(9):e300.
42. Nelson MI, Edelman L, Spiro DJ, Boyne AR, Bera J, Halpin R, et al. Molecular epidemiology of A/H3N2 and A/H1N1 influenza virus during a single epidemic season in the United States. PLoS Pathog. 2008;4(8):e1000133.
43. Nelson MI, Simonsen L, Viboud C, Miller MA, Taylor J, George KS, et al. Stochastic processes are key determinants of short-term evolution in influenza a virus. PLoS Pathog. 2006;2(12):e125.
44. Westgeest KB, Russell CA, Lin X, Spronken MI, Bestebroer TM, Bahl J, et al. Genomewide analysis of reassortment and evolution of human influenza A(H3N2) viruses circulating between 1968 and 2011. J Virol. 2014;88(5):2844-57.
45. Rambaut A, Pybus OG, Nelson MI, Viboud C, Taubenberger JK, Holmes EC. The genomic and epidemiological dynamics of human influenza A virus. Nature. 2008;453(7195):615-9.
46. Pauly MD, Procario MC, Lauring AS. A novel twelve class fluctuation test reveals higher than expected mutation rates for influenza A viruses. Elife. 2017;6.
47. Mehle A, Dugan VG, Taubenberger JK, Doudna JA. Reassortment and mutation of the avian influenza virus polymerase PA subunit overcome species barriers. J Virol. 2012;86(3):1750-7.
48. Carrat F, Flahault A. Influenza vaccine: the challenge of antigenic drift. Vaccine. 2007;25(39-40):6852-62.
49. Reid AH, Taubenberger JK. The origin of the 1918 pandemic influenza virus: a continuing enigma. J Gen Virol. 2003;84(Pt 9):2285-92.
50. Nakajima K. [The mechanism of antigenic shift and drift of human influenza virus]. Nihon Rinsho. 2003;61(11):1897-903.
51. Garten RJ, Davis CT, Russell CA, Shu B, Lindstrom S, Balish A, et al. Antigenic and genetic characteristics of swine-origin 2009 A(H1N1) influenza viruses circulating in humans. Science. 2009;325(5937):197-201.
52. Smith GL, Hay AJ. Replication of the influenza virus genome. Virology. 1982;118(1):96-108.
53. Kawaoka Y, Krauss S, Webster RG. Avian-to-human transmission of the PB1 gene of influenza A viruses in the 1957 and 1968 pandemics. J Virol. 1989;63(11):4603-8.
54. Kilbourne ED. Influenza pandemics of the 20th century. Emerg Infect Dis. 2006;12(1):9-14.
55. De Clercq E. Antiviral agents active against influenza A viruses. Nat Rev Drug Discov. 2006;5(12):1015-25.
56. Vergara-Alert J, Busquets N, Ballester M, Chaves AJ, Rivas R, Dolz R, et al. The NS segment of H5N1 avian influenza viruses (AIV) enhances the virulence of an H7N1 AIV in chickens. Vet Res. 2014;45:7.

57. Orlich M, Gottwald H, Rott R. Nonhomologous recombination between the hemagglutinin gene and the nucleoprotein gene of an influenza virus. Virology. 1994;204(1):462-5.
58. Suarez DL, Senne DA, Banks J, Brown IH, Essen SC, Lee CW, et al. Recombination resulting in virulence shift in avian influenza outbreak, Chile. Emerg Infect Dis. 2004;10(4):693-9.
59. Chare ER, Gould EA, Holmes EC. Phylogenetic analysis reveals a low rate of homologous recombination in negative-sense RNA viruses. J Gen Virol. 2003;84(Pt 10):2691-703.
60. Mossad SB. Influenza: Still more important than Zika virus in 2016-2017. Cleve Clin J Med. 2016;83(11):836-40.
61. Fox SJ, Miller JC, Meyers LA. Seasonality in risk of pandemic influenza emergence. PLoS Comput Biol. 2017;13(10):e1005749.
62. Deyle ER, Maher MC, Hernandez RD, Basu S, Sugihara G. Global environmental drivers of influenza. Proc Natl Acad Sci U S A. 2016;113(46):13081-6.
63. Pica N, Bouvier NM. Environmental factors affecting the transmission of respiratory viruses. Curr Opin Virol. 2012;2(1):90-5.
64. Taubenberger JK, Morens DM. 1918 Influenza: the mother of all pandemics. Emerg Infect Dis. 2006;12(1):15-22.
65. Nakajima K, Desselberger U, Palese P. Recent human influenza A (H1N1) viruses are closely related genetically to strains isolated in 1950. Nature. 1978;274(5669):334-9.
66. Morens DM, Folkers GK, Fauci AS. Emerging infections: a perpetual challenge. Lancet Infect Dis. 2008;8(11):710-9.
67. Bui CM, Chughtai AA, Adam DC, MacIntyre CR. An overview of the epidemiology and emergence of influenza A infection in humans over time. Arch Public Health. 2017;75:15.
68. Noda T. Native morphology of influenza virions. Front Microbiol. 2011;2:269.
69. Chu CM, Andrewes CH, Gledhill AW. Influenza in 1948-1949. Bull World Health Organ. 1950;3(2):187-214.
70. Kilbourne ED, Murphy JS. Genetic studies of influenza viruses. I. Viral morphology and growth capacity as exchangeable genetic traits. Rapid in ovo adaptation of early passage Asian strain isolates by combination with PR8. J Exp Med. 1960;111:387-406.
71. Smirnov Yu A, Kuznetsova MA, Kaverin NV. The genetic aspects of influenza virus filamentous particle formation. Arch Virol. 1991;118(3-4):279-84.
72. Hughey PG, Roberts PC, Holsinger LJ, Zebedee SL, Lamb RA, Compans RW. Effects of antibody to the influenza A virus M2 protein on M2 surface expression and virus assembly. Virology. 1995;212(2):411-21.
73. Roberts A, Kretzschmar E, Perkins AS, Forman J, Price R, Buonocore L, et al. Vaccination with a recombinant vesicular stomatitis virus expressing an influenza virus hemagglutinin provides complete protection from influenza virus challenge. J Virol. 1998;72(6):4704-11.
74. Bourmakina SV, Garcia-Sastre A. Reverse genetics studies on the filamentous morphology of influenza A virus. J Gen Virol. 2003;84(Pt 3):517-27.

75. Lamb RA, Lai CJ. Conservation of the influenza virus membrane protein (M1) amino acid sequence and an open reading frame of RNA segment 7 encoding a second protein (M2) in H1N1 and H3N2 strains. Virology. 1981;112(2):746-51.
76. Bouvier NM, Palese P. The biology of influenza viruses. Vaccine. 2008;26 Suppl 4:D49-53.
77. Muramoto Y, Noda T, Kawakami E, Akkina R, Kawaoka Y. Identification of novel influenza A virus proteins translated from PA mRNA. J Virol. 2013;87(5):2455-62.
78. McCauley JW, Mahy BW. Structure and function of the influenza virus genome. Biochem J. 1983;211(2):281-94.
79. Wang M, Veit M. Hemagglutinin-esterase-fusion (HEF) protein of influenza C virus. Protein Cell. 2016;7(1):28-45.
80. Briedis DJ, Lamb RA. Influenza B virus genome: sequences and structural organization of RNA segment 8 and the mRNAs coding for the NS1 and NS2 proteins. J Virol. 1982;42(1):186-93.
81. Fields S, Winter G. Nucleotide sequences of influenza virus segments 1 and 3 reveal mosaic structure of a small viral RNA segment. Cell. 1982;28(2):303-13.
82. Yamayoshi S, Watanabe M, Goto H, Kawaoka Y. Identification of a Novel Viral Protein Expressed from the PB2 Segment of Influenza A Virus. J Virol. 2016;90(1):444-56.
83. Chen W, Calvo PA, Malide D, Gibbs J, Schubert U, Bacik I, et al. A novel influenza A virus mitochondrial protein that induces cell death. Nat Med. 2001;7(12):1306-12.
84. Wise HM, Foeglein A, Sun J, Dalton RM, Patel S, Howard W, et al. A complicated message: Identification of a novel PB1-related protein translated from influenza A virus segment 2 mRNA. J Virol. 2009;83(16):8021-31.
85. Jagger BW, Wise HM, Kash JC, Walters KA, Wills NM, Xiao YL, et al. An overlapping protein-coding region in influenza A virus segment 3 modulates the host response. Science. 2012;337(6091):199-204.
86. Winter G, Fields S, Brownlee GG. Nucleotide sequence of the haemagglutinin gene of a human influenza virus H1 subtype. Nature. 1981;292(5818):72-5.
87. Winter G, Fields S, Gait MJ, Brownlee GG. The use of synthetic oligodeoxynucleotide primers in cloning and sequencing segment of 8 influenza virus (A/PR/8/34). Nucleic Acids Res. 1981;9(2):237-45.
88. Fields S, Winter G. Nucleotide-sequence heterogeneity and sequence rearrangements in influenza virus cDNA. Gene. 1981;15(2-3):207-14.
89. Winter G, Fields S. Cloning of influenza cDNA ino M13: the sequence of the RNA segment encoding the A/PR/8/34 matrix protein. Nucleic Acids Res. 1980;8(9):1965-74.
90. Shih SR, Suen PC, Chen YS, Chang SC. A novel spliced transcript of influenza A/WSN/33 virus. Virus Genes. 1998;17(2):179-83.
91. Wise HM, Hutchinson EC, Jagger BW, Stuart AD, Kang ZH, Robb N, et al. Identification of a novel splice variant form of the influenza A virus M2 ion channel with an antigenically distinct ectodomain. PLoS Pathog. 2012;8(11):e1002998.
92. Lin D, Lan J, Zhang Z. Structure and function of the NS1 protein of influenza A virus. Acta Biochim Biophys Sin (Shanghai). 2007;39(3):155-62.

93. Selman M, Dankar SK, Forbes NE, Jia JJ, Brown EG. Adaptive mutation in influenza A virus non-structural gene is linked to host switching and induces a novel protein by alternative splicing. Emerg Microbes Infect. 2012;1(11):e42.
94. Zhirnov OP, Syrtzev VV. Influenza virus pathogenicity is determined by caspase cleavage motifs located in the viral proteins. J Mol Genet Med. 2009;3(1):124-32.
95. Watanabe T, Watanabe S, Kawaoka Y. Cellular networks involved in the influenza virus life cycle. Cell Host Microbe. 2010;7(6):427-39.
96. Hofmann P, Sprenger H, Kaufmann A, Bender A, Hasse C, Nain M, et al. Susceptibility of mononuclear phagocytes to influenza A virus infection and possible role in the antiviral response. J Leukoc Biol. 1997;61(4):408-14.
97. Seo SH, Webby R, Webster RG. No apoptotic deaths and different levels of inductions of inflammatory cytokines in alveolar macrophages infected with influenza viruses. Virology. 2004;329(2):270-9.
98. Smed-Sorensen A, Chalouni C, Chatterjee B, Cohn L, Blattmann P, Nakamura N, et al. Influenza A virus infection of human primary dendritic cells impairs their ability to cross-present antigen to CD8 T cells. PLoS Pathog. 2012;8(3):e1002572.
99. Matsuoka Y, Matsumae H, Katoh M, Eisfeld AJ, Neumann G, Hase T, et al. A comprehensive map of the influenza A virus replication cycle. BMC Syst Biol. 2013;7:97.
100. Paterson D, Fodor E. Emerging roles for the influenza A virus nuclear export protein (NEP). PLoS Pathog. 2012;8(12):e1003019.
101. Baum LG, Paulson JC. Sialyloligosaccharides of the respiratory epithelium in the selection of human influenza virus receptor specificity. Acta Histochem Suppl. 1990;40:35-8.
102. Couceiro JN, Paulson JC, Baum LG. Influenza virus strains selectively recognize sialyloligosaccharides on human respiratory epithelium; the role of the host cell in selection of hemagglutinin receptor specificity. Virus Res. 1993;29(2):155-65.
103. Matrosovich MN, Matrosovich TY, Gray T, Roberts NA, Klenk HD. Human and avian influenza viruses target different cell types in cultures of human airway epithelium. Proc Natl Acad Sci U S A. 2004;101(13):4620-4.
104. Nicholls JM, Chan MC, Chan WY, Wong HK, Cheung CY, Kwong DL, et al. Tropism of avian influenza A (H5N1) in the upper and lower respiratory tract. Nat Med. 2007;13(2):147-9.
105. Shinya K, Ebina M, Yamada S, Ono M, Kasai N, Kawaoka Y. Avian flu: influenza virus receptors in the human airway. Nature. 2006;440(7083):435-6.
106. van Riel D, Munster VJ, de Wit E, Rimmelzwaan GF, Fouchier RA, Osterhaus AD, et al. H5N1 Virus Attachment to Lower Respiratory Tract. Science. 2006;312(5772):399.
107. Yao L, Korteweg C, Hsueh W, Gu J. Avian influenza receptor expression in H5N1-infected and noninfected human tissues. FASEB J. 2008;22(3):733-40.
108. Connor RJ, Kawaoka Y, Webster RG, Paulson JC. Receptor specificity in human, avian, and equine H2 and H3 influenza virus isolates. Virology. 1994;205(1):17-23.
109. Gambaryan AS, Tuzikov AB, Piskarev VE, Yamnikova SS, Lvov DK, Robertson JS, et al. Specification of receptor-binding phenotypes of influenza virus isolates

from different hosts using synthetic sialylglycopolymers: non-egg-adapted human H1 and H3 influenza A and influenza B viruses share a common high binding affinity for 6'-sialyl(N-acetyllactosamine). Virology. 1997;232(2):345-50.
110. Ito T, Kawaoka Y. Host-range barrier of influenza A viruses. Vet Microbiol. 2000;74(1-2):71-5.
111. Matrosovich M, Tuzikov A, Bovin N, Gambaryan A, Klimov A, Castrucci MR, et al. Early alterations of the receptor-binding properties of H1, H2, and H3 avian influenza virus hemagglutinins after their introduction into mammals. J Virol. 2000;74(18):8502-12.
112. Rogers GN, Paulson JC. Receptor determinants of human and animal influenza virus isolates: differences in receptor specificity of the H3 hemagglutinin based on species of origin. Virology. 1983;127(2):361-73.
113. Rogers GN, Pritchett TJ, Lane JL, Paulson JC. Differential sensitivity of human, avian, and equine influenza A viruses to a glycoprotein inhibitor of infection: selection of receptor specific variants. Virology. 1983;131(2):394-408.
114. Ito T, Suzuki Y, Suzuki T, Takada A, Horimoto T, Wells K, et al. Recognition of N-glycolylneuraminic acid linked to galactose by the alpha2,3 linkage is associated with intestinal replication of influenza A virus in ducks. J Virol. 2000;74(19):9300-5.
115. Pillai SP, Lee CW. Species and age related differences in the type and distribution of influenza virus receptors in different tissues of chickens, ducks and turkeys. Virol J. 2010;7:5.
116. Nicholls JM, Chan RW, Russell RJ, Air GM, Peiris JS. Evolving complexities of influenza virus and its receptors. Trends Microbiol. 2008;16(4):149-57.
117. Samji T. Influenza A: understanding the viral life cycle. Yale J Biol Med. 2009;82(4):153-9.
118. Skehel JJ, Wiley DC. Receptor binding and membrane fusion in virus entry: the influenza hemagglutinin. Annu Rev Biochem. 2000;69:531-69.
119. Huang Q, Sivaramakrishna RP, Ludwig K, Korte T, Bottcher C, Herrmann A. Early steps of the conformational change of influenza virus hemagglutinin to a fusion active state: stability and energetics of the hemagglutinin. Biochim Biophys Acta. 2003;1614(1):3-13.
120. Muramoto Y, Takada A, Fujii K, Noda T, Iwatsuki-Horimoto K, Watanabe S, et al. Hierarchy among viral RNA (vRNA) segments in their role in vRNA incorporation into influenza A virions. J Virol. 2006;80(5):2318-25.
121. Watanabe T, Watanabe S, Noda T, Fujii Y, Kawaoka Y. Exploitation of nucleic acid packaging signals to generate a novel influenza virus-based vector stably expressing two foreign genes. J Virol. 2003;77(19):10575-83.
122. Liang Y, Hong Y, Parslow TG. cis-Acting packaging signals in the influenza virus PB1, PB2, and PA genomic RNA segments. J Virol. 2005;79(16):10348-55.
123. Fujii K, Fujii Y, Noda T, Muramoto Y, Watanabe T, Takada A, et al. Importance of both the coding and the segment-specific noncoding regions of the influenza A virus NS segment for its efficient incorporation into virions. J Virol. 2005;79(6):3766-74.
124. Palese P, Tobita K, Ueda M, Compans RW. Characterization of temperature sensitive influenza virus mutants defective in neuraminidase. Virology. 1974;61(2):397-410.

125. Holsinger LJ, Lamb RA. Influenza virus M2 integral membrane protein is a homotetramer stabilized by formation of disulfide bonds. Virology. 1991;183(1):32-43.
126. Pinto LH, Holsinger LJ, Lamb RA. Influenza virus M2 protein has ion channel activity. Cell. 1992;69(3):517-28.
127. Pinto LH, Lamb RA. The M2 proton channels of influenza A and B viruses. J Biol Chem. 2006;281(14):8997-9000.
128. Bui M, Whittaker G, Helenius A. Effect of M1 protein and low pH on nuclear transport of influenza virus ribonucleoproteins. J Virol. 1996;70(12):8391-401.
129. Martin K, Helenius A. Nuclear transport of influenza virus ribonucleoproteins: the viral matrix protein (M1) promotes export and inhibits import. Cell. 1991;67(1):117-30.
130. Whittaker G, Bui M, Helenius A. Nuclear trafficking of influenza virus ribonuleoproteins in heterokaryons. J Virol. 1996;70(5):2743-56.
131. Wu WW, Sun YH, Pante N. Nuclear import of influenza A viral ribonucleoprotein complexes is mediated by two nuclear localization sequences on viral nucleoprotein. Virol J. 2007;4:49.
132. O'Neill RE, Jaskunas R, Blobel G, Palese P, Moroianu J. Nuclear import of influenza virus RNA can be mediated by viral nucleoprotein and transport factors required for protein import. J Biol Chem. 1995;270(39):22701-4.
133. O'Neill RE, Palese P. NPI-1, the human homolog of SRP-1, interacts with influenza virus nucleoprotein. Virology. 1995;206(1):116-25.
134. Wang P, Palese P, O'Neill RE. The NPI-1/NPI-3 (karyopherin alpha) binding site on the influenza a virus nucleoprotein NP is a nonconventional nuclear localization signal. J Virol. 1997;71(3):1850-6.
135. Cros JF, Garcia-Sastre A, Palese P. An unconventional NLS is critical for the nuclear import of the influenza A virus nucleoprotein and ribonucleoprotein. Traffic. 2005;6(3):205-13.
136. Helenius A. Unpacking the incoming influenza virus. Cell. 1992;69(4):577-8.
137. Crow M, Deng T, Addley M, Brownlee GG. Mutational analysis of the influenza virus cRNA promoter and identification of nucleotides critical for replication. J Virol. 2004;78(12):6263-70.
138. Deng T, Vreede FT, Brownlee GG. Different de novo initiation strategies are used by influenza virus RNA polymerase on its cRNA and viral RNA promoters during viral RNA replication. J Virol. 2006;80(5):2337-48.
139. Flick R, Neumann G, Hoffmann E, Neumeier E, Hobom G. Promoter elements in the influenza vRNA terminal structure. RNA. 1996;2(10):1046-57.
140. Azzeh M, Flick R, Hobom G. Functional analysis of the influenza A virus cRNA promoter and construction of an ambisense transcription system. Virology. 2001;289(2):400-10.
141. Plotch SJ, Tomasz J, Krug RM. Absence of detectable capping and methylating enzymes in influenza virions. J Virol. 1978;28(1):75-83.
142. Krug RM, Morgan MA, Shatkin AJ. Influenza viral mRNA contains internal N6-methyladenosine and 5'-terminal 7-methylguanosine in cap structures. J Virol. 1976;20(1):45-53.

143. Dhar R, Chanock RM, Lai CJ. Nonviral oligonucleotides at the 5' terminus of cytoplasmic influenza viral mRNA deduced from cloned complete genomic sequences. Cell. 1980;21(2):495-500.
144. Bouloy M, Plotch SJ, Krug RM. Globin mRNAs are primers for the transcription of influenza viral RNA in vitro. Proc Natl Acad Sci U S A. 1978;75(10):4886-90.
145. Plotch SJ, Bouloy M, Krug RM. Transfer of 5'-terminal cap of globin mRNA to influenza viral complementary RNA during transcription in vitro. Proc Natl Acad Sci U S A. 1979;76(4):1618-22.
146. Plotch SJ, Bouloy M, Ulmanen I, Krug RM. A unique cap(m7GpppXm)-dependent influenza virion endonuclease cleaves capped RNAs to generate the primers that initiate viral RNA transcription. Cell. 1981;23(3):847-58.
147. Bouloy M, Morgan MA, Shatkin AJ, Krug RM. Cap and internal nucleotides of reovirus mRNA primers are incorporated into influenza viral complementary RNA during transcription in vitro. J Virol. 1979;32(3):895-904.
148. Bouloy M, Plotch SJ, Krug RM. Both the 7-methyl and the 2'-O-methyl groups in the cap of mRNA strongly influence its ability to act as primer for influenza virus RNA transcription. Proc Natl Acad Sci U S A. 1980;77(7):3952-6.
149. Krug RM, Broni BA, Bouloy M. Are the 5' ends of influenza viral mRNAs synthesized in vivo donated by host mRNAs? Cell. 1979;18(2):329-34.
150. Robertson HD, Dickson E, Plotch SJ, Krug RM. Identification of the RNA region transferred from a representative primer, beta-globin mRNA, to influenza mRNA during in vitro transcription. Nucleic Acids Res. 1980;8(5):925-42.
151. Li ML, Rao P, Krug RM. The active sites of the influenza cap-dependent endonuclease are on different polymerase subunits. EMBO J. 2001;20(8):2078-86.
152. Engelhardt OG, Smith M, Fodor E. Association of the influenza A virus RNA-dependent RNA polymerase with cellular RNA polymerase II. J Virol. 2005;79(9):5812-8.
153. Fodor E, Pritlove DC, Brownlee GG. The influenza virus panhandle is involved in the initiation of transcription. J Virol. 1994;68(6):4092-6.
154. Hagen M, Chung TD, Butcher JA, Krystal M. Recombinant influenza virus polymerase: requirement of both 5' and 3' viral ends for endonuclease activity. J Virol. 1994;68(3):1509-15.
155. Poon LL, Fodor E, Brownlee GG. Polyuridylated mRNA synthesized by a recombinant influenza virus is defective in nuclear export. J Virol. 2000;74(1):418-27.
156. Poon LL, Pritlove DC, Fodor E, Brownlee GG. Direct evidence that the poly(A) tail of influenza A virus mRNA is synthesized by reiterative copying of a U track in the virion RNA template. J Virol. 1999;73(4):3473-6.
157. Shapiro GI, Gurney T, Jr., Krug RM. Influenza virus gene expression: control mechanisms at early and late times of infection and nuclear-cytoplasmic transport of virus-specific RNAs. J Virol. 1987;61(3):764-73.
158. Nguyen KT, Holloway MP, Altura RA. The CRM1 nuclear export protein in normal development and disease. Int J Biochem Mol Biol. 2012;3(2):137-51.
159. Boulo S, Akarsu H, Ruigrok RW, Baudin F. Nuclear traffic of influenza virus proteins and ribonucleoprotein complexes. Virus Res. 2007;124(1-2):12-21.

160. Akarsu H, Burmeister WP, Petosa C, Petit I, Muller CW, Ruigrok RW, et al. Crystal structure of the M1 protein-binding domain of the influenza A virus nuclear export protein (NEP/NS2). EMBO J. 2003;22(18):4646-55.
161. Baudin F, Petit I, Weissenhorn W, Ruigrok RW. In vitro dissection of the membrane and RNP binding activities of influenza virus M1 protein. Virology. 2001;281(1):102-8.
162. Nayak DP, Balogun RA, Yamada H, Zhou ZH, Barman S. Influenza virus morphogenesis and budding. Virus Res. 2009;143(2):147-61.
163. Rossman JS, Jing X, Leser GP, Balannik V, Pinto LH, Lamb RA. Influenza virus m2 ion channel protein is necessary for filamentous virion formation. J Virol. 2010;84(10):5078-88.
164. Iwatsuki-Horimoto K, Horimoto T, Noda T, Kiso M, Maeda J, Watanabe S, et al. The cytoplasmic tail of the influenza A virus M2 protein plays a role in viral assembly. J Virol. 2006;80(11):5233-40.
165. Chen BJ, Lamb RA. Mechanisms for enveloped virus budding: can some viruses do without an ESCRT? Virology. 2008;372(2):221-32.
166. Enami M, Sharma G, Benham C, Palese P. An influenza virus containing nine different RNA segments. Virology. 1991;185(1):291-8.
167. Bancroft CT, Parslow TG. Evidence for segment-nonspecific packaging of the influenza a virus genome. J Virol. 2002;76(14):7133-9.
168. Fujii Y, Goto H, Watanabe T, Yoshida T, Kawaoka Y. Selective incorporation of influenza virus RNA segments into virions. Proc Natl Acad Sci U S A. 2003;100(4):2002-7.
169. Fukuyama S, Kawaoka Y. The pathogenesis of influenza virus infections: the contributions of virus and host factors. Curr Opin Immunol. 2011;23(4):481-6.
170. Lessler J, Reich NG, Brookmeyer R, Perl TM, Nelson KE, Cummings DA. Incubation periods of acute respiratory viral infections: a systematic review. Lancet Infect Dis. 2009;9(5):291-300.
171. Godlee A, Almond MH, Dong T. Pathogenesis of influenza: virus-host interactions. Expert Rev Anti Infect Ther. 2011;9(8):573-5.
172. Diebold SS, Kaisho T, Hemmi H, Akira S, Reis e Sousa C. Innate antiviral responses by means of TLR7-mediated recognition of single-stranded RNA. Science. 2004;303(5663):1529-31.
173. Pichlmair A, Schulz O, Tan CP, Naslund TI, Liljestrom P, Weber F, et al. RIG-I-mediated antiviral responses to single-stranded RNA bearing 5'-phosphates. Science. 2006;314(5801):997-1001.
174. Kumagai Y, Takeuchi O, Akira S. Pathogen recognition by innate receptors. J Infect Chemother. 2008;14(2):86-92.
175. Geiss GK, Salvatore M, Tumpey TM, Carter VS, Wang X, Basler CF, et al. Cellular transcriptional profiling in influenza A virus-infected lung epithelial cells: the role of the nonstructural NS1 protein in the evasion of the host innate defense and its potential contribution to pandemic influenza. Proc Natl Acad Sci U S A. 2002;99(16):10736-41.
176. Li S, Min JY, Krug RM, Sen GC. Binding of the influenza A virus NS1 protein to PKR mediates the inhibition of its activation by either PACT or double-stranded RNA. Virology. 2006;349(1):13-21.

177. Sadler AJ, Williams BR. Structure and function of the protein kinase R. Curr Top Microbiol Immunol. 2007;316:253-92.
178. Nakayama Y, Plisch EH, Sullivan J, Thomas C, Czuprynski CJ, Williams BR, et al. Role of PKR and Type I IFNs in viral control during primary and secondary infection. PLoS Pathog. 2010;6(6):e1000966.
179. Perrone LA, Plowden JK, Garcia-Sastre A, Katz JM, Tumpey TM. H5N1 and 1918 pandemic influenza virus infection results in early and excessive infiltration of macrophages and neutrophils in the lungs of mice. PLoS Pathog. 2008;4(8):e1000115.
180. Herold S, Steinmueller M, von Wulffen W, Cakarova L, Pinto R, Pleschka S, et al. Lung epithelial apoptosis in influenza virus pneumonia: the role of macrophage-expressed TNF-related apoptosis-inducing ligand. J Exp Med. 2008;205(13):3065-77.
181. Dawson TC, Beck MA, Kuziel WA, Henderson F, Maeda N. Contrasting effects of CCR5 and CCR2 deficiency in the pulmonary inflammatory response to influenza A virus. Am J Pathol. 2000;156(6):1951-9.
182. Tate MD, Ioannidis LJ, Croker B, Brown LE, Brooks AG, Reading PC. The role of neutrophils during mild and severe influenza virus infections of mice. PLoS One. 2011;6(3):e17618.
183. Le Goffic R, Pothlichet J, Vitour D, Fujita T, Meurs E, Chignard M, et al. Cutting Edge: Influenza A virus activates TLR3-dependent inflammatory and RIG-I-dependent antiviral responses in human lung epithelial cells. J Immunol. 2007;178(6):3368-72.
184. de Wit E, Munster VJ, van Riel D, Beyer WE, Rimmelzwaan GF, Kuiken T, et al. Molecular determinants of adaptation of highly pathogenic avian influenza H7N7 viruses to efficient replication in the human host. J Virol. 2010;84(3):1597-606.
185. Tumpey TM, Maines TR, Van Hoeven N, Glaser L, Solorzano A, Pappas C, et al. A two-amino acid change in the hemagglutinin of the 1918 influenza virus abolishes transmission. Science. 2007;315(5812):655-9.
186. Liu Y, Childs RA, Matrosovich T, Wharton S, Palma AS, Chai W, et al. Altered receptor specificity and cell tropism of D222G hemagglutinin mutants isolated from fatal cases of pandemic A(H1N1) 2009 influenza virus. J Virol. 2010;84(22):12069-74.
187. Kiso M, Mitamura K, Sakai-Tagawa Y, Shiraishi K, Kawakami C, Kimura K, et al. Resistant influenza A viruses in children treated with oseltamivir: descriptive study. Lancet. 2004;364(9436):759-65.
188. Herlocher ML, Carr J, Ives J, Elias S, Truscon R, Roberts N, et al. Influenza virus carrying an R292K mutation in the neuraminidase gene is not transmitted in ferrets. Antiviral Res. 2002;54(2):99-111.
189. Le QM, Kiso M, Someya K, Sakai YT, Nguyen TH, Nguyen KH, et al. Avian flu: isolation of drug-resistant H5N1 virus. Nature. 2005;437(7062):1108.
190. Conenello GM, Zamarin D, Perrone LA, Tumpey T, Palese P. A single mutation in the PB1-F2 of H5N1 (HK/97) and 1918 influenza A viruses contributes to increased virulence. PLoS Pathog. 2007;3(10):1414-21.
191. Bussey KA, Bousse TL, Desmet EA, Kim B, Takimoto T. PB2 residue 271 plays a key role in enhanced polymerase activity of influenza A viruses in mammalian host cells. J Virol. 2010;84(9):4395-406.

192. Hatta M, Hatta Y, Kim JH, Watanabe S, Shinya K, Nguyen T, et al. Growth of H5N1 influenza A viruses in the upper respiratory tracts of mice. PLoS Pathog. 2007;3(10):1374-9.
193. Munster VJ, Baas C, Lexmond P, Waldenstrom J, Wallensten A, Fransson T, et al. Spatial, temporal, and species variation in prevalence of influenza A viruses in wild migratory birds. PLoS Pathog. 2007;3(5):e61.
194. Li Z, Chen H, Jiao P, Deng G, Tian G, Li Y, et al. Molecular basis of replication of duck H5N1 influenza viruses in a mammalian mouse model. J Virol. 2005;79(18):12058-64.
195. Song MS, Pascua PN, Lee JH, Baek YH, Lee OJ, Kim CJ, et al. The polymerase acidic protein gene of influenza a virus contributes to pathogenicity in a mouse model. J Virol. 2009;83(23):12325-35.
196. Jiao P, Tian G, Li Y, Deng G, Jiang Y, Liu C, et al. A single-amino-acid substitution in the NS1 protein changes the pathogenicity of H5N1 avian influenza viruses in mice. J Virol. 2008;82(3):1146-54.
197. Zhou H, Zhu J, Tu J, Zou W, Hu Y, Yu Z, et al. Effect on virulence and pathogenicity of H5N1 influenza A virus through truncations of NS1 eIF4GI binding domain. J Infect Dis. 2010;202(9):1338-46.
198. Pu J, Wang J, Zhang Y, Fu G, Bi Y, Sun Y, et al. Synergism of co-mutation of two amino acid residues in NS1 protein increases the pathogenicity of influenza virus in mice. Virus Res. 2010;151(2):200-4.
199. Min JY, Li S, Sen GC, Krug RM. A site on the influenza A virus NS1 protein mediates both inhibition of PKR activation and temporal regulation of viral RNA synthesis. Virology. 2007;363(1):236-43.
200. Seo SH, Hoffmann E, Webster RG. Lethal H5N1 influenza viruses escape host anti-viral cytokine responses. Nat Med. 2002;8(9):950-4.
201. Glezen WP, Decker M, Perrotta DM. Survey of underlying conditions of persons hospitalized with acute respiratory disease during influenza epidemics in Houston, 1978-1981. Am Rev Respir Dis. 1987;136(3):550-5.
202. Stephenson I, Nicholson KG. Influenza: vaccination and treatment. Eur Respir J. 2001;17(6):1282-93.
203. Sridhar S, Brokstad KA, Cox RJ. Influenza Vaccination Strategies: Comparing Inactivated and Live Attenuated Influenza Vaccines. Vaccines (Basel). 2015;3(2):373-89.
204. Fiore AE, Fry A, Shay D, Gubareva L, Bresee JS, Uyeki TM, et al. Antiviral agents for the treatment and chemoprophylaxis of influenza --- recommendations of the Advisory Committee on Immunization Practices (ACIP). MMWR Recomm Rep. 2011;60(1):1-24.
205. von Itzstein M, Wu WY, Kok GB, Pegg MS, Dyason JC, Jin B, et al. Rational design of potent sialidase-based inhibitors of influenza virus replication. Nature. 1993;363(6428):418-23.
206. Woods JM, Bethell RC, Coates JA, Healy N, Hiscox SA, Pearson BA, et al. 4-Guanidino-2,4-dideoxy-2,3-dehydro-N-acetylneuraminic acid is a highly effective inhibitor both of the sialidase (neuraminidase) and of growth of a wide range of influenza A and B viruses in vitro. Antimicrob Agents Chemother. 1993;37(7):1473-9.

207. Kim CU, Lew W, Williams MA, Liu H, Zhang L, Swaminathan S, et al. Influenza neuraminidase inhibitors possessing a novel hydrophobic interaction in the enzyme active site: design, synthesis, and structural analysis of carbocyclic sialic acid analogues with potent anti-influenza activity. J Am Chem Soc. 1997;119(4):681-90.
208. Service RF. Researchers seek new weapon against the flu. Science. 1997;275(5301):756-7.
209. Nguyen HT, Fry AM, Gubareva LV. Neuraminidase inhibitor resistance in influenza viruses and laboratory testing methods. Antivir Ther. 2012;17(1 Pt B):159-73.
210. Coombs KM, Berard A, Xu W, Krokhin O, Meng X, Cortens JP, et al. Quantitative proteomic analyses of influenza virus-infected cultured human lung cells. J Virol. 2010;84(20):10888-906.
211. Gorg A, Postel W, Gunther S. The current state of two-dimensional electrophoresis with immobilized pH gradients. Electrophoresis. 1988;9(9):531-46.
212. Klose J. Protein mapping by combined isoelectric focusing and electrophoresis of mouse tissues. A novel approach to testing for induced point mutations in mammals. Humangenetik. 1975;26(3):231-43.
213. Geiger T, Wehner A, Schaab C, Cox J, Mann M. Comparative proteomic analysis of eleven common cell lines reveals ubiquitous but varying expression of most proteins. Mol Cell Proteomics. 2012;11(3):M111 014050.
214. Mann M. Functional and quantitative proteomics using SILAC. Nat Rev Mol Cell Biol. 2006;7(12):952-8.
215. Rickwood D, MacGillivray AJ. Improved techniques for the fractionation of non-histone proteins of chromatin on hydroxyapatite. Eur J Biochem. 1975;51(2):593-601.
216. Lilley KS, Friedman DB. All about DIGE: quantification technology for differential-display 2D-gel proteomics. Expert Rev Proteomics. 2004;1(4):401-9.
217. Tong A, Wu L, Lin Q, Lau QC, Zhao X, Li J, et al. Proteomic analysis of cellular protein alterations using a hepatitis B virus-producing cellular model. Proteomics. 2008;8(10):2012-23.
218. Fu ZF, Li X, Dhingra V. Pathogenic rabies virus alters host protein expression in the central nervous system: implications for neuronal dysfunction. Developments in biologicals. 2008;131:83-91.
219. Vester D, Rapp E, Gade D, Genzel Y, Reichl U. Quantitative analysis of cellular proteome alterations in human influenza A virus-infected mammalian cell lines. Proteomics. 2009;9(12):3316-27.
220. Wu X, Wang S, Yu Y, Zhang J, Sun Z, Yan Y, et al. Subcellular proteomic analysis of human host cells infected with H3N2 swine influenza virus. Proteomics. 2013;13(22):3309-26.
221. Megger DA, Bracht T, Meyer HE, Sitek B. Label-free quantification in clinical proteomics. Biochim Biophys Acta. 2013;1834(8):1581-90.
222. Lai X, Wang L, Witzmann FA. Issues and applications in label-free quantitative mass spectrometry. Int J Proteomics. 2013;2013:756039.
223. Silva JC, Denny R, Dorschel C, Gorenstein MV, Li GZ, Richardson K, et al. Simultaneous qualitative and quantitative analysis of the Escherichia coli Proteome - A sweet tale. Mol Cell Proteomics. 2006;5(4):589-607.

224. Asara JM, Christofk HR, Freimark LM, Cantley LC. A label-free quantification method by MS/MS TIC compared to SILAC and spectral counting in a proteomics screen. Proteomics. 2008;8(5):994-9.
225. Ternette N, Wright C, Kramer HB, Altun M, Kessler BM. Label-free quantitative proteomics reveals regulation of interferon-induced protein with tetratricopeptide repeats 3 (IFIT3) and 5'-3'-exoribonuclease 2 (XRN2) during respiratory syncytial virus infection. Virol J. 2011;8(1):442.
226. Xiao H, Killip MJ, Staeheli P, Randall RE, Jackson D. The human interferon-induced MxA protein inhibits early stages of influenza A virus infection by retaining the incoming viral genome in the cytoplasm. J Virol. 2013;87(23):13053-8.
227. Fensterl V, Sen GC. Interferon-induced Ifit proteins: their role in viral pathogenesis. J Virol. 2015;89(5):2462-8.
228. Zhao X, Li J, Winkler CA, An P, Guo JT. IFITM Genes, Variants, and Their Roles in the Control and Pathogenesis of Viral Infections. Front Microbiol. 2018;9:3228.
229. Verhelst J, Parthoens E, Schepens B, Fiers W, Saelens X. Interferon-inducible protein Mx1 inhibits influenza virus by interfering with functional viral ribonucleoprotein complex assembly. J Virol. 2012;86(24):13445-55.
230. Everitt AR, Clare S, Pertel T, John SP, Wash RS, Smith SE, et al. IFITM3 restricts the morbidity and mortality associated with influenza. Nature. 2012;484(7395):519-23.
231. Pavlovic J, Haller O, Staeheli P. Human and mouse Mx proteins inhibit different steps of the influenza virus multiplication cycle. J Virol. 1992;66(4):2564-9.
232. Liu J, Shi X, Schwartz R, Kemble G. Use of MDCK cells for production of live attenuated influenza vaccine. Vaccine. 2009;27(46):6460-3.
233. Hussain AI, Cordeiro M, Sevilla E, Liu J. Comparison of egg and high yielding MDCK cell-derived live attenuated influenza virus for commercial production of trivalent influenza vaccine: in vitro cell susceptibility and influenza virus replication kinetics in permissive and semi-permissive cells. Vaccine. 2010;28(22):3848-55.
234. Xue J, Chambers BS, Hensley SE, Lopez CB. Propagation and Characterization of Influenza Virus Stocks That Lack High Levels of Defective Viral Genomes and Hemagglutinin Mutations. Front Microbiol. 2016;7:326.
235. Hegde NR. Cell culture-based influenza vaccines: A necessary and indispensable investment for the future. Hum Vaccin Immunother. 2015;11(5):1223-34.
236. Donis RO, Influenza Cell Culture Working G, Davis CT, Foust A, Hossain MJ, Johnson A, et al. Performance characteristics of qualified cell lines for isolation and propagation of influenza viruses for vaccine manufacturing. Vaccine. 2014;32(48):6583-90.
237. Govorkova EA, Murti G, Meignier B, de Taisne C, Webster RG. African green monkey kidney (Vero) cells provide an alternative host cell system for influenza A and B viruses. J Virol. 1996;70(8):5519-24.
238. Frank AL, Couch RB, Griffis CA, Baxter BD. Comparison of different tissue cultures for isolation and quantitation of influenza and parainfluenza viruses. J Clin Microbiol. 1979;10(1):32-6.
239. Schepetiuk SK, Kok T. The use of MDCK, MEK and LLC-MK2 cell lines with enzyme immunoassay for the isolation of influenza and parainfluenza viruses from clinical specimens. J Virol Methods. 1993;42(2-3):241-50.

240. Reina J, Fernandez-Baca V, Blanco I, Munar M. Comparison of Madin-Darby canine kidney cells (MDCK) with a green monkey continuous cell line (Vero) and human lung embryonated cells (MRC-5) in the isolation of influenza A virus from nasopharyngeal aspirates by shell vial culture. J Clin Microbiol. 1997;35(7):1900-1.
241. Romanova J, Katinger D, Ferko B, Voglauer R, Mochalova L, Bovin N, et al. Distinct host range of influenza H3N2 virus isolates in Vero and MDCK cells is determined by cell specific glycosylation pattern. Virology. 2003;307(1):90-7.
242. Seitz C, Frensing T, Hoper D, Kochs G, Reichl U. High yields of influenza A virus in Madin-Darby canine kidney cells are promoted by an insufficient interferon-induced antiviral state. J Gen Virol. 2010;91(Pt 7):1754-63.
243. Seitz C, Isken B, Heynisch B, Rettkowski M, Frensing T, Reichl U. Trypsin promotes efficient influenza vaccine production in MDCK cells by interfering with the antiviral host response. Appl Microbiol Biotechnol. 2012;93(2):601-11.
244. Frensing T, Seitz C, Heynisch B, Patzina C, Kochs G, Reichl U. Efficient influenza B virus propagation due to deficient interferon-induced antiviral activity in MDCK cells. Vaccine. 2011;29(41):7125-9.
245. Tobita K, Sugiura A, Enomote C, Furuyama M. Plaque assay and primary isolation of influenza A viruses in an established line of canine kidney cells (MDCK) in the presence of trypsin. Med Microbiol Immunol. 1975;162(1):9-14.
246. Organisation WH. WHO Manual on ANimal Influenza Diagnosis and Surveillance. 2002.
247. Guide AV. Tips and techniques for propagating virus in tissue culture and embryonated chicken eggs. 2016.
248. Wilson G, Ye Z, Xie H, Vahl S, Dawson E, Rowlen K. Automated interpretation of influenza hemagglutination inhibition (HAI) assays: Is plate tilting necessary? PLoS One. 2017;12(6):e0179939.
249. Killian ML. Hemagglutination assay for influenza virus. Methods Mol Biol. 2014;1161:3-9.
250. Brauer R, Chen P. Influenza virus propagation in embryonated chicken eggs. J Vis Exp. 2015(97).
251. (WHO) WHO. WHO Expert Committee on Biological Standardization. WHO Technical Report Series No 977. 2013.
252. Eisfeld AJ, Neumann G, Kawaoka Y. Influenza A virus isolation, culture and identification. Nat Protoc. 2014;9(11):2663-81.
253. Experts) VVp. Hemagglutination (HA) Assay Protocol. 2014.
254. Matrosovich M, Matrosovich T, Garten W, Klenk HD. New low-viscosity overlay medium for viral plaque assays. Virol J. 2006;3:63.
255. Baer A, Kehn-Hall K. Viral concentration determination through plaque assays: using traditional and novel overlay systems. J Vis Exp. 2014(93):e52065.
256. Sambrook J, Russell DW. SDS-Polyacrylamide Gel Electrophoresis of Proteins. CSH Protoc. 2006;2006(4).
257. Dong X, Armstrong SD, Xia D, Makepeace BL, Darby AC, Kadowaki T. Draft genome of the honey bee ectoparasitic mite, Tropilaelaps mercedesae, is shaped by the parasitic life history. Gigascience. 2017;6(3):1-17.
258. Kubiniok P, Finicle BT, Piffaretti F, McCracken AN, Perryman M, Hanessian S, et al. Dynamic phosphoproteomics uncovers signaling pathways modulated by anti-neoplastic sphingolipid analogs. Mol Cell Proteomics. 2018.

259. Derricott H, Luu L, Fong WY, Hartley CS, Johnston LJ, Armstrong SD, et al. Developing a 3D intestinal epithelium model for livestock species. Cell Tissue Res. 2018.
260. Jackson AP, Goyard S, Xia D, Foth BJ, Sanders M, Wastling JM, et al. Global Gene Expression Profiling through the Complete Life Cycle of Trypanosoma vivax. PLoS Negl Trop Dis. 2015;9(8):e0003975.
261. Jenjaroenpun P, Wongsurawat T, Pereira R, Patumcharoenpol P, Ussery DW, Nielsen J, et al. Complete genomic and transcriptional landscape analysis using third-generation sequencing: a case study of Saccharomyces cerevisiae CEN.PK113-7D. Nucleic Acids Res. 2018;46(7):e38.
262. Marriott AC, Dennis M, Kane JA, Gooch KE, Hatch G, Sharpe S, et al. Influenza A Virus Challenge Models in Cynomolgus Macaques Using the Authentic Inhaled Aerosol and Intra-Nasal Routes of Infection. PLoS One. 2016;11(6):e0157887.
263. Dong S, Liu L, Wu W, Armstrong SD, Xia D, Nan H, et al. Determination of the interactome of non-structural protein12 from highly pathogenic porcine reproductive and respiratory syndrome virus with host cellular proteins using high throughput proteomics and identification of HSP70 as a cellular factor for virus replication. J Proteomics. 2016;146:58-69.
264. Munday DC, Wu W, Smith N, Fix J, Noton SL, Galloux M, et al. Interactome analysis of the human respiratory syncytial virus RNA polymerase complex identifies protein chaperones as important cofactors that promote L-protein stability and RNA synthesis. J Virol. 2015;89(2):917-30.
265. Walsh KB, Teijaro JR, Wilker PR, Jatzek A, Fremgen DM, Das SC, et al. Suppression of cytokine storm with a sphingosine analog provides protection against pathogenic influenza virus. Proc Natl Acad Sci U S A. 2011;108(29):12018-23.
266. Rivas HG, Schmaling SK, Gaglia MM. Shutoff of Host Gene Expression in Influenza A Virus and Herpesviruses: Similar Mechanisms and Common Themes. Viruses. 2016;8(4):102.
267. Egorov A, Brandt S, Sereinig S, Romanova J, Ferko B, Katinger D, et al. Transfectant influenza A viruses with long deletions in the NS1 protein grow efficiently in Vero cells. J Virol. 1998;72(8):6437-41.
268. Garcia-Sastre A, Egorov A, Matassov D, Brandt S, Levy DE, Durbin JE, et al. Influenza A virus lacking the NS1 gene replicates in interferon-deficient systems. Virology. 1998;252(2):324-30.
269. Vreede FT, Chan AY, Sharps J, Fodor E. Mechanisms and functional implications of the degradation of host RNA polymerase II in influenza virus infected cells. Virology. 2010;396(1):125-34.
270. Llompart CM, Nieto A, Rodriguez-Frandsen A. Specific residues of PB2 and PA influenza virus polymerase subunits confer the ability for RNA polymerase II degradation and virus pathogenicity in mice. J Virol. 2014;88(6):3455-63.
271. Firth AE, Jagger BW, Wise HM, Nelson CC, Parsawar K, Wills NM, et al. Ribosomal frameshifting used in influenza A virus expression occurs within the sequence UCC_UUU_CGU and is in the +1 direction. Open Biol. 2012;2(10):120109.
272. Khaperskyy DA, Schmaling S, Larkins-Ford J, McCormick C, Gaglia MM. Selective Degradation of Host RNA Polymerase II Transcripts by Influenza A Virus PA-X Host Shutoff Protein. PLoS Pathog. 2016;12(2):e1005427.

273. Desmet EA, Bussey KA, Stone R, Takimoto T. Identification of the N-terminal domain of the influenza virus PA responsible for the suppression of host protein synthesis. J Virol. 2013;87(6):3108-18.
274. Killip MJ, Fodor E, Randall RE. Influenza virus activation of the interferon system. Virus Res. 2015;209:11-22.
275. Davidson S, McCabe TM, Crotta S, Gad HH, Hessel EM, Beinke S, et al. IFNlambda is a potent anti-influenza therapeutic without the inflammatory side effects of IFNalpha treatment. EMBO Mol Med. 2016;8(9):1099-112.
276. Weber-Gerlach M, Weber F. To Conquer the Host, Influenza Virus Is Packing It In: Interferon-Antagonistic Strategies beyond NS1. J Virol. 2016;90(19):8389-94.
277. Crotta S, Davidson S, Mahlakoiv T, Desmet CJ, Buckwalter MR, Albert ML, et al. Type I and type III interferons drive redundant amplification loops to induce a transcriptional signature in influenza-infected airway epithelia. PLoS Pathog. 2013;9(11):e1003773.
278. Seth RB, Sun L, Ea CK, Chen ZJ. Identification and characterization of MAVS, a mitochondrial antiviral signaling protein that activates NF-kappaB and IRF 3. Cell. 2005;122(5):669-82.
279. Kawai T, Takahashi K, Sato S, Coban C, Kumar H, Kato H, et al. IPS-1, an adaptor triggering RIG-I- and Mda5-mediated type I interferon induction. Nat Immunol. 2005;6(10):981-8.
280. Levy DE, Marie IJ, Durbin JE. Induction and function of type I and III interferon in response to viral infection. Curr Opin Virol. 2011;1(6):476-86.
281. Kotenko SV, Gallagher G, Baurin VV, Lewis-Antes A, Shen M, Shah NK, et al. IFN-lambdas mediate antiviral protection through a distinct class II cytokine receptor complex. Nat Immunol. 2003;4(1):69-77.
282. Onoguchi K, Yoneyama M, Takemura A, Akira S, Taniguchi T, Namiki H, et al. Viral infections activate types I and III interferon genes through a common mechanism. J Biol Chem. 2007;282(10):7576-81.
283. Munday DC, Emmott E, Surtees R, Lardeau CH, Wu W, Duprex WP, et al. Quantitative proteomic analysis of A549 cells infected with human respiratory syncytial virus. Mol Cell Proteomics. 2010;9(11):2438-59.
284. Wu W, Munday DC, Howell G, Platt G, Barr JN, Hiscox JA. Characterization of the interaction between human respiratory syncytial virus and the cell cycle in continuous cell culture and primary human airway epithelial cells. J Virol. 2011;85(19):10300-9.
285. Gibbs JD, Ornoff DM, Igo HA, Zeng JY, Imani F. Cell cycle arrest by transforming growth factor beta1 enhances replication of respiratory syncytial virus in lung epithelial cells. J Virol. 2009;83(23):12424-31.
286. Martinez I, Lombardia L, Garcia-Barreno B, Dominguez O, Melero JA. Distinct gene subsets are induced at different time points after human respiratory syncytial virus infection of A549 cells. J Gen Virol. 2007;88(Pt 2):570-81.
287. van Diepen A, Brand HK, Sama I, Lambooy LH, van den Heuvel LP, van der Well L, et al. Quantitative proteome profiling of respiratory virus-infected lung epithelial cells. J Proteomics. 2010;73(9):1680-93.
288. Fu Y, Quan R, Zhang H, Hou J, Tang J, Feng WH. Porcine reproductive and respiratory syndrome virus induces interleukin-15 through the NF-kappaB signaling pathway. J Virol. 2012;86(14):7625-36.

289. Bakre A, Wu W, Hiscox J, Spann K, Teng MN, Tripp RA. Human respiratory syncytial virus non-structural protein NS1 modifies miR-24 expression via transforming growth factor-beta. J Gen Virol. 2015;96(11):3179-91.
290. Ding X, Lu J, Yu R, Wang X, Wang T, Dong F, et al. Preliminary Proteomic Analysis of A549 Cells Infected with Avian Influenza Virus H7N9 and Influenza A Virus H1N1. PLoS One. 2016;11(5):e0156017.
291. Lieber M, Smith B, Szakal A, Nelson-Rees W, Todaro G. A continuous tumor-cell line from a human lung carcinoma with properties of type II alveolar epithelial cells. Int J Cancer. 1976;17(1):62-70.
292. Kugel D, Kochs G, Obojes K, Roth J, Kobinger GP, Kobasa D, et al. Intranasal administration of alpha interferon reduces seasonal influenza A virus morbidity in ferrets. J Virol. 2009;83(8):3843-51.
293. Haasbach E, Droebner K, Vogel AB, Planz O. Low-dose interferon Type I treatment is effective against H5N1 and swine-origin H1N1 influenza A viruses in vitro and in vivo. J Interferon Cytokine Res. 2011;31(6):515-25.
294. Vareille M, Kieninger E, Edwards MR, Regamey N. The airway epithelium: soldier in the fight against respiratory viruses. Clin Microbiol Rev. 2011;24(1):210-29.
295. Gazdar AF, Girard L, Lockwood WW, Lam WL, Minna JD. Lung cancer cell lines as tools for biomedical discovery and research. J Natl Cancer Inst. 2010;102(17):1310-21.
296. Kondo H, Miyoshi K, Sakiyama S, Tangoku A, Noma T. Differential Regulation of Gene Expression of Alveolar Epithelial Cell Markers in Human Lung Adenocarcinoma-Derived A549 Clones. Stem Cells Int. 2015;2015:165867.
297. Fuchs S, Hollins AJ, Laue M, Schaefer UF, Roemer K, Gumbleton M, et al. Differentiation of human alveolar epithelial cells in primary culture: morphological characterization and synthesis of caveolin-1 and surfactant protein-C. Cell Tissue Res. 2003;311(1):31-45.
298. Mao P, Wu S, Li J, Fu W, He W, Liu X, et al. Human alveolar epithelial type II cells in primary culture. Physiol Rep. 2015;3(2).
299. Doroshenko A, Halperin SA. Trivalent MDCK cell culture-derived influenza vaccine Optaflu (Novartis Vaccines). Expert Rev Vaccines. 2009;8(6):679-88.
300. Lugovtsev VY, Melnyk D, Weir JP. Heterogeneity of the MDCK cell line and its applicability for influenza virus research. PLoS One. 2013;8(9):e75014.
301. Liu X, Sun L, Yu M, Wang Z, Xu C, Xue Q, et al. Cyclophilin A interacts with influenza A virus M1 protein and impairs the early stage of the viral replication. Cell Microbiol. 2009;11(5):730-41.
302. Heather JM, Chain B. The sequence of sequencers: The history of sequencing DNA. Genomics. 2016;107(1):1-8.
303. Kulski JK. Next-Generation Sequencing — An Overview of the History, Tools, and “Omic” Applications. Next Generation Sequencing - Advances, Applications and Challenges2016.
304. Sanger F, Nicklen S, Coulson AR. DNA sequencing with chain-terminating inhibitors. Proc Natl Acad Sci U S A. 1977;74(12):5463-7.
305. Mardis ER. Next-generation DNA sequencing methods. Annu Rev Genomics Hum Genet. 2008;9:387-402.

306. Mardis ER. A decade's perspective on DNA sequencing technology. Nature. 2011;470(7333):198-203.
307. Metzker ML. Sequencing technologies - the next generation. Nat Rev Genet. 2010;11(1):31-46.
308. Wang Z, Gerstein M, Snyder M. RNA-Seq: a revolutionary tool for transcriptomics. Nat Rev Genet. 2009;10(1):57-63.
309. Thompson JF, Milos PM. The properties and applications of single-molecule DNA sequencing. Genome Biol. 2011;12(2):217.
310. GmbH EGB. 2017 [Available from: www.eurofinsgenomics.eu.
311. Lam HY, Clark MJ, Chen R, Chen R, Natsoulis G, O'Huallachain M, et al. Performance comparison of whole-genome sequencing platforms. Nat Biotechnol. 2011;30(1):78-82.
312. Kwong JC, McCallum N, Sintchenko V, Howden BP. Whole genome sequencing in clinical and public health microbiology. Pathology. 2015;47(3):199-210.
313. Liu L, Li Y, Li S, Hu N, He Y, Pong R, et al. Comparison of next-generation sequencing systems. J Biomed Biotechnol. 2012;2012:251364.
314. Lu H, Giordano F, Ning Z. Oxford Nanopore MinION Sequencing and Genome Assembly. Genomics Proteomics Bioinformatics. 2016;14(5):265-79.
315. Kall L, Storey JD, MacCoss MJ, Noble WS. Posterior error probabilities and false discovery rates: two sides of the same coin. J Proteome Res. 2008;7(1):40-4.
316. Quick J, Loman NJ, Duraffour S, Simpson JT, Severi E, Cowley L, et al. Real-time, portable genome sequencing for Ebola surveillance. Nature. 2016;530(7589):228-32.
317. Quick J, Ashton P, Calus S, Chatt C, Gossain S, Hawker J, et al. Rapid draft sequencing and real-time nanopore sequencing in a hospital outbreak of Salmonella. Genome Biol. 2015;16:114.
318. Gardy J, Loman NJ, Rambaut A. Real-time digital pathogen surveillance - the time is now. Genome Biol. 2015;16(1):155.
319. Hoenen T, Groseth A, Rosenke K, Fischer RJ, Hoenen A, Judson SD, et al. Nanopore Sequencing as a Rapidly Deployable Ebola Outbreak Tool. Emerg Infect Dis. 2016;22(2):331-4.
320. Wu X, Wang H, Bai L, Yu Y, Sun Z, Yan Y, et al. Mitochondrial proteomic analysis of human host cells infected with H3N2 swine influenza virus. J Proteomics. 2013;91:136-50.
321. Emmott E, Munday D, Bickerton E, Britton P, Rodgers MA, Whitehouse A, et al. The cellular interactome of the coronavirus infectious bronchitis virus nucleocapsid protein and functional implications for virus biology. J Virol. 2013;87(17):9486-500.
322. Emmott E, Rodgers MA, Macdonald A, McCrory S, Ajuh P, Hiscox JA. Quantitative proteomics using stable isotope labeling with amino acids in cell culture reveals changes in the cytoplasmic, nuclear, and nucleolar proteomes in Vero cells infected with the coronavirus infectious bronchitis virus. Mol Cell Proteomics. 2010;9(9):1920-36.
323. Emmott E, Smith C, Emmett SR, Dove BK, Hiscox JA. Elucidation of the avian nucleolar proteome by quantitative proteomics using SILAC and changes in cells

infected with the coronavirus infectious bronchitis virus. Proteomics. 2010;10(19):3558-62.
324. Lam YW, Evans VC, Heesom KJ, Lamond AI, Matthews DA. Proteomics analysis of the nucleolus in adenovirus-infected cells. Mol Cell Proteomics. 2010;9(1):117-30.
325. Baldwin MA. Protein identification by mass spectrometry: issues to be considered. Mol Cell Proteomics. 2004;3(1):1-9.
326. Lomize AL, Lomize MA, Krolicki SR, Pogozheva ID. Membranome: a database for proteome-wide analysis of single-pass membrane proteins. Nucleic Acids Res. 2017;45(D1):D250-D5.
327. Hsu PW, Lin LZ, Hsu SD, Hsu JB, Huang HD. ViTa: prediction of host microRNAs targets on viruses. Nucleic Acids Res. 2007;35(Database issue):D381-5.
328. Konig R, Stertz S, Zhou Y, Inoue A, Hoffmann HH, Bhattacharyya S, et al. Human host factors required for influenza virus replication. Nature. 2010;463(7282):813-7.
329. Haider S, Pal R. Integrated analysis of transcriptomic and proteomic data. Curr Genomics. 2013;14(2):91-110.
330. Hodge K, Have ST, Hutton L, Lamond AI. Cleaning up the masses: exclusion lists to reduce contamination with HPLC-MS/MS. J Proteomics. 2013;88:92-103.
331. Mogensen TH. Pathogen recognition and inflammatory signaling in innate immune defenses. Clin Microbiol Rev. 2009;22(2):240-73, Table of Contents.
332. Maringer K, Fernandez-Sesma A. Message in a bottle: lessons learned from antagonism of STING signalling during RNA virus infection. Cytokine Growth Factor Rev. 2014;25(6):669-79.
333. Regad T, Saib A, Lallemand-Breitenbach V, Pandolfi PP, de The H, Chelbi-Alix MK. PML mediates the interferon-induced antiviral state against a complex retrovirus via its association with the viral transactivator. EMBO J. 2001;20(13):3495-505.
334. Brint EK, Xu D, Liu H, Dunne A, McKenzie AN, O'Neill LA, et al. ST2 is an inhibitor of interleukin 1 receptor and Toll-like receptor 4 signaling and maintains endotoxin tolerance. Nat Immunol. 2004;5(4):373-9.
335. Iwasaki A, Pillai PS. Innate immunity to influenza virus infection. Nat Rev Immunol. 2014;14(5):315-28.
336. Jolly L, Stavrou A, Vanderstoken G, Meliopoulos VA, Habgood A, Tatler AL, et al. Influenza promotes collagen deposition via alphavbeta6 integrin-mediated transforming growth factor beta activation. J Biol Chem. 2014;289(51):35246-63.
337. Konishi K, Gibson KF, Lindell KO, Richards TJ, Zhang Y, Dhir R, et al. Gene expression profiles of acute exacerbations of idiopathic pulmonary fibrosis. Am J Respir Crit Care Med. 2009;180(2):167-75.
338. Teoh CM, Tan SS, Tran T. Integrins as Therapeutic Targets for Respiratory Diseases. Curr Mol Med. 2015;15(8):714-34.
339. Chen Y, Zhou J, Cheng Z, Yang S, Chu H, Fan Y, et al. Functional variants regulating LGALS1 (Galectin 1) expression affect human susceptibility to influenza A(H7N9). Sci Rep. 2015;5:8517.
340. Gaur P, Munjhal A, Lal SK. Influenza virus and cell signaling pathways. Med Sci Monit. 2011;17(6):RA148-54.

341. Kujime K, Hashimoto S, Gon Y, Shimizu K, Horie T. p38 mitogen-activated protein kinase and c-jun-NH2-terminal kinase regulate RANTES production by influenza virus-infected human bronchial epithelial cells. J Immunol. 2000;164(6):3222-8.
342. Mizumura K, Hashimoto S, Maruoka S, Gon Y, Kitamura N, Matsumoto K, et al. Role of mitogen-activated protein kinases in influenza virus induction of prostaglandin E2 from arachidonic acid in bronchial epithelial cells. Clin Exp Allergy. 2003;33(9):1244-51.
343. Fujioka Y, Tsuda M, Nanbo A, Hattori T, Sasaki J, Sasaki T, et al. A Ca(2+)-dependent signalling circuit regulates influenza A virus internalization and infection. Nat Commun. 2013;4:2763.
344. Tafforeau L, Chantier T, Pradezynski F, Pellet J, Mangeot PE, Vidalain PO, et al. Generation and comprehensive analysis of an influenza virus polymerase cellular interaction network. J Virol. 2011;85(24):13010-8.
345. Wozniak JSCaRW. Host Cell Factors Necessary for Influenza A Infection: Meta-Analysis of Genome Wide Studies. 2012.
346. Gack MU, Shin YC, Joo CH, Urano T, Liang C, Sun L, et al. TRIM25 RING-finger E3 ubiquitin ligase is essential for RIG-I-mediated antiviral activity. Nature. 2007;446(7138):916-20.
347. Meyerson NR, Zhou L, Guo YR, Zhao C, Tao YJ, Krug RM, et al. Nuclear TRIM25 Specifically Targets Influenza Virus Ribonucleoproteins to Block the Onset of RNA Chain Elongation. Cell Host Microbe. 2017;22(5):627-38 e7.
348. Liu L, Xiao L, Liang X, Chen L, Cheng L, Zhang L, et al. TRIM28 knockdown increases sensitivity to etoposide by upregulating E2F1 in non-small cell lung cancer. Oncol Rep. 2017;37(6):3597-605.
349. Liang Q, Deng H, Li X, Wu X, Tang Q, Chang TH, et al. Tripartite motif-containing protein 28 is a small ubiquitin-related modifier E3 ligase and negative regulator of IFN regulatory factor 7. J Immunol. 2011;187(9):4754-63.
350. Ozato K, Shin DM, Chang TH, Morse HC, 3rd. TRIM family proteins and their emerging roles in innate immunity. Nat Rev Immunol. 2008;8(11):849-60.
351. Hatakeyama S. TRIM Family Proteins: Roles in Autophagy, Immunity, and Carcinogenesis. Trends Biochem Sci. 2017;42(4):297-311.
352. Reperant LA, Moesker FM, Osterhaus AD. Influenza: from zoonosis to pandemic. ERJ Open Res. 2016;2(1).
353. Taubenberger JK, Kash JC. Influenza virus evolution, host adaptation, and pandemic formation. Cell Host Microbe. 2010;7(6):440-51.
354. Organisation WH. Influenza (seasonal). 2018, January 31.
355. Rimmelzwaan GF, Fouchier RA, Osterhaus AD. Age distribution of cases caused by different influenza viruses. Lancet Infect Dis. 2013;13(8):646-7.
356. Sun J, Han Z, Shao Y, Cao Z, Kong X, Liu S. Comparative proteome analysis of tracheal tissues in response to infectious bronchitis coronavirus, Newcastle disease virus, and avian influenza virus H9 subtype virus infection. Proteomics. 2014;14(11):1403-23.
357. Zou W, Ke J, Zhang A, Zhou M, Liao Y, Zhu J, et al. Proteomics analysis of differential expression of chicken brain tissue proteins in response to the neurovirulent H5N1 avian influenza virus infection. J Proteome Res. 2010;9(8):3789-98.

358. Widjaja I, de Vries E, Tscherne DM, Garcia-Sastre A, Rottier PJ, de Haan CA. Inhibition of the ubiquitin-proteasome system affects influenza A virus infection at a postfusion step. J Virol. 2010;84(18):9625-31.
359. Tisoncik-Go J, Gasper DJ, Kyle JE, Eisfeld AJ, Selinger C, Hatta M, et al. Integrated Omics Analysis of Pathogenic Host Responses during Pandemic H1N1 Influenza Virus Infection: The Crucial Role of Lipid Metabolism. Cell Host Microbe. 2016;19(2):254-66.
360. Gack MU, Albrecht RA, Urano T, Inn KS, Huang IC, Carnero E, et al. Influenza A virus NS1 targets the ubiquitin ligase TRIM25 to evade recognition by the host viral RNA sensor RIG-I. Cell Host Microbe. 2009;5(5):439-49.
361. Bouvier NM, Lowen AC. Animal Models for Influenza Virus Pathogenesis and Transmission. Viruses. 2010;2(8):1530-63.
362. Tchitchek N, Eisfeld AJ, Tisoncik-Go J, Josset L, Gralinski LE, Becavin C, et al. Specific mutations in H5N1 mainly impact the magnitude and velocity of the host response in mice. BMC Syst Biol. 2013;7:69.
363. Watanabe T, Tisoncik-Go J, Tchitchek N, Watanabe S, Benecke AG, Katze MG, et al. 1918 Influenza virus hemagglutinin (HA) and the viral RNA polymerase complex enhance viral pathogenicity, but only HA induces aberrant host responses in mice. J Virol. 2013;87(9):5239-54.
364. Shen S, Li J, Hilchey S, Shen X, Tu C, Qiu X, et al. Ion-Current-Based Temporal Proteomic Profiling of Influenza-A-Virus-Infected Mouse Lungs Revealed Underlying Mechanisms of Altered Integrity of the Lung Microvascular Barrier. J Proteome Res. 2016;15(2):540-53.
365. Fornek JL, Gillim-Ross L, Santos C, Carter V, Ward JM, Cheng LI, et al. A single-amino-acid substitution in a polymerase protein of an H5N1 influenza virus is associated with systemic infection and impaired T-cell activation in mice. J Virol. 2009;83(21):11102-15.
366. Fornek JL, Korth MJ, Katze MG. Use of functional genomics to understand influenza-host interactions. Adv Virus Res. 2007;70:81-100.
367. Baas T, Baskin CR, Diamond DL, Garcia-Sastre A, Bielefeldt-Ohmann H, Tumpey TM, et al. Integrated molecular signature of disease: analysis of influenza virus-infected macaques through functional genomics and proteomics. J Virol. 2006;80(21):10813-28.
368. Gardner MB, Luciw PA. Macaque models of human infectious disease. ILAR J. 2008;49(2):220-55.
369. Fritz RS, Hayden FG, Calfee DP, Cass LM, Peng AW, Alvord WG, et al. Nasal cytokine and chemokine responses in experimental influenza A virus infection: results of a placebo-controlled trial of intravenous zanamivir treatment. J Infect Dis. 1999;180(3):586-93.
370. Hayden FG, Fritz R, Lobo MC, Alvord W, Strober W, Straus SE. Local and systemic cytokine responses during experimental human influenza A virus infection. Relation to symptom formation and host defense. J Clin Invest. 1998;101(3):643-9.
371. Baskin CR, Bielefeldt-Ohmann H, Tumpey TM, Sabourin PJ, Long JP, Garcia-Sastre A, et al. Early and sustained innate immune response defines pathology and death in nonhuman primates infected by highly pathogenic influenza virus. Proc Natl Acad Sci U S A. 2009;106(9):3455-60.

372. Brown JN, Palermo RE, Baskin CR, Gritsenko M, Sabourin PJ, Long JP, et al. Macaque proteome response to highly pathogenic avian influenza and 1918 reassortant influenza virus infections. J Virol. 2010;84(22):12058-68.
373. Bricio-Moreno L, Sheridan VH, Goodhead I, Armstrong S, Wong JKL, Waters EM, et al. Evolutionary trade-offs associated with loss of PmrB function in host-adapted Pseudomonas aeruginosa. Nat Commun. 2018;9(1):2635.
374. Dubourg A, Xia D, Winpenny JP, Al Naimi S, Bouzid M, Sexton DW, et al. Giardia secretome highlights secreted tenascins as a key component of pathogenesis. Gigascience. 2018;7(3):1-13.
375. Chawade A, Alexandersson E, Levander F. Normalyzer: a tool for rapid evaluation of normalization methods for omics data sets. J Proteome Res. 2014;13(6):3114-20.
376. Ghosh S, Chaudhary R, Carpani M, Playford R. Interfering with interferons in inflammatory bowel disease. Gut. 2006;55(8):1071-3.
377. Tumpey TM, Basler CF, Aguilar PV, Zeng H, Solorzano A, Swayne DE, et al. Characterization of the reconstructed 1918 Spanish influenza pandemic virus. Science. 2005;310(5745):77-80.
378. Graham AC, Temple RM, Obar JJ. Mast cells and influenza a virus: association with allergic responses and beyond. Front Immunol. 2015;6:238.
379. Raj RS, Bonney EA, Phillippe M. Influenza, immune system, and pregnancy. Reprod Sci. 2014;21(12):1434-51.
380. Staples KJ, Nicholas B, McKendry RT, Spalluto CM, Wallington JC, Bragg CW, et al. Viral infection of human lung macrophages increases PDL1 expression via IFNbeta. PLoS One. 2015;10(3):e0121527.
381. Hatta M, Gao P, Halfmann P, Kawaoka Y. Molecular basis for high virulence of Hong Kong H5N1 influenza A viruses. Science. 2001;293(5536):1840-2.
382. Kamphuis E, Junt T, Waibler Z, Forster R, Kalinke U. Type I interferons directly regulate lymphocyte recirculation and cause transient blood lymphopenia. Blood. 2006;108(10):3253-61.
383. Dugas AF, Valsamakis A, Atreya MR, Thind K, Alarcon Manchego P, Faisal A, et al. Clinical diagnosis of influenza in the ED. Am J Emerg Med. 2015;33(6):770-5.
384. Burke TW, Henao R, Soderblom E, Tsalik EL, Thompson JW, McClain MT, et al. Nasopharyngeal Protein Biomarkers of Acute Respiratory Virus Infection. EBioMedicine. 2017;17:172-81.
385. Huang Y, Zaas AK, Rao A, Dobigeon N, Woolf PJ, Veldman T, et al. Temporal dynamics of host molecular responses differentiate symptomatic and asymptomatic influenza a infection. PLoS Genet. 2011;7(8):e1002234.
386. Ramilo O, Mejias A. Shifting the paradigm: host gene signatures for diagnosis of infectious diseases. Cell Host Microbe. 2009;6(3):199-200.
387. Woods CW, McClain MT, Chen M, Zaas AK, Nicholson BP, Varkey J, et al. A host transcriptional signature for presymptomatic detection of infection in humans exposed to influenza H1N1 or H3N2. PLoS One. 2013;8(1):e52198.
388. Julkunen I, Sareneva T, Pirhonen J, Ronni T, Melen K, Matikainen S. Molecular pathogenesis of influenza A virus infection and virus-induced regulation of cytokine gene expression. Cytokine Growth Factor Rev. 2001;12(2-3):171-80.

389. Ehrhardt C, Seyer R, Hrincius ER, Eierhoff T, Wolff T, Ludwig S. Interplay between influenza A virus and the innate immune signaling. Microbes Infect. 2010;12(1):81-7.
390. Katze MG, Fornek JL, Palermo RE, Walters KA, Korth MJ. Innate immune modulation by RNA viruses: emerging insights from functional genomics. Nat Rev Immunol. 2008;8(8):644-54.
391. Petridis D, Zarogoulidis P, Kallianos A, Kioumis I, Trakada G, Spyratos D, et al. Clinical differences between H3N2 and H1N1 influenza 2012 and lower respiratory tract infection found using a statistical classification approach. Ther Clin Risk Manag. 2014;10:77-86.
392. Cromer D, van Hoek AJ, Jit M, Edmunds WJ, Fleming D, Miller E. The burden of influenza in England by age and clinical risk group: a statistical analysis to inform vaccine policy. J Infect. 2014;68(4):363-71.
393. Teran LM, Ruggeberg S, Santiago J, Fuentes-Arenas F, Hernandez JL, Montes-Vizuet AR, et al. Immune response to seasonal influenza A virus infection: a proteomic approach. Arch Med Res. 2012;43(6):464-9.
394. Balch WE, Yates JR, 3rd. Application of mass spectrometry to study proteomics and interactomics in cystic fibrosis. Methods Mol Biol. 2011;742:227-47.
395. Chen H, Wang D, Bai C, Wang X. Proteomics-based biomarkers in chronic obstructive pulmonary disease. J Proteome Res. 2010;9(6):2798-808.
396. Crameri R. The potential of proteomics and peptidomics for allergy and asthma research. Allergy. 2005;60(10):1227-37.
397. Piasecka B, Duffy D, Urrutia A, Quach H, Patin E, Posseme C, et al. Distinctive roles of age, sex, and genetics in shaping transcriptional variation of human immune responses to microbial challenges. Proc Natl Acad Sci U S A. 2018;115(3):E488-E97.
398. Bahadoran A, Lee SH, Wang SM, Manikam R, Rajarajeswaran J, Raju CS, et al. Immune Responses to Influenza Virus and Its Correlation to Age and Inherited Factors. Front Microbiol. 2016;7:1841.
399. Ali Z, Bhaskar SB. Basic statistical tools in research and data analysis. Indian J Anaesth. 2016;60(9):662-9.
400. McHugh ML. The chi-square test of independence. Biochem Med (Zagreb). 2013;23(2):143-9.
401. Zarepour M, Bhullar K, Montero M, Ma C, Huang T, Velcich A, et al. The mucin Muc2 limits pathogen burdens and epithelial barrier dysfunction during Salmonella enterica serovar Typhimurium colitis. Infect Immun. 2013;81(10):3672-83.
402. Leeming GH, Kipar A, Hughes DJ, Bingle L, Bennett E, Moyo NA, et al. Gammaherpesvirus infection modulates the temporal and spatial expression of SCGB1A1 (CCSP) and BPIFA1 (SPLUNC1) in the respiratory tract. Lab Invest. 2015;95(6):610-24.
403. Bingle CD, Wilson K, Lunn H, Barnes FA, High AS, Wallace WA, et al. Human LPLUNC1 is a secreted product of goblet cells and minor glands of the respiratory and upper aerodigestive tracts. Histochem Cell Biol. 2010;133(5):505-15.
404. Fleming SB. Viral Inhibition of the IFN-Induced JAK/STAT Signalling Pathway: Development of Live Attenuated Vaccines by Mutation of Viral-Encoded IFN-Antagonists. Vaccines (Basel). 2016;4(3).

405. Reynolds SD, Reynolds PR, Pryhuber GS, Finder JD, Stripp BR. Secretoglobins SCGB3A1 and SCGB3A2 define secretory cell subsets in mouse and human airways. Am J Respir Crit Care Med. 2002;166(11):1498-509.
406. Raffay TM, Locy ML, Hill CL, Jindal NS, Rogers LK, Welty SE, et al. Neonatal hyperoxic exposure persistently alters lung secretoglobins and annexin A1. Biomed Res Int. 2013;2013:408485.
407. Platanias LC, Fish EN. Signaling pathways activated by interferons. Exp Hematol. 1999;27(11):1583-92.
408. Davidson S, Crotta S, McCabe TM, Wack A. Pathogenic potential of interferon alphabeta in acute influenza infection. Nat Commun. 2014;5:3864.
409. Hu Y. Progress in protein structure and function studies in China during 2010-2011. Sci China Life Sci. 2012;55(10):927-30.
410. Ayusawa D, Kaneda S, Itoh Y, Yasuda H, Murakami Y, Sugasawa K, et al. Complementation by a cloned human ubiquitin-activating enzyme E1 of the S-phase-arrested mouse FM3A cell mutant with thermolabile E1. Cell Struct Funct. 1992;17(2):113-22.
411. Cook JC, Chock PB. Isoforms of mammalian ubiquitin-activating enzyme. J Biol Chem. 1992;267(34):24315-21.
412. Ghaboosi N, Deshaies RJ. A conditional yeast E1 mutant blocks the ubiquitin-proteasome pathway and reveals a role for ubiquitin conjugates in targeting Rad23 to the proteasome. Mol Biol Cell. 2007;18(5):1953-63.
413. Gao G, Luo H. The ubiquitin-proteasome pathway in viral infections. Can J Physiol Pharmacol. 2006;84(1):5-14.
414. Byk LA, Iglesias NG, De Maio FA, Gebhard LG, Rossi M, Gamarnik AV. Dengue Virus Genome Uncoating Requires Ubiquitination. MBio. 2016;7(3).
415. Zhang Z, Miao L, Xin X, Zhang J, Yang S, Miao M, et al. Underexpressed CNDP2 participates in gastric cancer growth inhibition through activating the MAPK signaling pathway. Mol Med. 2014;20:17-28.
416. Li D, Jans DA, Bardin PG, Meanger J, Mills J, Ghildyal R. Association of respiratory syncytial virus M protein with viral nucleocapsids is mediated by the M2-1 protein. J Virol. 2008;82(17):8863-70.
417. Kipper S, Hamad S, Caly L, Avrahami D, Bacharach E, Jans DA, et al. New host factors important for respiratory syncytial virus (RSV) replication revealed by a novel microfluidics screen for interactors of matrix (M) protein. Mol Cell Proteomics. 2015;14(3):532-43.
418. Mindaye ST, Ilyushina NA, Fantoni G, Alterman MA, Donnelly RP, Eichelberger MC. Impact of Influenza A Virus Infection on the Proteomes of Human Bronchoepithelial Cells from Different Donors. J Proteome Res. 2017;16(9):3287-97.
419. Salazar GA, Meintjes A, Mazandu GK, Rapanoel HA, Akinola RO, Mulder NJ. A web-based protein interaction network visualizer. BMC Bioinformatics. 2014;15:129.
420. Fuller TL, Gilbert M, Martin V, Cappelle J, Hosseini P, Njabo KY, et al. Predicting hotspots for influenza virus reassortment. Emerg Infect Dis. 2013;19(4):581-8.
421. Peng X, Gralinski L, Armour CD, Ferris MT, Thomas MJ, Proll S, et al. Unique signatures of long noncoding RNA expression in response to virus infection and altered innate immune signaling. MBio. 2010;1(5).

422. Hao L, Sakurai A, Watanabe T, Sorensen E, Nidom CA, Newton MA, et al. Drosophila RNAi screen identifies host genes important for influenza virus replication. Nature. 2008;454(7206):890-3.
423. Dove BK, Surtees R, Bean TJ, Munday D, Wise HM, Digard P, et al. A quantitative proteomic analysis of lung epithelial (A549) cells infected with 2009 pandemic influenza A virus using stable isotope labelling with amino acids in cell culture. Proteomics. 2012;12(9):1431-6.
424. Sanford BA, Davison VE, Ramsay MA. Fibrinogen-mediated adherence of group A Streptococcus to influenza A virus-infected cell cultures. Infect Immun. 1982;38(2):513-20.
425. Millien VO, Lu W, Shaw J, Yuan X, Mak G, Roberts L, et al. Cleavage of fibrinogen by proteinases elicits allergic responses through Toll-like receptor 4. Science. 2013;341(6147):792-6.
426. Hafez MM, Abdel-Wahab KS, El-Fouhil DF. Augmented adherence and internalization of group A Streptococcus pyogenes to influenza A virus infected MDCK cells. J Basic Microbiol. 2010;50 Suppl 1:S46-57.
427. Akram KM, Moyo NA, Leeming GH, Bingle L, Jasim S, Hussain S, et al. An innate defense peptide BPIFA1/SPLUNC1 restricts influenza A virus infection. Mucosal Immunol. 2017.
428. Shin K, Wakabayashi H, Yamauchi K, Teraguchi S, Tamura Y, Kurokawa M, et al. Effects of orally administered bovine lactoferrin and lactoperoxidase on influenza virus infection in mice. J Med Microbiol. 2005;54(Pt 8):717-23.
429. Durmus Tekir S, Cakir T, Ulgen KO. Infection Strategies of Bacterial and Viral Pathogens through Pathogen-Human Protein-Protein Interactions. Front Microbiol. 2012;3:46.
430. Ritter JB, Wahl AS, Freund S, Genzel Y, Reichl U. Metabolic effects of influenza virus infection in cultured animal cells: Intra- and extracellular metabolite profiling. BMC Syst Biol. 2010;4:61.
431. Paquette SG, Banner D, Zhao Z, Fang Y, Huang SS, Leomicronn AJ, et al. Interleukin-6 is a potential biomarker for severe pandemic H1N1 influenza A infection. PLoS One. 2012;7(6):e38214.
432. Davey RT, Jr., Lynfield R, Dwyer DE, Losso MH, Cozzi-Lepri A, Wentworth D, et al. The association between serum biomarkers and disease outcome in influenza A(H1N1)pdm09 virus infection: results of two international observational cohort studies. PLoS One. 2013;8(2):e57121.
433. McHugh KJ, Mandalapu S, Kolls JK, Ross TM, Alcorn JF. A novel outbred mouse model of 2009 pandemic influenza and bacterial co-infection severity. PLoS One. 2013;8(12):e82865.
434. Dienz O, Rud JG, Eaton SM, Lanthier PA, Burg E, Drew A, et al. Essential role of IL-6 in protection against H1N1 influenza virus by promoting neutrophil survival in the lung. Mucosal Immunol. 2012;5(3):258-66.
435. Nalejska E, Maczynska E, Lewandowska MA. Prognostic and predictive biomarkers: tools in personalized oncology. Mol Diagn Ther. 2014;18(3):273-84.
436. Sadewasser A, Paki K, Eichelbaum K, Bogdanow B, Saenger S, Budt M, et al. Quantitative Proteomic Approach Identifies Vpr Binding Protein as Novel Host Factor Supporting Influenza A Virus Infections in Human Cells. Mol Cell Proteomics. 2017;16(5):728-42.

437. Emmott E, Wise H, Loucaides EM, Matthews DA, Digard P, Hiscox JA. Quantitative proteomics using SILAC coupled to LC-MS/MS reveals changes in the nucleolar proteome in influenza A virus-infected cells. J Proteome Res. 2010;9(10):5335-45.
438. Lietzen N, Ohman T, Rintahaka J, Julkunen I, Aittokallio T, Matikainen S, et al. Quantitative subcellular proteome and secretome profiling of influenza A virus-infected human primary macrophages. PLoS Pathog. 2011;7(5):e1001340.
439. Margine I, Krammer F. Animal models for influenza viruses: implications for universal vaccine development. Pathogens. 2014;3(4):845-74.
440. Uetani K, Hiroi M, Meguro T, Ogawa H, Kamisako T, Ohmori Y, et al. Influenza A virus abrogates IFN-gamma response in respiratory epithelial cells by disruption of the Jak/Stat pathway. Eur J Immunol. 2008;38(6):1559-73.
441. Hashimoto Y, Moki T, Takizawa T, Shiratsuchi A, Nakanishi Y. Evidence for phagocytosis of influenza virus-infected, apoptotic cells by neutrophils and macrophages in mice. J Immunol. 2007;178(4):2448-57.
442. Jorgensen SE, Christiansen M, Ryo LB, Gad HH, Gjedsted J, Staeheli P, et al. Defective RNA sensing by RIG-I in severe influenza virus infection. Clin Exp Immunol. 2018;192(3):366-76.
443. Wang Q, Li Q, Liu T, Chang G, Sun Z, Gao Z, et al. Host Interaction Analysis of PA-N155 and PA-N182 in Chicken Cells Reveals an Essential Role of UBA52 for Replication of H5N1 Avian Influenza Virus. Front Microbiol. 2018;9:936.
444. Phillips AM, Ponomarenko AI, Chen K, Ashenberg O, Miao J, McHugh SM, et al. Destabilized adaptive influenza variants critical for innate immune system escape are potentiated by host chaperones. PLoS Biol. 2018;16(9):e3000008.
445. Mehle A, Doudna JA. A host of factors regulating influenza virus replication. Viruses. 2010;2(2):566-73.
446. Bakre A, Andersen LE, Meliopoulos V, Coleman K, Yan X, Brooks P, et al. Identification of Host Kinase Genes Required for Influenza Virus Replication and the Regulatory Role of MicroRNAs. PLoS One. 2013;8(6):e66796.
447. Klemm C, Bruchhagen C, van Kruchten A, Niemann S, Loffler B, Peters G, et al. Mitogen-activated protein kinases (MAPKs) regulate IL-6 over-production during concomitant influenza virus and Staphylococcus aureus infection. Sci Rep. 2017;7:42473.
448. Liu X, Zhao Z, Xu C, Sun L, Chen J, Zhang L, et al. Cyclophilin A restricts influenza A virus replication through degradation of the M1 protein. PLoS One. 2012;7(2):e31063.
449. de Chassey B, Aublin-Gex A, Ruggieri A, Meyniel-Schicklin L, Pradezynski F, Davoust N, et al. The interactomes of influenza virus NS1 and NS2 proteins identify new host factors and provide insights for ADAR1 playing a supportive role in virus replication. PLoS Pathog. 2013;9(7):e1003440.
450. Pauli EK, Schmolke M, Wolff T, Viemann D, Roth J, Bode JG, et al. Influenza A virus inhibits type I IFN signaling via NF-kappaB-dependent induction of SOCS-3 expression. PLoS Pathog. 2008;4(11):e1000196.
451. Domingues P, Golebiowski F, Tatham MH, Lopes AM, Taggart A, Hay RT, et al. Global Reprogramming of Host SUMOylation during Influenza Virus Infection. Cell Rep. 2015;13(7):1467-80.

452. Estrin MA, Hussein ITM, Puryear WB, Kuan AC, Artim SC, Runstadler JA. Host-directed combinatorial RNAi improves inhibition of diverse strains of influenza A virus in human respiratory epithelial cells. PLoS One. 2018;13(5):e0197246.
453. Grow DA, McCarrey JR, Navara CS. Advantages of nonhuman primates as preclinical models for evaluating stem cell-based therapies for Parkinson's disease. Stem Cell Res. 2016;17(2):352-66.
454. Hong SG, Lin Y, Dunbar CE, Zou J. The Role of Nonhuman Primate Animal Models in the Clinical Development of Pluripotent Stem Cell Therapies. Mol Ther. 2016;24(7):1165-9.
455. Akram KM, Moyo NA, Leeming GH, Bingle L, Jasim S, Hussain S, et al. An innate defense peptide BPIFA1/SPLUNC1 restricts influenza A virus infection. Mucosal Immunol. 2018;11(1):71-81.
456. Berlutti F, Pantanella F, Natalizi T, Frioni A, Paesano R, Polimeni A, et al. Antiviral properties of lactoferrin--a natural immunity molecule. Molecules. 2011;16(8):6992-7018.
457. Scala MC, Sala M, Pietrantoni A, Spensiero A, Di Micco S, Agamennone M, et al. Lactoferrin-derived Peptides Active towards Influenza: Identification of Three Potent Tetrapeptide Inhibitors. Sci Rep. 2017;7(1):10593.
458. Pietrantoni A, Dofrelli E, Tinari A, Ammendolia MG, Puzelli S, Fabiani C, et al. Bovine lactoferrin inhibits influenza A virus induced programmed cell death in vitro. Biometals. 2010;23(3):465-75.